AWARD NUMBER: W81XWH-16-1-0634

TITLE: Understanding the Relative Contributions of and Critical Enzymes for the Three Pathways for Intracrine Metabolism of Testicular Androgens in Advanced Prostate Cancer

PRINCIPAL INVESTIGATOR: Dr. Robert Bies

RECIPIENT: Research Foundation for the State University
Buffalo, NY 14260

REPORT DATE: October 2017

TYPE OF REPORT: Annual

PREPARED FOR: U.S. Army Medical Research and Materiel Command
Fort Detrick, Maryland 21702-5012

REPORT DOCUMENTATION PAGE

Form Approved
OMB No. 0704-0188

1. REPORT DATE	2. REPORT TYPE	3. DATES COVERED
October 2017	Annual	30 Sep 2016 - 29 Sep 2017

4. TITLE AND SUBTITLE
Understanding the Relative Contributions of and Critical Enzymes for the Three Pathways for Intracrine Metabolism of Testicular Androgens in Advanced Prostate Cancer

5a. CONTRACT NUMBER

5b. GRANT NUMBER
W81XWH-16-1-0634

5c. PROGRAM ELEMENT NUMBER

6. AUTHOR(S)

Dr. Robert Bies
robertbi@buffalo.edu

5d. PROJECT NUMBER

5e. TASK NUMBER

5f. WORK UNIT NUMBER

7. PERFORMING ORGANIZATION NAME(S) AND ADDRESS(ES)

Research Foundation for the State University
Buffalo, NY 14260

8. PERFORMING ORGANIZATION REPORT NUMBER

9. SPONSORING / MONITORING AGENCY NAME(S) AND ADDRESS(ES)
U.S. Army Medical Research and Materiel Command
Fort Detrick, Maryland 21702-5012

10. SPONSOR/MONITOR'S ACRONYM(S)

11. SPONSOR/MONITOR'S REPORT NUMBER(S)

12. DISTRIBUTION / AVAILABILITY STATEMENT
Approved for Public Release; Distribution Unlimited

13. SUPPLEMENTARY NOTES

14. ABSTRACT

Castration depletes circulating testosterone (T) and prostate cancer (CaP) regresses, however androgen deprivation therapy (ADT) is palliative and CaP recurs as castration-recurrent/resistant CaP (CRPC) and causes death. One mechanism for CaP resistance is intratumoral intracrine androgen metabolism, which is the conversion of weak adrenal androgens, dehydroepiandrosterone (DHEA) or androstenedione (ASD) to testicular androgens, T and dihydrotestosterone (DHT). There are 3 androgen metabolism pathways for DHT synthesis, the frontdoor and primary and secondary backdoor pathways. The timeline of intratumoral T and DHT production, the relative contribution of the 3 pathways and enzyme and pathway redundancy that drive CaP persistence after initiation of ADT to allow recurrence remain poorly understood. The central hypothesis of this report, better understanding of intracrine androgen metabolism during ADT will identify new targets to reduce T and DHT production. These studies will lead to the identification of the dominant androgen metabolism pathway that drives CaP persistence during ADT will reveal new druggable targets. Fluorescent androgens will identify the critical enzymes that drive the terminal steps of the frontdoor and primary and secondary backdoor pathways of androgen metabolism. Inhibitors that target the lead enzymes will be developed. If successful in preclinical studies, these inhibitors could be tested in patients with advanced CaP for extent of response and extension of survival.

15. SUBJECT TERMS- Intratumoral backdoor androgen metabolism, dihydrotestosterone, prostate cancer, fluorescent-steroids, SRD5A, 3α-oxidoreductases, frontdoor androgen metabolism, testosterone, pharmacometrics, ordinary differential equations, nonlinear mixed effects modeling

16. SECURITY CLASSIFICATION OF:			17. LIMITATION OF ABSTRACT	18. NUMBER OF PAGES	19a. NAME OF RESPONSIBLE PERSON
					USAMRMC
a. REPORT	b. ABSTRACT	c. THIS PAGE			19b. TELEPHONE NUMBER *(include area code)*
U	U	U	UU	98	

TABLE OF CONTENTS

1. **INTRODUCTION:** Narrative that briefly (one paragraph) describes the subject, purpose and scope of the research.

Fig. 1: Androgen metabolism pathways for DHT synthesis

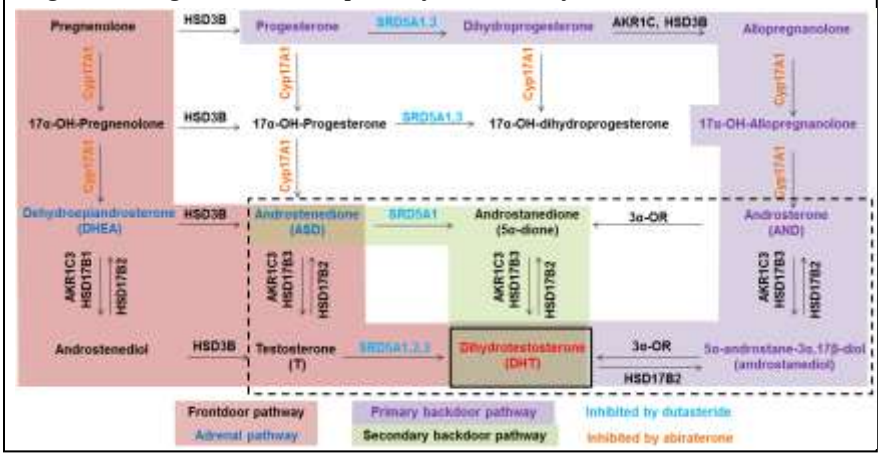

Prostate cancer (CaP) development and growth rely on the interaction between the androgen receptor (AR) and the testicular androgens, testosterone (T) and dihydrotestosterone (DHT). Most men who present with metastatic disease or men who have failed potentially curative therapy are treated with androgen deprivation therapy (ADT). ADT lowers circulating T levels and causes CaP regression in most men. However, ADT is palliative and CaP recurs as castration-recurrent/resistant CaP (CRPC) that causes death [1-5]. One mechanism that contributes to ADT resistance is intracrine intratumoral androgen metabolism. There are 3 androgen metabolism pathways to DHT, the frontdoor and primary and secondary backdoor pathways (Fig. 1). The confluence of front and backdoor pathways to DHT was appreciated only recently [6-9]. The frontdoor pathway uses the adrenal androgens dehydroepiandrosterone (DHEA) or androstenedione (ASD) to generate T, which is 5α-reduced to DHT by 5α-reductase (SRD5A) (Fig. 1;[10, 11]). The terminal substrate of the primary backdoor pathway, 5androstane3α,17β-diol (androstanediol; DIOL), is metabolized to DHT by four 3α-oxidoreductase enzymes. The secondary backdoor pathway uses a combination of SRD5A and 3α-xodiroedcutases to produce DHT from androstanedione (5α-dione). Inhibitors against the androgen metabolism enzymes such as, SRD5A inhibitors (finasteride or dutasteride), CYP17A1 inhibitors (abiraterone) and AKR1C3 inhibitors failed or produced modest responses in CRPC [12-22]. Improving response of advanced CaP to therapy requires a better understanding of intracrine androgen metabolism *in vivo* in the period immediately following initiation of ADT that can be achieved efficiently by the proposed research. The central hypothesis is **better understanding of intracrine androgen metabolism during ADT will identify new targets to reduce T and DHT production.** These studies will lead to the identification of the dominant androgen metabolism pathway that drives CaP persistence during ADT will reveal new druggable targets and development of inhibitors against the new targets. If successful in preclinical studies, these inhibitors could be tested in patients with advanced CaP for extent of response and extension of survival.

2. **KEYWORDS:** Provide a brief list of keywords (limit to 20 words).
Intratumoral backdoor androgen metabolism, dihydrotestosterone, prostate cancer, fluorescent-steroids, SRD5A, 3α-oxidoreductases, frontdoor androgen metabolism, testosterone, pharmacometrics, ordinary differential equations, nonlinear mixed effects modeling

3. **ACCOMPLISHMENTS:** The PI is reminded that the recipient organization is required to obtain prior written approval from the awarding agency Grants Officer whenever there are significant changes in the project or its direction.

What were the major goals of the project?
List the major goals of the project as stated in the approved SOW. If the application listed milestones/target dates for important activities or phases of the project, identify these dates and show actual completion dates or the percentage of completion.

The progress report focused on the goals achieved for Specific Aims 1 and 2.

Specific Aim 1. Determine the relative use of the 3 pathways for intracrine androgen metabolism *in vitro, in*

vivo and in clinical specimens **45% completed)**
Major Task 1 Identify whether provision of terminal steroid substrates confers xenograft resistance to ADT
Major Task 2 Develop mathematical models that define the dominant androgen metabolism

Specific Aim 2. Identify the principal androgen metabolism enzymes (i.e., 3α-oxidoreductases) responsible for primary backdoor DHT synthesis from androstanediol **(10% completed)**
Major Task 1 Establish 3α-oxidoreductase enzyme kinetics using fluorescent-steroids and fluorescent enzymes
Major Task 2 Establish 3α-oxidoreductase enzyme kinetics and refine Aim 1 mathematical model

Specific Aim 3. Determine the requirements for SRD5A1-3 in the front door pathway of DHT synthesis from T and its precursors and of SRD5A1 and HSD17B3
Major Task 1 Identify lead SRD5A enzyme using shRNA approaches
Major Task 2 Use mathematical model to conduct *in vivo* proof of principle experiment

What was accomplished under these goals?

J. Mohler, Project Director/Principal Investigator, RPCI:

Specific Aim 1, Major Task 1: Identify whether provision of terminal steroid substrates confers xenograft resistance to ADT
Subtask 1 Complete Sub aim 1 (DHEA) using CWR22, VCaP, LAPC-4 and LuCaP 35: **90% completed**
Subtask 2 Complete Sub aim 2 (androstanediol) using CWR22, VCaP, LAPC-4 and LuCaP 35: **to begin 11/2017**
Subtask 3 Complete Sub aim 3 (ASD) using CWR22, VCaP, LAPC-4 and LuCaP 35: **90% completed**
Subtask 4 Perform ImageStream, DHT ELISA, LC-MS/MS, qRT-PCR, and IHC analysis of samples generated in Sub aims 1-3: **Analysis to begin Jan 2018**

Fig. 2. Aim 1 experimental design

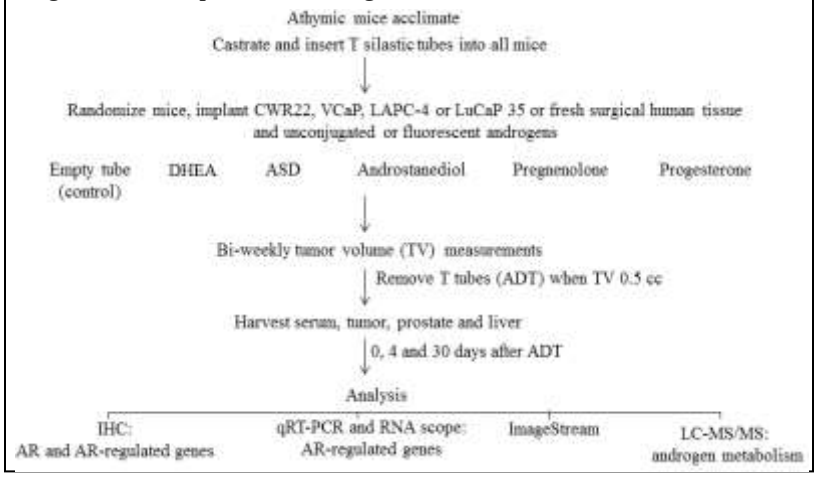

The hypothesis is adrenal androgen supplementation will facilitate CaP xenograft resistance to ADT. The experimental design (Fig. 2) was altered to include VCaP in addition to CWR22, LAPC-4 or LuCaP 35 for all Aim 1 studies. VCaP cells were included in the studies because LAPC-4 xenograft implantations failed to grow using our standard protocol. Therefore, VCaP were included to ensure we had 3 different xenograft models for comparison and data confirmation. VCaP cells are similar to LAPC-4 cells because both models have wild-type AR and do not regress after castration. However, VCaP cells use only primary backdoor metabolism, unlike LAPC-4, which uses frontdoor and primary backdoor metabolism.

J. Mohler, Project Director/Principal Investigator, RPCI, Subtasks 1 and 3: CWR22 and VCaP experiments were completed 10/22/16 and 7/7/17, respectively and the LuCaP 35 experiment was completed 10/15/17, except for two mice one for each of two control time points. CWR22 samples were analyzed using immunohistochemistry (IHC) to measure protein expression, quantitative real-time polymerase chain reaction (qRT-PCR) to measure changes in AR-regulated gene expression and liquid chromatography-tandem mass spectrometry (LC-MS/MS) to measure serum and tissue androgen levels.

Fig. 3. ASD supplementation maintained T and PSA levels

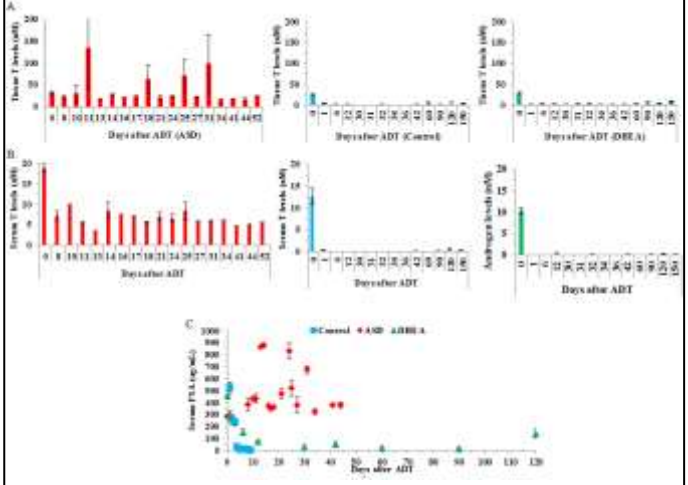

LC-MS/MS revealed ASD supplementation maintained CWR22 T levels during castration unlike mice with empty silastic tube (control) or mice supplemented with DHEA (Fig. 3A). Serum T (Fig. 3B; note different Y-axis). and PSA (Fig. 3C) levels were maintained with ASD supplementation and not in mice with control or mice supplemented with DHEA. IHC is in progress and expected to be completed Dec 2017 and a manuscript will be submitted Feb 2018.

J. Mohler, Project Director/Principal Investigator, RPCI: Subtask 2: Reports showed that DIOL is quickly glucuronidated and excreted from mice. DIOL-DP is a derivative of DIOL, which was reported to improve bioavailability of DIOL for tissue uptake [23]. Mohler laboratory performed a mouse study that assessed DIOL-DP uptake by castration-recurrent human CaP CWR22 (rCWR22) xenograft after intratumoral injection of DIOL-DP or IP injection of DIOL-DP into the subcutaneous space of the lower left flank in mice. Serum, prostate and rCWR22 androgen levels were measured using LC-MS/MS. LC-MS/MS revealed mouse prostate and/or rCWR22 xenografts produced DHT after intratumoral or IP left flank injection of DIOL-DP (Fig. 4). DIOL-DP was taken up by mouse prostate and rCWR22 xenograft after IP delivery, so a second study was performed to assess if DIOL or DIOL-DP could be administered to mice using silastic tube implants packed with DIOL or DIOL-DP. Samples were collected and LC-MS/MS to measure serum and prostate androgen levels is in progress. Subaim 2 experiments will begin after review of LC-MS/MS data and the best androstanediol delivery method is confirmed **(Nov 2017).**

Fig. 4. DHT levels increased after DIOL treatment

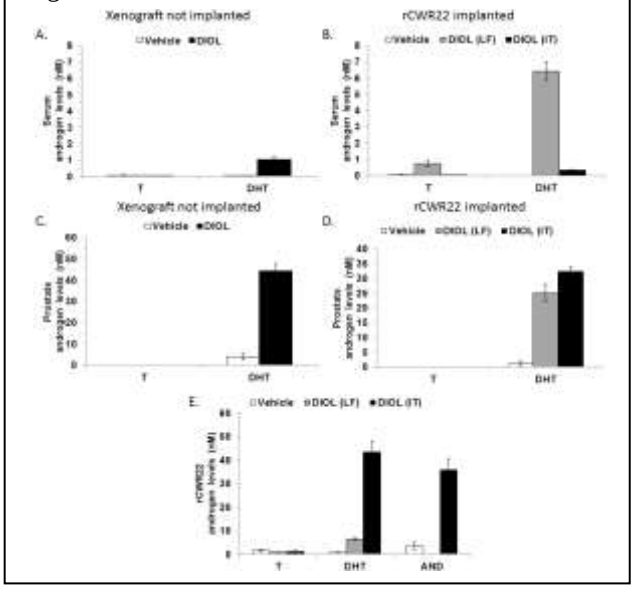

J. Mohler, Project Director/Principal Investigator, RPCI, Subtask 4: Perform ImageStream, DHT ELISA, LC-MS/MS, qRT-PCR, and IHC analysis of samples generated in Sub aims 1-3: **To begin once Subaim 2 samples are generated (Jan 2018)**

J. Mohler, Project Director/Principal Investigator, RPCI, Subtask 5: Complete Sub aim 4 (Fluorescent-steroids) using CWR22, LAPC-4 and LuCaP 35 **(begin Feb 2018)**

J. Mohler, Project Director/Principal Investigator, RPCI, Subtask 6: Perform ImageStream, DHT ELISA, LC-MS/MS, qRT-PCR, and IHC analysis of samples generated in Sub aim 5 **(immediately after completion of Subtask 5)**

D. Watt, Collaborating/Partnering PI, University of Kentucky, Subtask 6 cont': We synthesized and characterized fluorescent 5α-androgens that will be used by our collaborators to assess the contribution of the three androgen metabolism pathways (*i.e.*, front door, primary backdoor and secondary backdoor pathways). We introduced a fluorescent, aminocoumarin, namely 8-(2-aminoethyl)-2,3,4,5-tetrahydro-1*H*,4*H*-11-oxa-3a-azabenzo[*de*]anthracen-10-one, at either a C-17 keto or a C-17β hydroxyl group. Starting from isoandrostanolone (*i.e.*, 5α-androstan-3α-ol-17-one), we condensed this material with O-carboxymethyl hydroxylamine to introduce a suitable carboxylic acid functional group at the C-17 position. Subsequent

condensation with the fluorescent, aminocoumarin described above, furnished the fluorescent analog of 5α-androstan-3α-ol-17-one (AND). Oxidation of this fluorescent analog of 5α-androstan-3α-ol-17-one using sulfur trioxide-pyridine afforded the fluorescent analog of 5α-androstan-3,17-dione (5α-dione). Starting from 5α-dihydrotestosterone (DHT), the rhodium(II)-catalyzed condensation with ethyl diazoacetate and saponification provided DHT with a carboxymethoxy group at C-17. Subsequent condensation with the fluorescent-aminocoumarin described above, furnished the fluorescent analog of DHT. Selective reduction of the C-3 keto group in this modified DHT using lithium tri(tert-butoxy)aluminum hydride, Mitsunobu inversion, and saponification furnished 5α-androstan-3α,17β-diol(DIOL) with a carboxymethoxy group at C-17. Subsequent condensation with the fluorescent, aminocoumarin described above, furnished the fluorescent analog of DIOL. These fluorescent AND, 5α-dione and DIOL derivatives retained the needed level of biological activity in biological assays (*vida infra*). In summary, in accord with the Statement of Work (Specific Aim 1, Major Task 1, Subtask 6), we devised efficient syntheses of four fluorescent-5α-androstanes that possessed the desired fluorescent group need by our collaborators to study the frontdoor, primary backdoor and secondary backdoor pathways leading to DHT and T.

R. Bies, Collaborating/Partnering PI, University at Buffalo, Subtask 6, cont': We developed a detailed description of the CWR22 xenograft growth trajectory over time. The modeling framework incorporated a delayed signal architecture (Fig. 5), which was linked to a Gompertz growth model that could be perturbed based on time dependent interventions such as ADT. The model censored when mice were euthanized at various study time points or when xenografts exceeded veterinary limits (2 cc). censored tumors were accounted for in parallel with the growth model (Fig. 6). The model remains under development.

Fig. 5. Schematic of nonlinear mixed effects signal distribution model that describes CWR22 growth trajectories

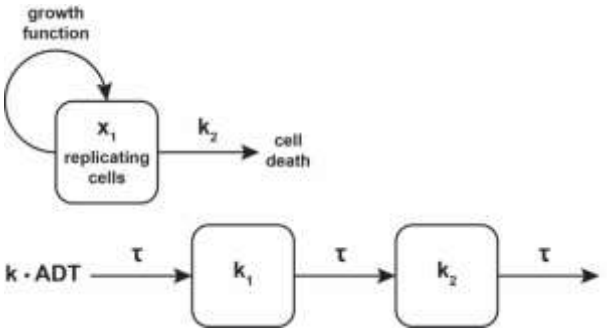

Fig. 6. Tumor growth trajectories with population average predictions from the nonlinear mixed effect model

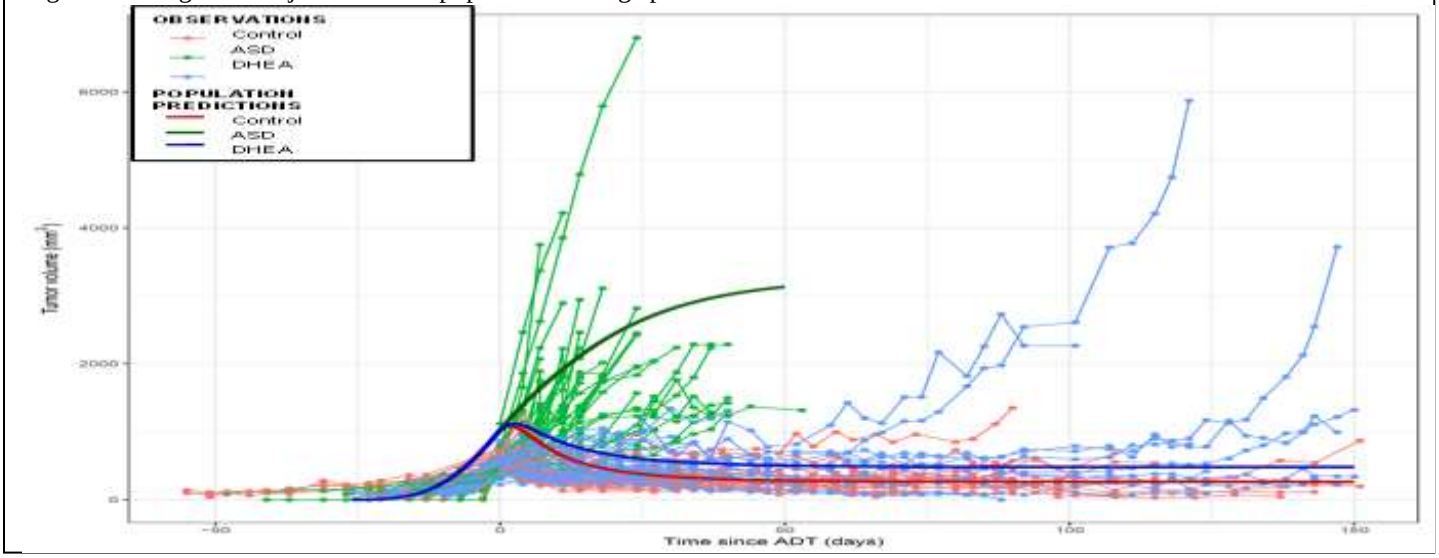

Specific Aim 2, Major Task 1: Establish 3α-oxidoreductase enzyme kinetics using fluorescent-steroids and fluorescent-enzymes

Subtask 1 Test PC-3 cells that stably express wild-type or double mutant 3α-oxidoreductase using live cell imaging and ImageStream **(In progress)**

Fig. 7. DHT levels increased after DIOL treatment

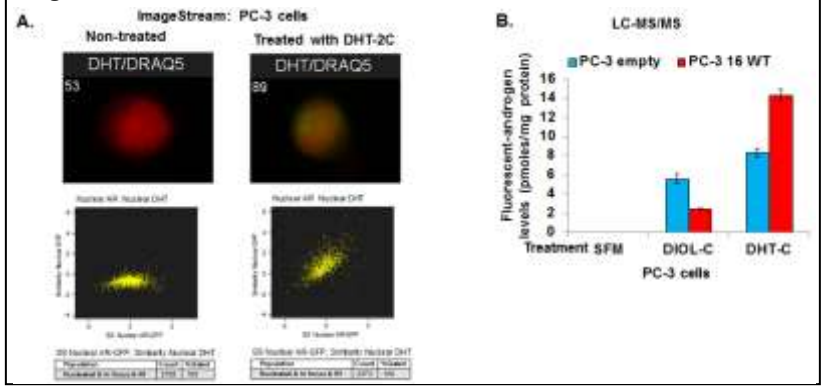

The androgen-independent PC-3 CaP cell line that stably expressed AR fused with green fluorescent protein (GFP) was used to determine cellular uptake of fluorescent-androgens, AR activation and nuclear translocation using ImageStream, and LC-MS/MS was used to determine if fluorescent-androgens were metabolized by androgen metabolism enzymes. PC-3 cells that stably expressed AR were treated with 20 nM DHT-2-coumarin (DHT-2C) and treated with nuclear dye Draq5 (red color) immediately before analysis. Draq5 was used to identify the nucleus in each cell and to confirm target nuclear localization when images were merged. ImageStream analysis revealed that fluorescent-DHT (DHT-2C; green) was taken up by PC-3 cells. DHT-2C bound to ARs, which led to nuclear translocation (Fig. 7A; yellow color produced when green and red colors overlap). PC-3 cells that stably expressed wild-type 3α-oxidoreductase RDH16 were treated with 20 nM DIOL-coumarin (DIOL-C) to assess if RDH16 metabolized DIOL-C to DHT-C. LC-MS/MS revealed PC-3 cells that stably expressed RDH16 metabolized DIOL-C to DHT-C (Fig. 7B) better compared to PC-3 cells without RDH16.

Fig. 8. DHT levels increased after DIOL treatment

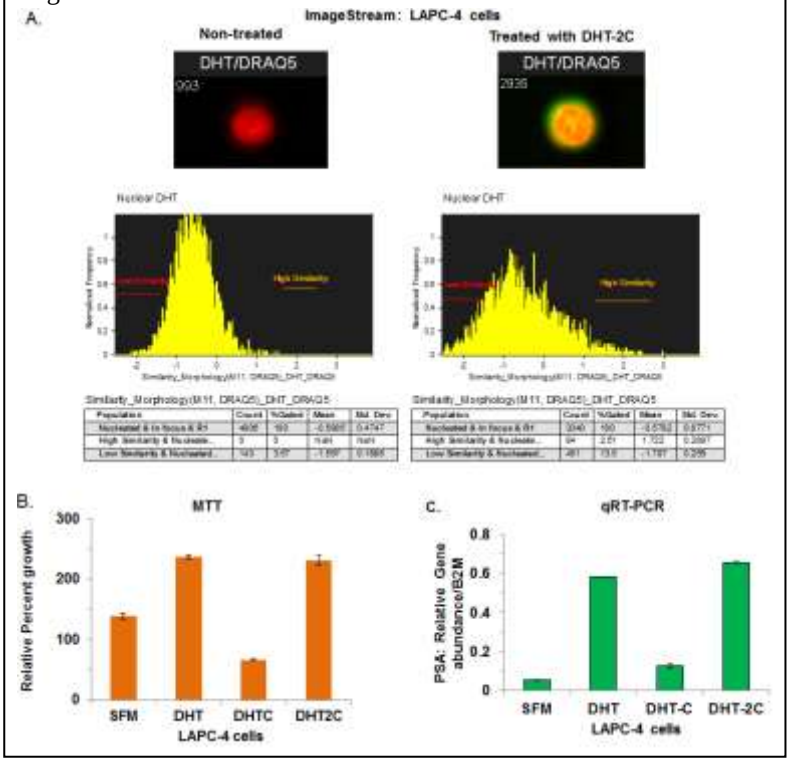

The androgen-sensitive LAPC-4 CaP cell line was used to determine DHT-2C cellular uptake, AR activation and nuclear translocation, and assess if DHT-2C rescues and restores LAPC-4 cell growth when cells were cultured in androgen-deprived media (serum-free complete media [SFM]). ImageStream revealed DHT-2C was taken into LAPC-4 cells and facilitated endogenous AR activation and nuclear translocation (Fig. 8A). DHT-2C treatment facilitated LAPC-4 cell growth during androgen deprivation (Fig. 8B). The increased LAPC-4 cell growth is due to AR activation as determined using prostate specific-antigen (PSA) induction (Fig. 7C). The data showed LAPC-4 cells treated with DHT-2C produced responses similar to LAPC-4 cells treated with unlabeled DHT, which suggests DHT-2C functions similar to DHT despite aminocoumarin addition.

Live-cell imaging experiment optimization is in progress and initial experiments will be completed end of October 2017.

Subtask 2 Repeat live-cell imaging and ImageStream experiments using LAPC-4 and VCaP **(In progress)**

Major task 2: Our laboratory developed a description of a subset of the metabolic network (Fig. 9) that uses first order rates of metabolism across the network to probe the nature of the metabolizing network. We focused on the conversion of androsterone to 5α-dione (Fig. 10) so that a full mass action model could be implemented.

This mass action network model provided flexibility to incorporate specific enzymes amounts, enzyme affinities, and catabolic rates and explicitly account for parallel pathways where competition can occur among enzymes and substrates. Matlab, toolbox SIMBIOLOGY (NAtik MA) was used to develop the model. A manuscript that detailed this mathematical description was drafted and prepared for submission after J. Mohler manuscript titled "Inhibition of dihydrotestosterone synthesis in prostate cancer by combined frontdoor and backdoor pathway Blockade" is accepted.

Fig.. 9. Androgen metabolism network model using first order transfer rates (subsets)

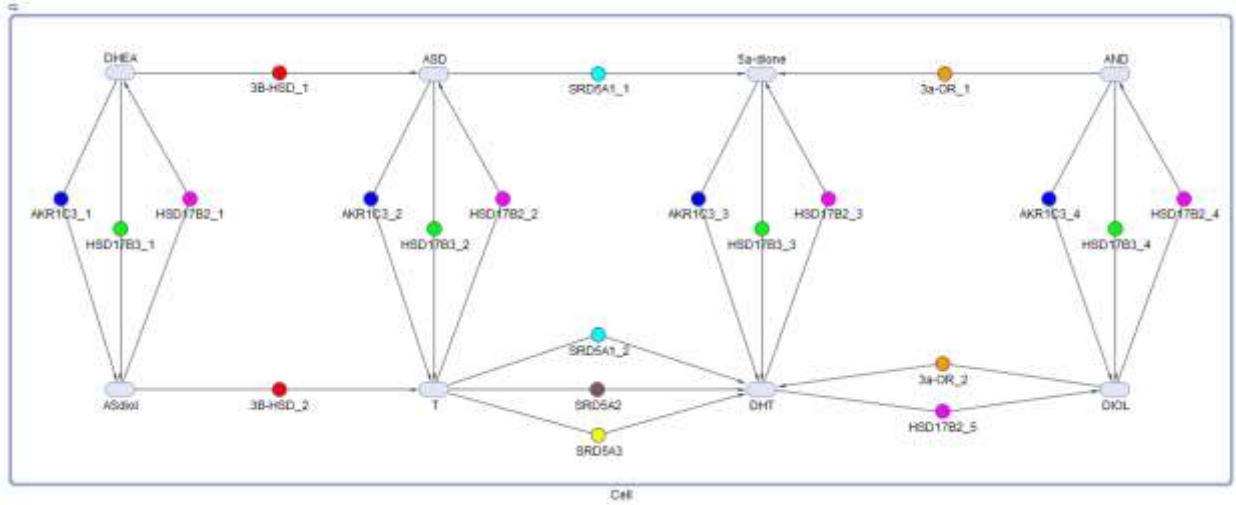

Fig.. 10. Schematic of androsterone to androstanedione (5α-dione) mathematical model structure

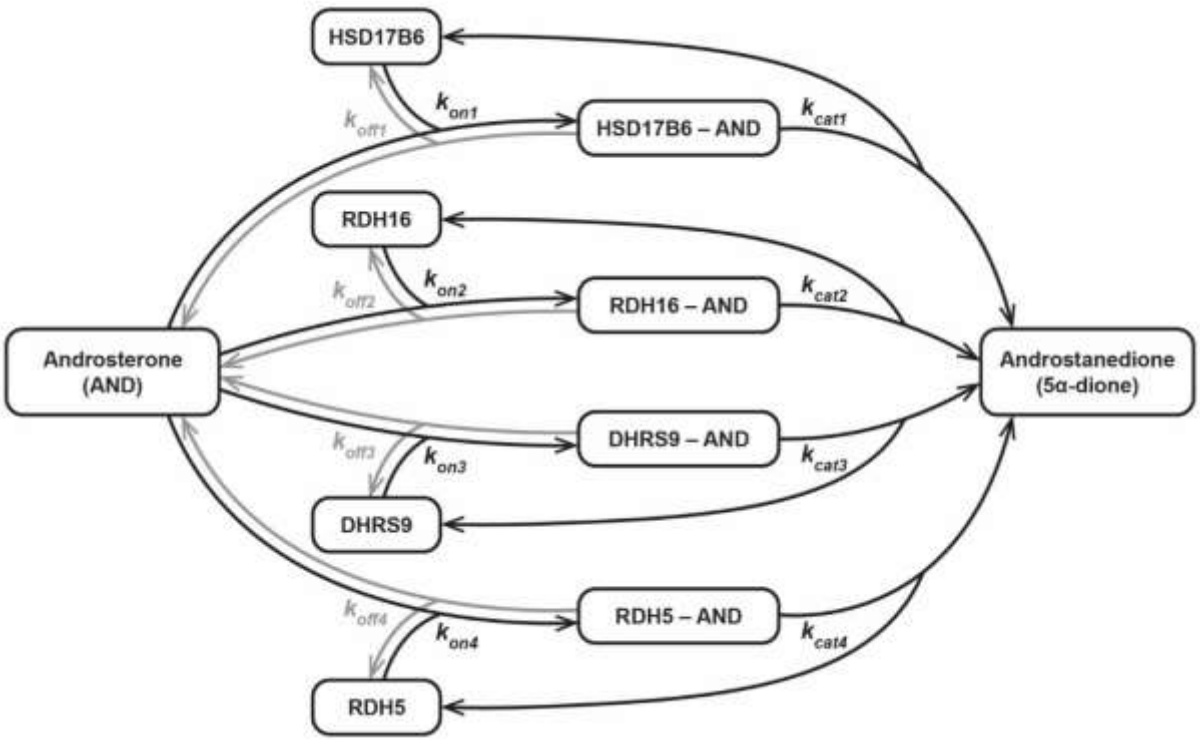

What opportunities for training and professional development has the project provided?

J. Mohler, Project Director/Principal Investigator, RPCI: Dr. Michael Fiandalo, Post-doctoral Fellow, gained additional experience with mouse project management and data analysis. Dr. Fiandalo learned how to design and perform ImageStream experiments and analyze ImageStream data. Dr. Fiandalo acquired additional experience with manuscript preparation and further developed scientific presentation skills at national conferences.

D. Watt, Collaborating/Partnering PI, University of Kentucky: Ms. Liliia Kril, Laboratory Technician Senior, gained research experience in the synthesis of fluorescent-steroids.

R. Bies, Collaborating/Partnering PI, University at Buffalo: Dr. Sarah Cook attended the Statistical Basis of Pharmacometrics course in Dublin, Ireland taught by Adrian Dunne in September 2016. This course helped to develop Dr. Cook's abilities in the area of nonlinear mixed effects modeling.

How were the results disseminated to communities of interest?

J. Mohler, Project Director/Principal Investigator, RPCI: Manuscripts were published in peer-reviewed journals.

D. Watt, Collaborating/Partnering PI, University of Kentucky: Manuscripts were published in peer-reviewed journals.

R. Bies, Collaborating/Partnering PI, University at Buffalo: Manuscript to be submitted after "Inhibition of dihydrotestosterone synthesis in prostate cancer by combined frontdoor and backdoor pathway blockade" is accepted.

What do you plan to do during the next reporting period to accomplish the goals?

J. Mohler, Project Director/Principal Investigator, RPCI: Aim 1, sub aims 1-3 experiments and sample analysis should be completed Feb 2018 and April 2018, respectively. The timeline remains consistent with the project statement of work. Subaim 4 *in vivo* experiments will begin May 2018 using CWR22, VCaP and LuCaP 35 xenografts. Watt laboratory will continue to produce fluorescent-ASD, -DHEA or –DIOL, pregnenolone and progesterone. Fluorescent-steroids will be tested *in vitro* using ImageStream and LC-MS/MS.

Aim 2 live-cell imaging experiments using PC-3 cells that express 3α-oxiodreductases will be completed October 2017 and experiment repeats using LAPC-4, CWR22pc or VCaP will be completed November 2017. Combination studies using wild-type RDH16 vs. catalytic inactive RDH16 will begin December 2017. Plasmid encoding fluorescent-wild-type or double mutant RDH5 for ImageStream and live-cell imaging experiments are in progress.

D. Watt, Collaborating/Partnering PI, University of Kentucky: The results generated in year 01 defined the pharmacological boundaries for biologically relevant fluorescent-androgens modified at the C-17 position. These androgens with an aminocoumarin at C-17 underwent absorption, translocated to the nucleus and bound AR but **did not activate** transcription. We will next synthesize fluorescent-steroids modified at the C-3 position. Preliminary results suggest that these androgens with an aminocoumarin at C-3 undergo absorption, translocate to the nucleus, bind to the AR and **activate** transcription.

R. Bies, Collaborating/Partnering PI, University at Buffalo: The key accomplishments anticipated for the next report are the extension of the metabolic network model to include at least four substrate to product conversions using data generated from the LAPC4 experimental system. In addition, there still appears to be

some mis-specification in the nonlinear mixed effects model describing the tumor trajectories using the CWR22 model system. These issues are being addressed and ideally will be corrected for the next reporting period utilizing a variety of strategies including but not limited to mixture distributions in parameter values, incorporation of biomarker measures and pathological measures of heterogeneity in the individual tumor xenografts.

Describe briefly what you plan to do during the next reporting period to accomplish the goals and objectives.

4. **IMPACT:** Describe distinctive contributions, major accomplishments, innovations, successes, or any change in practice or behavior that has come about as a result of the project relative to:

What was the impact on the development of the principal discipline(s) of the project?

J. Mohler, Project Director/Principal Investigator, RPCI: Specific Aim 1: The data produced from using multiple CaP xenografts will identify the preferred androgen metabolism pathway that facilitates CaP resistance to ADT. Identification of the preferred pathway will lead to identification of the critical enzymes necessary for CaP survival during ADT. Fluorescent-based screens will be used to identify compounds that inhibit the lead enzymes. The studies demonstrate adrenal androgen supplementation impacts xenograft response to ADT and data suggest *in vivo* models should include adrenal androgen supplementation when androgen metabolism inhibitors are tested. This is significant because mice lack adrenal androgens and adrenal androgen contribution to ADT or androgen metabolism inhibitor resistance is often overlooked.

D. Watt, Collaborating/Partnering PI, University of Kentucky: The results generated in year 1 provided the tools necessary to identify the principal androgen metabolism enzymes responsible for primary backdoor DHT synthesis from DIOL and to determine the requirements for specific enzymes in the late stages of androgen metabolism (*i.e.*, SRD5A1-3 in the frontdoor pathway and SRD5A1 and HSD17B3 in the secondary backdoor pathway).

R. Bies, Collaborating/Partnering PI, University at Buffalo: Nothing to report

What was the impact on other disciplines?

J. Mohler, Project Director/Principal Investigator, RPCI: Nothing to report

D. Watt, Collaborating/Partnering PI, University of Kentucky: The results generated in year 1 defined the pharmacological boundaries for biologically relevant fluorescent-androgens. We determined that androgens with an aminocoumarin (*i.e.*, 8-(2-aminoethyl)-2,3,4,5-tetrahydro-1*H*,4*H*-11-oxa-3a-azabenzo[*de*]anthracen-10-one) at C-17 underwent
absorption, bound AR, translocated to the nucleus, **but did not activate transcription**.

R. Bies, Collaborating/Partnering PI, University at Buffalo: Nothing to report

What was the impact on technology transfer?

J. Mohler, Project Director/Principal Investigator, RPCI: The results generated in year 1 identified shared catalytic amino acid residues among four 3α-oxidoreductases. The provisional patent "Inhibition of catalytic site common to multiple 3 alpha-oxidoreductases for treatment of prostate cancer" was converted to a Patent Cooperation Treaty (PCT/US2017/024322).

D. Watt, Collaborating/Partnering PI, University of Kentucky: The results generated in year 1 developed valuable tools for studying late-stage androgen metabolism. We are in the process of submitting a disclosure to the University of Kentucky's Intellectual Property Office. This Office will obtain an evaluation of our disclosure and if warranted, assist in filing a provisional U.S. patent application.

R. Bies, Collaborating/Partnering PI, University of Buffalo: Nothing to report

What was the impact on society beyond science and technology?
If there is nothing significant to report during this reporting period, state "Nothing to Report."

J. Mohler, Project Director/Principal Investigator, RPCI: Nothing to report

D. Watt, Collaborating/Partnering PI, University of Kentucky: The results generated in year 1 provide a reasonable expectation that it will be possible to identify specific enzymes targets late in androgen metabolism and ultimately to identify small-molecule agents to treat castration-recurrent/resistant prostate cancer (CRPC) that are better than current therapies.

R. Bies, Collaborating/Partnering PI, University at Buffalo: Nothing to report

5. **CHANGES/PROBLEMS:** The Project Director/Principal Investigator (PD/PI) is reminded that the recipient organization is required to obtain prior written approval from the awarding agency Grants Officer whenever there are significant changes in the project or its direction. If not previously reported in writing, provide the following additional information or state, "Nothing to Report," if applicable:

Changes in approach and reasons for change

J. Mohler, Project Director/Principal Investigator, RPCI: The experimental strategy was changed in two ways. First, human CaP VCaP xenograft was included for Aim 1 studies. Second mouse studies were performed to determine the best method of DIOL or DIOL-DP delivery to mice. VCaP cells are an ideal alternative to LAPC-4 cells because VCaP cells express wild-type AR and use primary backdoor metabolism.

D. Watt, Collaborating/Partnering PI, University of Kentucky: Nothing to report

R. Bies, Collaborating/Partnering PI, University at Buffalo: Nothing to report

Actual or anticipated problems or delays and actions or plans to resolve them
Describe problems or delays encountered during the reporting period and actions or plans to resolve them.

J. Mohler, Project Director/Principal Investigator, RPCI: Aim 1: LAPC-4 xenografts proved difficult to establish in nude mice. Studies using SCID mice implanted with LAPC-4 cells are in progress. If LAPC-4 xenografts fail to establish using various conditions, future studies will include CWR22, VCaP and LuCaP 35.

J. Mohler, Project Director/Principal Investigator, RPCI: Aim 2: Nothing to report

D. Watt, Collaborating/Partnering PI, University of Kentucky: Nothing to report

R. Bies, Collaborating/Partnering PI, University at Buffalo: Nothing to report

Changes that had a significant impact on expenditures

J. Mohler, Project Director/Principal Investigator, RPCI: Effort is being adjusted to cover a $1900 salary overage that occurred in year 1 and would cause a $7000 salary overage in year 2.

D. Watt, Collaborating/Partnering PI, University of Kentucky: Nothing to report

R. Bies, Collaborating/Partnering PI, University at Buffalo: Nothing to report

Significant changes in use or care of human subjects, vertebrate animals, biohazards, and/or select agents

Significant changes in use or care of human subjects

J. Mohler, Project Director/Principal Investigator, RPCI: Nothing to report because studies do not require human subjects

D. Watt, Collaborating/Partnering PI, University of Kentucky: Nothing to report; the Watt group does not work with human subjects

R. Bies, Collaborating/Partnering PI, University at Buffalo: Nothing to report; the Bies group does not work with human subjects

Significant changes in use or care of vertebrate animals.

J. Mohler, Project Director/Principal Investigator, RPCI: Nothing to report

D. Watt, Collaborating/Partnering PI, University of Kentucky: Nothing to report, the Watt group does not work with vertebrate animals

R. Bies, Collaborating/Partnering PI, University at Buffalo: Nothing to report, the Bies group does not work with vertebrate animals

Significant changes in use of biohazards and/or select agents

J. Mohler, Project Director/Principal Investigator, RPCI: Nothing to report because biohazards and select agents were not required.

D. Watt, Collaborating/Partnering PI, University of Kentucky: Nothing to report because biohazards and select agents were not required.

R. Bies, Collaborating/Partnering PI, University at Buffalo: Nothing to report because biohazards and select agents were not required.

6. **PRODUCTS:** List any products resulting from the project during the reporting period. If there is nothing to report under a particular item, state "Nothing to Report."

- **Publications, conference papers, and presentations**
  Report only the major publication(s) resulting from the work under this award.

  Journal publications.

J. Mohler, Project Director/Principal Investigator, RPCI: One manuscript under review, one ready for submission two in preparation.

Authors: Fiandalo, MV; Stocking, JS; Pop, EA; Wilton, JH; Mantione, KM; Li, Y; Attwood, KM; Azabdaftari, G; Wu, Y; Watt, DS; Wilson, EM; Mohler, JL
Title: Inhibition of Dihydrotestosterone Synthesis in Prostate Cancer by Combined Frontdoor and Backdoor Pathway Blockade
Journal: Oncotarget
Volume: N/A
Year: 2017
Page numbers: N/A
Status of publication: under review
Acknowledgement of federal support: Yes

D. Watt, Collaborating/Partnering PI, University of Kentucky: Two manuscripts published and two under review

Authors: Frasinyuk, MS; Mrug, GP; Bondarenko, SP; Khilya, VP; Sviripa, VM; Syrotchuk, OA; Zhang, W; Cai, X; Fiandalo, MV; Mohler, JL; Liu, C; Watt, DS
Title: Antineoplastic Isoflavonoids Derived from Intermediate *ortho*-Quinone Methides Generated from Mannich Bases
Journal: ChemMedChem
Volume: 11
Year: 2016
Page numbers: 600-611
Status of publication: published
Acknowledgement of federal support: Yes, but not for this DoD grant. Work was completed before start of funding period.

Authors: Frasinyuk, MS; Zhang, W; Wyrebek, P; Yu, T; Xu, X; Sviripa, VM; Bondarenko, SP; Xie, Y; Ngo, NG; Morris, AJ; Mohler, JL; Fiandalo, MV; Watt, DS; and Liu, C
Title: Developing Antineoplastic Agents that Targeting Peroxisomal Enzymes: Cytisine-linked Isoflavonoids as Inhibitors of Hydroxysteroid 17-beta-dehydrogenase-4 (HSD17B4)
Journal: Org Biomol Chem
Volume: N/A
Year: 2017
Page numbers: N/A
Status of publication: awaiting publication (doi: 10.1039/c7ob01584d)
Acknowledgement of federal support: Yes

Authors: Popova, AV; Frasinyuk, MS; Bondarenko, SP; Zhang, W; Xie, Y; Martin, ZM; Cai, X; Fiandalo, MV; Mohler, JL; Liu, C; Watt, DS; Sviripa, VM
Title: Efficient Synthesis of Aurone Mannich Bases and Evaluation of their Antineoplastic Activity in PC-3 Prostate Cancer Cells
Journal: Anticancer Agents Med Chem
Volume: N/A
Year: 2017
Page numbers: N/A
Status of publication: under review
Acknowledgement of federal support: Yes

R. Bies, Collaborating/Partnering PI, University at Buffalo: 1 manuscript ready for submission

J. Mohler, Project Director/Principal Investigator, RPCI: Presentations:

1) American Urologic Association (AUA) "Adrenal Androgens Facilitate Prostate Cancer Cell Resistance to Androgen Deprivation Therapy" Michael V. Fiandalo, James L. Mohler; Boston, MA, Poster Presentation, May 2017
2) Society for Basic Urologic Research (SBUR) "Adrenal Androgens Facilitate Prostate Cancer Cell Resistance to Androgen Deprivation Therapy" Michael V. Fiandalo, James L. Mohler; Paradise Valley, AZ, Poster Presentation, Nov 2016

Books or other non-periodical, one-time publications.

J. Mohler, Project Director/Principal Investigator, RPCI: No books or periodicals were published

D. Watt, Collaborating/Partnering PI, University of Kentucky: No books or periodicals were published

R. Bies, Collaborating/Partnering PI, University at Buffalo: No books or periodicals were published

Other publications, conference papers, and presentations.

J. Mohler, Project Director/Principal Investigator, RPCI Presentations:

1) *American Urologic Association (AUA) "Four Birds One Stone to Inhibit 5androstane-3α,17β-diol conversion to DHT. Michael V. Fiandalo, James L. Mohler; San Diego, CA, Poster Presentation, May 2016.
   Manuscript: "Inhibition of Dihydrotestosterone Synthesis in Prostate Cancer by Combined Frontdoor and Backdoor Pathway blockade Fiandalo MV, Wilton JH, Stocking JS, Mongiardo K, Pop EA, Li Y, Attwood K, Wilson EM, Mohler JL.
   Under review at Oncotarget and federal support was acknowledged

2) *Society for Basic Urologic Research (SBUR) "Adrenal Androgens Facilitate Prostate Cancer Cell Resistance to Androgen Deprivation Therapy" Michael V. Fiandalo, James L. Mohler; Paradise Valley, AZ, Poster Presentation, Nov 2016
   Manuscript: "Serum-free complete medium, an alternative medium to mimic androgen deprivation in human prostate cancer cell line models" Michael V. Fiandalo, John H Wilton, Krystin M. Mantione, Carol Wrzosek, Kristopher M. Attwood, Yue Wu and James L. Mohler
   Under review with Prostate and federal support was acknowledged

- **Website(s) or other Internet site(s)**

J. Mohler, Project Director/Principal Investigator, RPCI: No websites to list at this time

D. Watt, Collaborating/Partnering PI, University of Kentucky: No websites to list at this time

R. Bies, Collaborating/Partnering PI, University at Buffalo: No websites to list at this time

- **Technologies or techniques**

J. Mohler, Project Director/Principal Investigator, RPCI: ImageStream and live-cell imaging techniques allows identification of fluorescent-enzyme and fluorescent-substrate co-localization. The fluorescent-product binds the fluorescent-AR and localizes to the nucleus that's stained with a nuclear dye. These assays can be used to identify inhibitors against androgen metabolism enzymes and characterize lead inhibitors. The data produced from these studies can be used by the Bies laboratory to produce mathematical models.

D. Watt, Collaborating/Partnering PI, University of Kentucky: The results generated in year 1 provided the tools necessary to identify the principal androgen metabolism enzymes responsible for primary backdoor DHT synthesis from androstane-3α,17β-diol and to determine the requirements for specific enzymes in the late stages of androgen metabolism (*i.e.*, SRD5A1-3 in the frontdoor pathway and SRD5A1 and HSD17B3 in the secondary backdoor pathway).

R. Bies, Collaborating/Partnering PI, University at Buffalo: Nothing to report

- **Inventions, patent applications, and/or licenses**

J. Mohler, Project Director/Principal Investigator, RPCI: The provisional patent "Inhibition of Catalytic Site Common to Multiple 3 Alpha-Oxidoreductases for Treatment of Prostate Cancer" was converted to a Patent Cooperation Treaty (PCT/US2017/024322).

D. Watt, Collaborating/Partnering PI, University of Kentucky: We are in the process of disclosing information (working title for provisional patent: Development of Fluorescent-labeled Androgens as Tools for Antinenoplastic Drug Discovery) to the University of Kentucky's Intellectual Property Office in accord with University of Kentucky policy. The disclosure will involve the following inventors: Mohler, Fiandalo, Sviripa, and Watt. If evaluated and approved for patent protection, the University of Kentucky will identify a patent attorney who will file a provisional U.S. patent owned jointly by the University of Kentucky Research Foundation and Roswell Park Cancer Institute.

R. Bies, Collaborating/Partnering PI, University at Buffalo: Nothing to report

- **Other Products**

J. Mohler, Project Director/Principal Investigator, RPCI: No other reportable outcomes at this time

7. PARTICIPANTS & OTHER COLLABORATING ORGANIZATIONS

What individuals have worked on the project?

J. Mohler, Project Director/Principal Investigator, RPCI:

Name: James L. Mohler
Project Role: Director/Principal Investigator/Partnering PI
Research Identifier: ORCID ID: 0000-0002-7726-3795
Nearest person month worked: 1
Contribution to project: Dr. James L. Mohler (Urologic Oncology Surgeon, Principal Investigator) conceived the overall experimental question, assisted with the experimental design and supervised experiment completion, data analysis and manuscript development.
Funding Support: National Cancer Institute, National Institute of Diabetes and Digestive and Kidney Diseases, New York State Department of Health, Roswell Park Alliance Foundation

Name: Michael V. Fiandalo
Project Role: Post-doctoral fellow
Researcher Identifier: ORCID ID: /0000-0002-3558-2712
Nearest person month worked: 6

Contribution to project: Dr. Michael V. Fiandalo (Post-doctoral fellow) assisted with development of overall experimental question, refinement of the experimental question and experimental design and executed experiments, analyzed data and developed the manuscript.

D. Watt, Collaborating/Partnering PI, University of Kentucky:

Name: David S. Watt
Project Role: Collaborating/Partnering PI
Researcher Identifier: ORCID ID: orcid.org/0000-0002-3844-1712
Nearest person month worked: 1
Contribution to project: Dr. Watt contributed to the design of the synthetic pathways needed to synthesize various fluorescent-androgens, the writing of papers and reports, and the preparation of documents for submission to the University's Intellectual Property Office that will in turn evaluate the suitability of disclosed information for provisional U.S. patent application.
Funding Support: The University of Kentucky's College of Medicine; The University of Kentucky's College of Pharmacy through the Center for Pharmaceutical Research and Innovation; The National Institutes of Health.

Name: Liliia Kril
Project Role: Laboratory Technician Senior
Researcher Identifier: orcid.org/0000-0002-6469-0579
Nearest person month worked: 6
Contribution to project: Ms. Kril participates in the synthesis of organic compounds and their characterization by NMR, mass spectral and other means.
Funding Support: The University of Kentucky's College of Pharmacy through the Center for Pharmaceutical Research and Innovation

R. Bies, Collaborating/Partnering PI, University at Buffalo:

Name: Robert Bies
Project Role: Collaborating/Partnering PI
Research Identifier: ORCID ID: 0000-0003-3818-2252
Nearest person month worked: 1
Contribution to project: Dr. Bies has supervised and contributed to the development of mechanistic androgen metabolism and empirical nonlinear mixed effects modeling of tumor trajectories in the CWR22 tumor model
Funding Support: Nothing to report

Name: Sarah Cook
Project Role: Post-doctoral fellow
Researcher Identifier: 0000-0001-8612-882X
Nearest person month worked: 6
Contribution to project: Dr. Cook has worked directly on coding the metabolic and nonlinear mixed effects tumor trajectory models using SIMBIOLOGY/MATLAB and NONMEM. In addition, Dr. Cook wrote the first manuscript
Funding Support: Nothing to report

Has there been a change in the active other support of the PD/PI(s) or senior/key personnel since the last reporting period?
If there is nothing significant to report during this reporting period, state "Nothing to Report."

Yes, active other supports for Dr. James L. Mohler, Dr. David S. Watt, Dr. Kristopher A. Attwood, Dr. Michael V. Fiandalo, Dr. John H. Wilton were updated below. Nothing to report for Dr. Michael Moser

R. Bies, Collaborating/Partnering PI, University at Buffalo: Nothing to report

Changes in active support

Mohler, J.L.

Pending to Active
Title: A Small-Molecule Inhibitor of the Terminal Steps for Intracrine Androgen Synthesis in Advanced Prostate Cancer (Mohler)
Time Commitments: .975 calendar months
Supporting Agency: NCI-1R21CA205108-01
Name and address of the Funding Agency's Procuring Contracting/Grants Officer: Nicole Franklin, Grants Management Specialist, National Cancer Institute, 9609 Medical Center Drive, West Tower, Room 2W556, Bethesda, MD 20892 (regular mail), Phone: 240-276-5210, Email: nicole.franklin@nih.gov
Performance Period: 04/10/2016-04/09/2018
Level of Funding: $ 416,398
Brief description of project's goals: This research seeks to explore if a small-molecule inhibitor of the catalytic site shared by the five 3α−oxidoreductases will decrease T and DHT metabolism through the frontdoor and backdoor pathways.
List of specific aims:

1. Identify a candidate inhibitor against the catalytic site shared by the five 3α−oxidoreductases
2. Synthesize and test re-designed candidate inhibitors and conduct PK/PD and toxicity studies to produce a lead compound inhibitor of the five 3α−oxidoreductases
3. Determine whether the inhibitor of the 3α−oxidoreductases decreases tissue T and DHT levels and impairs CRPC growth

Overlap: None

Title: The NF-kappaB-androgen Receptor Axis Drives Failure of Medical Therapy in Human Benign Prostatic Hyperplasia (Matusik)
Time Commitments: 0.30 calendar months
Supporting Agency: NIH/NIDDK Melissa Haney, Manager, Dept of Urologic Surgery, Vanderbilt University. 615-322-3172, Melissa.haney@vanderbilt.edu
Name and address of the Funding Agency's Procuring Contracting/Grants Officer: not assigned
Performance Period: 09/16/2016 – 07/31/2021
Level of funding: $151,840 (sub)
Brief description of project's goals: NκB and AR signaling controls the failed response to 5ARIs in BPH.
List of specific aims:

1. Determine cross-talk between NFκB and AR signaling to regulate failure of edical therapy
2. Determine the SRD5A isoforms contribution during resistance to medical therapy
3. Determine if failure of medical therapy is driven by NFκB and/or AR-V7 in BPH patients. New insight into how BPH patients fail 5α-reductase inhibitors holds the promise to identify pathways to apply novel approaches to medical therapy in the treatment of BPH.

Overlap: None

Title: Genetic and Epigenetic Prostate Cancer Related alterations in early onset disease in African American Men (Woloszynska-Read)
Time Commitments: 1.20 calendar months

Supporting Agency: DoD
Name and address of the Funding Agency's Procuring Contracting/Grants Officer: Department of Defense, USA MED RESEARCH ACQ ACTIVITY 820 CHANDLER ST FORT DETRICK MD 21702-5014/ LYMOR BARNHARD
Performance Period: 04/01/2017-03/31/2020
Level of funding: $1,242,951
Brief description of project's goals: Proposed research aims to identify molecular alterations that distinguish aggressive forms of early onset prostate cancer commonly found in Afrinca American men will contribute to the development of African American tumor (epi)genetic signature(s) and ultimately will lead to personalized medicine strategies for this group of patients.
List of specific aims:
1. Determine the relative frequency of genetic lesions found in PCa in AAs and EAs.
2. Determine novel, clinically relevant methylomic and transcriptomic differences in PCa from AAs and EAsObtain and link vital status data and cause of death in PCaP research subjects

Overlap: None

Title: Racial differences in financial impact of prostate cancer treatment and outcome (Mohler)
Time Commitments: 1.44 calendar months Y1, 1.8 calendar months Y2, 2.40 calendar months Y3
Supporting Agency: DoD
Name and address of the Funding Agency's Procuring Contracting/Grants Officer: Not assigned
Performance Period: 07/01/2017-06/31/2020
Level of funding: $445,328
Brief description of project's goals: Recurrence of advanced CaP during androgen deprivation therapy leads to a variety of new FDA-approved treatments, which may include immunotherapy, androgen metabolism inhibitors, small molecule anti-androgens, radio-pharmaceuticals, and docetaxel, cabazitaxel or cisplatin, all of which can extend survival but cause side effects and are expensive. Complexities of insurance coverage and Medicare reimbursement, a trend toward increasing co-pays for covered medications and differences in availability of financial assistance from pharmaceutical companies for new agents makes challenging the anticipation of the amount of financial burden posed by advanced CaP. If cured of localized CaP, costs may result from treatment of side effects, such as incontinence and impotence. CaP has been reported to produce the highest level of financial distress among 7 common cancers studied. Patients and their family members have suffered loss of their home, had to quit or decrease job hours or intensity, or forego expensive treatments shown to prolong life. AAs compared to Caucasian Americans (CAs) have been reported to benefit from higher religiosity and "caregiverness" but suffer from lower socioeconomic reserve and medical sophistication. The central hypothesis is that the financial impact of CaP treatment and oncologic outcome differs between AAs and CAs newly diagnosed with CaP.
List of specific aims:
1. Locate and contact PCaP research subjects to update CaP status, CaP treatments received and comorbidities, repeat the QoL assessments performed at baseline and follow-up, and administer new surveys on financial burdens and stress and caregiver QoL and support
2. Locate and contact PCaP research subjects' treating physicians to update treatments received and oncologic outcome data
3. Obtain and link vital status data and cause of death in PCaP research subjects
4. Examine the role financial burden and stress have on CaP survival and QoL and whether this relationship was modified by race.

Overlap: None

Active to Completed
Title: Prostate Cancer: Transition to Androgen Independence, Project 1: Interference with the Androgen Receptor and Its Ligands in Recurrent Prostate Cancer (French - PI)
Time Commitments: 2.04 calendar months

Supporting Agency: National Cancer Institute P01-CA77739
Name and address of the Funding Agency's Procuring Contracting/Grants Officer:
Mark Kramer, Administrative Director, UNC Lineberger Comprehensive Cancer Center Campus Box 7295
102 Mason Farm Road, Chapel Hill, NC 27599-7295, Phone: (919) 966-0233, Fax: (919) 966-3015, mkramer@med.unc.edu
Performance Period: 04/01/2005-03/31/2017 (NCE)
Level of Funding: $2,292,618
Brief description of project's goals: Renewal of a project that tests the hypothesis that recurrence of prostate cancer during androgen deprivation therapy can be prevented or delayed by preventing the accumulation of tissue androgens and/or inhibiting the androgen receptor.
List of specific aims:
1. Prevent the changes in androgen metabolism that provide AR ligand(s) in the immediate post-castration period
2. Degrade AR ligand(s) formed in the immediate post-castration period
3. Diminish or eliminate AR in the immediate post-castration period

Overlap: None

Title: Prostate Cancer: Transition to Androgen Independence, Core A: Administration (Mohler – PI)
Time Commitments: 1.16 calendar months
Supporting Agency: National Cancer Institute P01-CA77739
Name and address of the Funding Agency's Procuring Contracting/Grants Officer: Mark Kramer, Administrative Director, UNC Lineberger Comprehensive Cancer Center Campus Box 7295
102 Mason Farm Road, Chapel Hill, NC 27599-7295, Phone: (919) 966-0233, Fax: (919) 966-3015, mkramer@med.unc.edu
Performance Period: 04/01/2005-03/31/2017 (NCE)
Level of Funding: $519,640
Brief description of project's goals: Renewal of an administrative core that provides the leadership for the overall Program Project in the daily execution of administrative matters common to the three projects and ImmunoAnalysis and Tumor Management Core B.
List of specific aims:
The objective of the Administration Core A is to provide leadership, direction and administrative services for the purposes of enhancing research productivity and maintaining a stimulating research environment conducive to study of prostate cancer biology. Administration Core A will foster exchange of ideas and promote collaboration through its interactions with the Project Leaders and research groups. A major effort will be to encourage and facilitate collaboration in translational research among investigators within the Program Project and other investigators within or outside UNC-Lineberger Comprehensive Cancer and Roswell Park Cancer Institute. Administration Core A will have direct responsibility for organization and facilitation of the monthly research conferences and annual review of the Program Project by the 5 external consultants. Administration Core A will monitor activities of ImmunoAnalysis and Research Specimen Management Core B, in particular, and the entire program, in general, to improve the efficiency and effectiveness of the entire program.
Overlap: None

Title: Prostate Cancer: Transition to Androgen Independence, Core B: ImmunoAnalysis and Tumor Management (French – PI)
Time Commitments: 0.48 calendar months
Supporting Agency: National Cancer Institute P01-CA77739
Name and address of the Funding Agency's Procuring Contracting/Grants Officer:
Mark Kramer, Administrative Director, UNC Lineberger Comprehensive Cancer Center Campus Box 7295
102 Mason Farm Road, Chapel Hill, NC 27599-7295, Phone: (919) 966-0233, Fax: (919) 966-3015, mkramer@med.unc.edu
Performance Period: 04/01/2005-03/31/2017 (NCE)
Level of Funding: $903,203

Brief description of project's goals: Renewal of a core that serves two primary functions to the three projects: Core B is involved in all aspects of clinical specimen and prostate cancer xenograft management and Core B processes and stores the invaluable prostate biopsy specimens obtained from men with advanced prostate cancer prior to and at regular intervals after beginning androgen deprivation therapy.

List of specific aims:

The ImmunoAnalysis and Research Specimen Management Core B will provide 3 primary services to the Program Project.

1. Core B will provide high quality, reliable and cost-effective technical services to participants of the Program Project for immunohistochemistry and quantitative image analysis.
2. Core B will manage the research specimens critical to the conduct of the research proposed by the Program Project.
3. Core B will provide expertise in biostatistics and genitourinary pathology.

Overlap: None

Title: Diet changes among prostate cancer patients under expectant management (Marshall - PI)
Time Commitments: 0.60 calendar months
Supporting Agency: National Cancer Institute
Name and address of the Funding Agency's Procuring Contracting/Grants Officer: Program Official: Howard L. Parnes, Email: hp24c@nih.gov Phone: 301-594-0920 Fax: 301-435-1564
Performance Period: 09/28/2009-01/31/2016
Level of Funding: $55,818
Brief description of project's goals: The focus of this study is to assess whether a diet emphasizing plant consumption decreases the probability that low grade, low-volume prostate cancer (LGLV)in expectant management(EM)patients progresses to a more aggressive form of cancer that merits active treatment. The intervention will be conducted through one of the leading cooperative oncology research groups: Cancer and Leukemia Group B (CALGB).

List of specific aims:

1. Assess the effect of a telephone-based dietary intervention on PSA, PSA doubling time, Gleason score and tumor extension in LGLV prostate cancer patients treated with EM.
2. Assess the effect of a telephone-based dietary intervention on treatment seeking, anxiety and coronary heart disease in prostate cancer patients treated with EM.

Overlap: None

Title: Defining intra- and intertumoral genomic heterogeneity in prostate cancer (Mohler - PI)
Time Commitments: 0.60 calendar months
Supporting Agency: Roswell Park Alliance Foundation
Name and address of the Funding Agency's Procuring Contracting/Grants Officer: Judith Epstein, Director Grants & Foundation Office, Elm & Carlton Streets, Research Studies Center Room 234, Buffalo, NY 14203, Judith.Epstein@RoswellPark.org
Performance Period: 12/10/2013-12/31/2015
Level of funding: $92,384
Brief description of project's goals:

Intra- and inter-tumoral CaP genomic heterogeneity necessitates extensive sampling of a radical prostatectomy specimen.

List of specific aims:

1. Determine intra- and inter-tumoral heterogeneity in CaP's mutational landscape using whole exome sequencing to determine heterogeneity within and among CaP foci derived from radical prostatectomy specimens from patients with high-risk disease who are expected to develop metastatic disease and require ADT
2. Define intra- and inter-tumoral CaP heterogeneity in structural gene rearrangement and gene expression patterns using RNA-Seq and RNA derived from the same CaP samples used in Aim 1

Overlap: None

Title: Deprive prostate cancer of DHEAS to prevent castration-recurrent prostate cancer (Wu – PI)
Time Commitments: 0.12 calendar months
Supporting Agency: NIH/NCI 1R21CA191895-01
Name and address of the Funding Agency's Procuring Contracting/Grants Officer: Viviana Knowles, 9609 Medical Center Drive, West Tower, Bethesda, MD 20892, phone: 240-276-5157, viviana.knowles@nih.gov
Performance Period: 09/17/2014-08/31/2017 (NCE)
Level of Funding: $419,884
Brief description of project's goals: This research seeks to address the racial differences in prostate cancer aggressiveness from a biological perspective.
List of specific aims:

1. Characterize the expression of STS and potential STS regulators in CRPC
2. Evaluate the value of targeting DHEAS usage by prostate cancer cells to prevent post-castration tumor growth
3. Identify DHEAS uptake mechanisms

Overlap: None

Watt, D.S.

Pending to Active
Title: A Small-Molecule Inhibitor of the Terminal Steps for Intracrine Androgen Synthesis in Advanced Prostate Cancer (Subcontract PI: Watt)
Time Commitments: 0.60 calendar months
Supporting Agency: NCI-1R21CA205108-01
Name and address of the Funding Agency's Procuring Contracting/Grants Officer: Nicole Franklin, Grants Management Specialist, National Cancer Institute, 9609 Medical Center Drive, West Tower, Room 2W556, Bethesda, MD 20892 (regular mail), Phone: 240-276-5210, Email: nicole.franklin@nih.gov
Performance Period: 04/10/2016-04/09/2018
Level of Funding: $ 97,187 (subcontract only)
Brief description of project's goals: This research seeks to explore if a small-molecule inhibitor of the catalytic site shared by the five 3α−oxidoreductases will decrease T and DHT metabolism through the frontdoor and backdoor pathways.
List of specific aims:

4. Identify a candidate inhibitor against the catalytic site shared by the five 3α−oxidoreductases
5. Synthesize and test re-designed candidate inhibitors and conduct PK/PD and toxicity studies to produce a lead compound inhibitor of the five 3α−oxidoreductases
6. Determine whether the inhibitor of the 3α−oxidoreductases decreases tissue T and DHT levels and impairs CRPC growth

Overlap: None

Active to Completed
Title: KLF4 as a novel biomarker and tumor suppressor in lung cancer (PI: C. Liu, co-PI: D. Watt)
Time commitment: 0.12 calendar months
Supporting Agency: Kentucky Lung Cancer Research Program
Name and address of the Funding Agency's Procuring Contracting/Grants Officer: Rogers, Jennifer F., Markey Cancer Center, University of Kentucky, 800 Rose Street, Lexington, KY 40536 telephone: 859-323-8775; email: jen.rogers@uky.edu.
Performance Period: 07/01/2015-06/30/2017
Level of Funding: $8,000 per year in direct costs for Watt

Brief description of project's goals: The objective is to perform a canse-control study, develop a specimen repository and develop a new HDAC inhibitors for the treatment of lung cancer.
List of specific aims:
1. Conduct a case-control study of lung cancer and matched controls in the 5th Congressional District of Kentucky to compare rates of moderate to high arsenic in lung cancer cases and controls (primary endpoint).
2. Create a biospecimen repository by collecting, annotating and archiving biologic and environmental samples from these subjects or their residences for analysis of DNA repair markers and, in the future, markers of oxidative stress and inflammation.
3. Fund four pilot projects including one on the development of novel HDAC inhibitors.
Overlap: None

Bies, R.R.

Attwood, K.A.

Pending to Active
Title: Assessing the impact of differing pharmacy tobacco retail displays on smokers awareness, perceptions, and intentions to quit (5 R21 CA198824-02)
Time Commitments: 0.12 calendar (PI-Bansal Travers)
Supporting Agency: NCI/NIH
Grants Officer: Phone: Annette Kaufman; Annette.kaufman@nih.gov; (240) 276-6706
Performance Period: 6/1/16-5/31/18
Level of Funding: $416,535
Brief description of project's goals: The goal of this timely project is to take advantage of the ongoing natural experiment in the three largest U.S. pharmacy chains to better understand consumer perceptions of differences in point-of-sale advertising for using and quitting tobacco, particularly how it is received, understood, and acted on by young adult cigarette smokers.
List of specific aims:
1) To determine consumer attention to current point-of-sale retail displays, the factors associated with different amounts and areas of attention, and whether attention to these displays influences consumer perceptions of the appeal and perceived relative risks of smoking cigarettes.
2) To determine consumer attention to current smoking cessation messages at point-of-sale retail displays, the factors associated with different amounts and areas of attention, and whether attention to these displays influences consumer perceptions of the perceived benefits of quitting.
3) To determine changes in quit intentions as a function of differences between pharmacy PoS retail displays.
4) To determine if consumer attention to cessation messages at the point-of-sale are associated with changes in intention to quit smoking.

Overlap: NONE

Title: Targeting ß-Adrenergic Signaling to Control GVH and GVL Responses (5 R21 CA202358-02)
Time Commitments: 0.30 calendar (PI-Cao)
Supporting Agency: NCI/NIH
Grants Officer: Karen Waddel Muszynski; Karen.muszynski2@nih.gov; Phone: (301) 846-1101
Performance Period: 07/15/16-06/30/18
Level of Funding: $435,234
Brief description of project's goals: Based on our recently published work, the goal of this study is to explore a new paradigm regarding β2-AR mediated stress response during alloHCT. Using established murine models, we have discovered that pharmacologic or physiologic manipulation of β2-AR signaling exhibits a significant impact on the outcome of alloHCT.
List of specific aims:

1) Examine norepinephrine blood levels and ßAR blocker or agonist usage in HCT patients as potential factors influencing clinical outcomes.
2) Evaluate the therapeutic potential of manipulating ßAR signaling to modulate GVH and GVT responses.
3) Study the cellular mechanisms by which ßAR-mediated stress signaling impacts GVH and GVT responses.

Overlap: NONE

Title: A Small-Molecule Inhibitor of the Terminal Steps for Intracrine Androgen Synthesis In Advanced Prostate Cancer (5 R21 CA205108-02)
Time Commitments: 0.30 calendar (PI-Mohler)
Supporting Agency: NCI/NIH
Grants Officer: Suresh Arya; suresh.arya@nih.gov; Phone: (240) 276-5906
Performance Period: 04/12/16-03/31/18
Level of Funding: $416,398
Brief description of project's goals: The central hypothesis is that a small-molecule inhibitor of the catalytic site shared by the five 3α-oxidoreductases will decrease T and DHT metabolism through the frontdoor and backdoor pathways.
List of specific aims:

1) Identify a candidate inhibitor against the catalytic site shared by the five 3α-oxidoreductases.
2) Synthesize and test re-designed candidate inhibitors and conduct PK/PD and toxicity studies to produce a lead compound inhibitor of the five 3α-oxidoreductases.
3) Determine whether the inhibitor of the 3α-oxidoreductases decreases tissue T and DHT levels and impairs CRPC growth.

Overlap: NONE

Title: Leveraging the methionine salvage pathway as a novel therapy for prostate cancer (5 R01 CA197996-02)
Time Commitments: 0.30 calendar (PI- Smiraglia)
Supporting Agency: NCI/NIH
Grants Officer: Elizabeth Woodhouse; Phone: (240) 276-6205; elizabeth.woodhouse@nih.gov
Performance Period: 05/01/2016-04/30/2021
Level of Funding: $1,928,005
Brief description of project's goals: The objective of the current proposal is to determine the therapeutic potential of polyamine catabolism upregulation methylthioadenosine phosphor-ylase inhibition, either alone or in combination, to enhance the extent and/or duration of clinical benefit of androgen deprivation therapy. The central hypothesis is that the MSP is critical to CaP due to high metabolic flux through polyamine biosynthesis, and that this dependence can be enhanced by increasing the activity of spermidine/spermine N1-acetyltransferase.
List of specific aims:

1) To determine mechanisms of action and synergistic potential of MSP inhibition and activation of polyamine catabolism in cell line models.
2) To measure efficacy of MSP inhibition and/or activation of polyamine catabolism to treat established androgen independent CaP in human cell line xenografts.
3) To measure drug efficacy to prevent castration recurrence in human xenograft and mouse models of progression to ADT-RCaP.

Overlap: NONE

Title: Prostate specific androgen transporters are the missing target for complete ADT (5 R01 CA193829-02)
Time Commitments: 0.30 calendar (PI- Smith)
Supporting Agency: NCI/NIH
Grants Officer: Neeraja Sathyamoorthy; neeraja.sathyamoorthy@nih.gov; Phone: (240) 276-6220
Performance Period: 12/09/2015-11/30/2020

Level of Funding: $2,193,750
Brief description of project's goals: This project will identify novel targets in prostate endothelial cells to provide a prostate-specific inhibition of uptake, metabolism and trans-cellular transport of the androgens from blood into the tissue, providing adjuvant therapies to make ADT durable/curative, minimize systemic side-effects, and improving therapeutic efficacy for use for treatment of organ-localized CaP.
List of specific aims:

1) Determine inter-patient variability in up-take and metabolism of circulating T and DHEA-S, expression profiles of genes associated with androgen uptake/metabolism in human pECs and CaP/pEpi cells, and the short-term effect of T-deprivation on these processes.
2) Define the molecular mechanisms that mediate uptake, trans-cellular transport and efflux of circulating androgens in human pECs and pEpi cells, and confirmed in pECs with CaP.
3) Determine whether interdiction of adrenal androgen usage by pEC and/or CaP/pEpi has the potential to enhance the effect of T-deprivation (ADT).

Overlap: NONE

Title: Genetic and Epigenetic Prostate Cancer Related Alterations in Early Onset Disease in African American Men (W81XWH-17-1-01-15)
Time Commitments: 0.60 calendar (PI- Woloszynska-Read)
Supporting Agency: DOD
Grants Officer: Department of Defense, USA Med Research ACQ Activity 820 Chandler St, Fort Detrick MD 21702-5014, Lymor Barnhard
Performance Period: 4/1/2017-3/31/2020
Level of Funding: $1,243,760
Brief description of project's goals: The objective of the proposal is to identify clinically relevant genomic and epigenomic events characteristic for prostate cancer in African American men and compare/contrast those with/to prostate cancer in European American men. These findings will be annotated with DNA methylation, gene expression, and demographic, environmental exposures, clinical, pathological and oncological outcomes.
List of specific aims:

1) Determine the relative frequency of genetic lesions found in PCa in AAs and EAs.
2) Determine novel, clinically relevant methylomic and transcriptomic differences in PCa from AAs and EAs.

Overlap: NONE

Active to Completed
Title: Deprive prostate cancer of DHEAS to prevent castration-recurrent prostate cancer (5 R21 CA191895-02)
Time Commitments: 0.30 calendar (PI-Wu)
Supporting Agency: NCI/NIH
Grants Officer: Neeraja Sathyamoorthy; neeraja.sathyamoorthy@nih.gov; Phone: (240) 276-6220
Performance Period: 09/17/14-08/31/17 (NCE)
Level of Funding: $446,950
Brief description of project's goals: The proposed studies are required to validate the concept that DHEAS is an important source of precursors for intracrine production of T and DHT by prostate cancer cells. In addition, the transporters, STS, and STS regulators provide potential targets for therapy.
List of specific aims:

1) Characterize the expression of STS and potential STS regulators in CRPC.
2) Evaluate the value of targeting DHEAS usage by prostate cancer cells to prevent post-castration tumor growth.
3) Identify DHEAS uptake mechanisms.

Overlap: NONE

Title: Multicenter phase 2 trial of nindetinib (BIBF 1120) in patients with carcinoid tumors (NCCN NINT 0016)
Time Commitments: 0.30 calendar (PI-Iyer)
Supporting Agency: NCCN
Grants Officer: Diane Paul, NCCN, 275 Commerce Drive, Suite 300, Fort Washington, PA, 19034, (215) 690-0232, paul@nccn.org
Performance Period: 11/25/14-11/24/15
Level of Funding: $480,611
Brief description of project's goals: We hypothesize that since fibroblast proliferation is a major driver of disease and clinical progression in non-pancreatic carcinoids that is shown in animal models to be driven by serotonin (5-HT) through FGFR2 (Hisaoka et al) that targeting angiogenesis and FGFR merits study in this tumor.
List of specific aims:

1) Targeting angiogenesis and the fibroblast growth factor pathway with nintedanib will result in clinical benefit measured as progression free survival (PFS) and radiographic response or stable disease in patients with progressing carcinoid tumors within the 12 months prior to study entry.
2) This therapy will be safe and tolerable in combination with octreotide. This will also lead to improved QOL measured using the Norfolk QOL-NET tool.
3) Using a previously developed PK/PD model, using decrease in circulating cytokines such as soluble vascular endothelial growth factor receptor (sVEGFR), VEGF, fibroblast growth factor (FGF) and FGFR by ELISA before and serially q12 week with steady state PK draw to correlate with drug level following start of therapy compared to pre therapy will correlate with clinical benefit and maybe a valuable biomarker.
4) Tumor expression of fibroblast growth factor receptor isoforms FGFR IIIb and IIIc, Ki-67 and microvessel density measured by immunohistochemistry (IHC) will correlate with clinical benefit.

Overlap: NONE

Title: Prosaposin: a novel biomarker of prostate cancer progression in African Americans (5 R01 MD005824-05)
Time Commitments: 0.30 calendar (PI- Koochekpour)
Supporting Agency: NIH
Grants Officer: Nishadi Rajapakse; chandima.rajapakse@nih.gov
Performance Period: 07/01/12-06/30/15
Level of Funding: $391,670
Brief description of project's goals: We hypothesized that PSAP contributes to PCa progression and has the characteristics of a novel biomarker discriminating the aggressive tumors from non-aggressive ones in African American patients.
List of specific aims:

1) Define the clinical significance of serum-PSAP as a marker of PCa progression or aggressiveness in African Americans.
2) Determine the association between tissue expression of PSAP and clinical and histopathological predictors or prognosticators of PCa progression or aggressiveness in African Americans.
3) Determine the association between PSAP and invasive and metastatic phenotypes in PSAP-overexpressed or -silenced African American PCa cells.

Overlap: NONE

Title: FACT as a Novel Marker and Target and Target of Aggressive Breast Cancer (CCR13264604)
Time Commitments: 0.60 calendar (PI-Gurova)
Supporting Agency: Susan G Komen National Foundation
Grants Officer: Nancy Martin; Phone: (972) 701-2085; fax: (972) 701-2121; nmartin@komen.org
Performance Period: 04/01/13-08/06/16

Level of Funding: $449,999
Brief description of project's goals: Our hypothesis is that we can measure FACT in BC to predict if a patient will develop metastatic disease and, therefore, requires additional treatment. We also propose that drug(s) which reduce or eliminate FACT would be effective in these types of patients and safe since FACT is not present in an adult organism (it is present only in so called "stem cells" of some organs and cells of embryos).
List of specific aims:

1) To confirm association of FACT expression with aggressive metastatic breast cancer.
2) To understand how FACT provides tumor cells with more aggressive features.
3) To define if artificial decrease in FACT activity or level would result in reduced tumor growth and loss of metastatic behavior of tumor cells in mouse models of BC.

Overlap: NONE

Title: Distinguishing Tumor- and Stromal- Mediated Mechanisms of Resistance and Rebound in Models of Metastatic Renal Cell Carcinoma (W81XWH-14-1-0210)
Time Commitments: 0.50 calendar (PI-Ebos)
Supporting Agency: DOD
Grants Officer: Wendy A. Baker, Contracting Officer; wendy.a.baker.civ@mail.mil; Phone: (301) 619-2034
Performance Period: 07/01/14-06/30/16
Level of Funding: $602,996
Brief description of project's goals: The purpose of the proposed studies is to investigate the contributions of stromal and tumor 'reactions' to antiangiogenic therapy in clinically-relevant metastatic models of RCC. The hypothesis guiding this research is that both tumor and host-stroma reactions collude to elicit metastatic cell behavior that drives resistance and rebound growth when therapy is halted.
List of specific aims:

1) To use an operative-metastatic RCC model to evaluate stromal host 'reactions' following therapy withdrawal in rebound and resistance 'reversibility'.
2) To identify whether tumor-stromal molecular gene signatures complement to activate pathways that promote drug-resistance and metastasis.
3) To assess the benefit of VEGF pathway inhibition in the neoadjuvant treatment setting.

Overlap: NONE

Title: Image-Guided Photodynamic Therapy of Lung Cancer (5 R21 CA176154-02)
Time Commitments: 2.50 calendar (PI-Nwogu)
Supporting Agency: NCI
Grants Officer: Anil Wali; anil.wali@nih.gov; Phone: (240) 276-6183
Performance Period: 08/01/14-07/31/16
Level of Funding: $466,950
Brief description of project's goals: Lung cancer is the most frequent cause of cancer death in both men and women in the United States and will account for about 27% of all estimated cancer deaths in 2013. This project seeks to study the ability of a novel compound to simultaneously image lung cancer using positron emission tomography (PET) and ablate it with photodynamic therapy (PDT).
List of specific aims:

1) Compare the effectiveness of 124I-PS2 and 18F-Fluorodeoxyglucose (FDG) in imaging of lung tumors and lymph node metastases using an orthotopic lung cancer model in SCID mice.
2) Compare the effectiveness of photodynamic therapy using PS2 and Porfimer Sodium (Photofrin®) in human NSCLC xenografts established subcutaneously in SCID mice.

Overlap: NONE

Title: Novel Mouse Models to Define Genetic Drivers of Aggressive Prostate Cancer (1R21 CA205627-01)
Time Commitments: 0.225 calendar (PI-Ellis)
Supporting Agency: NIH

Grants Officer: Grace Ault; grace.alt@nih.gov; Phone: (240) 276-6201
Performance Period: 04/15/16-01/31/17
Level of Funding: $471,625
Brief description of project's goals: Our principle objective is to characterize our genetically engineered mouse models to discover genetic switches which drive aggressive prostate cancer. Overall, our proposed studies will significantly impact prostate cancer research and how patients are clinically assessed to determine stratification of indolent from aggressive disease.
List of specific aims:

1) Specifically, aim 1 will determine if the retinoblastoma protein (Rb) is a suppressor of PCa metastasis.
2) Specific aim 2 will utilize a sleeping beauty mutagenesis screen to identify novel candidate genetic drivers of PCa metastasis.

Overlap: NONE

Title: Metabotropic Glutamate Receptor 1 in African American Prostate Cancer (5 R21 CA183892-02)
Time Commitments: 0.30 calendar (PI-Koochekpour)
Supporting Agency: NCI/NIH
Grants Officer: Elizabeth Woodhouse; elizabeth.woodhouse@nih.gov; Phone: (240) 276-6205
Performance Period: 04/01/14-03/31/17
Level of Funding: $406,247
Brief description of project's goals: Data generated from this exploratory study will define biological and/or clinicohistopathological significance or relevance of GRM1 expression in African American prostate cancer and may prove useful in discriminating clinically or biologically aggressive tumors from indolent (non-aggressive) tumors and minimizing prostate cancer disparity in African Americans.
List of specific aims:

1) Determine the association between tissue expression of GRM1 and clinicohistopathological predictors or prognosticators of prostate cancer progression or aggressiveness in African Americans.
2) Determine the association between GRM1 expression levels and invasive and metastatic phenotypes in African American prostate cancer cells.

Overlap: NONE

Title: Therapeutic Efficacy of Riluzole in Prostate Cancer (5 R21 CA181152-02)
Time Commitments: 0.30 calendar (PI-Koochekpour)
Supporting Agency: NCI/NIH
Grants Officer: Michael Alley; michael.alley@nih.gov; Phone: (301) 624-1246
Performance Period: 07/01/14-06/31/17
Level of Funding: $406,247
Brief description of project's goals: This is a translational prostate cancer research aimed at determining the effect of glutamate receptor antagonist on tumor growth and metastatic ability, fatty acid synthase (FAS) expression and apoptotic markers in prostate cancer. This study will investigate the underlying mechanisms by which glutamate receptor antagonist down regulates FAS expression in prostate cancer cell lines.
List of specific aims:

1) Determine the therapeutic efficacy of Riluzole in in-vivo tumorigenesis assays.
2) Determine the association between Riluzole treatment and androgen receptor expression in tumor xenografts and prostate cancer cell lines.

Overlap: NONE

Fiandalo, M.V.

Pending to Active
Title: A Small-Molecule Inhibitor of the Terminal Steps for Intracrine Androgen Synthesis in Advanced Prostate Cancer (Mohler)

Time Commitments: 7.20 calendar months (no salary requested)
Supporting Agency: NCI-1R21CA205108-01
Name and address of the Funding Agency's Procuring Contracting/Grants Officer: Nicole Franklin, Grants Management Specialist, National Cancer Institute, 9609 Medical Center Drive, West Tower, Room 2W556, Bethesda, MD 20892 (regular mail), Phone: 240-276-5210, Email: nicole.franklin@nih.gov
Performance Period: 04/10/2016-04/09/2018
Level of Funding: $ 416,398
Brief description of project's goals: This research seeks to explore if a small-molecule inhibitor of the catalytic site shared by the five 3α−oxidoreductases will decrease T and DHT metabolism through the frontdoor and backdoor pathways.
List of specific aims:

7. Identify a candidate inhibitor against the catalytic site shared by the five 3α−oxidoreductases
8. Synthesize and test re-designed candidate inhibitors and conduct PK/PD and toxicity studies to produce a lead compound inhibitor of the five 3α−oxidoreductases
9. Determine whether the inhibitor of the 3α−oxidoreductases decreases tissue T and DHT levels and impairs CRPC growth

Overlap: None

Active to Completed
Title: 4 Birds, 1 Stone to Inhibit 5androstane-3α,17β-diol Conversion to DHT (Fiandalo - PI)
Time Commitments: 12.00 calendar months
Supporting Agency: DoD Prostate Cancer Postdoctoral Training Award W81XWH-14-PCRP-PTA
Name and address of the Funding Agency's Procuring Contracting/Grants Officer: Not assigned yet
Performance Period: 07/01/2015-06/30/2017
Level of funding: $123,642
Brief description of project's goals: The central hypothesis of the proposed studies is that inhibition of the catalytic amino acid residues common to the 4 3α-oxidoreductases will block the conversion of androstanediol to DHT.
List of specific aims:
Aim 1. Determine which of the 4 3α-oxidoreductases are responsible for conversion of androstanediol to DHT and identify the key catalytic amino acids that are critical for enzyme activity
Aim 2. Discover small molecules that inhibit the critical catalytic sites common to the 4 3α-oxidoreductases
Aim.3. Determine if inhibition of specific 3α-oxidoreductase enzymes immediately proximate to intracrine synthesis of DHT blocks the growth of CR-CaP
Overlap: None

Wilton, J. H.

Pending to Active
Title: Prostate-Specific Androgen Transporters are the Missing Target for Complete ADT (Smith/Wu)
Time Commitments: 0.30 calendar months
Supporting Agency: NIH (1R01CA193829-01A1)
Name and address of the Funding Agency's Procuring Contracting/Grants Officer: Viviana Knowles, Grants Management Specialist, 9609 Medical Center Drive, West Tower, Bethesda, MD 20892, phone: 240-765-5157, viviana.knowles@nih.gov
Performance Period: 12/09/2015-11/30/2020
Level of Funding: $1,961,530
Brief description of project's goals: This research seeks to determine if interdiction of prostate endothelial cell-specific uptake and trans-cellular transport of circulating adrenal androgens through the blood-prostate barrier, will complement ADT to provide a curative/durable therapy for organ-localized and advanced prostate cancer.

List of specific aims:
Aim 1. Determine inter-patient variability in up-take and metabolism of circulating T and DHEA-S, expression profiles of genes associated with androgen uptake/metabolism in human pECs and CaP/pEpi cells, and the short-term effect of T-deprivation on these processes
Aim 2. Define the molecular mechanisms that mediate uptake, trans-cellular transport and efflux of circulating androgens in human pECs and pEpi cells, and confirmed in pECs with CaP
Aim 3. Determine whether interdiction of adrenal androgen usage by pEC and/or CaP/pEpi has the potential to enhance the effect of T-deprivation (ADT)
Overlap: None

Title: A Small-Molecule Inhibitor of the Terminal Steps for Intracrine Androgen Synthesis in Advanced Prostate Cancer (Mohler)
Time Commitments: no salary requested; included as key personnel
Supporting Agency: NCI- 1R21CA205108-01
Name and address of the Funding Agency's Procuring Contracting/Grants Officer: Nicole Franklin, Grants Management Specialist, National Cancer Institute, 9609 Medical Center Drive, West Tower, Room 2W556, Bethesda, MD 20892 (regular mail), Phone: 240-276-5210, Email: nicole.franklin@nih.gov
Performance Period: 04/10/2016-04/09/2018
Level of Funding: $ 416,398
Brief description of project's goals: This research seeks to explore if a small-molecule inhibitor of the catalytic site shared by the five 3α−oxidoreductases will decrease T and DHT metabolism through the frontdoor and backdoor pathways.
List of specific aims:
Aim 1. Identify a candidate inhibitor against the catalytic site shared by the five 3α−oxidoreductases
Aim 2. Synthesize and test re-designed candidate inhibitors and conduct PK/PD and toxicity studies to produce a lead compound inhibitor of the five 3α−oxidoreductases
Aim 3. Determine whether the inhibitor of the 3α−oxidoreductases decreases tissue T and DHT levels and impairs CRPC growth
Overlap: None

Active to Completed
Title: Deprive prostate cancer of DHEAS to prevent castration-recurrent prostate cancer (Wu)
Time Commitments: 0.60 calendar months
Supporting Agency: NIH/NCI (1R21CA191895-01)
Name and address of the Funding Agency's Procuring Contracting/Grants Officer: Viviana Knowles, 9609 Medical Center Drive, West Tower, Bethesda, MD 20892, phone: 240-276-5157, viviana.knowles@nih.gov
Performance Period: 09/17/2014-08/31/2016
Level of Funding: $419,884
Brief description of project's goals: This research seeks to address the racial differences in prostate cancer aggressiveness from a biological perspective.
List of specific aims:
Aim 1. Characterize the expression of STS and potential STS regulators in CRPC
Aim 2. Evaluate the value of targeting DHEAS usage by prostate cancer cells to prevent post-castration tumor growth
Aim 3. Identify DHEAS uptake mechanisms
Overlap: None

Nothing to report for Moser, M.

What other organizations were involved as partners?

J. Mohler, Project Director/Principal Investigator, RPCI: Nothing to report

D. Watt, Collaborating/Partnering PI, University of Kentucky:

Organization name: Institute of Bioorganic Chemistry and Petrochemistry, National Academy of Science of Ukraine
Location of organization: Kyiv 02094, Ukraine
Partner's contribution to the project: AV Popova and MS Frasinyuk synthesized, characterized and provided at no cost various compounds described in papers in Appendix.

Organization name: National University of Food Technologies
Location of organization: Kyiv, 01601, Ukraine
Partner's contribution to the project: SP Bondarenko synthesized, characterized and provided at no cost various compounds described in papers in Appendix.

R. Bies, Collaborating/Partnering PI, University at Buffalo: Nothing to report

8. SPECIAL REPORTING REQUIREMENTS

COLLABORATIVE AWARDS: For collaborative awards, independent reports are required from BOTH the Initiating PI and the Collaborating/Partnering PI. A duplicative report is acceptable; however, tasks shall be clearly marked with the responsible PI and research site. A report shall be submitted to **https://ers.amedd.army.mil** for each unique award.

QUAD CHARTS: If applicable, the Quad Chart (available on https://www.usamraa.army.mil) should be updated and submitted with attachments.

DoD Partnering PI Award: W81XWH-16-1-0635 (Grant Log# PC150326P2)
Title: Understanding the Relative Contributions of and Critical Enzymes for the Three Pathways for Intracrine Metabolism of Testicular Androgens in Advanced Prostate Cancer

9. APPENDICES:

Attach all appendices that contain information that supplements, clarifies or supports the text. Examples include original copies of journal articles, reprints of manuscripts and abstracts, a curriculum vitae, patent applications, study questionnaires, and surveys, etc.

J. Mohler, Project Director/Principal Investigator, RPCI: Nothing to report

D. Watt, Collaborating/Partnering PI, University of Kentucky: We have attached copies of publications described above.

R. Bies, Collaborating/Partnering PI, University at Buffalo: Nothing to report

1. Ryan CJ, Shah S, Efstathiou E et al. Phase II study of abiraterone acetate in chemotherapy-naive metastatic castration-resistant prostate cancer displaying bone flare discordant with serologic response. Clin Cancer Res 2011; 17: 4854-4861.

2. Ryan CJ, Smith MR, Fong L et al. Phase I clinical trial of the CYP17 inhibitor abiraterone acetate demonstrating clinical activity in patients with castration-resistant prostate cancer who received prior ketoconazole therapy. J Clin Oncol 2010; 28: 1481-1488.
3. Scher HI, Beer TM, Higano CS et al. Antitumour activity of MDV3100 in castration-resistant prostate cancer: a phase 1-2 study. Lancet 2010; 375: 1437-1446.
4. Scher HI, Fizazi K, Saad F et al. Effect of MDV3100, an androgen receptor signaling inhibitor (ARSI), on overall survivial in patients with prostate cancer postdocetaxel: Results from the phase III AFFIRM study. J Clin Oncol 2012; 30.
5. Small EJ, Schellhammer PF, Higano CS et al. Placebo-controlled phase III trial of immunologic therapy with sipuleucel-T (APC8015) in patients with metastatic, asymptomatic hormone refractory prostate cancer. J Clin Oncol 2006; 24: 3089-3094.
6. Chang KH, Li R, Papari-Zareei M et al. Dihydrotestosterone synthesis bypasses testosterone to drive castration-resistant prostate cancer. Proc Natl Acad Sci U S A 2011; 108: 13728-13733.
7. Chang KH, Li R, Kuri B et al. A gain-of-function mutation in DHT synthesis in castration-resistant prostate cancer. Cell 2013; 154: 1074-1084.
8. Penning T. Androgen biosynthesis in castration resistant prostate cancer. Endocr Relat Cancer 2014.
9. Chang KH, Sharifi N. Prostate cancer-from steroid transformations to clinical translation. Nat Rev Urol 2012; 9: 721-724.
10. Godoy A, Kawinski E, Li Y et al. 5alpha-reductase type 3 expression in human benign and malignant tissues: a comparative analysis during prostate cancer progression. Prostate 2011; 71: 1033-1046.
11. Titus MA, Li Y, Kozyreva OG et al. 5alpha-reductase type 3 enzyme in benign and malignant prostate. Prostate 2014; 74: 235-249.
12. Shah S, Trump D, Sartor O et al. Phase II study of dutasteride for recurrent prostate cancer during androgen deprivation therapy. J Urol 2009; 181: 621-626.
13. Fleshner NE, Trachtenberg J. Combination finasteride and flutamide in advanced carcinoma of the prostate: effective therapy with minimal side effects. J Urol 1995; 154: 1642-1645; discussion 1645-1646.
14. Leibowitz RL, Tucker SJ. Treatment of localized prostate cancer with intermittent triple androgen blockade: preliminary results in 110 consecutive patients. Oncologist 2001; 6: 177-182.
15. Dutkiewicz SA. Comparison of maximal and more maximal intermittent androgen blockade during 5-year treatment of advanced prostate cancer T3NxMx-1. Int Urol Nephrol 2012; 44: 487-492.
16. Tay MH, Kaufman DS, Regan MM et al. Finasteride and bicalutamide as primary hormonal therapy in patients with advanced adenocarcinoma of the prostate. Ann Oncol 2004; 15: 974-978.
17. Ornstein DK, Rao GS, Johnson B et al. Combined finasteride and flutamide therapy in men with advanced prostate cancer. Urology 1996; 48: 901-905.
18. Fiandalo MV, Wilton J, Mohler JL. Roles for the backdoor pathway of androgen metabolism in prostate cancer response to castration and drug treatment. Int J Biol Sci 2014; 10: 596-601.
19. Cai C, Chen S, Ng P et al. Intratumoral de novo steroid synthesis activates androgen receptor in castration-resistant prostate cancer and is upregulated by treatment with CYP17A1 inhibitors. Cancer Res 2011; 71: 6503-6513.
20. Mostaghel EA, Marck BT, Plymate SR et al. Resistance to CYP17A1 inhibition with abiraterone in castration-resistant prostate cancer: induction of steroidogenesis and androgen receptor splice variants. Clin Cancer Res 2011; 17: 5913-5925.
21. Cai C, Chen S, Ng P et al. Intratumoral de novo steroid synthesis activates androgen receptor in castration-resistant prostate cancer and is upregulated by treatment with CYP17A1 inhibitors. Cancer Res 2011; 71: 6503-6513.
22. Loriot Y, Fizazi K, Jones RJ et al. Safety, tolerability and anti-tumour activity of the androgen biosynthesis inhibitor ASP9521 in patients with metastatic castration-resistant prostate cancer: multi-centre phase I/II study. Invest New Drugs 2014.
23. Mohler JL, Titus MA, Bai S et al. Activation of the androgen receptor by intratumoral bioconversion of androstanediol to dihydrotestosterone in prostate cancer. Cancer Res 2011; 71: 1486-1496.

ChemPubSoc Europe

DOI: 10.1002/cmdc.201600008

CHEMMEDCHEM Full Papers

Antineoplastic Isoflavonoids Derived from Intermediate *ortho*-Quinone Methides Generated from Mannich Bases

Mykhaylo S. Frasinyuk,*[a, b, c] Galyna P. Mrug,[c] Svitlana P. Bondarenko,[d] Volodymyr P. Khilya,[d] Vitaliy M. Sviripa,[a, b] Oleksandr A. Syrotchuk,[e] Wen Zhang,[a, f] Xianfeng Cai,[a, f] Michael V. Fiandalo,[g] James L. Mohler,[g] Chunming Liu,[a, f] and David S. Watt*[a, b, f]

The regioselective condensations of various 7-hydroxyisoflavonoids with bis(*N*,*N*-dimethylamino)methane in a Mannich reaction provided C-8 *N*,*N*-dimethylaminomethyl-substituted isoflavonoids in good yield. Similar condensations of 7-hydroxy-8-methylisoflavonoids led to the C-6-substituted analogs. Thermal eliminations of dimethylamine from these C-6 or C-8 *N*,*N*-dimethylaminomethyl-substituted isoflavonoids generated *ortho*-quinone methide intermediates within isoflavonoid frameworks for the first time. Despite other potential competing outcomes, these *ortho*-quinone methide intermediates trapped dienophiles including 2,3-dihydrofuran, 3,4-dihydro-2*H*-pyran, 3-(*N*,*N*-dimethylamino)-5,5-dimethyl-2-cyclohexen-1-one, 1-morpholinocyclopentene, and 1-morpholinocyclohexene to give various inverse electron-demand Diels–Alder adducts. Several adducts derived from 8-*N*,*N*-dimethylaminomethyl-substituted isoflavonoids displayed good activity in the 1–10 μM concentration range in an in vitro proliferation assay using the PC-3 prostate cancer cell line.

Introduction

Androgen-deprivation therapy produces temporary palliation but fails to cure advanced prostate cancer in which tissue levels of testosterone and 5α-dihydrotestosterone are sufficient to activate the androgen receptor.[1] Although the steroidal drug, abiraterone, interferes with the metabolism of adrenal androgens to testosterone and 5α-dihydrotestosterone by inhibiting cytochrome 17A1 (CYP17A1),[2] its effects are only short-lived when used after the failure of androgen-deprivation therapy.[3] Prostate cancer remains the second leading cause of cancer-related mortality in men,[4] and new therapies focused on the selective inhibition of enzymes participating in the backdoor pathway[5] to dihydrotestosterone from 4-androstene-3,17-dione remain a worthy goal for enhancing the extent or duration of response to androgen-deprivation therapy.

Isoflavones, particularly daidzein (**1a**) and genistein (**1b**) (Figure 1), attracted interest as potential agents for the treatment of prostate cancer,[6] but these natural products and their metabolites have a spectrum biological effects, including those that act on androgen receptor expression and enzymes associated with androgen metabolism.[7] We selected 7-hydroxyisoflavones as candidates as part of a program to develop antineoplastic agents against *selective* biological targets. Prior work in our laboratories demonstrated that the removal or transformation of hydroxy groups from natural products and replacement

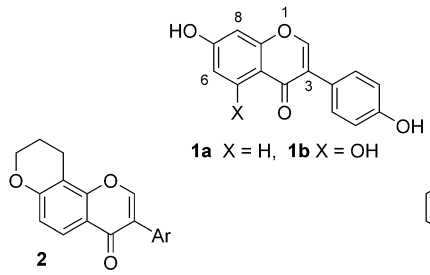

Figure 1. Naturally occurring isoflavones daidzein (**1a**) and genistein (**1b**), and synthetic isoflavonoids **2** and **3**.

[a] *Dr. M. S. Frasinyuk, Dr. V. M. Sviripa, W. Zhang, Dr. X. Cai, Prof. C. Liu, Prof. D. S. Watt*
Department of Molecular and Cellular Biochemistry, College of Medicine
University of Kentucky, Lexington, KY 40536-0596 (USA)
E-mail: dwatt@uky.edu

[b] *Dr. M. S. Frasinyuk, Dr. V. M. Sviripa, Prof. D. S. Watt*
Center for Pharmaceutical Research and Innovation, College of Pharmacy
University of Kentucky, Lexington, KY 40536-0509 (USA)

[c] *Dr. M. S. Frasinyuk, Dr. G. P. Mrug*
Department of Chemistry of Bioactive Nitrogen-Containing Heterocyclic Bases, Institute of Bioorganic Chemistry and Petrochemistry
National Academy of Science of Ukraine, Kyiv 02094 (Ukraine)
E-mail: mykhaylo.frasinyuk@ukr.net

[d] *Dr. S. P. Bondarenko, Prof. V. P. Khilya*
Department of Chemistry
Taras Shevchenko Kyiv National University, Kyiv 01601 (Ukraine)

[e] *O. A. Syrotchuk*
Central Laboratory for Quality Control of Medicines and Medical Products
Kyiv 04053 (Ukraine)

[f] *W. Zhang, Dr. X. Cai, Prof. C. Liu, Prof. D. S. Watt*
Lucille Parker Markey Cancer Center
University of Kentucky, Lexington, KY 40536-0093 (USA)

[g] *Dr. M. V. Fiandalo, Prof. J. L. Mohler*
Department of Urology
Roswell Park Cancer Institute, Buffalo, NY 14263 (USA)

Supporting information for this article can be found under http://dx.doi.org/10.1002/cmdc.201600008.

of these groups with functional groups capable of hydrogen bonding and van der Waals interactions led to new agents with singular and important biological targets.[8]

Results and Discussion

The removal of hydroxy groups found frequently in naturally occurring isoflavones limited competitive redox processes as well as phase II metabolism (e.g., sulfation or glucuronidation) and provided an opportunity to acquire a pharmacophore with a singular mechanism of action. For example, the elimination of hydroxy groups in resveratrol, a hackneyed natural product with a multiplicity of biological effects, led to the fluorinated stilbenes.[8a,9] These antineoplastic agents act as epigenetic regulators of a single molecular target, the catalytic subunit of methionine adenosyltransferase-2. Additional modifications of the stilbene pharmacophore led to the fluorinated 3-arylquinolines[8b] as antineoplastic agents that bind uniquely to the intermediate filament protein, vimentin, and promote the secretion of the natural tumor suppressor, Prostate apoptosis response-4 protein (Par-4). In the same fashion, we initiated a structure–activity study on semisynthetic isoflavones using an in vitro proliferation assay based on the PC-3 human prostate cancer cell line to interrogate structures, identify potent analogs and provide a framework for biotinylation and target identification. This decision distanced us from the debate surrounding the naturally occurring isoflavone and allowed us to focus on developing synthetic isoflavonoids with substituent patterns not seen in natural products. As part of this effort to identify enzyme inhibitors within new, heterocyclic platforms, we explored Diels–Alder cycloadditions involving the chromone core, which appears in isoflavones. Although chromones were used previously in Diels–Alder reactions with various dienes, invariably successful Diels–Alder reactions required the presence of electron-withdrawing carbonyl- or cyano- group in position 3 of chromone ring.[10]

This limitation would appear to exclude the use of semisynthetic flavonoids or isoflavonoids in Diels–Alder reactions because they possess electron-donating phenyl substituent at positions 2 or 3, respectively. The in situ generation of *ortho*-quinone methides from phenolic Mannich bases,[11] hydroxybenzyl alcohol derivatives,[12] and oxygen-containing heterocycles[13] provided chromane derivatives in hetero-Diels–Alder reaction, but the generation of *ortho*-quinone methides in a chromone platform was without precedent. It was unclear at the outset of this work if the reactive 1,4-benzopyrone functionality in isoflavonoids would accommodate a transitory *ortho*-quinone methides and trap dieneophiles without competitive, interfering reactions. Specifically, we wanted to synthesize substituted 3-aryl-9,10-dihydropyrano[2,3-f]chromen-4(8H)-ones **2** and 3-aryl-3,4-dihydro-2H,6H-pyrano[3,2 g]chromen-6-ones **3** (Figure 1).[14]

To accomplish this aim, aminomethyl-, hydroxymethyl-, and methoxymethyl derivatives of 7-hydroxyflavones were tested as precursors to *ortho*-quinone methides and as dienes in an inverse electron-demand Diels–Alder addition. Synthesis of these precursors involved the application of the Mannich reaction to 7-hydroxyisoflavonoids **4** with bis(*N*,*N*-dimethylamino)-methane in isopropanol at reflux to provide regioselectively the C-8 substituted *N*,*N*-dimethylaminomethyl analogs **5** (Scheme 1) in good yields.[15] The 7-hydroxy-8-methyisoflavonoids **6** gave, as expected, the isomeric C-6 analogs **7**.

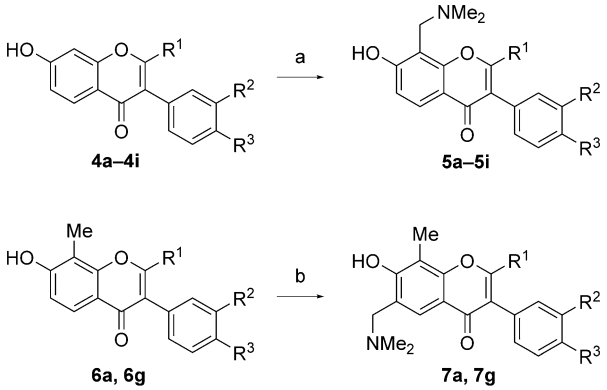

Scheme 1. Regioselective modification of 7-hydroxyisoflavones **4** and 7-hydroxy-8-methylisoflavones **6**. *Reagents and conditions*: a) $CH_2(NMe)_2$, *i*PrOH, 80 °C, 2–4 h, 68–91%; b) $CH_2(NMe)_2$, dioxane, 100 °C, 16 h, 72–99%.

Heating the *N*,*N*-dimethylaminomethyl-substituted isoflavonoids **5** generated the intermediate *ortho*-quinone methides **8** (Scheme 2) that trapped various electron-rich dienophiles including 2,3-dihydrofuran, 3,4-dihydro-2*H*-pyran, 3-(*N*,*N*-dimethylamino)-5,5-dimethyl-2-cyclohexen-1-one, 1-morpholino-cyclopentene, and 1-morpholinocyclohexene. These reactions led to Diels–Alder adducts **11**–**15** (Scheme 2) in yields that varied with dienophile reactivity (Table 1). Table 1 summarizes representative combinations of dienophiles and *N*,*N*-dimethylamino-substituted isoflavonoids that led to biologically active adducts. Among the various dienophiles, dihydrofuran and dihydropyran produced the most biologically active compounds, and consequently, these dienophiles were explored in the most detail. The few adducts synthesized from other dienophiles, such as the enamines, had low activity, or in the case of 3-(*N*-*N*-dimethylamino)-5,5-dimethyl-2-cyclohexen-1-one, produced very insoluble adducts that could not be evaluated in a biological assay.

The further transformation of hemi-aminals **10** that were intermediates in some cases depended on substituents (Scheme 2). The presence of an electron-withdrawing carbonyl group led to dimethylamine elimination (path A) with formation of **13**. In cases of 1-morpholinocyclopentene or 1-morpholinocyclohexene, the hydrolysis of hemi-aminals **10** (path B) led to 2-substituted ketones or tautomeric hemi-ketals **14** or **15**. The yields were low (< 50%) using either 2,3-dihydrofuran or 3,4-dihydro-2*H*-pyran due to dimerization and polymerization reactions, but were acceptable using other dienophiles. Similar reactions with dienophiles were observed for the intermediate *ortho*-quinone methides **9** derived from 6-dimethylaminomethyl isoflavones **7**. In these cases, linear 6a,7,8,9a-tetrahydro-4*H*,6*H*-furo[2,3-*b*]pyrano[3,2 *g*]chromen-4-ones **16** and 6,8,9,10-tetrahydro-4*H*,7*H*-pyrano[3,2-*b*]xanthene-4,7-dione **17** were

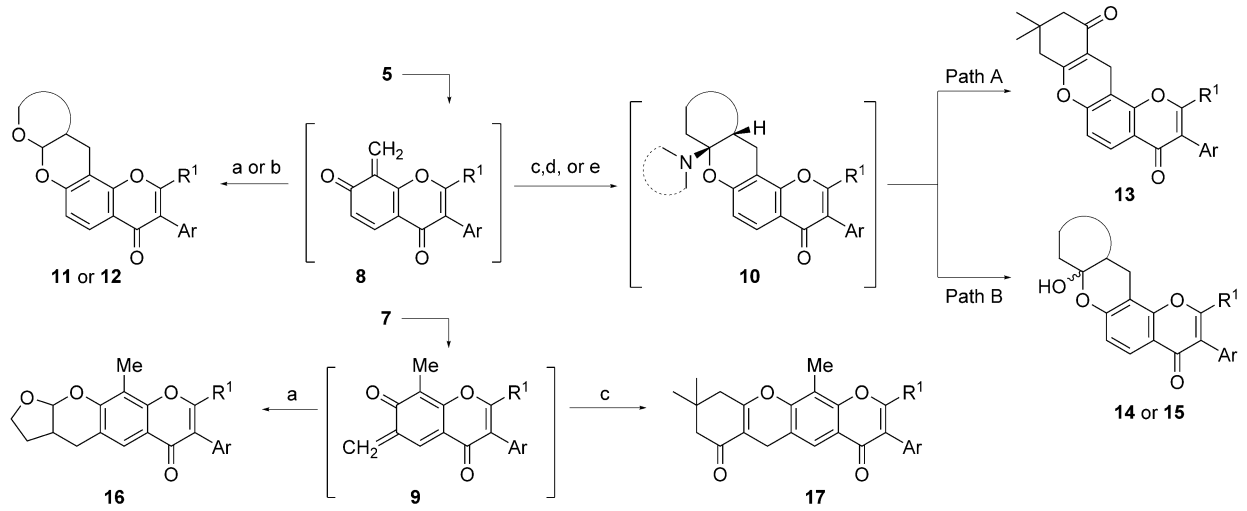

Scheme 2. Diels–Alder reaction of *N*,*N*-dimethylaminoisoflavones **5** and **7** with dienophiles *Reagents and conditions*: a) 2,3-dihydrofuran, DMF, reflux; 24–40 h; b) 3,4-dihydro-2*H*-pyran, DMF, reflux; 36–40 h; c) 3-(dimethylamino)-5,5-dimethylcyclohex-2-en-1-one, DMF, reflux; 4 h; d) 4-cyclopent-1-en-1-yl morpholine, DMF, reflux; 4 h; e) 4-cyclohex-1-en-1-yl morpholine, DMF, reflux; 4 h. Yields are reported in Table 1 and the Experimental Section.

formed. Attempts to employ common electron-deficient dienophiles were unsuccessful.

The Diels–Alder reactions of **5** with either 2,3-dihydrofuran or 3,4-dihydro-2*H*-pyran led to a 1:1 ratio of enantiomeric, *cis*-fused adducts **11** or **12**, respectively, which was confirmed by the coupling constants ^{3}J between the acetal proton at C-7a and bridgehead proton at C-10a and by chiral-phase high-performance liquid chromatography (HPLC). The structures of the *cis*-fused adducts **11** and **12** were also confirmed by 2D nuclear Overhauser effect spectroscopy (NOESY). The Diels–Alder reaction of the isomeric isoflavonoids **7** with 2,3-dihydrofuran led to the corresponding *cis*-fused adduct **16**. The 2,3,3a,9a-tetrahydro-4*H*-furo[2,3-*b*]chromene skeleton within adducts **11** and **16** appears in bioactive xyloketals isolated from fungi.[14] The Diels–Alder reactions of **5** and **7** with 3-(*N*,*N*-dimethylamino)-5,5-dimethyl-2-cyclohexen-1-one led to initial adducts that suffered concomitant thermal eliminations of dimethylamine to give the isolated adducts **13** and **17**, respectively, in excellent yield. A study of the reaction of **5a** with the 3-(*N*,*N*-dimethylamino)-5,5-dimethyl-2-cyclohexen-1-one in various solvents led to the selection of refluxing *N*,*N*-dimethylformamide (DMF) as the optimal conditions for these reactions (Table 1). Finally, Diels–Alder reactions with 1-morpholinocyclopentene and 1-morpholinocyclohexene led to the adducts **14** and **15**, respectively. The mechanism leading to each of these adducts involved an initial cycloaddition and the subsequent hydrolysis of intermediate hemi-aminals. The adducts adopted either the open-chain tautomer **14** in the case of 1-morpholinocyclopentene or the cyclic hemiacetal **15** in the case of 1-morpholinocyclohexene. Figure 2 summarizes the Diels–Alder adducts **11**–**17**.

In place of the Mannich bases as precursors to the *ortho*-quinone methides, we also investigated 8-hydroxymethyl- and 8-methoxymethyl-substituted 7-hydroxyisoflavones **18a**, **18g**, **19a**, and **19g** and diacetates **20a** and **20g**[15] as intermediates for generation of *ortho*-quinone methides in model reaction with 3-(*N*,*N*-dimethylamino)-5,5-dimethyl-2-cyclohexen-1-one in DMF (Scheme 3). Although 8-methoxymethyl-7-hydroxyisofla-

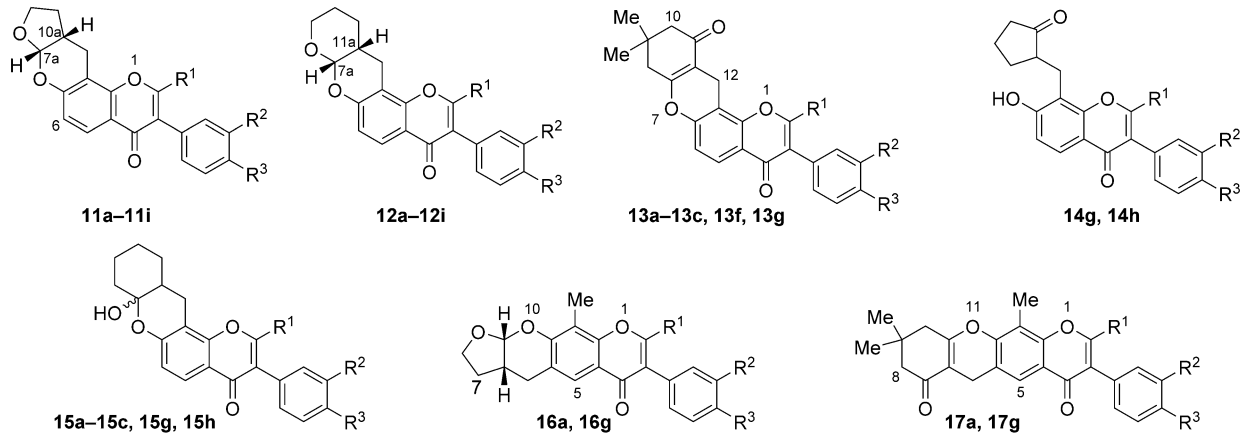

Figure 2. Diels–Alder adducts **11**–**17** derived from thermal reactions of Mannich bases **5** or **7** with various dienophiles.

Table 1. Isolated yields of Diels–Alder adducts **11**–**17** from the reaction of dienophiles and *ortho*-quinone methides derived from **5** and **7**.

		Dienophile:	A 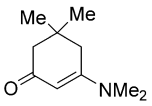		B 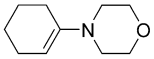	C 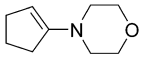			
Sub-strate	Dienophile	Solvent T [°C], t [h]	Diels–Alder Adduct	Isolated Yield [%]	Sub-strate	Dienophile	Solvent T [°C], t [h]	Diels–Alder Adduct	Isolated Yield [%]
5a	2,3-dihydrofuran	DMF 154, 24	**11a**	70	**5e**	3,4-dihydro-2*H*-pyran	DMF 154, 36	**12e**	19
5a	3,4-dihydro-2*H*-pyran	DMF 154, 36	**12a**	30	**5f**	2,3-dihydrofuran	DMF 154, 40	**11f**	73
5a	**A**	1,4-dioxane 100, 12	**13a**[a]	81	**5f**	3,4-dihydro-2*H*-pyran	DMF 154, 38	**12f**	33
5a	**A**	toluene 110 12	**13a**[a]	68	**5f**	**A**	DMF 154, 4	**13f**[a]	84
5a	**A**	2-methoxyethanol 124, 8	**13a**[a]	69	**5g**	2,3-dihydrofuran	DMF 154, 24	**11g**	62
5a	**A**	DMSO 160, 4	**13a**[a]	71	**5g**	3,4-dihydro-2*H*-pyran	DMF 154, 40	**12g**	34
5a	**A**	DMF 154, 4	**13a**[a]	92	**5g**	**A**	DMF 154, 4	**13g**[a]	81
5a	**B**	DMF 154, 16	**15a**[b]	91	**5g**	**C**	DMF 154, 4	**14g**[b]	58
5b	2,3-dihydrofuran	DMF 154, 40	**11b**	29	**5g**	**B**	DMF 154, 4	**15g**[b]	69
5b	3,4-dihydro-2*H*-pyran	DMF 154, 40	**12b**	55	**5h**	2,3-dihydrofuran	DMF 154, 30	**11h**	56
5b	**A**	DMF 154, 4	**13b**[a]	75	**5h**	3,4-dihydro-2*H*-pyran	DMF 154, 36	**12h**	15
5b	**B**	DMF 154, 4	**15b**[b]	85	**5h**	**C**	DMF 154, 4	**14h**[b]	53
6c	2,3-dihydrofuran	DMF 154, 36	**11c**	64	**5h**	**B**	DMF 154, 4	**15h**[b]	51
5c	3,4-dihydro-2*H*-pyran	DMF 154, 40	**12c**	25	**5i**	2,3-dihydrofuran	DMF 154, 40	**11i**	60
5c	**A**	DMF 154, 4	**13c**[a]	81	**5i**	3,4-dihydro-2*H*-pyran	DMF 154, 40	**12i**	15
5c	**B**	DMF 154, 4	**15c**[b]	76	**7a**	2,3-dihydrofuran	DMF 154, 16	**16a**	27
6d	2,3-dihydrofuran	DMF 154, 36	**11d**	75	**7a**	**A**	DMF 154, 4	**17a**	80
5d	3,4-dihydro-2*H*-pyran	DMF 154, 40	**12d**	36	**7g**	2,3-dihydrofuran	DMF 154, 16	**16g**	46
6e	2,3-dihydrofuran	DMF 154, 24	**11e**	55	**7g**	**A**	DMF 154, 4	**17g**	72

[a] Product of elimination of dimethylamine. [b] Product of hydrolysis of hemi-aminals.

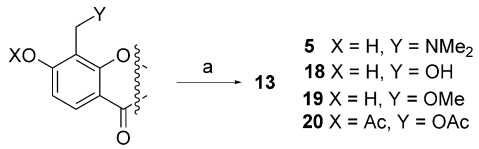

5 X = H, Y = NMe_2
18 X = H, Y = OH
19 X = H, Y = OMe
20 X = Ac, Y = OAc

Scheme 3. Regioselective modification of 7-hydroxyisoflavones **5** and 7-hydroxy-8-methylisoflavones **7**. *Reagents and conditions*: a) $CH_2(NMe)_2$, *i*PrOH, 80 °C, 2–4 h; b) $CH_2(NMe)_2$, dioxane, 100 °C, 16 h. Yields are reported in Table 2 and the Experimental Section.

vonoids gave only marginally improved yields of pyranoxanthones **13a** and **13g** than the 8-dimethylaminomethylisoflavonoids **5a** and **5g** (Table 2), the use of the Mannich bases was preferred given their ready availability. These findings suggest that other naturally ocurring hydroxymethyl- or methoxymethyl hydroxychromones could be deployed in inverse electron-demand Diels–Alder reactions.

Proliferation studies using PC-3 cells revealed that Diels–Alder adducts formed from 2,3-dihydrofuran or 3,4-dihydro-2*H*-pyran with the *ortho*-quinone methide derived from C-8 *N*,*N*-dimethylaminomethyl-substituted isoflavonoids **6** produced the most active adducts **11** and **12** (Table 3). Adduct **12** was more active than other adducts, with a few exceptions. Among the exceptions, adducts **11a** and **11e** were comparable in activity to **12a** and **12e**, and adduct **15g** was slightly superior in activity to **12g**. With respect to substituents on the isoflavonoid framework, those adducts bearing 3-(4′-methoxyphenyl), 3-(3′,4′-dimethoxyphenyl), 3-(3′,4′-methylenedioxyphenyl), or 3-

Table 2. Isolated yields of Diels–Alder adducts **13a,g** from the reaction of 3-(*N,N*-dimethylamino)-5,5-dimethyl-2-cyclohexen-1-one and precursors of *ortho*-quinone methides.[a]

Substrate	Substituents on Isoflavonoid		Diels–Alder Adduct	Isolated Yield [%]
	X	Y		
5a	H	NMe_2	**13a**	92
5g	H	NMe_2	**13g**	81
18a	H	OH	**13a**	96
18g	H	OH	**13g**	88
19a	H	OMe	**13a**	84
19g	H	OMe	**13g**	78
20a	Ac	OAc	**13a**	87
20g	Ac	OAc	**13g**	74

[a] Reactions in DMF at 154 °C, 4 h.

Table 3. Percent inhibition of PC-3 proliferation by some isoflavonoid-based Diels–Alder adducts.

Isoflavonoid Diels–Alder Adduct	Substituents on Isoflavonoid		Inhibition[a] at 10 μM [%]	Cell Diameter [μm][a,b]
	C-2	C-3		
Genistein (**1b**)	H	C_6H_4OH-4	46 ± 4.5	17.41 ± 0.46
11a	H	C_6H_4OMe-4	62 ± 7	16.43 ± 0.19
11c	H	$C_6H_3(OCH_2O)$-3,4	47 ± 4	16.37 ± 0.34
11e	H	C_6H_4Cl-4	63 ± 10	16.50 ± 0.19
12a	H	C_6H_4OMe-4	73 ± 6	17.08 ± 0.34
12b	H	$C_6H_3(OMe)_2$-3,4	35 ± 10	16.56 ± 0.17
12c	H	$C_6H_3(OCH_2O)$-3,4	68 ± 0.5	16.39 ± 0.11
12d	H	$C_6H_3(OCH_2CH_2O)$-3,4	48 ± 3	16.50 ± 0.29
12e	H	C_6H_4Cl-4	44 ± 4	16.53 ± 0.08
12g	Me	C_6H_4OMe-4	62 ± 0.4	17.08 ± 0.27
12h	Me	$C_6H_3(OMe)_2$-3,4	44 ± 3	16.55 ± 0.18
12i	Me	C_6H_4Cl-4	74 ± 3	16.30 ± 0.35
13b	H	$C_6H_3(OMe)_2$-3,4	86 ± 1	13.68 ± 0.74
15a	H	C_6H_4OMe-4	30 ± 15	17.25 ± 1.03
15b	H	$C_6H_3(OMe)_2$-3,4	56 ± 5	17.11 ± 0.17
15g	Me	C_6H_4OMe-4	78 ± 1	17.11 ± 0.45
16a	H	C_6H_4OMe-4	78 ± 3	15.89 ± 0.10
16g	Me	C_6H_4OMe-4	61 ± 2	16.77 ± 0.59

[a] Mean ± SD for at least three experiments; [b] 16.24 ± 0.34 for DMSO alone.

(4′-chlorophenyl) substituents were most active. In a promising outcome, the adduct **13b**, which was generated using 3-(*N,N*-dimethylamino)-5,5-dimethyl-2-cyclohexen-1-one, displayed 86% inhibition at 10 μM and 31% inhibition at 1 μM.

In a preliminary study of cell toxicity, the treated cells were analyzed by a Vi-Cell XR viability analyzer (Beckman Coulter, Brea, CA, USA) that took 50 images per sample and permitted the determination of cell concentrations, viability, and size. The viability of each sample was greater than 95%; however, the cell numbers were significantly decreased by active compounds. The cell sizes were similar (Table 3) except for cells treated with **13b**, which was the most potent compound. Isoflavonoid **13b** significantly decreased the size of PC-3 cells, suggesting that it may inhibit PC-3 cell proliferation by inhibiting the cell cycle as well as inducing apoptosis. Additional studies will be needed to clarify this point.

Conclusions

A regioselective condensation of 7-hydroxyisoflavonoids **4** or 7-hydroxy-8-methylisoflavonoids **6** with bis(*N,N*-dimethylamino)methane in isopropanol at reflux provided **5** or **7**, respectively. Thermal eliminations of dimethylamine from these Mannich bases as well as elimination of methanol or water from corresponding 8-methoxymethyl- or 8-hydroxymethyl 7-hydroxyisoflavones generated *ortho*-quinone methide intermediates that trapped a variety of dienophiles to give various Diels–Alder adducts **11**–**17** in good yields. Some of these adducts, particularly those derived from 2,3-dihydrofuran, 3,4-dihydro-2*H*-pyran, or 3-(*N,N*-dimethylamino)-5,5-dimethyl-2-cyclohexen-1-one, displayed good activity in a proliferation assay using PC-3 prostate cancer cells. Subsequent studies will focus on identifying the biological target of these isoflavonoids.

Experimental Section

Chemicals and instruments. ^1H and ^{13}C NMR spectra were recorded on a Varian 500 spectrometer (Palo Alto, CA, USA; at 500 MHz or at 125 MHz, respectively) or on a Varian 400 spectrometer (at 400 MHz or at 100 MHz, respectively) in deuteriochloroform ($CDCl_3$) or deuterated dimethylsulfoxide ($[D_6]$DMSO). ^{13}C NMR Chemical shifts for minor isomers compounds **15** are given in brackets. IR spectra were recorded on a Bruker Vertex 70 FT/IR spectrometer (Billerica, MA, USA). Melting points were determined in open capillarity tubes with a Büchi B-535 apparatus (Flawil, Switzerland) and were uncorrected. Mass spectra were obtained with an Agilent 1100 spectrometer (Santa Clara, CA, USA) under chemical ionization conditions. Column chromatography was performed using Macherey–Nagel Silica 60, 0.04–0.063 mm silica gel (Düren, Germany).

General procedure for the synthesis of Mannich bases 5a–5i. To a stirred suspension of isoflavonoids **4a–4i** (2 mmol) in isopropanol (10 mL), bis(*N,N*-dimethylamino)methane (0.3 mL, 2.2 mmol, 1.1 eq) was added at 25 °C. The mixture was heated at 80 °C for 2 h and cooled to afford a precipitate that was collected by gravity filtration. In the absence of crystallization, the residue was triturated with hexane to induce crystallization. The Mannich bases **5** were recrystallized from 1:1 isopropanol/hexane.

8-[(*N,N*-Dimethylamino)methyl]-7-hydroxy-3-(4-methoxyphenyl)-4*H*-chromen-4-one (5a). Pale yellow solid (83% yield); m.p. 174–176 °C; IR (KBr): $\tilde{\nu}_{max}$ = 3448, 2951, 1626, 1427, 1246, 1178, 1028 cm^{-1}; ^1H NMR (400 MHz, $CDCl_3$): δ = 2.44 (s, 6H, $N(CH_3)_2$), 3.85 (s, 3H, 4′-OCH_3), 3.99 (s, 2H, 8-CH_2), 6.90 (d, 1H, ^3J = 8.8 Hz, 6-H), 6.97 (d, 2H, ^3J = 8.8 Hz, 3′, 5′-H), 7.50 (d, 2H, ^3J = 8.8 Hz, 2′, 6′-H), 7.89 (s, 1H, 2-H), 8.14 (d, 1H, ^3J = 8.8 Hz, 5-H), 10.21 ppm (br s, 1H, 7-OH); ^{13}C NMR (125 MHz, $CDCl_3$): δ = 44.41, 54.87, 55.20, 107.27, 113.80, 115.44, 116.89, 124.22, 124.32, 126.67, 130.00, 151.25, 154.96, 159.41, 163.97, 175.74 ppm; MS (CI): *m/z* 326.1 (MH^+, 100). Anal. Calcd for $C_{19}H_{19}NO_4$: C, 70.14; H, 5.89; N, 4.30. Found: C, 69.88; H, 5.97; N, 4.39.

3-(3,4-Dimethoxyphenyl)-8-[(*N,N*-dimethylamino)methyl]-7-hydroxy-4*H*-chromen-4-one (5b). Pale yellow solid (77% yield); m.p. 154–155 °C; IR (KBr): $\tilde{\nu}_{max}$ = 2948, 1636, 1602, 1517, 1266, 1145, 1024 cm^{-1}; ^1H NMR (400 MHz, $CDCl_3$): δ = 2.44 (s, 6H, $N(CH_3)_2$), 3.91, 3.93 (2s, 6H, 3′, 4′-OCH_3), 3.99 (s, 2H, 8-CH_2), 6.86–6.96 (m, 2H, 6, 6′-H), 7.00–7.07 (m, 1H, 5′-H), 7.18–7.23 (m, 1H, 2′-H), 7.92 (s, 1H,

2-H), 8.13 (d, 1H, ^3J=8.8 Hz, 5-H), 9.79 ppm (s, 1H, 7-OH); ^{13}C NMR (125 MHz, $CDCl_3$): δ=44.52, 55.04, 55.88, 55.89, 107.40, 111.04, 112.46, 115.58, 116.93, 120.90, 124.45, 124.70, 126.68, 148.64, 148.95, 151.44, 154.93, 164.05, 175.86 ppm; MS (CI): *m/z* 356.2 (*M*H$^+$, 100). Anal. Calcd for $C_{20}H_{21}NO_5$: C, 67.59; H, 5.96; N, 3.94. Found: C, 67.88; H, 5.97; N, 4.39.

3-(1,3-Benzodioxol-5-yl)-8-[(*N,N*-dimethylamino)methyl]-7-hydroxy-4*H*-chromen-4-one (5c). Pale yellow solid (73% yield); m.p. 160–161 °C; IR (KBr): $\tilde{\nu}_{max}$=2960, 2987, 1639, 1488, 1425, 1246, 1017 cm^{-1}; ^{1}H NMR (400 MHz, $CDCl_3$): δ=2.44 (s, 6H, $N(CH_3)_2$), 3.98 (s, 2H, 8-CH_2), 5.98 (s, 2H, 3′, 4′-OCH_2O), 6.80–7.00 (m, 3H, 6, 5′, 6′-H), 7.06-7.13 (m, 1H, 2′-H), 7.86 (s, 1H, 2-H), 8.11 (d, 1H, ^3J=8.8 Hz, 5-H), 9.95 ppm (s, 1H, 7-OH); ^{13}C NMR (125 MHz, $CDCl_3$): δ=44.60, 55.15, 101.13, 107.49, 108.34, 109.78, 115.62, 116.94, 122.34, 124.61, 125.78, 126.78, 147.56, 147.62, 151.46, 154.97, 164.12, 175.73 ppm; MS (CI): *m/z* 340.3 (*M*H$^+$, 100). Anal. Calcd for $C_{19}H_{17}NO_5$: C, 67.25; H, 5.05; N, 4.13. Found: C, 67.48; H, 4.97; N, 4.39.

3-(2,3-Dihydro-1,4-benzodioxin-6-yl)-8-[(*N,N*-dimethylamino)-methyl]-7-hydroxy-4*H*-chromen-4-one (5d). Pale yellow solid (68% yield); m.p. 179–180 °C; IR (KBr): $\tilde{\nu}_{max}$=3072, 2955, 1643, 1602, 1509, 1289, 1060, 1027 cm^{-1}; ^{1}H NMR (400 MHz, $CDCl_3$): δ=2.42 (s, 6H, $N(CH_3)_2$), 3.97 (s, 2H, 8-CH_2), 4.27 (s, 4H, 3′,4′-OCH_2CH_2O), 6.88 (d, 1H, ^3J=8.7 Hz, 6-H), 6.91 (d, 1H, ^3J=8.4 Hz, 8′-H), 7.02 (dd, 1H, ^3J=8.7 Hz, ^4J=2.0 Hz, 7′-H), 7.09 (d, 1H, ^4J=2.0 Hz, 5′-H), 7.86 (s, 1H, 2-H), 8.11 (d, 1H, ^3J=8.7 Hz, 5-H), 10.04 ppm(s, 1H, 7-OH); ^{13}C NMR (125 MHz, $CDCl_3$): δ=44.39, 54.63, 64.24, 64.38, 107.04, 115.54, 116.87, 117.16, 117.88, 122.08, 124.27, 125.10, 126.94, 143.32, 143.57, 151.46, 155.02, 164.03, 175.67 ppm; MS (CI): *m/z* 354.2 (*M*H$^+$, 100). Anal. Calcd for $C_{20}H_{19}NO_5$: C, 67.98; H, 5.42; N, 3.96. Found: C, 68.10; H, 5.67; N, 4.79.

3-(4-Chlorophenyl)-8-[(*N,N*-dimethylamino)methyl]-7-hydroxy-4*H*-chromen-4-one (5e). Pale yellow solid (78% yield); m.p. 174–176 °C; IR (KBr): $\tilde{\nu}_{max}$=3061, 2958, 2838, 1881, 1632, 1590, 1466, 1378, 1257, 1204, 1176, 1011, 824 cm^{-1}; ^{1}H NMR (400 MHz, $CDCl_3$): δ=2.43 (s, 6H, $N(CH_3)_2$), 3.97 (s, 2H, 8-CH_2), 6.90 (d, 1H, ^3J=8.8 Hz, 6-H), 7.36-7.41 (m, 2H, 3′, 5′-H), 7.46–7.52 (m, 2H, 2′, 6′-H), 7.89 (s, 1H, H-2), 8.11 (d, 1H, ^3J=8.8 Hz, 5-H), 12.48 ppm (s, 1H, 7-OH); ^{13}C NMR (100 MHz, $CDCl_3$): δ=44.59, 55.14, 107.55, 115.79, 116.89, 123.84, 126.75, 128.60, 130.21, 130.51, 134.01, 151.79, 155.00, 164.32, 175.37 ppm; MS (CI): *m/z* 330.2 (*M*H$^+$, 100), 332.2 (*M*H$^+$, 28). Anal. Calcd for $C_{18}H_{16}ClNO_3$: C, 65.56; H, 4.89; N, 4.25. Found: C, 65.81; H, 5.07; N, 4.47.

8-[(*N,N*-Dimethylamino)methyl]-7-hydroxy-2-methyl-3-phenyl-4*H*-chromen-4-one (5f). Pale yellow solid (81% yield); m.p. 168–170 °C; IR (KBr): $\tilde{\nu}_{max}$=3052, 2952, 1633, 1599, 1399, 1287, 1258, 1018 cm^{-1}; ^{1}H NMR (400 MHz, $CDCl_3$): δ=2.29 (s, 3H, 2-CH_3), 2.44 (s, 6H, $N(CH_3)_2$), 3.98 (s, 2H, 8-CH_2), 6.84 (d, 1H, ^3J=8.8 Hz, 6-H), 7.24-7.47 (m, 5H, 3-Ph), 8.05 (d, 1H, ^3J=8.8 Hz, 5-H), 11.79 ppm (s, 1H, 7-OH); ^{13}C NMR (125 MHz, $CDCl_3$): δ=19.32, 44.41, 54.67, 106.69, 115.12, 115.83, 122.95, 126.83, 127.58, 128.24, 130.38, 133.17, 154.73, 161.90, 163.78, 176.29 ppm; MS (CI): *m/z* 310 (*M*H$^+$, 100). Anal. Calcd for $C_{19}H_{19}NO_3$: C, 73.77; H, 6.19; N, 4.53. Found: C, 73.92; H, 5.99; N, 4.43.

8-[(*N,N*-Dimethylamino)methyl]-7-hydroxy-3-(4-methoxyphenyl)-2-methyl-4*H*-chromen-4-one (5g). Pale yellow solid (91% yield); m.p. 185–187 °C decom.p.; IR (KBr): $\tilde{\nu}_{max}$=3450, 2958, 1626, 1603, 1255, 1176, 1016 cm^{-1}; ^{1}H NMR (400 MHz, $CDCl_3$): δ=2.30 (s, 3H, 2-CH_3), 2.44 (s, 6H, $N(CH_3)_2$), 3.84 (s, 3H, 4′-OCH_3), 3.98 (s, 2H, 8-CH_2), 6.85 (d, 1H, ^3J=8.8 Hz, 6-H), 6.97 (d, 2H, ^3J=8.7 Hz, 3′, 5′-H), 7.20 (d, 2H, ^3J=8.7 Hz, 2′, 6′-H), 8.04 (d, 1H, ^3J=8.8 Hz, 5-H), 11.30 ppm (br s, 1H); ^{13}C NMR (125 MHz, $CDCl_3$): δ=19.28, 44.44, 54.85, 55.21, 106.83, 113.78, 115.03, 115.89, 122.51, 125.33, 126.74, 131.51, 154.68, 158.99, 161.76, 163.69, 176.47 ppm; MS (CI): *m/z* 340.1 (*M*H$^+$, 100). Anal. Calcd for $C_{20}H_{21}NO_4$: C, 70.78; H, 6.24; N, 4.13. Found: C, 70.91; H, 5.95; N, 4.33.

3-(3,4-dimethoxyphenyl)-8-[(*N,N*-dimethylamino)methyl]-7-hydroxy-2-methyl-4*H*-chromen-4-one (5h). Pale yellow solid (87% yield); m.p. 150–152 °C; IR (KBr): $\tilde{\nu}_{max}$=2995, 2841, 1635, 1516, 1393, 1262, 1020 cm^{-1}; ^{1}H NMR (400 MHz, $CDCl_3$): δ=2.31 (s, 3H, 2-CH_3), 2.45 (s, 6H, $N(CH_3)_2$), 3.87, 3.91 (2s, 6H, 3′, 4′-OCH_3), 3.99 (s, 2H, 8-CH_2), 6.78-6.83 (m, 2H, 2′, 6′-H), 6.85 (d, 1H, ^3J=8.8 Hz, 6-H), 6.92 (d, 1H, ^3J=8.7 Hz, 5′-H), 8.05 ppm (d, 1H, ^3J=8.8 Hz, 5-H); ^{13}C NMR (125 MHz, $CDCl_3$): δ=19.39, 44.62, 55.24, 55.88, 55.89, 107.14, 111.11, 113.67, 115.11, 115.94, 122.76, 122.80, 125.84, 126.64, 148.50, 148.70, 154.61, 161.89, 163.78, 176.50 ppm; MS (CI): *m/z* 370.3 (*M*H$^+$, 100). Anal. Calcd for $C_{21}H_{23}NO_5$: C, 68.28; H, 6.28; N, 3.79. Found: C, 67.97; H, 6.14; N, 4.56.

3-(4-Chlorophenyl)-8-[(*N,N*-dimethylamino)methyl]-7-hydroxy-2-methyl-4*H*-chromen-4-one (5i). Pale yellow solid (86% yield); m.p. 174–175 °C; IR (KBr): $\tilde{\nu}_{max}$=2974, 2835, 1631, 1407, 1371, 1285, 1258, 1014 cm^{-1}; ^{1}H NMR (400 MHz, $CDCl_3$): δ=2.29 (s, 3H, 2-CH_3), 2.44 (s, 6H, $N(CH_3)_2$), 3.98 (s, 2H, 8-CH_2), 6.86 (d, 1H, ^3J=8.8 Hz, 6-H), 7.19-7.25 (m, 2H, 3′, 5′-H), 7.36-7.42 (m, 2H, 2′, 6′-H), 8.03 (d, 1H, ^3J=8.8 Hz, 5-H), 12.14 ppm (s, 7-OH); ^{13}C NMR (100 MHz, $CDCl_3$): δ=19.32, 44.63, 55.24, 107.18, 115.29, 115.80, 121.99, 126.65, 128.54, 131.76, 131.88, 133.61, 154.63, 161.76, 163.99, 176.03 ppm; MS (CI): *m/z* 344.3 (*M*H$^+$, 100), 346.3 (*M*H$^+$, 29). Anal. Calcd for $C_{19}H_{18}ClNO_3$: C, 66.38; H, 5.28; N, 4.07. Found: C, 66.10; H, 4.99; N, 3.85.

6-[(*N,N*-Dimethylamino)methyl]-7-hydroxy-3-(4-methoxyphenyl)-8-methyl-4*H*-chromen-4-one (7a). To a suspension of **6a** (2 mmol) in 1,4-dioxane (10 mL), bis(*N,N*-dimethylamino)methane (1 mL, 7.4 mmol) was added at 70 °C. The mixture was heated at 100 °C for 16 h, cooled, and diluted with hexane (20 mL). The precipitate was collected to afford 672 mg (99%) of **7a** as a yellow solid: m.p. 182–183 °C; IR (KBr): $\tilde{\nu}_{max}$=3069, 2954, 2831, 1627, 1512, 1461, 1369, 1290, 1223, 1176, 830 cm^{-1}; ^{1}H NMR (400 MHz, $CDCl_3$): δ=2.32 (s, 3H, 8-CH_3), 2.37 (s, 6H, $N(CH_3)_2$), 3.78 (s, 2H, 6-CH_2), 3.84 (s, 3H, 4′-OCH_3), 6.97 (d, 2H, ^3J=8.7 Hz, 3′, 5′-H), 7.50 (d, 2H, ^3J=8.7 Hz, 2′, 6′-H), 7.81 (s, 1H, 5-H), 7.97 (s, 1H, 2-H), 9.81 ppm (br s, 1H, 7-OH); ^{13}C NMR (125 MHz, $CDCl_3$): δ=7.81, 44.21, 55.30, 62.37, 111.80, 113.88, 116.63, 120.31, 122.69, 124.02, 124.60, 130.07, 152.01, 155.76, 159.38, 161.30, 176.30 ppm; MS (CI): *m/z* 340.3 (*M*H$^+$, 100). Anal. Calcd for $C_{20}H_{21}NO_4$: C, 70.87; H, 6.24; N, 4.13. Found: C, 70.62; H, 6.43; N, 4.11.

6-[(*N,N*-Dimethylamino)methyl]-7-hydroxy-3-(4-methoxyphenyl)-2,8-dimethyl-4*H*-chromen-4-one (7g). The procedure described for **6a** was repeated to afford 509 mg of **7g** as a white solid (72% yield); m.p. 176–177 °C; IR (KBr): $\tilde{\nu}_{max}$=3039, 2952, 2834, 1643, 1606, 1511, 1397, 1239, 1158 cm^{-1}; ^{1}H NMR (400 MHz, $CDCl_3$): δ=2.32 (s, 6H, 2, 8-CH_3), 2.36 (s, 6H, $N(CH_3)_2$), 3.76 (s, 2H, 6-CH_2), 3.85 (s, 3H, 4′-OCH_3), 6.97 (d, 2H, ^3J=8.7 Hz, 3′, 5′-H), 7.21 (d, 2H, ^3J=8.7 Hz, 2′, 6′-H), 7.74 ppm (s, 1H, 5-H); ^{13}C NMR (125 MHz, $CDCl_3$): δ=7.83, 19.43, 44.20, 55.23, 62.34, 111.39, 113.77, 115.55, 119.84, 122.14, 122.62, 125.67, 131.55, 155.31, 158.87, 161.02, 162.34, 176.92 ppm; MS (CI): *m/z* 354.2 (*M*H$^+$, 100). Anal. Calcd.for $C_{21}H_{23}NO_4$: C, 71.37; H, 6.56; N, 3.96. Found: C, 71.46; H, 6.31; N, 4.17.

General procedure for synthesis of Diels–Alder adducts 11 and 16. To a solution of **5** or **7** (2 mmol) in DMF (10 mL) was added 2,3-dihydrofuran (2 mL, 26 mmol, 13 eq). The use of 13 equivalents of 2,3-dihydrofuran per mmol of **5** or **7** was chosen arbitrarily and does not represent an optimized ratio. Increased equivalents, however, lowered the reflux temperature, slowed the generation of the *ortho*-quinone methide, and decreased the product yield. The solution was left at reflux for 24–40 h. The solvent and excess 2,3-dihydrofuran were evaporated in vacuo, and the residue was purified by chromatography using MeOH/CH_2Cl_2 1:50 to afford adducts **11** or **16**.

3-(4-Methoxyphenyl)-9,10,10 a,11-tetrahydro-4 *H*,7 a*H*-furo[2,3-*b*]-pyrano[2,3-*f*]chromen-4-one (11 a). Pale yellow solid (70% yield); m.p. 201-.202 °C; IR (KBr): $\tilde{\nu}_{max}$ = 2903, 2844, 1643, 1610, 1510, 1435, 1295, 1242, 1205, 1052 cm^{-1}; ^1H NMR (400 MHz, $CDCl_3$): δ = 1.69–1.82 (m, 1H, 10α-CH), 2.10-2.20 (m, 1H, 10β-CH), 2.75-2.86 (m, 1H, 10a-CH), 3.09 (dd, 1H, ^2J = 17.5 Hz, ^3J = 6.2 Hz, 11α-CH), 3.19 (dd, 1H, ^2J = 17.5 Hz, ^3J = 2.0 Hz, 11β-CH), 3.85 (s, 3H, 4′-OMe), 4.01-4.10 (m, 1H, 9α-CH), 4.16-4.24 (m, 1H, 9β-CH), 5.68 (d, 1H, ^3J = 4.2 Hz, 7a-CH), 6.94 (d, 1H, ^3J = 8.8 Hz, 6-H), 6.96-7.00 (m, 2H, 3′, H-5′-H), 7.48-7.54 (m, 2H, 2′, H-6′-H), 7.96 (s, 1H, 2-H), 8.10 ppm (d, 1H, ^3J = 8.8 Hz, 5-H); ^{13}C NMR (400 MHz, $CDCl_3$): δ = 19.46, 27.72, 36.27, 55.34, 68.45, 100.86, 107.02, 113.95, 115.55, 118.49, 124.19, 124.79, 125.49, 130.11, 151.74, 155.39, 157.14, 159.57, 175.95 ppm; MS (CI): *m/z* 351.2 (*M*H^+, 100). Anal. Calcd. for $C_{21}H_{18}O_5$: C, 71.99; H, 5.18. Found: C, 72.17; H, 4.92.

3-(3,4-Dimethoxyphenyl)-9,10,10 a,11-tetrahydro-4 *H*,7 a*H*-furo-[2,3-*b*]pyrano[2,3-*f*]chromen-4-one (11 b). Pale yellow solid (29% yield); m.p. 193-.195 °C; IR (KBr): $\tilde{\nu}_{max}$ = 2900, 2843, 1637, 1607, 1510, 1437, 1398, 1290, 1244, 1057, 1025, 840 cm^{-1}; ^1H NMR (400 MHz, $CDCl_3$): δ = 1.68-1.82 (m, 1H, 10α-CH), 2.10-2.21 (m, 1H, 10β-CH), 2.75-2.86 (m, 1H, 10a-CH), 3.09 (dd, 1H, ^2J = 17.5, ^3J = 6.0 Hz, 11α-CH), 3.14-3.24 (m, 1H, 11β-CH), 3.92 (s, 3H, 3′-OMe), 3.93 (s, 3H, 4′-OMe), 4.01-4.12 (m, 1H, 9α-CH), 4.15-4.24 (m, 1H, 9β-CH), 5.68 (d, 1H, ^3J = 4.1 Hz, 7a-CH), 6.91-6.98 (m, 2H, 6, 5′-H), 7.03-7.09 (m, 1H, 6′-H), 7.22 (d, 1H, ^4J = 1.8 Hz, 2′-H), 7.99 (s, 1H, 2-H), 8.10 ppm (d, 1H, ^3J = 8.9 Hz, 5-H); ^{13}C NMR (400 MHz, $CDCl_3$): δ = 19.47, 27.71, 36.26, 55.96, 55.99, 68.46, 100.87, 107.03, 111.15, 112.52, 115.65, 118.47, 121.01, 124.62, 124.85, 125.47, 148.76, 149.10, 151.94, 155.38, 157.21, 176.00 ppm; MS (CI): *m/z* 381.2 (*M*H^+, 100). Anal. Calcd for $C_{22}H_{20}O_6$: C, 69.46; H, 5.30. Found: C, 69.21; H, 5.01.

3-(1,3-Benzodioxol-5-yl)-9,10,10 a,11-tetrahydro-4 *H*,7 a*H*-furo[2,3-*b*]pyrano[2,3-*f*]chromen-4-one (11 c). Pale yellow solid (64% yield); m.p. 203-.205 °C; IR (KBr): $\tilde{\nu}_{max}$ = 2986, 2903, 1641, 1600, 1490, 1435, 1245, 1226, 1056, 1032 cm^{-1}; ^1H NMR (400 MHz, $CDCl_3$): δ = 1.67-1.81 (m, 1H, 10α-CH), 2.10-2.20 (m, 1H, 10β-CH), 2.75-2.86 (m, 1H, 10a-CH), 3.09 (dd, 1H, ^2J = 17.6, ^3J = 6.2 Hz, 11α-CH), 3.19 (dd, 1H, ^2J = 17.6, ^3J = 2.0 Hz, 11β-CH), 4.00-4.11 (m, 1H, 9α-CH), 4.14-4.24 (m, 1H, 9β-CH), 5.68 (d, 1H, ^3J = 4.2 Hz, 7a-CH), 6.00 (s, 2H, OCH_2O), 6.87 (d, 1H, ^3J = 8.0 Hz, 7′-H), 6.94 (d, 1H, ^3J = 8.8 Hz, 6-H), 6.98 (dd, 1H, ^3J = 8.0, ^4J = 1.7 Hz, 6′-H), 7.10 (d, 1H, ^3J = 1.7 Hz, 4′-H), 7.95 (s, 1H, 2-H), 8.09 ppm (d, 1H, ^3J = 8.8 Hz, 5-H); ^{13}C NMR (400 MHz, $CDCl_3$): δ = 19.46, 27.71, 36.26, 68.46, 100.87, 101.16, 107.04, 108.36, 109.75, 115.63, 118.41, 122.35, 124.93, 125.50, 125.64, 147.63, 147.66, 151.91, 155.37, 157.21, 175.79 ppm; MS (CI): *m/z* 365.1 (*M*H^+, 100). Anal. Calcd. for $C_{21}H_{16}O_6$: C, 69.23; H, 4.43. Found: C, 69.52; H, 4.18.

3-(2,3-Dihydro-1,4-benzodioxin-6-yl)-9,10,10 a,11-tetrahydro-4 *H*,7 a*H*-furo[2,3-*b*]pyrano[2,3-*f*]chromen-4-one (11 d). Pale yellow solid (75% yield); m.p. 188–189 °C; IR (KBr): $\tilde{\nu}_{max}$ = 2936, 2862, 1656, 1611, 1512, 1437, 1281, 1219, 1198, 1138 cm^{-1}; ^1H NMR (400 MHz, $CDCl_3$): δ = 1.68-1.82 (m, 1H, 10α-CH), 2.09-2.20 (m, 1H, 10β-CH), 2.75-2.86 (m, 1H, 10a-CH), 3.09 (dd, 1H, ^2J = 17.4, ^3J = 6.4 Hz, 11α-CH), 3.19 (dd, 1H, ^2J = 17.4, ^3J = 2.0 Hz, 11β-CH), 3.99-4.09 (m, 1H, 9α-CH), 4.14-4.23 (m, 1H, 9β-CH), 4.25-4.32 (m, 4H, OCH_2CH_2O), 5.68 (d, 1H, ^3J = 4.2 Hz, 7a-CH), 6.90-6.96 (m, 2H, 6, 8′-H), 7.04 (dd, 1H, ^3J = 8.3, ^4J = 2.0 Hz, 7′-H), 7.11 (d, 1H, ^3J = 2.0 Hz, 2′-H), 7.94 (s, 1H, 7-H), 8.09 ppm (d, 1H, ^3J = 8.8 Hz, 5-H); ^{13}C NMR (400 MHz, $CDCl_3$): δ = 19.45, 27.70, 36.25, 64.32, 64.46, 68.45, 100.87, 107.05, 115.55, 117.25, 117.94, 118.46, 122.13, 124.63, 125.09, 125.48, 143.42, 143.69, 151.92, 155.35, 157.15, 175.79 ppm; MS (CI): *m/z* 379.2 (*M*H^+, 100). Anal. Calcd. for $C_{22}H_{18}O_6$: C, 69.84; H, 4.79. Found: C, 70.07; H, 4.95.

3-(4-Chlorophenyl)-9,10,10 a,11-tetrahydro-4 *H*,7 a*H*-furo[2,3-*b*]-pyrano[2,3-*f*]chromen-4-one (11 e). Pale yellow solid (55% yield); m.p. 194–195 °C; IR (KBr): $\tilde{\nu}_{max}$ = 2961, 2899, 1637, 1598, 1492, 1438, 1377, 1244, 1092, 1064, 1012, 819 cm^{-1}; ^1H NMR (400 MHz, $CDCl_3$): δ = 1.70-1.82 (m, 1H, 10α-CH), 2.12-2.21 (m, 1H, 10β-CH), 2.77-2.86 (m, 1H, 10a-CH), 3.09 (dd, 1H, ^2J = 17.5, ^3J = 6.3 Hz, 11α-CH), 3.19 (dd, 1H, ^2J = 17.5, ^3J = 2.0 Hz, 11β-CH), 4.02-4.11 (m, 1H, 9α-CH), 4.16-4.25 (m, 1H, 9β-CH), 5.69 (d, 1H, ^3J = 4.2 Hz, 7a-CH), 6.96 (d, 1H, ^3J = 8.9 Hz, 6-H), 7.39-7.44 (m, 2H, 3′, 5′-H), 7.49-7.55 (m, 2H, 2′, 6′-H), 7.99 (s, 1H, 2-H), 8.10 ppm (d, 1H, ^3J = 8.9 Hz, 5-H); ^{13}C NMR (400 MHz, $CDCl_3$): δ = 19.46, 27.70, 36.22, 68.48, 100.90, 107.10, 115.83, 118.38, 124.19, 125.50, 128.65, 130.22, 130.36, 134.15, 152.27, 155.42, 157.40, 175.50 ppm; MS (CI): *m/z* 355.2 (*M*H^+, 100), 357.1 (MH^+, 30). Anal. Calcd for $C_{20}H_{15}ClO_4$: C, 67.71; H, 4.26. Found: C, 67.55; H, 4.43.

2-Methyl-3-phenyl-9,10,10 a,11-tetrahydro-4 *H*,7 a*H*-furo[2,3-*b*]-pyrano[2,3-*f*]chromen-4-one (11 f). Pale yellow solid (73% yield); m.p. 181–182 °C; IR (KBr): $\tilde{\nu}_{max}$ = 2966, 2900, 1634, 1607, 1579, 1510, 1437, 1398, 1244, 1057, 840 cm^{-1}; ^1H NMR (400 MHz, $CDCl_3$): δ = 1.70-1.83 (m, 1H, 10α-CH), 2.11-2.21 (m, 1H, 10β-CH), 2.32 (s, 3H, 2-CH_3), 2.75-2.85 (m, 1H, 10a-CH), 3.10 (dd, 1H, ^2J = 17.4, ^3J = 6.1 Hz, 11α-CH), 3.21 (dd, 1H, ^2J = 17.4, ^3J = 2.0 Hz, 11β-CH), 4.01-4.10 (m, 1H, 9α-CH), 4.16-4.23 (m, 1H, 9β-CH), 5.68 (d, 1H, ^3J = 4.2 Hz, 7a-CH), 6.91 (d, 1H, ^3J = 8.8 Hz, 6-H), 7.27-7.30 (m, 2H, 2′, 6′-H), 7. 46-7.34 (m, 3H, 3′, 4′, 5′, H), 8.02 ppm (d, 1H, ^3J = 8.8 Hz, 5-H); ^{13}C NMR (400 MHz, $CDCl_3$): δ = 19.39, 19.52, 27.76, 36.31, 68.44, 100.84, 106.71, 115.15, 117.44, 123.38, 125.40, 127.68, 128.33, 130.42, 133.20, 155.01, 157.00, 162.28, 176.34 ppm; MS (CI): *m/z* 335.2 (*M*H^+, 100). Anal. Calcd for $C_{21}H_{18}O_4$: C, 75.43; H, 5.43. Found: C 75.85; H, 5.72.

3-(4-Methoxyphenyl)-2-methyl-9,10,10 a,11-tetrahydro-4 *H*,7 a*H*-furo[2,3-*b*]pyrano[2,3-*f*]chromen-4-one (11 g). Pale yellow solid (62% yield); m.p. 227–229 °C; IR (KBr): $\tilde{\nu}_{max}$ = 2900, 2825, 1634, 1607, 1510, 1437, 1398, 1290, 1244, 1057, 1025 cm^{-1}; ^1H NMR (400 MHz, $CDCl_3$): δ = 1.68-1.82 (m, 1H, 10α-CH), 2.09-2.20 (m, 1H, 10β-CH), 2.33 (s, 3H, 2-CH_3), 2.74-2.85 (m, 1H, 10a-CH), 3.09 (dd, 1H, ^2J = 17.4, ^3J = 6.2 Hz, 11α-CH), 3.19 (dd, 1H, ^2J = 17.4, ^3J = 1.6 Hz, 11β-CH), 3.85 (s, 3H, 4′-OMe), 4.00-4.09 (m, 1H, 9α-CH), 4.15-4.22 (m, 1H, 9β-CH), 5.67 (d, 1H, ^3J = 4.2 Hz, 7a-CH), 6.90 (d, 1H, ^3J = 8.8 Hz, 6-H), 6.97 (d, 2H, ^3J = 8.7 Hz, 3′, 5′-H), 7.21 (d, 2H, ^3J = 8.7 Hz, 2′, 6′-H), 8.01 ppm (d, 1H, ^3J = 8.8 Hz, 5-H); ^{13}C NMR (400 MHz, $CDCl_3$): δ = 19.41, 19.53, 27.78, 36.33, 55.29, 68.43, 100.84, 106.69, 113.87, 115.08, 117.43, 122.92, 125.31, 125.42, 131.55, 154.98, 156.94, 159.07, 162.22, 176.55 ppm; MS (CI): *m/z* 365.1 (*M*H^+, 100). Anal. Calcd for $C_{22}H_{20}O_5$: C, 72.51; H, 5.53. Found: C, 72.80; H, 5.82.

3-(3,4-Dimethoxyphenyl)-2-methyl-9,10,10 a,11-tetrahydro-4 *H*,7 a*H*-furo[2,3-*b*]pyrano[2,3-*f*]chromen-4-one (11 h). Pale

yellow solid (56% yield); m.p. 217–219 °C; IR (KBr): $\tilde{\nu}_{max}$ = 2936, 2859, 1634, 1602, 1578, 1506, 1436, 1386, 1242, 1216, 1067 cm^{-1}; ^1H NMR (400 MHz, $CDCl_3$): δ = 1.69-1.82 (m, 1H, 10α-CH), 2.10-2.19 (m, 1H, 10β-CH), 2.33 (s, 3H, 2-CH_3), 2.75-2.84 (m, 1H, 10a-CH), 3.10 (dd, 1H, ^2J = 17.5, ^3J = 6.1 Hz, 11α-CH), 3.20 (dd, 1H, ^2J = 17.5, ^2J = 2.0 Hz, 11β-CH), 3.88 (s, 3H, 3′-OMe), 3.92 (s, 3H, 4′-OMe), 4.02-4.10 (m, 1H, 9α-CH), 4.15-4.23 (m, 1H, 9β-CH), 5.68 (d, 1H, ^3J = 4.2 Hz, 7a-CH), 6.80-6.83 (m, 2H, 2′, 6′-H), 6.90 (d, 1H, ^3J = 8.8 Hz, 6-H), 6.93 (d, 1H, ^3J = 8.6 Hz, 5′-H), 8.02 ppm (d, 1H, ^3J = 8.8 Hz, 5-H); ^{13}C NMR (400 MHz, $CDCl_3$): δ = 19.45, 19.53, 27.77, 36.32, 55.90, 55.92, 68.43, 100.85, 106.68, 111.18, 113.68, 115.16, 117.42, 122.80, 123.14, 125.41, 125.73, 148.60, 148.77, 154.99, 156.99, 162.44, 176.57 ppm; MS (CI): *m/z* 395.3 (*M*H$^+$, 100). Anal. Calcd for $C_{23}H_{22}O_6$: C, 70.04; H, 5.62. Found: C, 69.85; H, 5.90.

3-(4-Chlorophenyl)-2-methyl-9,10,10 a,11-tetrahydro-4 *H*,7 a*H*-furo[2,3-*b*]pyrano[2,3-*f*]chromen-4-one (11 i). Pale yellow solid (60% yield); m.p. 266–268 °C; IR (KBr): $\tilde{\nu}_{max}$ = 2971, 2903, 1641, 1605, 1582, 1491, 1438, 1399, 1251, 1088, 1068 cm^{-1}; ^1H NMR (400 MHz, $CDCl_3$): δ = 1.69-1.83 (m, 1H, 10α-CH), 2.11-2.20 (m, 1H, 10β-CH), 2.32 (s, 3H, 2-CH_3), 2.75-2.85 (m, 1H, 10a-CH), 3.10 (dd, 1H, ^2J = 17.4, ^3J = 6.3 Hz, 11α-CH), 3.20 (dd, 1H, ^2J = 17.4, ^2J = 2.1 Hz, 11β-CH), 4.02-4.11 (m, 1H, 9α-CH), 4.16-4.23 (m, 1H, 9β-CH), 5.68 (d, 1H, ^3J = 4.2 Hz, 7a-CH), 6.91 (d, 1H, ^3J = 8.8 Hz, 6-H), 7.19-7.25 (m, 2H, 3′, 5′-H), 7.38-7.44 (m, −2′, 6′-H), 8.01 ppm (d, 1H, ^3J = 8.8 Hz, 5-H); ^{13}C NMR (400 MHz, $CDCl_3$): δ = 19.38, 19.52, 27.74, 36.28, 68.45, 100.87, 106.75, 115.32, 117.27, 122.34, 125.38, 128.59, 131.65, 131.86, 133.71, 155.01, 157.16, 162.32, 176.10 ppm; MS (CI): *m/z* 369.1 (*M*H$^+$, 100)., 371.1 (*M*H$^+$, 29). Anal. Calcd for $C_{21}H_{17}ClO_4$: C, 68.39; H, 4.65. Found: C, 68.70; H, 4.87.

3-(4-Methoxyphenyl)-11-methyl-6 a,7,8,9 a-tetrahydro-4 *H*,6 *H*-furo[2,3-*b*]pyrano[3,2 *g*]chromen-4-one (16 a). Pale yellow solid (27% yield); m.p. 155–157 °C; IR (KBr): $\tilde{\nu}_{max}$ = 2963, 2907, 1640, 1606, 1512, 1462, 1289, 1219, 1176, 1056 cm^{-1}; ^1H NMR (400 MHz, $CDCl_3$): δ = 1.53-1.67 (m, 1H, 7α-CH), 2.00-2.14 (m, 1H, 7β-CH), 2.33 (s, 3H, 11-CH_3), 2.79-2.93 (m, 2H, 6a-CH, 6α-CH), 3.10 (dd, ^2J = 16.4, ^3J = 5.9 Hz, 1H, 6β-CH), 3.83 (s, 3H, 4′-OCH_3), 3.88-3.98 (m, 2H, 8-CH_2), 5.83 (d, 1H, ^3J = 5.1 Hz, 9a-CH), 6.98 (d, 2H, ^3J = 8.8 Hz, 3′, 5′-H), 7.51 (d, 2H, ^3J = 8.8 Hz, 2′, 6′-H), 7.91 (s, 1H, 5-H), 8.00 ppm (s, 1H, 2-H); ^{13}C NMR (100 MHz, $CDCl_3$): δ = 8.20, 26.53, 27.97, 37.67, 55.34, 68.33, 102.87, 113.96, 118.62, 120.49, 123.20, 124.19, 124.49, 130.11, 152.27, 154.78, 155.98, 159.49, 176.33 ppm; MS (CI): *m/z* 365.3 (*M*H$^+$, 100). Anal. Calcd for $C_{22}H_{20}O_5$: C, 72.51; H, 5.53. Found: C, 72.80; H, 5.35.

3-(4-Methoxyphenyl)-2,11-methyl-6 a,7,8,9 a-tetrahydro-4 *H*,6 *H*-furo[2,3-*b*]pyrano[3,2 *g*]chromen-4-one (16 g). Pale yellow solid (24% yield); m.p. 155–157 °C; IR (KBr): $\tilde{\nu}_{max}$ = 2933, 2837, 1635, 1608, 1513, 1462, 1238, 1932 cm^{-1}; ^1H NMR (400 MHz, $CDCl_3$): δ = 1.52-1.62 (m, 1H, 7α-CH), 2.02-2.12 (m, 1H, 7β-CH), 2.33, 2.35 (2 s, 3H, 3H, 2, 11-CH_3), 2.80-2.91 (m, 2H, 6a-CH, 6α-CH), 3.09 (dd, ^2J = 16.0, ^3J = 5.7 Hz, 1H, 6β-CH), 3.84 (s, 3H, 4′-OCH_3), 3.88-3.99 (m, 2H, 8-CH_2), 5.83 (d, 1H, ^3J = 5.3 Hz,9a-CH), 6.97 (d, 2H, ^3J = 8.6 Hz, 3′, 5′-H), 7.21 (d, 2H, ^3J = 8.6 Hz, 2′, 6′-H), 7.82 ppm (s, 1H, 5-H); ^{13}C NMR (100 MHz, $CDCl_3$): δ = 8.24, 19.50, 26.54, 28.03, 37.76, 55.29, 68.32, 102.91, 113.60, 113.88, 117.58, 120.15, 122.38, 123.09, 125.59, 131.59, 154.37, 155.79, 159.00, 162.77, 176.94 ppm; MS (CI): *m/z* 365.3 (*M*H$^+$, 100). Anal. Calcd for $C_{22}H_{20}O_5$: C, 72.51; H, 5.53. Found: C, 72.80; H, 5.35.

General procedure for synthesis of Diels–Alder adducts 12. To a solution of **5** (2 mmol) in DMF (10 mL) was added 3,4-dihydro-2*H*-dihydropyran (2 mL, 22 mmol, 11 eq). The solution was refluxed for 36-40 h. The solvent and excess 2*H*,3,4-dihydropyran were evaporated in vacuo, and the residue was purified by chromatography with MeOH/CH_2Cl_2 to afford **12**.

3-(4-Methoxyphenyl)-10,11,11 a,12-tetrahydro-4 *H*,7 a*H*,9 *H*-dipyrano[2,3-*b*:2′,3′-*f*]chromen-4-one (12 a). Pale yellow solid (30% yield); m.p. 182–183 °C; IR (KBr): $\tilde{\nu}_{max}$ = 2966, 2933, 1636, 1598, 1511, 1437, 1248, 1205, 1178, 1090, 1029 cm^{-1}; ^1H NMR (400 MHz, $CDCl_3$): δ = 1.47-1.92 (m, 4H, 10, 11-CH_2), 2.24-2.40 (m, 1H, 11a-CH), 2.90 (dd, 1H, ^2J = 17.4 Hz, ^3J = 4.2 Hz, 12α-CH), 3.01 (dd, 1H, ^2J = 17.4, ^3J = 6.1 Hz, 12β-CH), 3.75-3.82 (m, 1H, 9α-CH), 3.85 (s, 3H, 4′-OMe), 3.95-4.09 (m, 1H, 9β-CH), 5.44 (d, 1H, ^3J = 2.0 Hz, 7a-CH), 6.93-7.02 (m, 3H, 6, 3′, 5′-H), 7.50 (d, 2H, ^3J = 8.7 Hz, 2′, 6′-H), 7.96 (s, 1H, 2-H), 8.10 ppm (d, 1H, ^3J = 8.8 Hz, 5-H); ^{13}C NMR (400 MHz, $CDCl_3$): δ = 23.17, 23.57, 24.02, 30.62, 55.33, 62.58, 96.94, 107.86, 113.94, 115.27, 118.45, 124.19, 124.79, 125.29, 130.13, 151.79, 155.37, 157.15, 159.55, 176.07 ppm; MS (CI): *m/z* 365.1 (*M*H$^+$, 100). Anal. Calcd for $C_{22}H_{20}O_5$: C, 72.51; H, 5.53. Found: C, 72.38; H, 5.67.

3-(3,4-Dimethoxyphenyl)-10,11,11 a,12-tetrahydro-4 *H*,7 a*H*,9 *H*-dipyrano[2,3-*b*:2′,3′-*f*]chromen-4-one (12 b). Pale yellow solid (54% yield); m.p. 177–178 °C; IR (KBr): $\tilde{\nu}_{max}$ = 3076, 2925, 1642, 1600, 1515, 1436, 1267, 1249, 1139, 1090, 1023 cm^{-1}; ^1H NMR (400 MHz, $CDCl_3$): δ = 1.61-1.82 (m, 4H, 10, 11-CH_2), 2.27-2.37 (m, 1H, 11a-CH), 2.91 (dd, 1H, ^2J = 17.3, ^3J = 4.1 Hz, 12α-CH), 2.99 (dd, 1H, ^2J = 17.3, ^3J = 6.1 Hz, 12β-CH), 3.76-3.83 (m, 1H, 9α-CH), 3.92 (s, 3H, 3′-OMe), 3.93 (s, 3H, 4′-OMe), 4.00-4.08 (m, 1H, 9β-CH), 5.45 (d, 1H, ^3J = 2.0 Hz, 7a-CH), 6.93 (d, 1H, ^3J = 8.3 Hz, 5′-H), 6.98 (d, 1H, ^3J = 8.9 Hz, 6-H), 7.04 (dd, 1H, ^3J = 8.3, ^4J = 2.0 Hz, 6′-H), 7.22 (d, 1H, ^4J = 2.0 Hz, 2′-H), 7.99 (s, 1H, 2-H), 8.09 ppm (d, 1H, ^3J = 8.9 Hz, 5-H); ^{13}C NMR (400 MHz, $CDCl_3$): δ = 23.15, 23.56, 24.05, 30.64, 55.96, 55.98, 62.61, 96.97, 107.89, 111.16, 112.55, 115.34, 118.46, 121.02, 124.67, 124.83, 125.26, 148.76, 149.10, 151.96, 155.35, 157.22, 176.06 ppm; MS (CI): *m/z* 395.3 (*M*H$^+$, 100). Anal. Calcd for $C_{23}H_{22}O_6$: C, 70.04; H, 5.62. Found: C, 70.27; H, 5.90.

3-(1,3-Benzodioxol-5-yl)-10,11,11 a,12-tetrahydro-4 H,7 a*H*,9 *H*-dipyrano[2,3-b:2′,3′-*f*]chromen-4-one (12 c). Pale yellow solid (25% yield); m.p. 179–181 °C; IR (KBr): $\tilde{\nu}_{max}$ = 2925, 1637, 1599, 1434, 1247, 1142, 1033 cm^{-1}; ^1H NMR (400 MHz, $CDCl_3$): δ = 1.68-1.84 (m, 4H, 10, 11-CH_2), 2.25-2.37 (m, 1H, 11a-CH), 2.83-3.08 (m, 2H, 12α, 12β-CH), 3.75-3.85 (m, 1H, 9α-CH), 4.00-4.09 (m, 1H, 9β-CH), 5.44 (d, 1H, ^3J = 2.4 Hz, 7a-CH), 6.00 (s, 2H, OCH_2O), 6.88 (d, 1H, ^3J = 8.0 Hz, 7′-H), 6.95-7.01 (m, 2H, 6, 6′-H), 7.10 (d, 1H, ^3J = 1.7 Hz, 4′-H), 7.95 (s, 1H, 2-H), 8.09 ppm (d, 1H, ^3J = 8.8 Hz, 5-H); ^{13}C NMR (400 MHz, $CDCl_3$): δ = 23.19, 23.58, 24.05, 30.63, 62.58, 96.91, 101.11, 107.82, 108.31, 109.71, 115.29, 118.30, 122.31, 124.86, 125.23, 125.56, 147.53, 147.55, 151.88, 155.25, 157.13, 175.82 ppm; MS (CI): *m/z* 379.2 (*M*H$^+$, 100). Anal. Calcd for $C_{22}H_{18}O_6$: C, 69.84; H, 4.79. Found: C, 70.07; H, 4.61.

3-(2,3-Dihydro-1,4-benzodioxin-6-yl)-10,11,11 a,12-tetrahydro-4 *H*,7 a*H*,9 *H*-dipyrano[2,3-*b*:2′,3′-*f*]chromen-4-one (12 d). Pale yellow solid (36% yield); m.p. 160–162 °C; IR (KBr): $\tilde{\nu}_{max}$ = 2943, 2924, 2860, 1635, 1599, 1507, 1436, 1303, 1287, 1249, 1091 cm^{-1}; ^1H NMR (400 MHz, $CDCl_3$): δ = 1.67-1.82 (m, 4H, 10, 11-CH_2), 2.27-2.35 (m, 1H, 11a-CH), 2.91 (dd, 1H, ^2J = 17.3, ^3J = 4.1 Hz, 12α-CH), 2.99 (dd, 1H, ^2J = 17.3, ^3J = 6.1 Hz, 12β-CH), 3.75-3.83 (m, 1H, 9α-CH), 4.00-4.09 (m, 1H, 9β-CH), 4.27-4.31 (m, 4H, OCH_2CH_2O), 5.44 (d, 1H, ^3J = 2.4 Hz, 7a-CH), 6.93 (d, 1H, ^3J = 8.3 Hz, 8′-H), 6.97 (d, 1H, ^3J = 8.9 Hz, 6-H), 7.03 (dd, 1H, ^3J = 8.3, ^4J = 2.1 Hz, 7′-H), 7.10 (d, 1H, ^4J = 2.1 Hz, 5′-H), 7.94 (s, 1H, 2-H), 8.09 ppm (d, 1H, ^3J = 8.9 Hz, 5-H); ^{13}C NMR (400 MHz, $CDCl_3$): δ = 23.19, 23.58, 24.01, 30.63, 62.56, 64.32, 64.46, 96.94, 107.85, 115.27, 117.28, 117.96, 118.45, 122.18,

124.67, 125.12, 125.32, 143.42, 143.68, 151.93, 155.33, 157.17, 175.90 ppm; MS (CI): *m/z* 393.2 (*M*H$^+$, 100). Anal. Calcd for $C_{23}H_{20}O_6$: C, 70.40; H, 5.14. Found: C, 70.15; H, 5.40.

3-(4-Chlorophenyl)-10,11,11 a,12-tetrahydro-4 *H*,7 a*H*,9 *H*-dipyrano[2,3-*b*:2′,3′-*f*]chromen-4-one (12 e). Pale yellow solid (19% yield); m.p. 195–197 °C; IR (KBr): $\tilde{\nu}_{max}$ = 2930, 1643, 1597, 1437, 1256, 1206, 1094, 826 cm^{-1}; ^{1}H NMR (400 MHz, $CDCl_3$): δ = 1.67-1.84 (m, 4H, 10, 11-CH_2), 2.28-2.38 (m, 1H, 11a-CH), 2.85-3.07 (m, 2H, 12α, 12β-CH), 3.76-3.85 (m, 1H, 9α-CH), 3.99-4.11 (m, 1H, 9β-CH), 5.45 (d, 1H, ^3J = 2.4 Hz, 7a-CH), 6.99 (d, 1H, ^3J = 8.8 Hz, 6-H), 7.42 (d, 2H, ^3J = 8.7 Hz, 3′, 5′-H), 7.52 (d, 2H, ^3J = 8.7 Hz, 2′, 6′-H), 7.99 (s, 1H, 2-H), 8.09 ppm (d, 1H, ^3J = 8.9 Hz, 5-H); ^{13}C NMR (400 MHz, $CDCl_3$): δ = 23.20, 23.59, 24.05, 30.61, 62.60, 96.93, 107.89, 115.47, 118.33, 124.13, 125.25, 128.60, 130.16, 130.32, 134.06, 152.16, 155.28, 157.28, 175.27 ppm; MS (CI): *m/z* 369.2 (*M*H$^+$, 100), 371.2 (*M*H$^+$, 25). Anal. Calcd for $C_{21}H_{17}ClO_4$: C, 68.39; H, 4.65. Found: C, 68.17; H, 4.43.

2-Methyl-3-phenyl-10,11,11 a,12-tetrahydro-4 *H*,7 a*H*,9 *H*-dipyrano[2,3-*b*:2′,3′-*f*]chromen-4-one (12 f). Pale yellow solid (33% yield); m.p. 165–167 °C; IR (KBr): $\tilde{\nu}_{max}$ = 2927, 1626, 1600, 1440, 1400, 1255, 1139, 1090 cm^{-1}; ^{1}H NMR (400 MHz, $CDCl_3$): δ = 1.66-1.81 (m, 4H, 10, 11-CH_2), 2.32 (s, 4H, 2-CH_3, 11a-CH), 2.86-3.08 (m, 2H, 12α, 12β-CH), 3.75-3.86 (m, 1H, 9α-CH), 4.01-4.11 (m, 1H, 9β-CH), 5.45 (d, 1H, ^3J = 2.4 Hz, 7a-CH), 6.94 (d, 1H, ^3J = 8.8 Hz, 6-H), 7.28-7.32 (m, 2H, 2′, 6′-H), 7.36 (t, 1H, ^3J = 7.3 Hz, 4′-H), 7.44 (t, 2H, ^3J = 7.3 Hz, 3′, 5′-H), 8.02 ppm (d, 1H, ^3J = 8.9 Hz, 5-H); ^{13}C NMR (400 MHz, $CDCl_3$): δ = 19.43, 23.24, 23.62, 24.09, 30.72, 62.58, 96.86, 107.44, 114.77, 117.37, 123.30, 125.15, 127.59, 128.25, 130.36, 133.16, 154.87, 156.87, 162.15, 176.26 ppm; MS (CI): *m/z* 349.2 (*M*H$^+$, 100). Anal. Calcd for $C_{22}H_{20}O_4$: C, 75.84; H, 5.79. Found: C, 76.01; H, 5.95.

3-(4-Methoxyphenyl)-2-methyl-10,11,11 a,12-tetrahydro-4 *H*,7 a*H*,9 *H*-dipyrano[2,3-*b*:2′,3′-*f*]chromen-4-one (12 g). Pale yellow solid (34% yield); m.p. 199–200 °C; IR (KBr): $\tilde{\nu}_{max}$ = 2931, 2901, 1637, 1606, 1510, 1440, 1397, 1255, 1243, 1136, 1091, 1030 cm^{-1}; ^{1}H NMR (400 MHz, $CDCl_3$): δ = 1.61-1.82 (m, 4H, 10, 11-CH_2), 2.28-2.35 (m, 4H, 2-CH_3, 11a-CH), 2.92 (dd, 1H, ^2J = 17.3, ^3J = 4.2 Hz, 12α-CH), 3.00 (dd, 1H, ^2J = 17.3, ^3J = 6.3 Hz, 12β-CH), 3.76-3.83 (m, 1H, 9α-CH), 3.85 (s, 3H, 4′-OMe), 4.00-4.10 (m, 1H, 9β-CH), 5.44 (d, 1H, ^3J = 2.2 Hz, 7a-CH), 6.93 (d, 1H, ^3J = 8.8 Hz, 6-H), 6.97 (d, 2H, ^3J = 8.7 Hz, 3′, 5′-H), 7.21 (d, 2H, ^3J = 8.7 Hz, 2′, 6′-H), 8.01 ppm (d, 1H, ^3J = 8.8 Hz, 5-H); ^{13}C NMR (400 MHz, $CDCl_3$): δ = 19.41, 23.18, 23.58, 24.06, 30.69, 55.28, 62.59, 96.90, 107.48, 113.84, 114.76, 117.38, 122.88, 125.19, 125.32, 131.55, 154.94, 156.91, 159.02, 162.25, 176.63 ppm; MS (CI): *m/z* 379.3 (*M*H$^+$, 100). Anal. Calcd for $C_{23}H_{22}O_5$: C, 73.00; H, 5.86. Found: C, 73.18; H, 6.02.

3-(3,4-Dimethoxyphenyl)-2-methyl-10,11,11 a,12-tetrahydro-4 *H*,7 a*H*,9 *H*-dipyrano[2,3-*b*:2′,3′-*f*]chromen-4-one (12 h). Pale yellow solid (15% yield); m.p. 209–210 °C; IR (KBr): $\tilde{\nu}_{max}$ = 2934, 1636, 1581, 1513, 1438, 1394, 1258, 1138 cm^{-1}; ^{1}H NMR (400 MHz, $CDCl_3$): δ = 1.56-1.82 (m, 4H, 10, 11-CH_2), 2.27-2.35 (m, 4H, 2-CH_3, 11a-CH), 2.98 (dd, 1H, ^2J = 17.2, ^3J = 4.4 Hz, 12α-CH), 3.00 (dd, 1H, ^2J = 17.2, ^3J = 6.3 Hz, 12β-CH), 3.75–3.83 (m, 1H, 9α-CH), 3.88 (s, 3H, 3′-OMe), 3.92 (s, 3H, 4′-OMe), 4.00-4.10 (m, 1H, 9β-CH), 5.44 (d, 1H, ^3J = 2.4 Hz, 7a-CH), 6.79-6.83 (m, 2H, 2′, 6′-H), 6.91-6.95 (m, 2H, 6, 5′-H), 8.02 ppm (d, 1H, ^3J = 8.8 Hz, 5-H); ^{13}C NMR (400 MHz, $CDCl_3$): δ = 19.45, 23.17, 23.57, 24.08, 30.69, 55.90, 55.91, 62.61, 96.93, 107.51, 111.17, 113.68, 114.86, 117.37, 122.81, 123.12, 125.19, 125.76, 148.58, 148.76, 154.97, 156.99, 162.51, 176.68 ppm; MS (CI): *m/z* 409.2 (*M*H$^+$, 100). Anal. Calcd for $C_{24}H_{24}O_6$: C, 70.58; H, 5.92. Found: C, 70.69; H, 6.17.

3-(4-Chlorophenyl)-2-methyl-10,11,11 a,12-tetrahydro-4 *H*,7 a*H*,9 *H*-dipyrano[2,3-*b*:2′,3′-*f*]chromen-4-one (12 i). Pale yellow solid (15% yield); m.p. 205–206 °C; IR (KBr): $\tilde{\nu}_{max}$ = 2927, 1635, 1605, 1439, 1398, 1257, 1139, 1094, 895 cm^{-1}; ^{1}H NMR (400 MHz, $CDCl_3$): δ = 1.82-1.64 (m, 4H, 10, 11-CH_2), 2.28-2.37 (m, 4H, 2-CH_3, 11a-CH), 2.84-3.07 (m, 2H, 12α, 12β-CH), 3.75–3.84 (m, 1H, 9α-CH), 4.00-4.10 (m, 1H, 9β-CH), 5.44 (d, 1H, ^3J = 2.5 Hz, 7a-CH), 6.95 (d, 1H, ^3J = 8.8 Hz, 6-H), 7.20-7.25 (m, 2H, 2′, 6′-H), 7.38-7.43 (m, 2H, 3′, 5′-H), 8.01 ppm (d, 1H, ^3J = 8.8 Hz, 5-H); ^{13}C NMR (400 MHz, $CDCl_3$): δ = 19.38, 23.12, 23.51, 24.03, 30.60, 62.59, 96.90, 107.55, 115.03, 117.15, 122.27, 125.16, 128.57, 131.59, 131.83, 133.67, 154.96, 157.15, 162.44, 176.20 ppm; MS (CI): *m/z* 383.2 (*M*H$^+$, 100), 385.2 (*M*H$^+$, 25). Anal. Calcd for $C_{22}H_{19}ClO_3$: C, 72.03; H, 5.22. Found: C, 72.31; H, 5.43.

General procedure for synthesis of pyranoxanthenediones 13 and 17. To a solution of **5** or **7** (1 mmol), 3-(*N*,*N*-dimethylamino)-5,5-dimethylcyclohex-2-en-1-one (1.25 mmol, 1.25 eq) in DMF (10 mL) was added. The solution was left at reflux for 4 h. The mixture was diluted with MeOH (20 mL), and the precipitate was collected by filtration and recrystallized from 1:2 DMF/MeOH to afford **13** or **17**.

3-(4-Methoxyphenyl)-9,9-dimethyl-8,9,10,12-tetrahydro-4 *H*,11 *H*-pyrano[2,3-*a*]xanthene-4,11-dione (13 a). Beige solid (92% yield); m.p. 223–225 °C; IR (KBr): $\tilde{\nu}_{max}$ = 2949, 1647, 1606, 1511, 1438, 1237, 1032 cm^{-1}; ^{1}H NMR (400 MHz, [D_6]DMSO): δ = 1.10 (s, 6H, 9-CH_3), 2.33 (s, 2H, 10-CH_2), 2.53 (2, 2H, 8-CH_2), 3.52 (s, 2H, 12-CH_2), 3.81 (s, 3H, 4′-OCH_3), 7.01 (d, 2H, ^3J = 8.6, 3′, 5′-H), 7.18 (d, 1H, ^3J = 8.8, 6-H), 7.54 (d, 2H, ^3J = 8.6, 2′, 6′-H), 8.00 (d, 2H, ^3J = 8.8, 5-H), 8.50 ppm (s, 1H, 2-H); ^{13}C NMR (125 MHz, $CDCl_3$ and [D_6]DMSO 1:1): δ = 16.01, 27.89, 31.67, 40.57, 50.07, 54.80, 107.61, 109.39, 113.36, 113.84, 120.34, 123.22, 124.36, 124.84, 129.51, 151.86, 152.47, 153.99, 159.01, 163.63, 174.96, 196.87 ppm; MS (CI): *m/z* 403.2 (*M*H$^+$, 100). Anal. Calcd for $C_{25}H_{22}O_5$: C, 74.61; H, 5.51. Found: C, 74.47; H, 5.27.

3-(3,4-Dimethoxyphenyl)-9,9-dimethyl-8,9,10,12-tetrahydro-4 *H*,11 *H*-pyrano[2,3-*a*]xanthene-4,11-dione (13 b). Beige solid (75% yield); m.p. 196–198 °C; IR (KBr): $\tilde{\nu}_{max}$ = 2955, 1654, 1640, 1516, 1440, 1261, 1237, 1195 cm^{-1}; ^{1}H NMR (400 MHz, $CDCl_3$): δ = 1.17 (s, 6H, 9-CH_3), 2.39 (s, 2H, 10-CH_2), 2.50 (s, 2H, 8-CH_2), 3.65 (s, 2H, 12-CH_2), 3.93, 3.94 (2 s, 6H, 3′, 4′-OCH_3), 6.94 (d, 1H, ^3J = 8.3 Hz, 5′-H), 7.02-7.10 (m, 2H, 6, 6′-H), 7.21 (d, 1H, ^4J = 1.8 Hz, 2′-H), 8.04 (s, 1H, 2-H), 8.15 ppm (d, 1H, ^3J = 8.3 Hz, 5-H); ^{13}C NMR (400 MHz, $CDCl_3$): δ = 16.51, 28.42, 32.20, 41.17, 50.60, 55.94, 55.96, 108.31, 109.99, 111.18, 112.39, 114.45, 121.02, 121.07, 124.17, 125.20, 125.60, 148.80, 149.24, 152.51, 153.12, 154.62, 164.28, 175.76, 197.69 ppm; MS (CI): *m/z* 433.3 (*M*H$^+$, 100). Anal. Calcd for $C_{26}H_{24}O_6$: C, 72.21; H, 5.59. Found: C, 72.49; H, 5.22.

3-(1,3-Benzodioxol-5-yl)-9,9-dimethyl-8,9,10,12-tetrahydro-4 *H*,11 *H*-pyrano[2,3-*a*]xanthene-4,11-dione (13 c). Beige solid (80% yield); m.p. 258–260 °C; IR (KBr): $\tilde{\nu}_{max}$ = 2950, 2897, 1649, 1599, 1429, 1240, 1194, 1037 cm^{-1}; ^{1}H NMR (400 MHz, $CDCl_3$): δ = 1.17 (s, 6H, 9-CH_3), 2.39 (s, 2H, 10-CH_2), 2.50 (s, 2H, 8-CH_2), 3.64 (s, 2H, C, 12-CH_2), 6.00 (s, 2H, OCH_2O), 6.88 (d, 1H, ^3J = 8.0 Hz, 5′-H), 6.99 (dd, 1H, ^4J = 1.7 Hz, ^3J = 8.0 Hz, 6′-H), 7.05 (d, 1H, ^3J = 8.8 Hz, 6-H), 7.10 (d, 1H, ^4J = 1.7 Hz, 2′-H), 8.00 (s, 1H, 2-H), 8.15 ppm (d, 1H, ^3J = 8.8 Hz, 5-H); ^{13}C NMR (100 MHz, $CDCl_3$): δ = 16.52, 28.43, 32.21, 41.19, 50.61, 101.22, 108.33, 108.45, 109.71, 110.01, 114.46, 120.99,

122.42, 125.23, 125.32, 125.69, 147.74, 147.81, 152.49, 153.15, 154.65, 164.28, 175.62, 197.69 ppm; MS (CI): *m/z* 417.3 (MH^+, 100). Anal. Calcd for $C_{25}H_{20}O_6$: C, 72.11; H, 4.84. Found: C, 72.29; H, 5.11.

2,9,9-trimethyl-3-phenyl-8,9,10,12-tetrahydro-4 H,11 H-pyrano[2,3-a]xanthene-4,11-dione (13 f). Beige solid (84% yield); m.p. 265–266 °C; IR (KBr): $\tilde{\nu}_{max}$ = 3047, 2947, 2885, 1646, 1590, 1390, 1235, 1215, 700 cm^{-1}; ^1H NMR (400 MHz, $CDCl_3$): δ = 1.17 (s, 6H, 9-CH_3), 2.35 (s, 3H, 2-CH_3), 2.40 (s, 2H, 10-CH_2), 2.51 (s, 2H, 8-CH_2), 3.66 (s, 2H, 12-CH_2), 7.01 (d, 1H, ^3J = 8.8 Hz, 6-H), 7.26-7.30 (m, 2H, 2′, 6′-H), 7.35-7.40 (m, 1H, 4′-H), 7.41-7.47 (m, 2H, 3′, 5′-H), 8.08 ppm (d, 1H, ^3J = 8.8 Hz, 5-H); ^{13}C NMR (100 MHz, $CDCl_3$): δ = 16.48, 19.55, 28.42, 32.20, 41.22, 50.64, 108.34, 109.56, 113.99, 120.04, 123.73, 125.56, 127.85, 128.41, 130.34, 132.82, 152.94, 154.29, 163.30, 164.46, 176.08, 197.89 ppm; MS (CI): *m/z* 387.3 (MH^+, 100). Anal. Calcd for $C_{25}H_{22}O_4$: C, 77.70; H, 5.74. Found: C, 77.92; H, 5.88.

3-(4-Methoxyphenyl)-2,9,9-trimethyl-8,9,10,12-tetrahydro 4 H,11 H-pyrano[2,3–a]xanthene-4,11-dione (13 g). Beige solid (90% yield); m.p. 236–237 °C; IR (KBr): $\tilde{\nu}_{max}$ = 2958, 2890, 1653, 1586, 1515, 1440, 1393, 1239, 1174, 1026 cm^{-1}; ^1H NMR (400 MHz, $CDCl_3$): δ = 1.14 (s, 6H, 9-CH_3), 2.32 (s, 3H, 2-CH_3), 2.36 (s,2H, 10-CH_2), 2.47 (s, 2H, 8-CH_2), 3.62 (s, 2H, 12-CH_2), 3.82 (s, 3H, 4′-OCH_3), 6.92-6.99 (m, 3H, 6, 3′, 5′-H), 7.15-7.21 (m, 2H, 2′, 6′-H), 8.04 ppm (d, 1H, ^3J = 8.8 Hz, 5-H); ^{13}C NMR (100 MHz, $CDCl_3$): δ = 16.47, 19.56, 28.42, 32.19, 41.23, 50.65, 55.28, 108.36, 109.52, 113.92, 113.93, 120.02, 123.28, 124.91, 125.56, 131.50, 152.90, 154.26, 159.17, 163.25, 164.46, 176.30, 197.86 ppm; MS (CI): *m/z* 417.3 (MH^+, 100). Anal. Calcd for $C_{26}H_{24}O_5$: C, 74.98; H, 5.81. Found: C, 74.70; H, 6.10.

3-(4-Methoxyphenyl)-9,9,12-trimethyl-6,8,9,10-tetrahydro-4 H,7 H-pyrano[3,2-b]xanthene-4,7-dione (17 a). Beige solid (80% yield); m.p. 230–232 °C; IR (KBr): $\tilde{\nu}_{max}$ = 3079, 2958, 2835, 1645, 1612, 1514, 1463, 1391, 1296, 1220, 1179 cm^{-1}; ^1H NMR (400 MHz, $CDCl_3$): δ = 1.16 (s, 6H, 9-CH_3), 2.35 (s, 2H, 8-CH_2), 2.39 (s, 3H, 12-CH_3), 2.52 (s, 2H, 10-CH_2), 3.62 (s, 2H, 6-CH_2), 3.84 (s, 3H, 4′-OCH_3), 6.97 (d, 2H, ^3J = 8.8 Hz, 3′, 5′-H), 7.50 (d, 2H, ^3J = 8.8 Hz, 2′, 6′-H), 7.96 (s, 1H, 5-H), 8.00 ppm (s, 1H, 2-H); ^{13}C NMR (100 MHz, $CDCl_3$): δ = 8.32, 20.97, 28.45, 32.20, 41.29, 50.62, 55.34, 109.16, 113.99, 114.18, 118.85, 120.88, 124.05, 124.16, 124.49, 130.05, 151.43, 152.48, 153.96, 159.62, 163.91, 175.92, 197.56 ppm; MS (CI): *m/z* 417.3 (MH^+, 100). Anal. Calcd for $C_{26}H_{14}O_5$: C, 74.98; H, 5.81. Found: C, 75.22; H, 5.64.

3-(4-Methoxyphenyl)-2,9,9,12-tetramethyl-6,8,9,10-tetrahydro-4 H,7 H-pyrano[3,2-b]xanthene-4,7-dione (17 g). Beige solid (72% yield); m.p. 270–272 °C; IR (KBr): $\tilde{\nu}_{max}$ = 2954, 2878, 1642, 1609, 1395, 1238, 1220, 1142 cm^{-1}; ^1H NMR (400 MHz, $CDCl_3$): δ = 1.16 (s, 6H, 9-CH_3), 2.34 (s, 3H, 2-CH_3), 2.36 (s, 2H, 8-CH_2), 2.40 (s, 3H, 12-CH_3), 2.52 (2H, 10-CH_2), 3.61 (s, 2H, 6-CH_2), 3.85 (s, 3H, 4′-OCH_3), 6.97 (d, 2H, ^3J = 8.7 Hz, 3′, 5′-H), 7.20 (d, 2H, ^3J = 8.7 Hz, 2′, 6′-H), 7.89 ppm (s, 1H, 5-H); ^{13}C NMR (100 MHz, $CDCl_3$): δ = 8.33, 19.54, 20.95, 28.47, 32.20, 41.33, 50.63, 55.29, 109.19, 113.70, 113.91, 118.35, 119.84, 122.75, 124.08, 125.16, 131.54, 151.26, 153.58, 159.11, 163.11, 163.96, 176.53, 197.61 ppm; MS (CI): *m/z* 431.1 (MH^+, 100). Anal. Calcd for $C_{27}H_{26}O_5$: C, 75.33; H, 6.09. Found: C, 75.52; H, 5.87.

General procedure for synthesis of Diels–Alder adducts 14 and 15. To a solution of **5** (2 mmol) in DMF (10 mL) was added 1-morpholinocyclopentene or 1-morpholinocyclohexene (2.2 mmol, 1.1 eq). The mixture was heated at 154 °C for 4 h. The solvent was evaporated in vacuo, and residue was purified by chromatography using MeOH/CH_2Cl_2 1:50 to afford **14** or **15**.

7-Hydroxy-3-(4-methoxyphenyl)-2-methyl-8-[(2-oxocyclopentyl)-methyl]-4 H-chromen-4-one (14 g). Pale yellow solid (58% yield); m.p. 210–211 °C; IR (KBr): $\tilde{\nu}_{max}$ = 2960, 1735, 1631, 1580, 1512, 1436, 1291, 1244 cm^{-1}; ^1H NMR (400 MHz, $CDCl_3$): δ = 1.62-2.25 (m, 4H, 4″, 5″-CH_2), 2.33 (s, 3H, 2-CH_3), 2.38-2.63 (m, 2H, 3″-CH_2), 3.01-3.17 (m, 2H, 8-CH_2), 3.37-3.74 (m, 1H, 1″-H), 3.84 (s, 3H, 4′-OCH_3), 6.91-7.00 (m, 3H, 6, 3′, 5′-H), 7.21 (d, 2H, ^3J = 8.6 Hz, 2′, 6′-H), 7.99 ppm (d, 1H, ^3J = 8.7 Hz, 5-H); ^{13}C NMR (125 MHz, [D_6]DMSO): δ = 19.15, 20.05, 22.40, 28.91, 37.40, 48.03, 55.04, 113.25, 113.43, 113.69, 115.56, 121.25, 124.27, 125.31, 131.67, 155.07, 158.46, 159.94, 162.29, 175.36, 219.25 ppm; MS (CI): *m/z* 379.1 (MH^+, 100). Anal. Calcd for $C_{23}H_{22}O_5$: C, 73.00; H, 5.86. Found: C, 73.26; H, 5.62.

3-(3,4-Dimethoxyphenyl)-7-hydroxy-2-methyl-8-[(2-oxocyclopentyl)methyl]-4 H-chromen-4-one (14 h). Pale yellow solid (53% yield); m.p. 88–90 °C; IR (KBr): $\tilde{\nu}_{max}$ = 2924, 1736, 1633, 1515, 1440, 1265 cm^{-1}; ^1H NMR (400 MHz, [D_6]DMSO): δ = 1.51-2.07 (m, 4H, 4″, 5″-CH_2), 2.27 (s, 3H, 2-CH_3), 2.66-3.16 (m, 4H, 8, 3″-CH_2), 3.36-3.60 (m, 1H, 1″-H), 3.74, 3.79 (2 s, 6H, 3′, 4′- OCH_3), 6.74-6.88 (m, 2H, 2′, 6′-H), 6.93-7.03 (m, 2H, 6, 5′-H), 7.76 (d, 1H, ^3J = 8.7 Hz, 5-H), 10.64 ppm (s, 1H, 7-OH); ^{13}C NMR (125 MHz, [D_6]DMSO): δ = 19.63, 20.47, 29.33, 37.83, 48.43, 55.93, 55.97, 111.89, 113.68, 114.12, 114.80, 116.05, 122.01, 123.24, 124.70, 126.17, 148.54, 148.68, 155.50, 160.34, 162.85, 175.75, 219.65 ppm; MS (CI): *m/z* 409.2 (MH^+, 100). Anal. Calcd for $C_{24}H_{24}O_6$: C, 70.58; H, 5.92. Found: C, 70.28; H, 6.18.

7 a-Hydroxy-3-(4-methoxyphenyl)-8,9,10,11,11 a,12-hexahydro-4 H,7 aH-pyrano[2,3-a]xanthen-4-one (15 a). Pale yellow solid (91% yield); m.p. 222–223 °C; IR (KBr): $\tilde{\nu}_{max}$ = 2987, 1613, 1513, 1439, 1251, 1030 cm^{-1}; ^1H NMR (400 MHz, $CDCl_3$): δ = 1.30-2.18 (m, 9H, 8, 9, 10, 11-CH_2, 11a-CH), 2.35-3.26 (m, 2H, 12-CH_2), 3.85 (s, 3H, 4′-OCH_3), 6.81-6.89 (m, 1H, 6-H), 6.98 (d, 2H, ^3J = 8.6 Hz, 3′, 5′-H), 7.51 (d, 2H, ^3J = 8.6 Hz, 2′, 6′-H), 7.96 (s, 1H, 2-H), 8.02-8.09 ppm (m, 1H, 5-H); ^{13}C NMR (125 MHz, [D_6]DMSO): δ = 21.82 (21.73), 22.82 (23.00), 24.93 (24.30), 29.11 (28.59), 36.33 (35.45), 37.51 (37.28), 55.13, 98.10 (97.70), 111.20 (108.97), 113.58, 115.63 (115.65), 117.11 (117.33), 123.13 (123.18), 123.84, 124.16, 130.06 (130.08), 153.15, 154.26 (154.95), 156.84 (156.37), 158.96, 174.88 ppm (174.86); MS (CI): *m/z* 349.2 (MH^+, 100). Anal. Calcd for $C_{23}H_{22}O_5$: C, 73.00; H, 5.86. Found: C, 72.71; H, 5.98.

3-(3,4-Dimethoxyphenyl)-7 a-hydroxy-8,9,10,11,11 a,12-hexahydro-4 H,7 aH-pyrano[2,3-a]xanthen-4-one (15 b). Pale yellow solid (85% yield); m.p. 214–216 °C; IR (KBr): $\tilde{\nu}_{max}$ = 2930, 1629, 1612, 1516, 1439, 1263, 1143, 1027 cm^{-1}; ^1H NMR (400 MHz, [D_6]DMSO): δ = 1.40–2.62 (m, 9H, 8, 9, 10, 11-CH_2, 11a-CH), 2.70-3.60 (m, 2H, 12-CH_2), 3.75 (s, 6H, 3′, 4′-OCH_3), 6.84-6.99, 7.07–7.19 (2 m, 4H, 6, 2′, 5′, 6′-H), 7.81-7.87 (m, 1H, 5-H), 8.42, 8.43 ppm (2 s, 1H, 2-H); ^{13}C NMR (125 MHz, [D_6]DMSO): δ = 22.22 (22.13), 23.25 (23.42), 25.35 (24.73), 29.54 (29.02), 36.76 (35.87), 37.94 (37.71), 55.96, 55.96, 98.54 (98.13), 109.39 (109.30), 111.95 (111.62), 113.17, 116.10 (116.07), 117.56 (117.78), 121.63 (121.66), 123.63 (123.63), 124.28, 124.90 (124.91), 148.68, 149.03, 153.79, 154.63 (155.32), 157.27 (156.79), 175.28 ppm (175.26); MS (CI): *m/z* 409.2 (MH^+, 100). Anal. Calcd for $C_{24}H_{24}O_6$: C, 70.58; H, 5.92. Found: C, 70.31; H, 6.21.

3-(1,3-Benzodioxol-5-yl)-7 a-hydroxy-8,9,10,11,11 a,12-hexahydro-4 H,7 aH-pyrano[2,3-a]xanthen-4-one (15 c). Pale yellow solid (76% yield); m.p. 197–197 °C; IR (KBr): $\tilde{\nu}_{max}$ = 2937, 1630, 1587, 1435, 1251, 1027 cm^{-1}; ^1H NMR (400 MHz, [D_6]DMSO): δ = 1.23-2.62

(m, 9H, 8, 9, 10, 11-CH_2, 11a-CH), 2.70-3.60 (m, 2H, 12-CH_2), 6.05 (s, 2H, OCH_2O), 6.88-7.18 (2 m, 4H, 6, 2′, 5′, 6′-H), 7.81-7.99 (m, 1H, 5-H), 8.41, 8.45 ppm (2 s, 1H, 2-H); ^{13}C NMR (125 MHz, [D_6]DMSO): δ = 22.24 (22.14), 23.24 (23.42), 25.35 (24.72), 29.53 (29.02), 36.76 (35.88), 37.95 (37.70), 98.56 (98.15), 101.45, 108.51, 109.83 (109.86), 111.65, 116.13 (116.10), 117.49 (117.72), 122.81 (122.84), 123.58 (123.63), 124.29, 126.11 (126.13), 147.34, 147.41, 153.86 (153.64), 154.64 (155.33), 157.32 (156.86), 175.16 ppm (175.15); MS (CI): *m/z* 393.2 (*M*H$^+$, 100). Anal. Calcd for $C_{23}H_{20}O_6$: C, 70.40; H, 5.14. Found: C, 70.14; H, 4.85.

7a-Hydroxy-3-(4-methoxyphenyl)-2-methyl-8,9,10,11,11a,12-hexahydro-4*H*,7a*H*-pyrano[2,3-*a*]xanthen-4-one (15g). Pale yellow solid (69% yield); m.p. 212–213 °C; IR (KBr): $\tilde{\nu}_{max}$ = 2924, 1632, 1608, 1514, 1435, 1251, 1177 cm^{-1}; ^{1}H NMR (400 MHz, $CDCl_3$): δ = 1.57-2.17 (m, 9H, 8, 9, 10, 11-CH_2, 11a-CH), 2.33 (s, 3H, 2-CH_3), 2.54- 3.27 (m, 2H, 12-CH_2), 3.85 (s, 3H, 4′-OCH_3), 6.70-6.81 (m, 1H, 6-H), 6.97 (d, 2H, ^3J = 8.5 Hz, 3′, 5′-H), 7.21 (d, 2H, ^3J = 8.5 Hz, 2′, 6′-H), 7.87-7.97 ppm (m, 1H, 5-H); ^{13}C NMR (400 MHz, $CDCl_3$): δ = 19.43 (19.44), 22.12 (21.97), 23.09 (23.34), 25.51 (24.92), 29.44 (29.13), 36.64 (38.54), 37.80 (37.85), 55.29, 97.93 (97.76), 110.68 (108.50), 113.85, 115.24 (115.21), 116.93 (117.14), 122.74 (122.77), 124.61 (124.70), 125.50 (125.51), 131.61, 154.48 (155.18), 155.81 (156.39), 159.02, 162.51 (162.51), 177.10 ppm (177.07); MS (CI): *m/z* 393.2 (*M*H$^+$, 100). Anal. Calcd for $C_{24}H_{24}O_5$: C, 73.45; H, 6.16. Found: C, 73.18; H, 6.42.

3-(3,4-Dimethoxyphenyl)-7a-hydroxy-2-methyl-8,9,10,11,11a,12-hexahydro-4*H*,7a*H*-pyrano[2,3-*a*]xanthen-4-one (15h). Pale yellow solid (51% yield); m.p. 193–194 °C; IR (KBr): $\tilde{\nu}_{max}$ = 2938, 1631, 1610, 1577, 1514, 1437, 1264, 1028 cm^{-1}; ^{1}H NMR (400 MHz, $CDCl_3$): δ = 1.30-2.16 (m, 9H, 8, 9, 10, 11-CH_2, 11a-CH), 2.34 (s, 3H, 2-CH_3), 2.53-3.28 (m, 2H, 12-CH_2), 3.88, 3.92 (2 s, 6H, 3′, 4′-OCH_3), 6.62-6.99 (m, 1H, 6-H), 6.78-6.86, 6.90-6.96 (2 m, 3H, 2′, 5′, 6′-H), 7.84-7.92 ppm (m, 1H, 5-H); ^{13}C NMR (125 MHz, [D_6]DMSO): δ = 19.19 (19.21), 21.76 (21.69), 22.80 (22.99), 24.96 (24.32), 29.10 (28.59), 36.36 (35.46), 37.57 (37.31), 55.47, 55.50, 97.97 (97.58), 110.87 (108.64), 111.41, 114.31, 115.20 (115.17), 116.05 (116.27), 122.02 (122.08), 122.80, 123.64, 125.65 (125.67), 148.13, 148.22, 153.81 (154.50), 156.65 (156.16), 162.53, 175.20 ppm (175.17); MS (CI): *m/z* 423.2 (*M*H$^+$, 100). Anal. Calcd for $C_{25}H_{26}O_6$: C, 71.07; H, 6.20. Found: C, 71.33; H, 6.07.

Cell proliferation assay. PC-3 human prostate cancer cells (ATCC CRL-1435; ATCC, Manassas, VA) were grown in Dulbecco's modified Eagle medium nutrient mixture F-12 (DMEM/F-12 HAM) (Sigma D8437) with 10% fetal bovine serum (Atlanta Biological S11150). For cell proliferation assays, 3.5×10^4 cells per well were placed into 12-well plates. After 1 d, 10 μM of each compound was added to each well. DMSO was used as a control. The experiments were performed in triplicate. Cell viability and number were analyzed using Vi-Cell XR Cell Viability Analyzer (Beckman Coulter) as previously described.[8a] Inhibition data represent the mean ± SD for at least three experiments.

Acknowledgements

D.S.W. and C.L. were supported by R21 CA139359 and CA172379 from the US National Institutes of Health (NIH), by the Office of the Dean of the College of Medicine (University of Kentucky), and by NIH Grant Number P30 GM110787. J.L.M. and M.V.F. were supported by P01 CA77739 from the NIH. The contents are solely the responsibility of the authors and do not necessarily represent the official views of the NIH or the National Institute of General Medical Sciences (NIGMS).

Keywords: inverse electron-demand Diels–Alder reaction · isoflavonoids · Mannich reactions · *ortho*-quinone methides · prostate cancer PC-3 cell line

[1] a) J. L. Mohler, C. W. Gregory, O. H. Ford, D. Kim, C. M. Weaver, P. Petrusz, E. M. Wilson, F. S. French, *Clin. Cancer Res.* **2004**, *10*, 440–448; b) M. A. Titus, M. J. Schell, F. B. Lih, K. B. Tomer, J. L. Mohler, *Clin. Cancer Res.* **2005**, *11*, 4653–4657.

[2] a) V. C. O. Njar, M. Hector, R. W. Hartmann, *Bioorg. Med. Chem.* **1996**, *4*, 1447–1453; b) G. Attard, A. H. M. Reid, R. A'Hern, C. Parker, N. B. Oommen, E. Folkerd, C. Messiou, L. R. Molife, G. Maier, E. Thom.p. son, D. Olmos, R. Sinha, G. Lee, M. Dowsett, S. B. Kaye, D. Dearnaley, T. Kheoh, A. Molina, J. S. de Bono, *J. Clin. Oncol.* **2009**, *27*, 3742–3748; c) M. Jarman, S. E. Barrie, J. M. Llera, *J. Med. Chem.* **1998**, *41*, 5375–5381; d) P. Purushottamachar, A. Khandelwal, T. S. Vasaitis, R. D. Bruno, L. K. Gediya, V. C. O. Njar, *Bioorg. Med. Chem.* **2008**, *16*, 3519–3529.

[3] a) G. Attard, A. H. M. Reid, T. A. Yap, F. Raynaud, M. Dowsett, S. Settatree, M. Barrett, C. Parker, V. Martins, E. Folkerd, J. Clark, C. S. Cooper, S. B. Kaye, D. Dearnaley, G. Lee, J. S. de Bono, *J. Clin. Oncol.* **2008**, *26*, 4563–4571; b) J. S. de Bono, C. J. Logothetis, A. Molina, K. Fizazi, S. North, L. Chu, K. N. Chi, R. J. Jones, O. B. Goodman, F. Saad, J. N. Staffurth, P. Mainwaring, S. Harland, T. W. Flaig, T. E. Hutson, T. Cheng, H. Patterson, J. D. Hainsworth, C. J. Ryan, C. N. Sternberg, S. L. Ellard, A. Fléchon, M. Saleh, M. Scholz, E. Efstathiou, A. Zivi, D. Bianchini, Y. Loriot, N. Chieffo, T. Kheoh, C. M. Haqq, H. I. Scher, *N. Engl. J. Med.* **2011**, *364*, 1995–2005; c) C. J. Ryan, M. R. Smith, J. S. de Bono, A. Molina, C. J. Logothetis, P. de Souza, K. Fizazi, P. Mainwaring, J. M. Piulats, S. Ng, J. Carles, P. F. A. Mulders, E. Basch, E. J. Small, F. Saad, D. Schrijvers, H. Van Poppel, S. D. Mukherjee, H. Suttmann, W. R. Gerritsen, T. W. Flaig, D. J. George, E. Y. Yu, E. Efstathiou, A. Pantuck, E. Winquist, C. S. Higano, M.-E. Taplin, Y. Park, T. Kheoh, T. Griffin, H. I. Scher, D. E. Rathkopf, *N. Engl. J. Med.* **2013**, *368*, 138–148.

[4] R. Siegel, J. Ma, Z. Zou, A. Jemal, *Ca-Cancer J. Clin.* **2014**, *64*, 9–29.

[5] M. V. Fiandalo, J. Wilton, J. L. Mohler, *Int. J. Biol. Sci.* **2014**, *10*, 596–601.

[6] a) I. C. Munro, M. Harwood, J. J. Hlywka, A. M. Stephen, J. Doull, W. G. Flamm, H. Adlercreutz, *Nutr. Rev.* **2003**, *61*, 1–33; b) H. Adlercreutz, *Scand. J. Clin. Lab. Invest.* **1990**, *50*, 3–23; c) S. Andres, K. Abraham, K. E. Appel, A. Lam.p. en, *Crit. Rev. Toxicol.* **2011**, *41*, 463–506.

[7] J. M. Hamilton-Reeves, S. A. Rebello, W. Thomas, J. W. Slaton, M. S. Kurzer, *J. Nutr.* **2007**, *137*, 1769–1775.

[8] a) W. Zhang, V. Sviripa, X. Chen, J. Shi, T. Yu, A. Hamza, N. D. Ward, L. M. Kril, C. W. Vander Kooi, C.-G. Zhan, B. M. Evers, D. S. Watt, C. Liu, *ACS Chem. Biol.* **2013**, *8*, 796–803; b) R. Burikhanov, V. M. Sviripa, N. Hebbar, W. Zhang, W. J. Layton, A. Hamza, C.-G. Zhan, D. S. Watt, C. Liu, V. M. Rangnekar, *Nat. Chem. Biol.* **2014**, *10*, 924–926.

[9] a) W. Zhang, V. Sviripa, L. M. Kril, X. Chen, T. Yu, J. Shi, P. Rychahou, B. M. Evers, D. S. Watt, C. Liu, *J. Med. Chem.* **2011**, *54*, 1288–1297; b) V. M. Sviripa, W. Zhang, A. G. Balia, O. V. Tsodikov, J. R. Nickell, F. Gizard, T. Yu, E. Y. Lee, L. P. Dwoskin, C. Liu, D. S. Watt, *J. Med. Chem.* **2014**, *57*, 6083–6091.

[10] a) A. Sandulache, A. M. S. Silva, J. A. S. Cavaleiro, *Tetrahedron* **2002**, *58*, 105–114; b) R. M. Kamble, M. M. V. Ramana, *Can. J. Chem.* **2010**, *88*, 1233–1239; c) R. A. Valiulin, T. M. Arisco, A. G. Kutateladze, *J. Org. Chem.* **2011**, *76*, 1319–1332; d) P. J. Cremins, S. T. Saengchantara, T. W. Wallace, *Tetrahedron* **1987**, *43*, 3075–3082; e) R. P. Hsung, *J. Org. Chem.* **1997**, *62*, 7904–7905.

[11] a) M. Von Strandtmann, M. P. Cohen, J. Shavel, *J. Heterocycl. Chem.* **1970**, *7*, 1311–1319; b) V. A. Osyanin, E. A. Ivleva, Y. N. Klimochkin, *Synth. Commun.* **2012**, *42*, 1832–1847; c) P. D. Gardner, H. S. Rafsanjani, L. Rand, *J. Am. Chem. Soc.* **1959**, *81*, 3364–3367; d) V. A. Osyanin, D. V. Osipov, Y. N. Klimochkin, *J. Org. Chem.* **2013**, *78*, 5505–5520.

[12] a) V. Kumbaraci, D. Ergunes, M. Midilli, S. Begen, N. Talinli, *J. Heterocycl. Chem.* **2009**, *46*, 226–230; b) A. k. Shaikh, A. J. A. Cobb, G. Varvounis, *Org. Lett.* **2012**, *14*, 584–587; c) C. D. Bray, *Org. Biomol. Chem.* **2008**, *6*,

2815 – 2819; d) L. René, *Synthesis* **1989**, 69 – 70; e) R. Rodriguez, R. M. Adlington, J. E. Moses, A. Cowley, J. E. Baldwin, *Org. Lett.* **2004**, *6*, 3617 – 3619.

[13] H. Sugimoto, S. Nakamura, T. Ohwada, *Adv. Synth. Catal.* **2007**, *349*, 669 – 679.

[14] a) X. Wu, X. Liu, G. Jiang, Y. Lin, W. Chan, L. L. P. Vrijmoed, *Chem. Br. Chem. Nat. Com.p.d.* **2005**, *41*, 27 – 29; b) X. Y. Wu, X. H. Liu, Y. C. Lin, J. H. Luo, Z. G. She, L. Houjin, W. L. Chan, S. Antus, T. Kurtan, B. Elsässer, K. Krohn, *Eur. J. Org. Chem.* **2005**, 4061 – 4064; c) Y. Lin, X. Wu, S. Feng, G. Jiang, J. Luo, S. Zhou, L. L. P. Vrijmoed, E. B. G. Jones, K. Krohn, K. Steingröver, F. Zsila, *J. Org. Chem.* **2001**, *66*, 6252 – 6256; d) Z.-X. Li, J.-W. Chen, F. Yuan, Y.-Y. Huang, L.-Y. Zhao, J. Li, H.-X. Su, J. Liu, J.-Y. Pang, Y.-C. Lin, X.-L. Lu, Z. Pei, G.-L. Wang, Y.-Y. Guan, *Mar. Drugs* **2013**, *11*, 504 – 522; e) X. Liu, F. Xu, Y. Zhang, L. Liu, H. Huang, X. Cai, Y. Lin, W. Chan, *Russ. Chem. Bull.* **2006**, *55*, 1091 – 1092.

[15] M. Frasinyuk, G. P. Mrug, S. P. Bondarenko, V. M. Sviripa, W. Zhang, X. Cai, M. Fiandalo, J. L. Mohler, C. Liu, D. Watt, *Org. Biomol. Chem.* **2015**, *13*, 11292 – 11301.

Received: January 6, 2016
Revised: February 8, 2016
Published online on February 17, 2016

Organic & Biomolecular Chemistry

PAPER

View Article Online
View Journal

Cite this: DOI: 10.1039/c7ob01584d

Developing antineoplastic agents that target peroxisomal enzymes: cytisine-linked isoflavonoids as inhibitors of hydroxysteroid 17-beta-dehydrogenase-4 (HSD17B4)†

Mykhaylo S. Frasinyuk,‡[a,b,c] Wen Zhang,‡[a,d] Przemyslaw Wyrebek,‡[a,b] Tianxin Yu,‡[a,d] Xuehe Xu,[a,d] Vitaliy M. Sviripa,[b,e] Svitlana P. Bondarenko,[f] Yanqi Xie,[a,b,d] Huy X. Ngo,[e] Andrew J. Morris,[g] James L. Mohler,[h] Michael V. Fiandalo,[h] David S. Watt*[a,b,d] and Chunming Liu*[a,d]

Received 29th June 2017,
Accepted 24th August 2017

DOI: 10.1039/c7ob01584d

rsc.li/obc

Cytisine-linked isoflavonoids (CLIFs) inhibited PC-3 prostate and LS174T colon cancer cell proliferation by inhibiting a peroxisomal bifunctional enzyme. A pull-down assay using a biologically active, biotin-modified CLIF identified the target of these agents as the bifunctional peroxisomal enzyme, hydroxysteroid 17β-dehydrogenase-4 (HSD17B4). Additional studies with truncated versions of HSD17B4 established that CLIFs specifically bind the C-terminus of HSD17B4 and selectively inhibited the enoyl CoA hydratase but not the D-3-hydroxyacyl CoA dehydrogenase activity. HSD17B4 was overexpressed in prostate and colon cancer tissues, knocking down HSD17B4 inhibited cancer cell proliferation, suggesting that HSD17B4 is a potential biomarker and drug target and that CLIFs are potential probes or therapeutic agents for these cancers.

Introduction

A program to develop semisynthetic, natural products as antineoplastic agents[1,2] with unexpected biological targets utilized the inhibition of cancer cell proliferation as a screening tool to identify semisynthetic isoflavonoids as potential candidates. Naturally occurring isoflavones appear largely in plants belonging to the Fabaceae family and have a long, albeit dubious, history as compounds for the treatment of human diseases.[3,4] Isoflavones, such as daidzein **1** and genistein **2** (Fig. 1A), have alleged health benefits for the treatment of cancer,[5–8] but the spectrum of biological activities ascribed to isoflavones raises cautionary concerns when exploring these natural products as potential drugs. The synthetic modifications of isoflavones to include pharmacophores not found in nature provide semi-

[a]Department of Molecular and Cellular Biochemistry, College of Medicine, University of Kentucky, Lexington, KY 40536-0509, USA. E-mail: dwatt@uky.edu, chunming.liu@uky.edu
[b]Center for Pharmaceutical Research and Innovation, College of Pharmacy, University of Kentucky, Lexington, KY 40536-0596, USA
[c]Institute of Bioorganic Chemistry and Petrochemistry, National Academy of Science of Ukraine, Kyiv 02094, Ukraine
[d]Lucille Parker Markey Cancer Center, University of Kentucky, Lexington, KY 40536-0093, USA
[e]Department of Pharmaceutical Sciences, College of Pharmacy, University of Kentucky, Lexington, KY 40535-0596, USA
[f]National University of Food Technologies, Kyiv, 01601, Ukraine
[g]Department of Pharmacology and Nutritional Sciences, College of Medicine, University of Kentucky, Lexington, KY 40536-0596, USA
[h]Department of Urology, Roswell Park Cancer Institute, Buffalo, NY 14263, USA

†Electronic supplementary information (ESI) available: General procedure for the synthesis and characterization of isoflavones. See DOI: 10.1039/c7ob01584d

‡Contributed equally to this work.

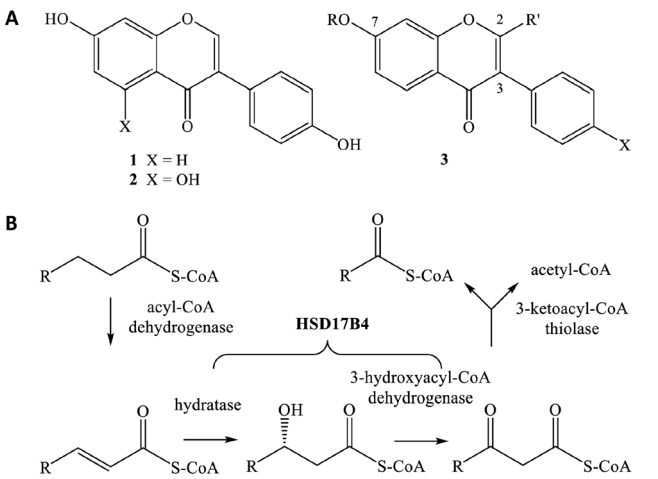

Fig. 1 A. Naturally occurring isoflavones **1** and **2** and semisynthetic isoflavonoid **3**. B. Biological function of HSD17B4.

synthetic isoflavonoids **3** (Fig. 1A) with the potential to escape this polypharmacology. Structure–activity studies[1,2] utilizing cancer cell proliferation as a guide established that the inclusion of C-3 *para*-chlorophenyl and C-7 ω-(*N*,*N*-dialkylamino)alkoxy groups in the semisynthetic isoflavonoid scaffold **3** led to potent agents in either PC-3 prostate cancer or LS174T colorectal cancer cell proliferation assays. After examining different C-7 ω-(*N*,*N*-dialkylamino)alkoxy substituents, we found that the inclusion of the alkaloid, (−)-cytisine, in the C-7 side-chain produced potent cytisine-linked isoflavonoids (CLIFs). We now report that CLIFs specifically inhibit the enoyl CoA hydratase activity in the peroxisomal bifunctional enzyme, hydroxysteroid 17β-dehydrogenase-4 (HSD17B4). HSD17B4 plays a normal role in the catabolism[9,10] of very long-chain fatty acids (Fig. 1B), branched fatty acids, and steroid hormones,[11] and its overexpression in prostate cancer cells compared to matched, benign epithelia cells may play a potential role in prostate cancer progression.[12] Small molecules such as the CLIFs that selectively inhibit HSD17B4 provide a useful tool for studying HSD17B4 as a therapeutic target.

Results

Initial structure–activity (SAR) studies focused on modifications at C-2, C-3, and C-7 in the isoflavonoid scaffold **3** (Fig. 1A). The synthesis of these isoflavonoids required the condensation of resorcinol with substituted phenylacetic acids **4** to furnish deoxybenzoins **5** (Fig. 2A).[13,14] The subsequent condensation of deoxybenzoins **5** either with *N*,*N*-dimethylformamide[2] under acidic conditions or with acetic anhydride[15] under basic conditions provided isoflavonoids **3** (Fig. 2A). Preliminary screening using cell proliferation assays as guides identified the most active isoflavonoids **3** as those with hydrogen or methyl groups at C-2, *para*-chlorophenyl groups at C-3, and hydroxyl groups at C-7. Most isoflavonoids **3** exhibited substantial cancer cell inhibition only at relatively high concentrations (30–50 μM; data not shown).

Isoflavonoids **3c** (R = H and X = Cl) and **3d** (R = CH_3 and X = Cl) displayed the modest inhibition of PC-3 cells at 10 μM (Fig. 2B). Additional modifications that improved potency in PC-3 cell inhibition included the attachment of various ω-(*N*,*N*-dialkylamino)alkyl groups to the C-7 hydroxyl group in **3** through the spacers of varied carbon-chain lengths. The alkylation of isoflavonoids **3** with 1,2-dibromoethane afforded 7-(2-bromoethoxy)isoflavonoids **6**. The condensation of **6** with either piperazine or *N*-(2-hydroxyethyl)piperazine afforded 2-(piperazin-1-yl)ethoxy-substituted isoflavonoids **7c** and **8**, respectively (Fig. 2A). These piperazine-substituted isoflavonoids **7c** and **8** inhibited PC-3 cells at lower concentrations (*i.e.*, <10 μM) than those at which the unmodified isoflavonoids **3** were active (Fig. 2B). We examined naturally occurring alkaloids as potential partners for the *N*-alkylation of 7-(2-bromoethoxy)isoflavonoids **6** in addition to screening

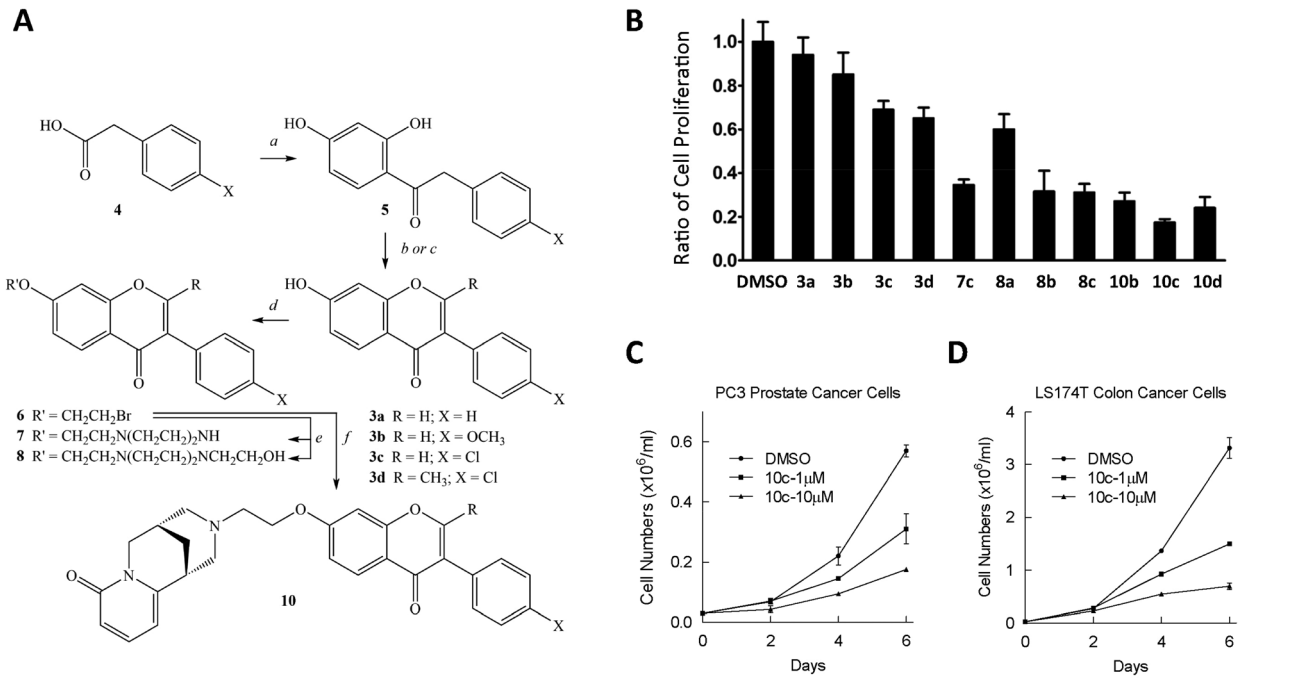

Fig. 2 A. Synthesis of isoflavonoids. Substituent key: a: R = H and X = H; b: R = H and X = OCH_3; c: R = H and X = Cl; and d: R = CH_3 and X = Cl. Reagent legend: a, resorcinol, BF_3-Et_2O (yields: 49–60%); b, DMF, BF_3-Et_2O, $POCl_3$ (yields: 53–69%); c, Ac_2O, K_2CO_3, DMF (yield: 88% for **3d**); d, K_2CO_3, $BrCH_2CH_2Br$ (yields: 62–88%); e, piperazine, NaI, K_2CO_3, DMF (yield: 79% for **7c**); or *N*-(2-hydroxyethyl)piperazine, NaI, K_2CO_3, DMF (yield: 60–74%); f, cytisine, NaI, iPr_2NH, DMF (yield: 62–76%). Specific yields for individual compounds are given in the ESI.† B. Effects of isoflavonoids **3**, **7**, **8** and **10** on the proliferation of PC-3 prostate cancer cells. C and D. Effects of **10c** on the proliferation of PC-3 prostate and LS174T colon cancer cells.

similarly substituted isoflavonoids bearing other monocyclic, nitrogen-containing heterocycles (data not shown). The coupling of **6** with the alkaloid, (−)-cytisine **9**, afforded CLIF **10c** that displayed potent PC-3 cell inhibition in the low μM range (Fig. 2B and C). CLIF **10c** also significantly inhibited the proliferation of other cancer cell lines, such as LS174T colon cancer cells (Fig. 2D). However, **10c** only weakly inhibited normal cell lines, BEAS-2B and BCL-299 (Table S1†). Cytisine **9** alone had limited activity for cancer cell inhibition (Table S1†).

The identification of the cellular target or targets of CLIF **10c** required a biotinylated analog that retained biological activity as an inhibitor of cell proliferation. It was important to position the biotin moiety within CLIF **10c** sufficiently far from the isoflavonoid pharmacophore to permit the capture of the targets using streptavidin-bound beads. After experimentation to find the appropriate combination of the spacer length and covalent attachment site (data not shown), we found that the alkylation of isoflavonoid **3d** with a six-carbon spacer attached to the C-7 hydroxyl group met these preconditions. The alkylation of the C-7 hydroxyl group in isoflavonoid **3d** with 6-bromo-1-hexene furnished 5-hexenyloxyisoflavonoid **11d**, and the treatment of **11d** with *meta*-chloroperoxybenzoic acid afforded the epoxide **12d** (Fig. 3A). The regiospecific alkylation of **12d** with (−)-cytisine (**9**) gave the intermediate secondary alcohol **13d** as a mixture of (1*R*,5*S*,2′ζ)-diastereomers. Oxidation with Dess–Martin's reagent removed the epimeric center at C-2 and afforded the ketone **14d**, and condensation

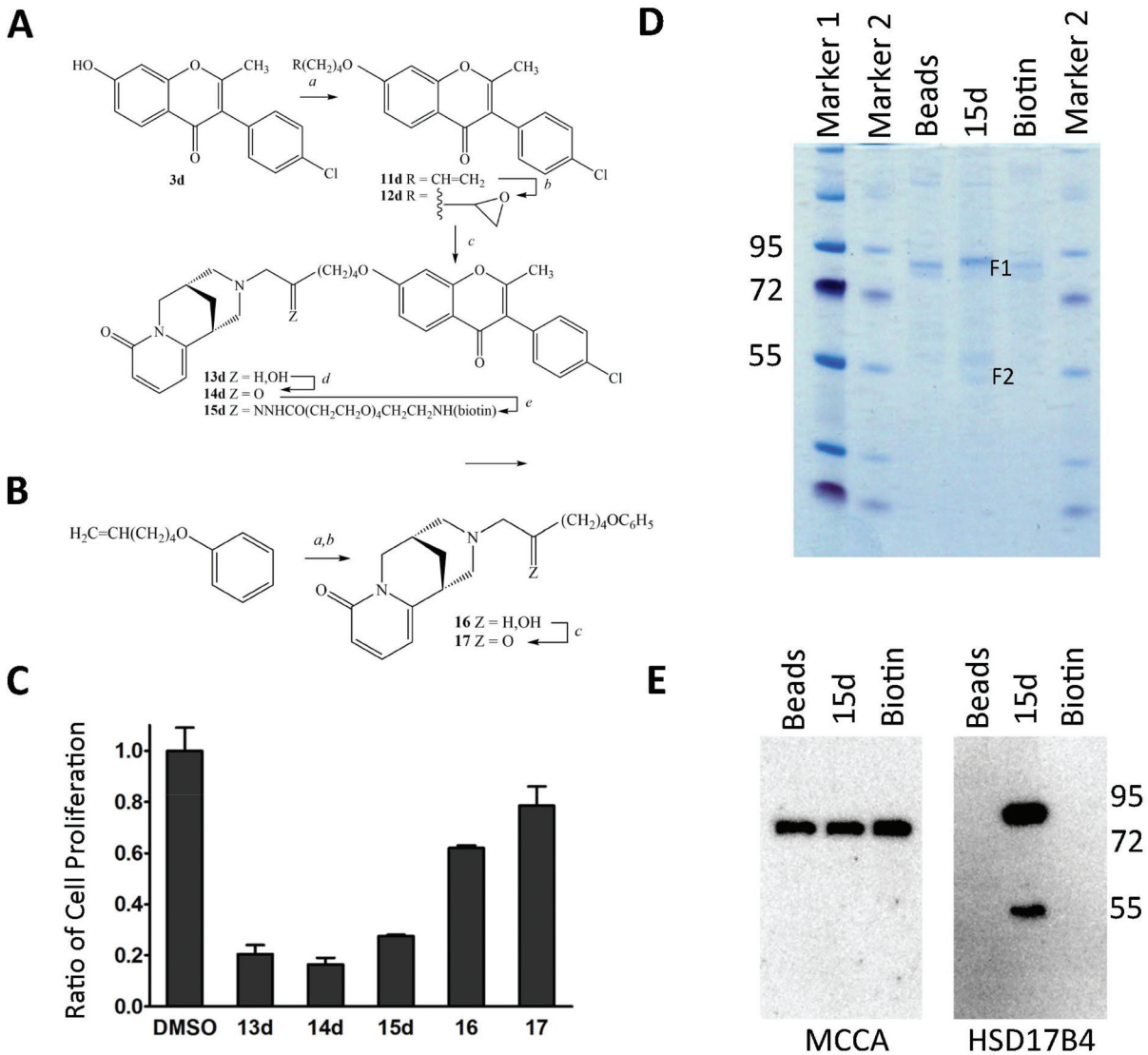

Fig. 3 A. Synthesis of a biotinylated cytisine-linked isoflavone **15d**. Reagent legend: a, K_2CO_3, 6-bromo-1-hexene (yield: 81%); b, MCPBA (yield: 76%); c, cytisine, EtOH, 90 °C, pressure tube (yield: 96%); d, Dess–Martin reagent (yield: 81%); e, PEG hydrazide, $CeCl_3$ (yield: 24%). B. Reagent legend: a, MCPBA (yield: 81%); b, cytisine, EtOH, 90 °C, pressure tube (yield: 98%); c, Dess–Martin reagent (yield: 57%). Specific yields for individual compounds are given in the ESI.† C. Effects of isoflavonoids **13–17** on the proliferation of PC-3 cells. D. Purification of binding proteins of isoflavonoids. E. Validation of potential targets using western blotting.

with a D-biotin-PEG-hydrazide afforded the biotinylated CLIF **15d** as a mixture of *E* and *Z*-isomers. The intermediate alcohol **13d**, the ketone **14d**, and the biotinylated CLIF **15d** significantly inhibited PC-3 cell proliferation (Fig. 3C) at 10 μM. This level of activity was sufficient to implement a successful pull-down assay. Controls to establish the requirement for both the (−)-cytisinyl and isoflavonoid moieties for PC-3 cell inhibition required the synthesis of the cytisinyl-substituted alcohol **16** and ketone **17**, respectively (Fig. 3B). The alcohol **16** and ketone **17** possessed a phenoxy group in place of the isoflavonoid and proved less effective as PC-3 cell inhibitors (Fig. 3C).

Identification of the direct target of these CLIFs involved the incubation of biotinylated CLIF **15d** with LS174T cell lysates and a subsequent pull-down assay using streptavidin beads. The proteins that bound to these beads were eluted with 2.5 mM D-biotin and analyzed using 4–12% SDS-PAGE gel and colloidal blue staining (Fig. 3D). The gel displayed two specific bands (F1 and F2) in the CLIF **15d**-containing sample compared with the control samples that contained either beads alone or beads and D-biotin. These two bands were excised from gels and analyzed using mass spectrometry (NanoLC-ESI-MS/MS). The band F1 (Fig. 3D) contained two proteins: peroxisomal hydroxysteroid 17β-dehydrogenase-4 (HSD17B4) and mitochondrial methylcrotonoyl-CoA carboxylase subunit alpha (MCCA). The band F2 also contained HSD17B4.

Validation of these results included western blotting using antibodies against HSD17B4 and MCCA. The MCCA enzyme that appeared in both the CLIF **15d**-containing sample and the control sample was a non-specific binding protein of the streptavidin complex with CLIF **15d**. As a biotin-containing carboxylase, it was not surprising that MCCA bound to the streptavidin beads. The bifunctional HSD17B4 protein that appeared only in the CLIF **15d**-containing sample (Fig. 3E) was a specific binding protein of the biotinylated CLIF **15d**. The HSD17B4 antibody (GeneTex) recognized the full-length and the C-terminal cleaved fragment that contained the enoyl CoA hydratase domain (Fig. 3E).

The D-3-hydroxyacyl CoA dehydrogenase activity resided in the N-terminus of HSD17B4, and the enoyl CoA hydratase activity resided in the C-terminus.[9,10] The binding of biotinylated CLIF **15d** to a panel of truncated, purified HSD17B4 constructs and the full-length protein from *E. coli* (Fig. 4A) using the streptavidin bead-based pull-down assay demonstrated that the full-length HSD17B4, but not the C-terminus-truncated fragments, N318 and N634, interacted with CLIF **15d** (Fig. 4B). The N-terminus-truncated fragment C919 bound CLIF **15d** (Fig. 4C), a finding that established that the CLIFs bound to the C-terminus of HSD17B4 containing the enoyl CoA hydratase activity and the solute carrier protein-2-linked (SCP2L) domain.

Studies on the N-terminal D-3-hydroxyacyl CoA dehydrogenase fragment, the C-terminal enoyl CoA hydratase fragment, and the full-length protein using substrates for HSD17B4 provided supporting evidence. We evaluated the D-3-hydroxyacyl CoA dehydrogenase activity using DL-β-hydroxylbutyryl CoA as a

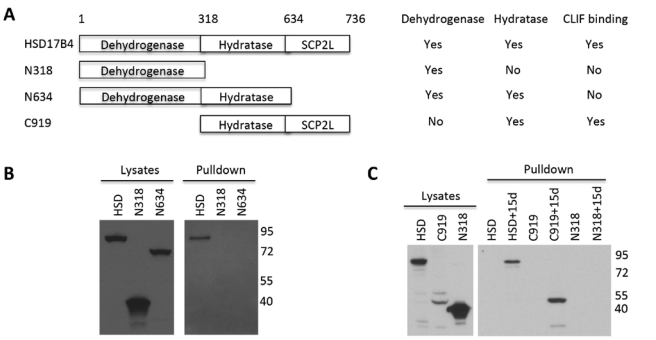

Fig. 4 A. Schematic diagram of HSD17B4. B and C. Interactions of isoflavanoid **15d** with full-length and truncated HSD17B4.

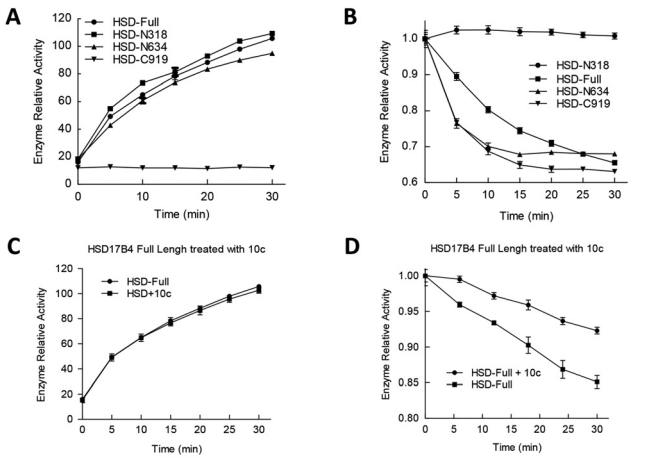

Fig. 5 A. D-3-Hydroxyacyl CoA dehydrogenase activities of full-length and truncated HSD17B4. B. Enoyl CoA hydratase activities of full-length and truncated HSD17B4. C. Effects of **10c** on the D-3-hydroxyacyl CoA dehydrogenase activity of HSD17B4. D. Effects of **10c** on the enoyl CoA hydratase activity of HSD17B4.

substrate and the conversion of NAD^+ to NADH as a readout.[16] We concomitantly measured the enoyl CoA hydratase activity using crotonoyl CoA as a substrate and the diminished ultraviolet absorption of the α,β-unsaturated thioester chromophore as a readout.[16] The full-length protein, as expected, had activities of both enzymes (Fig. 5A and B). The C-terminal-truncated fragments, N318 and N634, but not the N-terminal-truncation fragment, C919, had the D-3-hydroxyacyl CoA dehydrogenase activity (Fig. 5A). The N-terminal fragment N634 and the C-terminal fragment C919, but not the N-terminal fragment N318, had the enoyl CoA hydratase activity (Fig. 5B; summarized in Fig. 4A). We tested the effects of CLIF **10c** on each enzyme activity and found that CLIF **10c** had no effect on the D-3-hydroxyacyl CoA dehydrogenase activity (Fig. 5C) but inhibited the enoyl CoA hydratase activity (Fig. 5D). These results were consistent with those of previous reports about the interlocking roles of the different domains in HSD17B4.[9,17]

We validated the importance of the overexpression of HSD17B4 in prostate cancer[12] by analyzing the expression

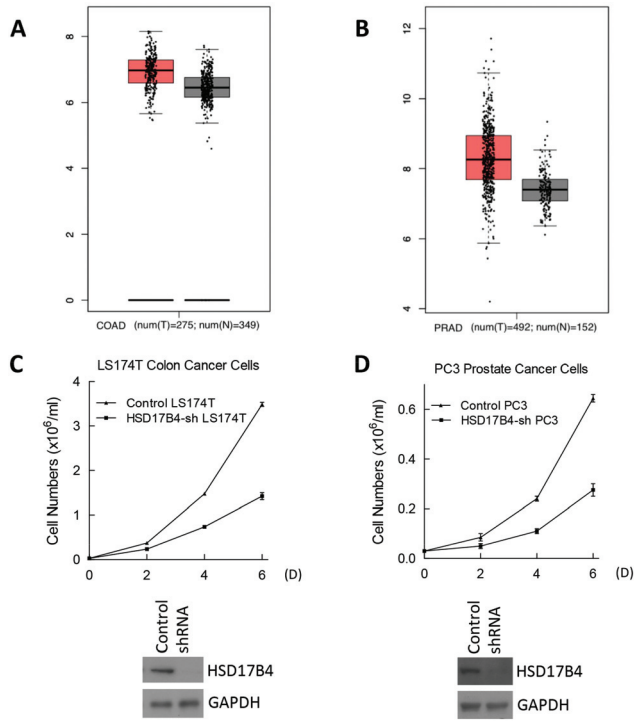

Fig. 6 A and B. The expression levels of HSD17B4 were significantly increased in colon adenocarcinoma (COAD) and prostate adenocarcinoma (PRAD). Data were extracted using the Expression DIY – Box plot from GEPIA (http://gepia.cancer-pku.cn/). $|\log_2 FC|$ Cutoff is 1; *p*-value cutoff is 0.01. Jitter size is 0.4 and the data of normal and tumor samples were matched with TCGA and GTEx data. Red color: tumor samples; grey color: normal samples. C and D. HSD17B4 depletion inhibited LS174T and PC-3 cell proliferation.

profile of HSD17B4 in The Cancer Genome Atlas (TCGA) database. A two-sample *t*-test showed that HSD17B4 expression was significantly upregulated in prostate cancer patients *versus* normal controls (Fig. 6A). We also found that HSD17B4 was overexpressed (Fig. 6B) using data from colon adenocarcinoma. Validation of HSD17B4 as an antineoplastic target of these CLIF inhibitors involved a knockdown of HSD17B4 using shRNA in PC-3 prostate cancer cells and LS174T colon cancer cells. As expected, HSD17B4 depletion inhibited the proliferation of both PC-3 and LS174T cells (Fig. 6C and D). These results were consistent with the results from the treatment of these same cells with CLIF **10c** (Fig. 2C and D) and suggested that HSD17B4 is a potential target for cancer treatment.

Discussion

Semisynthetic natural products continue to provide instructive probes for biological processes and sources of potential drug candidates. We explored the isoflavone family as part of our interest in the development of new antineoplastic agents with specific molecular targets. The naturally occurring isoflavones, daidzein **1** and genistein **2** (Fig. 1A), appeared in dietary supplements with alleged utility for the treatment of cancer,[5–7] and other isoflavones possess biological activities potentially useful for the treatment of other diseases. The synthetic modifications of isoflavones that introduce pharmacophores not found in nature provided semisynthetic isoflavonoids with the potential to bind distinct biological targets and to escape the polypharmacology associated with the natural products.

A screening program identified semisynthetic isoflavonoids **3** (Fig. 1A) with modifications at C-2, C-3, and C-7 as inhibitors of LS174T and PC-3 cancer cell proliferation. A study of structure–activity relationships (SAR) identified 7-alkoxyisoflavonoids bearing terminal, piperazinyl substituents on the alkoxy group, such as **7** and **8** (Fig. 2A), as effective cancer cell inhibitors in the 10 μM concentration range. Efforts to improve upon this potency led to the synthesis and evaluation of alkaloid-linked isoflavonoids, such as the cytisine-linked isoflavonoids (CLIFs) **10c** (Fig. 2A), with potencies as cancer cell proliferation inhibitors in the high nanomolar to low micromolar concentration range. (−)-Cytisine **9** alone had minimal effect on cancer cell proliferation at these concentrations (<15% inhibition at 10 μM, Table S1†). Several groups reported isoflavonoids with amine substituents as antineoplastic agents,[18] antibacterials,[19] and antipsychotics,[20] and still other groups explored the linkage of (−)-cytisine to known drugs such as phenothiazines.[21] The work reported here is the first to explore covalently linked cytisine isoflavonoids as antineoplastic agents. Compared with two chemotherapy drugs, doxorubicin and 5-FU, **10c** was less toxic to normal cells at 10 μM (23–33% *vs.* 64–99% inhibition, Table S1†). Compared with two targeted cancer therapy drugs, erlotinib and sorafenib, **10c** was less toxic to normal cells at 10 μM (23–33% *vs.* 25–98% inhibition, Table S1†) but was a little more potent at 1 μM (33–54% *vs.* 10–33% inhibition, Table S1†).

Elucidation of the biological target of CLIFs utilized the introduction of a biotin tag that would facilitate a streptavidin pull-down assay but would not eradicate the biological activity of the biotinylated CLIFs. Synthetic efforts ultimately provided a solution to this problem in the form of a biotinylated CLIF **15d** (Fig. 3A) with a six-carbon linker between (−)-cytisine and the isoflavonoid and with a carbonyl group in the linker suitable for the attachment of a biotin-PEG-hydrazide. The biologically active biotinylated CLIF **15d** pulled down two protein bands using cancer cell lysates (Fig. 3D). According to mass spectral analysis, the 80 kDa band contained a bifunctional peroxisomal enzyme, hydroxysteroid 17β-dehydrogenase-4 (HSD17B4), and a mitochondrial enzyme, methylcrotonoyl-CoA carboxylase subunit alpha (MCCA). Because MCAA was a carboxylase enzyme, it contained biotin[22] and was also present in the control sample. It was reasonable to assume that MCCA was a non-specific, biotin-containing carboxylase that bound to streptavidin independent of CLIF **15d**. The mass spectrum of the 50 kDa band also matched HSD17B4. Post-translational cleavage of HSD17B4 was known to provide a 32 kDa N-terminal fragment with D-3-hydroxyacyl CoA dehydrogenase (SCAD) activity and a 50 kDa C-terminal fragment with enoyl CoA hydratase activity and 3-ketoacyl CoA thiolase (SCP2) activity (Fig. 4A).[9,10] As we subsequently learned, the CLIFs

bound preferentially to the C-terminus of HSD17B4 and for this reason, pulled down both the full-length and the 50 kDa fragments.

The multiplicity of normal substrates for HSD17B4 (*i.e.*, very long chain fatty acids, branched fatty acids, and androgens/estrogens) made it challenging to establish the connection between the CLIF inhibition of the enoyl CoA hydratase activity in HSD17B4 and the effect on cancer cell proliferation. We validated HSD17B4 as an antineoplastic target by knocking down HSD17B4 using shRNA in PC-3 prostate cancer cells and LS174T colon cancer cells. On this basis, we concluded that the inhibition of HSD17B4 by CLIFs and the inhibition of PC-3 and LS174T cell proliferation were not independent events. In summary, cytisine-linked isoflavonoids (CLIFs) functioned as selective inhibitors of the fatty acid enoyl CoA hydratase activity in the bifunctional peroxisomal enzyme, hydroxysteroid 17β-dehydrogenase-4 (HSD17B4). On-going studies will establish the interconnection between these events and determine the potential utility of CLIFs as therapeutic agents.

Experimental

Chemistry

Chemicals were purchased from Sigma Aldrich (Milwaukee, WI) or Fisher Scientific (Pittsburgh, PA) or were synthesized according to literature procedures as described in the ESI†. Hydrazide-PEG_4-biotin was purchased from Thermo Fisher Scientific (Florence, KY). Solvents were purchased from commercial vendors without further purification unless otherwise noted. Nuclear magnetic resonance spectra were recorded on a Varian instrument (^{1}H, 400 MHz; ^{13}C, 100 Mz). High resolution electrospray ionization (ESI) mass spectra were recorded on a ThermoScientific Q Exactive Orbitrap mass spectrometer. Resolution was set at 100 000 (at 400 *m*/*z*). Samples were introduced through direct infusion using a syringe pump (flow rate: 5 μL min^{-1}). The purity of compounds was greater than 95% as established using combustion analyses determined by Atlantic Microlabs, Inc. (Norcross, GA).

Biology

Cell culture. LS174T colon cancer cells were cultured in MEM/EBSS (Hyclone SH30024) and PC-3 prostate cancer cells were cultured in a DMEM/F-12 HAM mixture (Sigma D8437) containing 10% fetal bovine serum (Atlanta Biological S11150). Cells (3.5×10^4 cells per well) were split into 12-well plates. After 24 h, each compound (10 μM) was added to each well. DMSO was used as a control. Each experiment was performed in triplicate. Cell viability and number were analyzed using the Vi-Cell XR cell viability analyzer (Beckman Coulter). PC-3 and LS174T cell lines were infected with lentivirus carrying pLKO.1-control shRNA and pLKO.1-HSD17B4b shRNA, respectively, to knockdown the HSD17B4 levels. Control shRNA and HSD17B4 shRNA cloned in pLKO.1 vectors with a puromycin-resistance selection marker were purchased from Sigma. Lentiviral stocks were prepared as previously described.[23]

Biochemistry. Cells were lysed in an appropriate volume of lysis buffer (50 mM HEPES, 100 mM NaCl, 2 mM EDTA, 1% glycerol, 50 mM NaF, 1 mM Na_3VO_4 and 1% Triton X-100 with protease inhibitors). The following antibodies were used: HSD17B4 (GeneTex, GTX103864), MCCA (GeneTex, GTX110062) and His-tag (BD Pharmingen, 552564).

Biotinylated compound **15d** (Fig. 3A) was incubated with cell lysates and streptavidin beads. The binding proteins were pulled down and analyzed by 4–12% SDS-PAGE as described previously.[24] The protein bands were identified using a NanoLC-ESI-MS/MS at ProtTech, Inc. For binding and enzymatic assays, His-tagged HSD17B4 constructs were cloned and truncated using PCR and pET28. The full-length and truncated proteins were purified from bacteria BL21.

Enzyme reaction. The enzymatic activities of HSD17B4 were analyzed using the method reported by Novikov *et al.*[16] D-3-Hydroxyacyl CoA dehydrogenase assay: the purified HSD17B4 enzyme was diluted in 200 μL reaction buffer (60 mM hydrazine, pH 8.0; 1 mM NAD^+; 50 mM KCl; 0.01% Triton-X100 and 0.05% BSA) and incubated with the 25 μM substrate, DL-β-hydroxybutyryl CoA lithium salt (Sigma H0261). The reaction was quantified by measuring the fluorescent product NADH (excitation: 340 nm; emission 460 nm). Hydratase assay: the purified HSD17B4 enzyme was diluted in 200 μL reaction buffer (0.32 M Tris-HCl, pH 7.4; 5.9 mM EDTA, 0.006% BSA) and incubated with the 0.2 mM substrate, crotonyl CoA (Sigma 28007). The reaction was quantified by measuring the remaining substrate using absorbance at 280 nm.

Statistics. Cell proliferation and enzymatic studies were performed in triplicates. Microarray and patient clinical data from colon cancer and prostate cancer studies were downloaded from the TCGA and GTEx databases. A two-sample *t*-test was used to compare the HSD17B4 expression in colon adenocarcinoma and prostate adenocarcinoma patients *versus* normal controls using the GEPIA program.[25]

Conclusions

Cytisine-linked isoflavonoids (CLIFs) functioned as selective inhibitors of the fatty acid enoyl CoA hydratase activity in the bifunctional peroxisomal enzyme, hydroxysteroid 17β-dehydrogenase-4 (HSD17B4). Our findings suggest that peroxisomal enzymes could be novel targets for cancer therapeutics.

Author contributions

WZ, XX, TY, and YX performed the biological experiments. MSF, PPW, SPB, VMS and HXN synthesized and analyzed the compounds. WZ, VMS, AJM, JLM, MVF, DSW, and CL designed the studies, analyzed the data, and wrote the manuscript.

Conflicts of interest

CL and DSW have partial ownership in a private venture, Epionc Inc., to develop small-molecule inhibitors for cancer

treatment. In accord with the University of Kentucky policies, CL and DSW have disclosed this work to the University of Kentucky's Intellectual Property Committee and complied with stipulations of the University's Conflict of Interest Oversight Committee.

Acknowledgements

CL and DSW were supported by NIH R01 CA172379. DSW was also supported by the Office of the Dean of the College of Medicine, the Center for Pharmaceutical Research and Innovation in the College of Pharmacy, and NIH R21 CA205108 (to J. Mohler), the Department of Defense Idea Development Award W81XWH-16-1-0635, NIH P20 RR020171 from the National Institute of General Medical Sciences (to L. Hersh), and NIH UL1 TR000117 from the National Institutes of Health for the University of Kentucky's Center for Clinical and Translational Science.

References

1 M. S. Frasinyuk, G. P. Mrug, S. P. Bondarenko, V. P. Khilya, V. M. Sviripa, O. A. Syrotchuk, W. Zhang, X. Cai, M. V. Fiandalo, J. L. Mohler, C. Liu and D. S. Watt, *ChemMedChem*, 2016, **11**, 600.
2 M. S. Frasinyuk, G. P. Mrug, S. P. Bondarenko, V. M. Sviripa, W. Zhang, X. Cai, M. V. Fiandalo, J. L. Mohler, C. Liu and D. S. Watt, *Org. Biomol. Chem.*, 2015, **13**, 11292.
3 C. H. Arrowsmith, J. E. Audia, C. Austin, J. Baell, J. Bennett, J. Blagg, C. Bountra, P. E. Brennan, P. J. Brown, M. E. Bunnage, C. Buser-Doepner, R. M. Campbell, A. J. Carter, P. Cohen, R. A. Copeland, B. Cravatt, J. L. Dahlin, D. Dhanak, A. M. Edwards, M. Frederiksen, S. V. Frye, N. Gray, C. E. Grimshaw, D. Hepworth, T. Howe, K. V. M. Huber, J. Jin, S. D. Knapp, J. Kotz, R. G. Kruger, D. Lowe, M. M. Mader, B. Marsden, A. Mueller-Fahrnow, S. Müller, R. C. O'Hagan, J. P. Overington, D. R. Owen, S. H. Rosenberg, R. Ross, B. Roth, M. Schapira, S. L. Schreiber, B. Shoichet, M. Sundström, G. Superti-Furga, J. Taunton, L. Toledo-Sherman, C. Walpole, M. A. Walters, T. M. Willson, P. Workman, R. N. Young and W. J. Zuercher, *Nat. Chem. Biol.*, 2015, **11**, 536.
4 W. J. H. Wuttke and D. Seidlová-Wuttke, *Ageing Res. Rev.*, 2007, **6**, 150.
5 H. Adlercreutz, *Scand. J. Clin. Lab. Invest.*, 1990, **201**, 3.
6 S. Andres, K. Abraham, K. E. Appel and A. Lampen, *Crit. Rev. Toxicol.*, 2011, **41**, 463.
7 I. C. Munro, M. Harwood, J. J. Hlywka, A. M. Stephen, J. Doull, W. G. Flamm and H. Adlercreutz, *Nutr. Rev.*, 2003, **61**, 1.
8 P. B. Kaufman, J. A. Duke, H. Brielmann, J. Boik and J. E. Hoyt, *J. Altern. Complement. Med.*, 1997, **3**, 7.
9 S. Huyghe, G. P. Mannaerts, M. Baes and P. P. Van Veldhoven, *Biochim. Biophys. Acta, Mol. Cell Biol. Lipids*, 2006, **1761**, 973.
10 R. J. Wanders, *Mol. Genet. Metab.*, 2004, **83**, 16.
11 H. Peltoketo, V. Luu-Tee, J. Simard and J. Adamski, *J. Mol. Endocrinol.*, 1999, **23**, 1.
12 K. K. Rasiah, M. Gardiner-Garden, E. J. Padilla, G. Moller, J. G. Kench, M. C. Alles, S. A. Eggleton, P. D. Stricker, J. Adamski, R. L. Sutherland, S. M. Henshall and V. M. Hayes, *Mol. Cell. Endocrinol.*, 2009, **301**, 89.
13 S. Békássy, J. Farkas, B. Ágai and F. Figueras, *Top. Catal.*, 2000, **13**, 287.
14 A. R. L. Dohme, E. H. Cox and E. Miller, *J. Am. Chem. Soc.*, 1926, **48**, 1688.
15 A. Martin, N. Gavande, M. S. Kim, N. X. Yang, N. K. Salam, J. R. Hanrahan, R. H. Roubin and D. E. Hibbs, *J. Med. Chem.*, 2009, **52**, 6835.
16 D. K. Novikov, G. F. Vanhove, H. Carchon, S. Asselberghs, H. J. Eyssen, P. P. Van Veldhoven and G. P. Mannaerts, *J. Biol. Chem.*, 1994, **269**, 27125.
17 Y. de Launoit and J. Adamski, *J. Mol. Endocrinol.*, 1999, **22**, 227.
18 L. Betti, M. Floridi, G. Giannaccini, F. Manetti, C. Paparelli, G. Strappaghetti and M. Botta, *Bioorg. Med. Chem.*, 2004, **12**, 1527.
19 K. S. Babu, T. H. Babu, P. Srinivas, K. H. Kishore, U. Murthy and J. M. Rao, *Bioorg. Med. Chem. Lett.*, 2006, **16**, 221.
20 J. Bolós, L. Anglada, S. Gubert, J. M. Planas, J. Agut, M. Príncep, À. De la Fuente, A. Sacristán and J. A. Ortiz, *J. Med. Chem.*, 1998, **41**, 5402.
21 I. V. Kulakov, *Chem. Nat. Compd.*, 2010, **46**, 68.
22 K. F. T. Obata, R. Morishita, S. Abe, S. Asakawa, S. Yamaguchi, M. Yoshino, K. Ihara, K. Murayama, K. Shigemoto, N. Shimizu and I. Kondo, *Genomics*, 2001, **72**, 145.
23 T. Yu, X. Chen, W. Zhang, D. Colon, J. Shi, D. Napier, P. Rychahou, W. Lu, E. Y. Lee and H. L. Weiss, *J. Biol. Chem.*, 2012, **287**, 3760.
24 W. Zhang, V. Sviripa, X. Chen, J. Shi, T. Yu, A. Hamza, N. D. Ward, L. M. Kril, C. W. Vander Kooi, C. G. Zhan, B. M. Evers, D. S. Watt and C. Liu, *ACS Chem. Biol.*, 2013, **8**, 796.
25 Z. Tang, C. Li, B. Kang, G. Gao, C. Li and Z. Zhang, *Nucleic Acids Res.*, 2017, **45**, W98.

Inhibition of Dihydrotestosterone Synthesis in Prostate Cancer by Combined Frontdoor and Backdoor Pathway Blockade

Michael V. Fiandalo[1], John J. Stocking[1], Elena A. Pop[1], John H. Wilton[1,2], Krystin M. Mantione[2], Yun Li[1], Kristopher M. Attwood[3], Gissou Azabdaftari[4], Yue Wu[1], David S. Watt[5], Elizabeth M. Wilson[6] and James L. Mohler[1]

Departments of Urology[1], Pharmacology and Therapeutics[2], Biostatistics and Bioinformatics[3] and Pathology[4], Roswell Park Cancer Institute, Buffalo, NY 14263, USA, Center for Pharmaceutical Research and Innovation and Department of Molecular and Cellular Biochemistry[5], University of Kentucky, Lexington, KY, 40536, USA and Department of Pediatrics, Department of Biochemistry and Biophysics and Lineberger Comprehensive Cancer Center, University of North Carolina, Chapel Hill, NC 27599[6] USA

Keywords: Androstanediol, dihydrotestosterone, dutasteride, 3α-oxidoreductases, androgen deprivation therapy

Correspondence to: James L. Mohler, M.D.
Department of Urology
Roswell Park Cancer Institute
Elm and Carlton Streets
Buffalo, NY 14263
Telephone: (716) 845-8433
Fax: (716) 845-3300
Email: James.Mohler@RoswellPark.org

Word count: 4,198 **Total figures:** 6 **Total tables:** 10 supplemental tables

Abstract

Androgen deprivation therapy (ADT) is palliative and prostate cancer (CaP) recurs as lethal castration-recurrent/resistant CaP (CRPC). One mechanism that provides CaP resistance to ADT is primary backdoor androgen metabolism, which uses up to four 3α-oxidoreductases to convert 5α-androstane-3α,17β-diol (DIOL) to dihydrotestosterone (DHT). The goal was to determine whether inhibition of 3α-oxidoreductase activity decreased conversion of DIOL to DHT. Protein sequence analysis showed that the four 3α-oxidoreductases have identical catalytic amino acid residues. Mass spectrometry data showed combined treatment using catalytically inactive 3α-oxidoreductase mutants and the 5α-reductase inhibitor, dutasteride, decreased DHT levels in CaP cells better than dutasteride alone. Combined blockade of frontdoor and backdoor pathways of DHT synthesis provides a therapeutic strategy to inhibit CRPC development and growth.

Introduction

Prostate cancer (CaP) growth and progression rely on the activation of the androgen receptor (AR) by the testicular androgen, testosterone (T), or its more potent metabolite, dihydrotestosterone (DHT) [1]. Almost all men who present with advanced CaP and some men who fail potentially curative therapy are treated with androgen deprivation therapy (ADT). ADT lowers circulating T levels, deprives AR of ligand and induces CaP regression [2, 3]; however, ADT is only a temporary palliative measure. After ADT, intratumoral androgen levels remain sufficient to activate AR [1, 4] and CaP recurs as lethal, castration-recurrent/resistant CaP (CRPC).

One mechanism that may contribute to CaP resistance to ADT is intratumoral DHT synthesis from adrenal androgens or T [5]. Three androgen pathways produce DHT (Fig. 1A, modified from [6]) from three different, penultimate precursors: reduction of the Δ^4-double bond in T by 5α-reductase (SRD5A) 1, 2 or 3; reduction of the 17-keto group in 5α-androstane-3,17-

dione (5α-dione) by ARK1C3 or HSD17B3; or oxidation of the 3α-hydroxyl group in 5α-androstane-3α,17β-diol (DIOL) by 3α-oxidoreductases. The frontdoor pathway uses the adrenal androgens, dehydroepiandrosterone (DHEA) or 4-androstene-3,17-dione (ASD), as precursors to generate T that undergoes reduction to DHT by SRD5A 1, 2 or 3 [7]. Two backdoor pathways generate DHT without using T as an intermediate. The primary and secondary backdoor pathways convert DIOL or 5α-dione, respectively, to DHT (Fig. 1A).

Previous work from our laboratory and others demonstrated that CaP cells use both primary and secondary backdoor pathways to synthesize DHT [5, 8-10]. The terminal step in the primary backdoor pathway is the conversion of DIOL to DHT [5, 10, 11] by any of the four 3α-oxidoreductases: [1] 17β-hydroxysteroid dehydrogenase (HSD) 6 (HSD17B6); [2] retinol dehydrogenase (RDH) 16 (RDH16); [3] dehydrogenase/reductase family member 9 (DHRS9, formerly RDH15); and [4] dehydrogenase/reductase family member 5 (RDH5) [5, 11-13]. The secondary backdoor pathway involves the conversion of DHEA to ASD by HSD3B1 or HSD3B2. ASD is converted subsequently to 5α-dione by SRD5A1 and 5α-dione is converted to DHT by AKR1C3 or HSD17B3 [9, 14-16].

Androgen metabolism inhibitors, such as the SRD5A inhibitor, dutasteride, or the CYP17A1 inhibitor, abiraterone [7, 17], have been disappointing clinically. Dutasteride inhibited SRD5A activity [18], depressed T uptake and lowered DHT levels *in vitro* [19], but dutasteride proved ineffective against CRPC in a Phase II clinical trial [20]. CYP17A1 metabolized steroids, such as pregnenolone or progesterone to adrenal androgens, such as DHEA, that provided intermediates for the androgen pathways that generated T and DHT [21]. Abiraterone decreased intratumoral DHT levels [22], but abiraterone extended survival by only approximately 4 months [23]. CaP resistance to abiraterone presumably resulted from enzyme redundancy, progesterone accumulation that led to increased CYP17A1 expression and/or the generation of AR splice variants [24-27]. The need to produce an androgen metabolism inhibitor

that performs better than abiraterone has become more important since abiraterone will become used earlier in the disease as a result of the demonstration of improved survival when used with standard ADT for newly diagnosed metastatic CaP [28, 29].

No inhibitors are available clinically to block the conversion of DIOL to DHT by 3α-oxidoreductases. In this report, we show that the catalytic activity of the 3α-oxidoreductases is critical for metabolism of 5α-androstan-3α-ol-17-one (androsterone; AND) to 5α-dione and DIOL to DHT. Inhibition of the terminal steps of the frontdoor pathway using dutasteride and the primary backdoor pathway using 3α-oxidoreductase catalytic mutants lowered DHT more effectively than either alone.

Results

3α-oxidoreductase enzymes shared a conserved catalytic site

The primary backdoor pathway uses one or more of four 3α-oxidoreductases to convert DIOL to DHT or AND to 5α-dione (Fig. 1B). DHT synthesis from adrenal androgens was suggested to contribute to the development and growth of CRPC [5, 8, 10, 30]. Inhibition of a single 3α-oxidoreductase enzyme could fail due to enzyme redundancy and/or expression of more than one enzyme. Therefore, an optimal therapeutic approach is to inhibit all four 3α-oxidoreductases. Constraint-based Multiple Protein Alignment Tool (COBALT) protein sequence analysis showed that the four 3α-oxidoreductases shared a common catalytic site (Fig. 1C).

HSD17B6, RDH16, DHRS9 and RDH5 were expressed in clinical CaP

Analysis of immunohistochemistry performed on TMA sections from a total of 72 patients showed that HSD17B6, RDH16, DHRS9 and RDH5 were expressed in androgen-stimulated (AS) benign prostate (BP), AS-CaP and CRPC (Fig. 1D). DHRS9 was expressed only in the cytoplasm. Nuclear expression levels of HSD17B6 and RDH16, but not RDH5, were higher in CRPC tissues than in AS-BP or AS-CaP tissues (Fig. 1E; Supplemental Table S4). RDH16 levels were higher in the nucleus than the cytoplasm (Fig. 1E; Supplemental Table S4). Peri-

nuclear enhancement was observed for each 3α-oxidoreductase except DHRS9, in AS-BP, AS-CaP and CRPC tissues.

3α-oxidoreductase gene expression varied among CaP cell lines

Although 3α-oxidoreductases were detected in clinical samples using IHC, they were not detectable in CaP cell lines using western blot analysis. Therefore, quantitative real-time polymerase chain reaction (qRT-PCR) was performed to determine 3α-oxidoreductase, SRD5A and AR gene expression profiles in CaP cell lines and the androgen-dependent human CWR22 and castration-recurrent CWR22 (rCWR22) CaP xenografts. RDH5 mRNA levels were higher than the expression of the other three 3α-oxidoreductases in all cell lines, except VCaP, PC-3 and DU145 (Fig. 2A). SRD5A3 mRNA levels were higher than SRD5A1 in all cell lines, except PC-3 and DU145 (Fig. 2B). SRD5A2 mRNA was not measurable, which is consistent with reports of low SRD5A2 gene expression in CaP cell lines [19] and clinical specimens [31]. AR mRNA was expressed in all CaP cell lines, except PC-3 and DU145, and in both xenografts (Fig. 2C) [32, 33]. The data suggested that analysis of 3α-oxidoreductase activity in human CaP cell lines required transient expression.

DHT levels increased when RDH16, DHRS9 or RDH5 were expressed in LAPC-4 cells

The effect of 3α-oxidoreductase expression on DHT levels was determined in the androgen-sensitive LAPC-4 cell line that expressed wild-type AR and RDH5 (Fig. 2A) and exhibited 5α-reductase activity [19]. VCaP and LNCaP-RPCI (LNCaP) cells [19] were not used initially because conversion of T to DHT was not detected. Wild-type 3α-oxidoreductases were expressed transiently in LAPC-4 cells. Results were compared to LAPC-4 cells transfected with empty plasmid, which were expected to have low endogenous 3α-oxidoreductase activity based on endogenous RDH5 in LAPC-4 cells (Fig. 2A). LAPC-4 cells were treated with DIOL, AND or T. DIOL and AND were used for treatment because 3α-oxidoreductases convert DIOL to DHT or AND to 5α-dione (Fig. 1B) [5, 12, 13]. T treatment was used as a control condition because 3α-oxidoreductases do not convert T to DHT [12, 13].

Liquid chromatography-tandem mass spectrometry (LC-MS/MS) analysis revealed that LAPC-4 cells transfected with empty plasmid in Serum Free Complete Media (SFM; medium without exogenous androgen) produced low levels of DHT (0.0211 pmoles/mg protein) (Fig. 3A empty plasmid). This finding was consistent with qRT-PCR data (Fig. 2A) and previous reports [5] that LAPC-4 cells expressed endogenous RDH5 that metabolized DIOL to DHT. DHT levels were higher ($p = 0.008$) in SFM treated LAPC-4 cells that expressed RDH16 compared to SFM treated LAPC-4 cells with empty plasmid (Fig. 3A [RDH16 vs. empty plasmid] and Supplemental Table S6), which suggested that RDH16 enhanced DHT synthesis in LAPC-4 cells.

LAPC-4 cells with empty plasmid treated with DIOL produced higher levels of DHT compared to SFM treated LAPC-4 cells with empty plasmid (Fig. 3B [note the change in Y axis between panels A and B]; Supplemental Table S6). DIOL treated LAPC-4 cells that expressed RDH16 produced higher ($p = 0.022$) levels of DHT than SFM treated LAPC-4 cells with empty plasmid (Fig. 3A and Supplemental Table S6). DIOL treated LAPC-4 cells that expressed HSD17B6 produced lower DHT levels ($p < 0.001$) compared to LAPC-4 cells with empty plasmid, which suggested that LAPC-4 cells may possess inhibitory mechanisms that impaired HSD17B6 activity.

DHT levels were higher ($p = 0.024$) when LAPC-4 cells with empty plasmid were treated with T (Fig. 3C and Supplemental Table S6) compared to SFM treated LAPC-4 cells with empty plasmid, which is consistent with T to DHT conversion by endogenous SRD5A [19]. DHT levels were not significantly different among T treated LAPC-4 cells that expressed 3α-oxidoreductases or LAPC-4 cells with empty plasmid (Supplemental Table S6).

5α-dione was produced when LAPC-4 cells with empty plasmid were treated with DIOL or AND (Fig. 3B). The data were consistent with the levels of endogenous RDH5 mRNA found in LAPC-4 cells (Fig. 2A). DIOL treated LAPC-4 cells that transiently expressed HSD17B6, RDH16 or DHRS9 produced 5α-dione, but only LAPC-4 cells that expressed HSD17B6 ($p = 0.022$) or RDH16 ($p = 0.003$) produced higher 5α-dione levels compared to LAPC-4 cells with

empty plasmid (Fig. 3B; Supplemental Table S6). The data suggested LAPC-4 cells endogenously converted DIOL to DHT and HSD17B6 or RDH16 converted AND to 5α-dione. AND treated LAPC-4 cells that transiently expressed 3α-oxidoreductases produced similar 5α-dione levels as AND treated LAPC-4 cells with empty plasmid (Fig. 3D). The data suggested that LAPC-4 cells may not be an appropriate CaP cell model to study the ability of 3α-oxdioredcutases to convert AND to 5α-dione.

Taken together, these data were consistent with reports that 3α-oxidoreductases metabolize DIOL to DHT or AND to 5α-dione [5, 10, 12, 13].

Catalytic amino acid substitution or deletion impaired 3α-oxidoreductase activity

Previous reports showed that 3α-oxidoreductases contained a catalytic tyrosine (Y) and lysine (K) that lowered the binding energy requirements and promoted the metabolism of androgen precursors [12, 13, 34]. Site-directed mutagenesis of the 3α-oxidoreductase catalytic residues confirmed Y176/175 and K179/180 were essential for 3α-oxidoreductase activity for all four enzymes. The mutants included Δcat (deletion of the catalytic residues) or double mutants, Y→F, K→R (Y176F for HSD17B6, RDH16, DHRS9 or Y175F for RDH5 and K180R for HSD17B6, RDH16 and DHRS9 or K179R for RDH5). Rationale for the Y→F mutation rested on their similarity in size but difference in an essential hydroxyl group. This mutation was not expected to alter protein folding but would affect enzyme activity. The K→R mutation was chosen because R would maintain a positive charge but was not expected to alter protein folding [34, 35].

qRT-PCR confirmed that CV-1 cells had low endogenous AR and 3α-oxidoreductase mRNA levels that suggested RDH5 converted AND to 5α-dione in control CV-1 cells (Fig. 4A). 3α-oxidoreductase protein expression was not detected using western blotting (data not shown). Therefore, despite low expression of RDH5, CV-1 cells were used to express wild-type or mutant 3α-oxidoreductases to evaluate the effect of the mutations on the activity of 3α-oxidoreductases.

CV-1 cells treated with AND produced only a small amount of 5α-dione that was measurable only in the media (Fig. 4B). T or DHT was not detected in the media or CV-1 cell pellets. Therefore, subsequent experiments measured only androgens in media. CV-1 cells that expressed wild-type HSD17B6, RDH16 or RDH5 and were treated with AND produced 5α-dione at levels higher than levels observed in media from CV-1 cells with empty plasmid (Supplemental Table S8). ∆cat or the Y→F,K→R mutations reduced 5α-dione levels to background. Wild-type DHRS9 activity was impaired in CV-1 cells, which suggested CV-1 cells possessed inhibitory mechanisms that interfered with DHRS9 activity (Fig. 4B). 5α-dione levels were not increased in CV-1 cells that expressed Y→F,K→R or ∆cat 3α-oxidoreductase mutants. 3α-oxidoreductase enzyme expression was verified using western blot (Fig. 4C). The findings suggested that Y176 (Y175) and K180 (K179) were critical residues for enzyme activity for three of the four 3α-oxidoreductases.

3α-oxidoreductase expression in AS-BP and CaP specimens from research subjects treated with finasteride

To address the clinical relevance of the 3α-oxidoreductases, LC-MS/MS was applied to tissues obtained from a randomized, double-blind, placebo-controlled clinical trial of selenium supplementation and finasteride treatment of research subjects with CaP for two to four weeks prior to radical prostatectomy (Selenium and Finasteride Pre-Treatment Trial, I104607). Research subjects who received finasteride alone or in combination with selenium were compared to research subjects who received selenium alone or placebo. Research subjects treated with finasteride had decreased CaP tissue levels of DHT in both benign and malignant macro-dissected samples, although DHT levels remained sufficient to activate AR (data not shown). TMAs generated from the clinical trial were sectioned and analyzed using IHC. HSD17B6, RDH16, DHRS9 and RDH5 were expressed in AS-BP and AS-CaP (Figs. 5A and B). HSD17B6, RDH16, DHRS9 and RDH5 expression levels and subcellular localization were similar to the 72 research subjects' specimens analyzed previously (Figs. 1D and 1E). The data

suggested that DHT synthesis persisted in spite of finasteride inhibition of SRD5A either from incomplete inhibition of SRD5A or from backdoor DHT synthesis.

Combination dutasteride and 3α-oxidoreductase mutants decreased DHT greater than dutasteride alone

Primary backdoor DHT synthesis may facilitate CaP resistance to 5α-reductase inhibition. Therefore, simultaneous inhibition of the terminal steps of the frontdoor and primary backdoor pathways could lower DHT levels more effectively than targeting either terminal step alone. LAPC-4 cells exhibited SRD5A activity and dutasteride treatment decreased LAPC-4 DHT levels [19]. LAPC-4 cells also were capable of backdoor DHT synthesis using 3α-oxidoreductases to convert DIOL to DHT (Fig. 3A). Therefore, LAPC-4 cells were used to test the effect of inhibition of the terminal steps of the frontdoor and primary backdoor androgen pathways. Dutasteride was used to inhibit SRD5A activity and block the frontdoor pathway. Activity impairing mutants were used to block enzymatic activity in the primary backdoor pathway, since no effective inhibitors are available for the four 3α-oxidoreductases.

DHT levels were higher in LAPC-4 cell pellets that overexpressed RDH16 ($p < 0.001$) or DHRS9 ($p < 0.001$) compared to LAPC-4 cell pellets with empty plasmid (Fig. 6A [SFM alone]; Supplemental Table S10); no androgens were measurable in media. DHT levels were lower in dutasteride treated LAPC-4 cells with empty plasmid compared to SFM treated LAPC-4 cells with empty plasmid (Fig. 6A; $p = 0.041$; Supplemental Table S10). No effect of dutasteride was observed in LAPC-4 cells that expressed wild-type RDH16 or DHRS9, which suggested that RDH16 or DHRS9 was sufficient for primary backdoor DHT synthesis. LAPC-4 cells that expressed Δcat of RDH5 or Y→F,K→R mutants of RDH16 or DHRS9 had lower DHT levels (RDH5, $p = 0.046$; RDH16, $p = 0.006$; DHRS9, $p = 0.004$) compared to LAPC-4 cells that expressed wild-type RDH16, DHRS9 or RDH5. DHT levels were lowered further by dutasteride treatment of LAPC-4 cells that expressed mutant RDH16 or DHRS9 compared to LAPC-4 cells treated with dutasteride alone. DHT levels were significantly lower in LAPC-4 cells that

expressed RDH16-Δcat ($p = 0.008$), RDH16-Y176F,K180R ($p = 0.004$), DHRS9-Δcat ($p = 0.029$) or DHRS9-Y176F,K180R ($p = 0.004$) after dutasteride treatment compared to LAPC-4 cells that overexpressed wild-type RDH16 or DHRS9 (Fig. 6A; Supplemental Table S10). Subsequent experiments focused on RDH16 because [1] wild-type RDH16 expression rendered dutasteride ineffective in LAPC-4 cells; and [2] DHT levels were lowered significantly by expression of RDH16-Y176F,K180R and dutasteride treatment.

Empty plasmid, or plasmids for over-expression of RDH16 wild-type or RDH16-Y176F,K180R were expressed into VCaP, LNCaP-C4-2 (C4-2) or CWR-R1 cells and DHT levels were measured using LC-MS/MS. DHT levels were similar in VCaP cells in SFM treated with or without dutasteride, which suggested that dutasteride treatment did not lower VCaP DHT levels (Fig. 6B). The data were consistent with data reported previously [19]. Expression of wild-type RDH16 increased DHT levels ($p = 0.031$) that were affected minimally by dutasteride treatment. RDH16-Y176F,K180R expression resulted in DHT levels similar to VCaP cells that contained the empty plasmid. C4-2 cells produced measurable levels of DHT that were reduced by dutasteride treatment ($p = 0.001$; Fig. 6C; Supplemental Table S10). Expression of wild-type RDH16 increased DHT levels ($p = 0.001$) that appeared to be reduced by dutasteride treatment. C4-2 cells that expressed RDH16-Y176,K180R produced DHT levels similar to C4-2 cells with empty plasmid. RDH16 did not appear to increase DHT levels in CWR-R1 cells and dutasteride did not lower DHT levels of CWR-R1 cells that contained empty plasmid or expressed wild-type RDH16 (Fig. 6D). DHT levels appeared lower when CWR-R1 cells that expressed RDH16-Y176F,K180R were treated with dutasteride.

Western blot analysis demonstrated wild-type, Δcat or Y→F,K→R mutant 3α-oxidoreductase expression in the four CaP cell lines (Fig. 6E-H). LC-MS/MS revealed that dutasteride appeared to lower T levels in all LAPC-4 cells, except in LAPC-4 cells that expressed RDH5-Δcat (data available upon request). LNCaP cells did not have measurable DHT, and T was not detected after dutasteride treatment (data available upon request).

Discussion

The findings provide proof of principal that the catalytic site shared by HSD176, RDH16, DHRS9 and RDH5 plays a role in intracrine androgen metabolism. RDH16 or DHRS9 enhanced DHT synthesis in LAPC-4 cells, which was consistent with previous reports from our group and others [5, 11-13, 34, 36, 37]. LAPC-4 and CV-1 LC-MS/MS data suggested 3α-oxidoreductase activity may be cell line-specific because CV-1 cells could not use DHRS9 to convert AND to 5α-dione and LAPC-4 cells could not use HSD17B6 to convert DIOL to DHT. However, HSD17B6 has been shown to convert DIOL to DHT in VCaP and LNCaP cell lines [38]. LC-MS/MS revealed that all four 3α-oxidoreductases converted AND to 5α-dione. Mutation of the common catalytic amino acids diminished 3α-oxidoreductase activity, which impaired CaP cells' DHT synthesis using the primary backdoor pathway.

The current study is novel because the data showed that 3α-oxidoreductases are expressed in specimens of AS-BP, AS-CaP and CRPC, and AS-BP and AS-CaP after finasteride treatment. The primary backdoor pathway may facilitate DHT synthesis to overcome abiraterone treatment for CRPC and finasteride treatment for benign prostate enlargement or CaP chemoprevention. LC-MS/MS data provided evidence that all four 3α-oxidoreductases have similar enzymatic activity and that amino acid residues Y176/175 and K180/179 are essential for conversion of DIOL to DHT or AND to 5α-dione. The combination of dutasteride treatment and 3α-oxidoreductase mutation decreased DHT levels more effectively than dutasteride or 3α-oxidoreductase mutants alone.

The studies demonstrated that 3α-oxidoreductase expression may provide AS-BP, AS-CaP and CRPC with a mechanism for resistance to SRD5A inhibitors that primarily block frontdoor DHT synthesis.

A potential limitation of the study is that experiments could not be performed using endogenous 3α-oxidoreductases because enzyme expression was so low in CaP cell lines. Therefore, 3α-oxidoreductases were expressed transiently in CaP and CV-1 cells. Expression

variability in cell-to-cell expression was a potential complication in cells that expressed 3α-oxidoreductases transiently. However, western blot analysis showed expression levels were consistent among wild-type enzymes. Western blots also showed 3α-oxidoreductase mutant expression was lower than the expression of wild-type 3α-oxidoreductases, which suggested amino acid substitutions may impair post-translational modification. However, sufficient enzyme was present based on the reproducibility of the replicates and differences in androgen metabolism observed among CaP cells transfected with control, wild-type or mutant 3α-oxidoreductases.

LC-MS/MS analyses were consistent across nine analytical runs conducted over a twenty month period. Sample generation, LC-MS/MS sample preparation and analysis improved over twenty months, which led to reduced replicate variability observed in later experiments. Reduced replicate variability explains why DHT levels produced from SFM only treated LAPC-4 cells that expressed DHRS9 were significantly higher than LAPC-4 cells with empty plasmid in Fig. 6A, but not Fig. 3A. Results were reliable over time and across replicates because the extracted calibration standards and plasma quality controls used to control and assess the quality of each LC-MS/MS analysis had an overall mean accuracy of 100% and 97.9%, respectively, for the androgens analyzed in CaP cell pellets and media over nine independent sets of experiments.

The LC-MS/MS method used for these studies was limited to six androgens and therefore, glucuronidated or sulfated androgens or androgen metabolites with activity in the glucocorticoid pathway were not measured. Cellular uptake and export of androgens and their metabolites were not considered [39]. The LC-MS/MS method could not measure DIOL because DIOL did not display a mass spectrum sufficiently different from other androgens. Therefore, AND conversion to 5α-dione was used to measure individual enzyme activity for the expression studies in CV-1 cells. The studies suggested that the conversion of AND to 5α-dione may provide an opportunity to use the secondary backdoor pathway to produce DHT [9].

The combination of dutasteride treatment and 3α-oxidoreductase mutation showed DHT levels were suppressed for 12 h. Clinical effectiveness will require longer studies of any potential inhibitor of the four 3α-oxidoreductases alone or in combination with dutasteride.

Taken together, the data [1] show that 3α-oxidoreductases are expressed in AS-BP, AS-CaP and CRPC; [2] demonstrate the catalytic residues necessary for the terminal step of the primary backdoor pathway, DIOL to DHT, are essential to all four 3α-oxidoreductases; and [3] provide evidence that combined SRD5A and 3α-oxidoreductase blockade lowered DHT levels more effectively than inhibition of either enzyme family alone. Inhibitors against the 3α-oxidoreductases are not yet available for clinical use and need to be identified. A new treatment strategy to block the key enzymatic steps of the frontdoor and primary and secondary backdoor pathways may decrease DHT levels more effectively than ADT alone. Further reduction of tissue DHT by inhibiting the last step of intracrine DHT synthesis should improve the clinical response to ADT or induce re-remission of CRPC and improve survival of men with advanced CaP.

Materials and Methods

Experimental Models

Human male CaP lines LAPC-4 [40], LNCaP-RPCI (LNCaP) [41], PC-3 cells (ATCC, Manassas, VA) and LNCaP-C4-2 (C4-2) cells [42, 43] were cultured in RPMI 1640 (Mediatech, Inc., Manassas, VA). CWR-R1 cells [44] were cultured using Richter's Improved media (Corning). CV-1 monkey kidney cells, DU145 [45] and VCaP cells (ATCC) were cultured in DMEM (Corning, Corning, NY). RPMI and DMEM media were supplemented with 10% fetal bovine serum (FBS, Corning) and 2 mM glutamine (Corning). CWR-R1 cells were cultured in Richter's Improved Media (Corning) supplemented with 1% epidermal growth factor (Thermo Fisher Scientific, Waltham, MA), 1% insulin-transferrin-sodium selenite supplement (Roche, Indianapolis, IN), 1% nicotinamide (Calbiochem, Billerica, MA) and 2% FBS. Androgen-

dependent CWR22 [46] and ADT-recurrent CWR22 (rCWR22) [47] human CaP xenografts were propagated in immunocompromised nude mice.

All cell lines and xenografts were authenticated using genomic profiling in the RPCI Genomics Shared Resource. DNA profiles were acquired using 15 short tandem repeat (STR) loci and an amelogenin gender-specific marker. Test and control samples were amplified using the AmpFLSTR® Identifiler® Plus PCR Amplification Kit (Thermo Fisher Scientific, Waltham, MA) using the Verti 96-well Thermal Cycler (Applied Biosystems, Foster City, CA) in 9600 Emulation Mode (initial denature: 95°C 11 min, 28 cycles of denature: 94°C 20 sec and anneal/extend: 59°C 3 min, final extension: 60°C 10 min and hold: 12°C). PCR products were evaluated using the 3130xl Genetic Analyzer (Applied Biosystems) and analyzed using GeneMapper v4.0 (Applied Biosystems). Eight of the 15 STRs and amelogenin from the DNA profile for the cell lines were compared to the ATCC STR database (https://www.atcc.org/STR%20Database.aspx?slp=1) and the DSMZ combined Online STR Matching Analysis (http://www.dsmz.de/fp/cgi-bin/str.html). All matches above 80% were considered the same lineage.

Method Details

COBALT

The COBALT protein sequence alignment tool [48] was accessed using the National Center for Biotechnology (NCBI) website (http://www.ncbi.nlm.nih.gov/tools/cobalt/cobalt.cgi). Accession numbers for the 3α-oxidoreductases, HSD17B6, RDH16, DHRS9 and RDH5, were acquired using the NCBI protein database (http://www.ncbi.nlm.nih.gov/protein) and UniProtKB (http://www.uniprot.org/). Amino acid sequences of the four 3α-oxidoreductases were analyzed using COBALT and compared to other 3α-oxidoreductases and the SRD5A and CYP17 families to determine whether the catalytic site was conserved and specific to HSD17B6, RDH16, DHRS9 and RDH5.

Site-directed mutagenesis

Site-directed mutagenesis was performed using the QuikChange® Lightning Site-Directed Mutagenesis Kit (Strategene, Foster City, CA) and Strategene's protocol. pCMV6-entry expression plasmids with C-terminal MYC-DDK tag encoded with HSD17B6, RDH16, DHRS9 or RDH5 were purchased from Origene (Origene, Rockville, MD). 3α-oxidoreductase primers (Integrated DNA Technologies, Coralville, IA) were used to generate ∆cat or Y→F,K→R 3α-oxidoreductase mutants (Supplemental Table S1). Plasmids were purified using PureYield Plasmid Miniprep System (Promega, Madison, WI) and sequenced at the Genomics Shared Resource. PCR for plasmid sequencing was performed using plasmid templates and Big Dye Terminator v3.1 Master Mix Kit (Life Technologies, Carlsbad, CA). PCR products were purified using Sephadex-G50 (Sigma-Aldrich, St. Louis, MO) into multiscreen HV plates (Thermo Fisher Scientific). Eluted samples were analyzed using 3130xl ABI Prism Genetic Analyzer. Sequence data were analyzed using Sequencing Analysis 5.2 software (Life Technologies).

qRT-PCR

RNA extraction was performed using the RNeasy Plus Mini Kit (Qiagen, Valencia, CA). Samples generated from 9 cell lines were plated at 1 x 10^6 cells/T25 cell culture flask (Corning). Cells were harvested using 0.05% trypsin and washed 3 times using Dulbecco's phosphate buffered saline (PBS). PBS was removed and RLT lysis buffer was added to lyse the cell pellets. Frozen tissues from 2 xenografts (CWR22 and rCWR22) were Dounce homogenized in RLT lysis buffer. Lysates were passed through QIAshredder columns and RNA was extracted using RNeasy spin columns. Genomic DNA contamination was assessed using PCR and intron spanning GAPDH primers. Genomic DNA contamination was removed using a DNA-free DNA Removal Kit (Life Technologies). RNA was analyzed using PCR after DNase treatment to confirm genomic DNA was removed.

First strand complementary DNA (cDNA) was generated using 2 µg RNA and the High-Capacity cDNA Reverse Transcription Kit (10X RT Buffer, 10X Random Primers, 25X 100 mM deoxyNTP mix and 50 U/µL MultiScribe-Reverse Transcriptase; Applied Biosystems) and

RNAse inhibitor in 10 µL reactions. The Primer Quest Primer Design Tool was used to design qRT-PCR primers (Integrated DNA Technologies) (Supplemental Table S1).

qRT-PCR reactions included 12.5 µL of SYBR Green PCR Master Mix (Applied Biosystems), 0.1 µL of 10 mM forward and reverse primers, 2.5 µL of 100 ng/µL cDNA (250 ng final concentration) and 9.8 µL distilled deionized (dd-H_2O) for a final reaction volume 25 µL. Reactions were performed in 96-well plates. Gene expression was analyzed using 7300 Real Time System (Applied Biosystems). The qRT-PCR reaction parameters were 95°C for 30 sec, 60°C for 30 sec repeated 39 times, 95°C for 5 sec and melt curve 65°C-95°C. All procedures were performed with 3 technical replicates and 3 biological replicates. Cycle threshold (Ct) values were normalized against β2 microglobulin (B2M) that was selected based on unchanged B2M expression in SFM (data not shown). Ct values for negative RT controls and no template controls were reported as undefined. Relative gene abundance was calculated using 2^-(normalized Ct).

Cell lysate and media preparation for LC-MS/MS analysis

LAPC-4, LNCaP, C4-2 or CWR-R1 cells were plated at 1.2 x 10^5/well, VCaP cells at 2.5 x 10^5 and CV-1 cells at 1 x 10^4/well in 6-well tissue culture plates (Corning). Media and cell pellets from two 6-well plates were combined to generate 1 media and 1 cell pellet sample for LC-MS/MS analysis. LAPC-4, LNCaP, C4-2 or CWR-R1 cells were transfected using the Effectene Transfection Kit (Invitrogen, Grand Island, NY). Forty-eight h after transfection, growth media was removed and LAPC-4 cells were washed once with PBS (Corning). LAPC-4 cells were treated with serum-free complete media (SFM, Corning) alone or with 1 nM T, 20 nM DIOL 20 nM AND (Steraloids, Newport, RI) or 1 µM dutasteride (Selleckchem, Houston, TX) for 12 h. VCaP or CV-1 cells were transfected using X-tremeGene HP transfection reagent (Roche Diagnostics Corporation, Indianapolis, IN). After 48 h, growth media were aspirated, CV-1 cells were washed once with PBS and incubated in SFM alone or with 20 nM AND (Steraloids) for 12 h.

After 12 h treatment, media (total 24 mL) were collected in 50 mL conical tubes (Corning). Cells were released using trypsin and collected in 15 mL conical tubes (Corning). The cells were washed 3 times using PBS, re-suspended in 1 mL PBS and 5% of the cell suspension was removed for protein concentration measurement and western blot analysis. The remaining 95% of the cell suspension was centrifuged and the supernatant was removed and discarded. Cell pellets were stored at -80ºC until analyzed using LC-MS/MS.

LC-MS/MS

Cell pellet and media samples were analyzed over 9 runs for 5 androgens T, DHT, DHEA, ASD and AND using a validated LC-MS/MS method (Supplemental Methods and [49]). 5α-dione was also measured using this assay and data were included although results did not pass the strict validation acceptance criteria used for other androgens. Study samples were quantitated using aqueous-based spiked calibration standards and pre-spiked quality control samples prepared in 2X charcoal-stripped human postmenopausal female plasma (Bioreclamation, LLC, Westbury, NY). Performance data for calibrators, quality controls and calibration ranges were listed in Supplemental Table S2.

Androgen concentrations (pmoles/mg protein) in cell lysates measured using LC-MS/MS (ng/mL) were multiplied by the total volume of the lysate (1 mL), normalized by the total amount of protein of the cell pellet (mg), divided by the molecular weight of the androgen (ng/nmole), and converted to pmoles. Media androgen concentrations (ng/mL) were multiplied by the total volume of media (24 mL), normalized against total protein of the cell culture (mg), divided by the molecular weight of the androgen (ng/nmole) and converted to pmoles. Cell pellet and media androgen concentrations were reported combined in Results. Data from cell pellets or media and their statistical analysis provided upon similar results and are available on request. Experiments were performed in triplicate (n = 3).

Western blotting

Cells removed from -80°C storage were resuspended in ubiquitin extraction lysis buffer

(150 mM NaCl, 50 mM Tris-HCl, pH 7.4, 5 mM EDTA, 1% NP40, 0.5% sodium deoxycholate [all from Fisher, Pittsburg, PA]) and 0.1% SDS (Quality Biological, Gathersburg, MD). Halt Protease Inhibitor Cocktail (Sigma) was added to the ubiquitin lysis buffer just before cells were lysed. Cells were freeze-thawed three times and centrifuged at 14,000 x g for 15 min. Supernatants were transferred to clean microfuge tubes. Protein was quantified using the Protein Determination Kit (BioRad) and analyzed in flat bottom 96-well plates using an EL800 University Microplate Reader (BioTek Instruments) and KC Junior software (Bio-Tek Instruments). SDS-polyacrylamide gel electrophoresis (PAGE) was performed using 4-15% Mini Trans-Blot cell (BioRad). Protein was transferred to Immuno-Blot PVDF membranes for Protein Blot (BioRad) and blocked in 5% milk in Tris-buffered saline with Tween 20 (TBST, Amersham Bioscience, GE Healthcare Bio-Sciences, Pittsburg, PA) for 30 min.

Membranes were incubated with DDK targeted antibody (Origene) 1:1000 overnight at room temperature. After incubation, blots were washed three times with TBST (Amersham Bioscience) for 10 min each. Washed blots were incubated with goat anti-mouse secondary antibody (Jackson ImmunoResearch Laboratories, West Grove, PA) 1:1000 for 1 h at room temperature. Blots were washed with TBST three times for 10 min each and protein expression was measured using the Pierce ECL Western Blotting Substrate (Life Technologies). Immunoblots were washed with TBST, blocked in 5% milk in TBST, reprobed for tubulin (1:1000 for 1 h at room temperature; Abcam, Cambridge, MA) and incubated with goat anti-rabbit secondary antibody (1:1000 for 1 h at room temperature; Jackson ImmunoResearch Laboratories).

Tissue microarray (TMA) construction

Matched AS-BP and AS-CaP tissue specimens were collected from 36 patients who underwent radical prostatectomy. CRPC specimens were collected from 36 patients who underwent transurethral resection of the prostate for urinary retention from CaP that recurred during ADT. Specimens were collected between 1991 and 2011 at the Roswell Park Cancer

Institute or the University of North Carolina (Chapel Hill, NC). TMAs were constructed (0.6 millimeter tissue cores) from formalin-fixed, paraffin-embedded donor blocks from each patient, which was guided by genitourinary pathologists. TMAs contained control tissue from lung, tonsil, liver, kidney, colon, spleen, cervix, thyroid, ovary, testis, myometrium and brain.

TMAs were constructed using the same process on tissues collected from a randomized, double-blind, placebo-controlled clinical trial of selenium supplementation and finasteride treatment of patients with CaP prior to robotic prostatectomy (Selenium and Finasteride Pre-Treatment Trial ID:NCT00736645). Forty-seven patients scheduled for radical prostatectomy were randomized into one of four treatment groups: placebo, finasteride, selenium or combination finasteride and selenium.

IHC

TMA sections were de-paraffinized, rehydrated under an alcohol gradient and antigen retrieved using Reveal Decloaker (Biocare Medical, Concord, CA) for 30 min at 110°C and 5.5-6.0 psi. Sections were immunostained for the four 3α-oxidoreductases and AR as described (Supplemental Table S3). Enzymatic activity was assayed using 3,3'-Diaminobenzidine (Sigma-Aldrich) and sections were counterstained with hematoxylin (Vector Laboratories, Burlingame, CA). Sections were dehydrated and mounted using permanent mounting medium. Section images were collected using a Leica DFC0425C camera mounted on a Leica DMRA2 microscope (Leica Microsystems Inc., Buffalo Grove, IL). Protein expression was determined by three scorers who assessed the immunostain intensity and assigned values between zero (no immunostain) and three (dark immunostain) for 100 cells per core that generated an average final score between zero and 300 [50-52].

Quantification and Statistical Analysis

IHC and qRT-PCR expression data were summarized graphically using mean and standard error. IHC experiments produced average scores between 0 and 300 for each tissue specimen from each patient in each TMA; qRT-PCR experiments had a sample size of n = 9

(three biological replicates analyzed using three technical replicates) per treatment group. Specific treatment groups details or changes in sample size for each experiment were listed in the figure legends.

IHC and qRT-PCR expression data, and androgen concentrations, were modeled as a function of tissue type (AS-BP, AS-CaP or CRPC), cell-line (VCaP, LNCaP, LAPC-4, C4-2, PC-3, DU145, CWR-R1, CWR22 or rCWR22), enzyme (HSD17B6, RDH16, DHRS9 or RDH5) or empty plasmid, treatment (SFM, T, DIOL, AND or dutasteride), expressed 3α-oxidoreductase (wild-type, Δcat or Y→F,K→R mutant enzymes), interaction terms and random replicate effects using general linear models (GLMs) or linear mixed models (LMMs). Factors, factor levels, interaction terms and random effects were included in each model depended on the specific experiment and research question that was addressed. Mean differences of interest were evaluated using Dunnett or Tukey-Kramer adjusted tests about the appropriate least square means. All tests were two-sided, unless stated otherwise. All model assumptions were verified graphically using quantile-quantile and residual plots, with Box-Cox transformations applied as appropriate. Additional details for experiment specific analyses were provided in the appropriate figure legends.

All analyses were conducted in SAS v9.4 (Cary, NC) at a nominal significance level of 0.05; therefore a *P*-value less than 0.05 denoted a statistical significant result. No randomization techniques were utilized and no observations were excluded from analysis.

Abbreviations

4androstene-3α,17β-dione (ASD)

5androstane3α,17β-diol (androstanediol; DIOL)

5α-reductase (SRD5A)

5α-androstan-3α-ol-17-one (Androsterone; AND)

5α-androstan-3,17-dione (5α-dione)

17β-hydrosteroid dehydrogenase (HSD) 6 (HSD17B6)

Androgen receptor (AR)

Androgen Deprivation Therapy (ADT)

Androgen-stimulated benign prostate (AS-BP)

Androgen-stimulated prostate cancer (AS-CaP)

Castration-recurrent prostate cancer (CRPC)

Complementary DNA (cDNA)

Constraint-based Multiple Protein Alignment Tool (COBALT)

Dehydroepiandrosterone (DHEA)

Dehydrogenase/reductase family member 9 (DHRS9)

Dehydrogenase/reductase family member 5 (RDH5)

Dihydroteosterone (DHT)

General linear models (GLMs)

Immunohistochemistry (IHC)

Linear mixed models (LMMs)

Liquid-chromatography tandem mass spectrometry (LC-MS/MS)

LNCaP-RPCI (LNCaP)

LNCaP-C4-2 (C4-2)

National Center for Biotechnology (NCBI)

Prostate Cancer (CaP)

Quantitative Real-Time Polymerase Chain Reaction (qRT-PCR)

Retinol Dehydrogenase 16 (RDH16)

Serum-free Complete Media (SFM)

Testosterone (T)

Tissue microarray (TMA)

Author contributions

Dr. James L. Mohler (Urologic Oncology Surgeon, Principal Investigator) conceived the overall experimental question, assisted with the experimental design and supervised experiment completion, data analysis and manuscript development. Dr. Michael V. Fiandalo (Post-doctoral fellow) assisted with development of overall experimental question, refinement of the experimental question and experimental design and executed experiments, analyzed data and developed the manuscript. Dr. Elena Pop (Senior Research Specialist) sectioned paraffin-embedded tissues and performed IHC. John Stocking assisted Dr. Fiandalo with qRT-PCR, assisted Dr. Pop with IHC and scored tissues. Dr. John Wilton (Mass spectrometry specialist) performed mass spectrometry measurements and assisted with data analysis. Yun Li generated mutant 3α-oxidoreductase plasmids and assisted with RNA extractions. Krystin Mantione assisted Dr. Wilton with mass spectrometry measurements. Dr. Kristopher Attwood (biostatistician) performed all statistical analysis. Dr. Gissou Azabdaftari (genitourinary pathologist) characterized prostate tissue and assisted with data analysis. Dr. Yue Wu assisted with experiment design and data analysis. Dr. David Watt assisted with data analysis and manuscript preparation. Dr. Elizabeth Wilson assisted with the experimental design and manuscript preparation. All co-authors reviewed the manuscript.

Acknowledgements

Conflicts of interest Authors have no conflicts of interest.

Funding James L. Mohler: P01-CA77739, DoD Prostate Cancer Research Program Award No. W81XWH-16-1-0635; Michael V. Fiandalo: Post-doctoral Training Award W81XWH-15-1-0409; and, in part, by the NCI Cancer Center Support Grant to RPCI (P30-CA016056) for the Bioanalytics, Metabolomics and Pharmacokinetics, Pathology Network and Genomics Shared Resources; David S. Watt: P20-RR020171

References

1. Titus MA, Schell MJ, Lih FB, Tomer KB, Mohler JL. Testosterone and dihydrotestosterone tissue levels in recurrent prostate cancer. Clin Cancer Res. 2005; 11: 4653-7. doi: 10.1158/1078-0432.CCR-05-0525.
2. Isaacs JT. Antagonistic effect of androgen on prostatic cell death. Prostate. 1984; 5: 545-57.
3. Huggins C, Hodges CV. Studies on prostatic cancer: I. The effect of castration, of estrogen and of androgen injection on serum phosphatases in metastatic carcinoma of the prostate. Cancer Res. 1941; 1: 293-7.
4. Mohler JL, Gregory CW, Ford OH, 3rd, Kim D, Weaver CM, Petrusz P, Wilson EM, French FS. The androgen axis in recurrent prostate cancer. Clin Cancer Res. 2004; 10: 440-8.
5. Mohler JL, Titus MA, Bai S, Kennerley BJ, Lih FB, Tomer KB, Wilson EM. Activation of the androgen receptor by intratumoral bioconversion of androstanediol to dihydrotestosterone in prostate cancer. Cancer Res. 2011; 71: 1486-96. doi: 10.1158/0008-5472.CAN-10-1343.
6. Stocking JJ, Fiandalo MV, Pop EA, Wilton JH, Azabdaftari G, Mohler JL. Characterization of Prostate Cancer in a Functional Eunuch. J Natl Compr Canc Netw. 2016; 14: 1054-60. doi:
7. Godoy A, Kawinski E, Li Y, Oka D, Alexiev B, Azzouni F, Titus MA, Mohler JL. 5alpha-reductase type 3 expression in human benign and malignant tissues: a comparative analysis during prostate cancer progression. Prostate. 2011; 71: 1033-46. doi: 10.1002/pros.21318.
8. Mohler J, Titus M. (2009). Tissue levels of androgens in castration-recurrent prostate cancer. In: Mohler JL and Tindall D, eds. Androgen Action in Prostate Cancer. (New York, NY: Springer Science), pp. 175-85.
9. Chang KH, Li R, Papari-Zareei M, Watumull L, Zhao YD, Auchus RJ, Sharifi N. Dihydrotestosterone synthesis bypasses testosterone to drive castration-resistant prostate cancer. Proc Natl Acad Sci U S A. 2011; 108: 13728-33. doi: 10.1073/pnas.1107898108.
10. Auchus RJ. The backdoor pathway to dihydrotestosterone. Trends Endocrinol Metab. 2004; 15: 432-8. doi: 10.1016/j.tem.2004.09.004.
11. Bauman DR, Steckelbroeck S, Williams MV, Peehl DM, Penning TM. Identification of the major oxidative 3alpha-hydroxysteroid dehydrogenase in human prostate that converts 5alpha-androstane-3alpha,17beta-diol to 5alpha-dihydrotestosterone: a potential therapeutic target for androgen-dependent disease. Mol Endocrinol. 2006; 20: 444-58. doi: 10.1210/me.2005-0287.
12. Day JM, Tutill HJ, Purohit A, Reed MJ. Design and validation of specific inhibitors of 17beta-hydroxysteroid dehydrogenases for therapeutic application in breast and prostate cancer, and in endometriosis. Endocr Relat Cancer. 2008; 15: 665-92. doi: 10.1677/ERC-08-0042.
13. Biswas MG, Russell DW. Expression cloning and characterization of oxidative 17beta- and 3alpha-hydroxysteroid dehydrogenases from rat and human prostate. J Biol Chem. 1997; 272: 15959-66. doi:
14. Kavanagh KL, Jornvall H, Persson B, Oppermann U. Medium- and short-chain dehydrogenase/reductase gene and protein families : the SDR superfamily: functional and structural diversity within a family of metabolic and regulatory enzymes. Cell Mol Life Sci. 2008; 65: 3895-906. doi: 10.1007/s00018-008-8588-y.
15. Fankhauser M, Tan Y, Macintyre G, Haviv I, Hong MK, Nguyen A, Pedersen JS, Costello AJ, Hovens CM, Corcoran NM. Canonical androstenedione reduction is the predominant source of signaling androgens in hormone-refractory prostate cancer. Clin Cancer Res. 2014; 20: 5547-57. doi: 10.1158/1078-0432.CCR-13-3483.
16. Penning T. Androgen biosynthesis in castration resistant prostate cancer. Endocr Relat Cancer. 2014. doi: 10.1530/ERC-14-0109.

17. Ryan CJ, Smith MR, Fong L, Rosenberg JE, Kantoff P, Raynaud F, Martins V, Lee G, Kheoh T, Kim J, Molina A, Small EJ. Phase I clinical trial of the CYP17 inhibitor abiraterone acetate demonstrating clinical activity in patients with castration-resistant prostate cancer who received prior ketoconazole therapy. J Clin Oncol. 2010; 28: 1481-8. doi: 10.1200/JCO.2009.24.1281.
18. Yamana K, Labrie F, Luu-The V. Human type 3 5alpha-reductase is expressed in peripheral tissues at higher levels than types 1 and 2 and its activity is potently inhibited by finasteride and dutasteride. Horm Mol Biol Clin Investig. 2010; 2: 293-9. doi: 10.1515/hmbci.2010.035.
19. Wu Y, Godoy A, Azzouni F, Wilton JH, Ip C, Mohler JL. Prostate cancer cells differ in testosterone accumulation, dihydrotestosterone conversion, and androgen receptor signaling response to steroid 5alpha-reductase inhibitors. Prostate. 2013; 73: 1470-82. doi: 10.1002/pros.22694.
20. Shah SK, Trump DL, Sartor O, Tan W, Wilding GE, Mohler JL. Phase II study of Dutasteride for recurrent prostate cancer during androgen deprivation therapy. J Urol. 2009; 181: 621-6. doi: 10.1016/j.juro.2008.10.014.
21. Ferraldeschi R, Sharifi N, Auchus RJ, Attard G. Molecular Pathways: Inhibiting Steroid Biosynthesis in Prostate Cancer. Clin Cancer Res. 2013; 19: 3353-9. doi: 10.1158/1078-0432.CCR-12-0931.
22. Attard G, Reid AH, A'Hern R, Parker C, Oommen NB, Folkerd E, Messiou C, Molife LR, Maier G, Thompson E, Olmos D, Sinha R, Lee G, et al. Selective inhibition of CYP17 with abiraterone acetate is highly active in the treatment of castration-resistant prostate cancer. J Clin Oncol. 2009; 27: 3742-8. doi: 10.1200/JCO.2008.20.0642.
23. Ryan CJ, Smith MR, de Bono JS, Molina A, Logothetis CJ, de Souza P, Fizazi K, Mainwaring P, Piulats JM, Ng S, Carles J, Mulders PF, Basch E, et al. Abiraterone in metastatic prostate cancer without previous chemotherapy. N Engl J Med. 2013; 368: 138-48. doi: 10.1056/NEJMoa1209096.
24. Cai C, Chen S, Ng P, Bubley GJ, Nelson PS, Mostaghel EA, Marck B, Matsumoto AM, Simon NI, Wang H, Balk SP. Intratumoral de novo steroid synthesis activates androgen receptor in castration-resistant prostate cancer and is upregulated by treatment with CYP17A1 inhibitors. Cancer Res. 2011; 71: 6503-13. doi: 10.1158/0008-5472.CAN-11-0532.
25. Mostaghel EA, Marck BT, Plymate SR, Vessella RL, Balk S, Matsumoto AM, Nelson PS, Montgomery RB. Resistance to CYP17A1 inhibition with abiraterone in castration-resistant prostate cancer: induction of steroidogenesis and androgen receptor splice variants. Clin Cancer Res. 2011; 17: 5913-25. doi: 10.1158/1078-0432.CCR-11-0728.
26. Bremmer F, Jarry H, Strauss A, Behnes CL, Trojan L, Thelen P. Increased expression of CYP17A1 indicates an effective targeting of the androgen receptor axis in castration resistant prostate cancer (CRPC). Springerplus. 2014; 3: 574. doi: 10.1186/2193-1801-3-574.
27. Titus MA, Li Y, Kozyreva OG, Maher V, Godoy A, Smith GJ, Mohler JL. 5alpha-reductase type 3 enzyme in benign and malignant prostate. Prostate. 2014; 74: 235-49. doi: 10.1002/pros.22745.
28. Fizazi K, Tran N, Fein L, Matsubara N, Rodriguez-Antolin A, Alekseev BY, Ozguroglu M, Ye D, Feyerabend S, Protheroe A, De Porre P, Kheoh T, Park YC, et al. Abiraterone plus Prednisone in Metastatic, Castration-Sensitive Prostate Cancer. N Engl J Med. 2017 ; 377: 352-360. doi: 10.1056/NEJMoa1704174.
29. James ND, de Bono JS, Spears MR, Clarke NW, Mason MD, Dearnaley DP, Ritchie AWS, Amos CL, Gilson C, Jones RJ, Matheson D, Millman R, Attard G, et al. Abiraterone for Prostate Cancer Not Previously Treated with Hormone Therapy. N Engl J Med. 2017. doi: 10.1056/NEJMoa1702900.
30. Mostaghel EA, Page ST, Lin DW, Fazli L, Coleman IM, True LD, Knudsen B, Hess DL, Nelson CC, Matsumoto AM, Bremner WJ, Gleave ME, Nelson PS. Intraprostatic androgens and

androgen-regulated gene expression persist after testosterone suppression: therapeutic implications for castration-resistant prostate cancer. Cancer Res. 2007; 67: 5033-41. doi: 10.1158/0008-5472.CAN-06-3332.
31. Titus MA, Gregory CW, Ford OH, 3rd, Schell MJ, Maygarden SJ, Mohler JL. Steroid 5alpha-reductase isozymes I and II in recurrent prostate cancer. Clin Cancer Res. 2005; 11: 4365-71. doi: 10.1158/1078-0432.CCR-04-0738.
32. Chlenski A, Nakashiro K, Ketels KV, Korovaitseva GI, Oyasu R. Androgen receptor expression in androgen-independent prostate cancer cell lines. Prostate. 2001; 47: 66-75. doi: 10.1002/pros.1048.
33. Tilley WD, Bentel JM, Aspinall JO, Hall RE, Horsfall DJ. Evidence for a novel mechanism of androgen resistance in the human prostate cancer cell line, PC-3. Steroids. 1995; 60: 180-6.
34. Tanaka N. SDR: Structure, Mechanism of Action, and Substrate Recognition. Curr Org Chem. 2001; 5: 89-11.
35. Schlegel BP, Jez JM, Penning TM. Mutagenesis of 3 alpha-hydroxysteroid dehydrogenase reveals a "push-pull" mechanism for proton transfer in aldo-keto reductases. Biochemistry. 1998; 37: 3538-48. doi: 10.1021/bi9723055.
36. Locke JA, Guns ES, Lubik AA, Adomat HH, Hendy SC, Wood CA, Ettinger SL, Gleave ME, Nelson CC. Androgen levels increase by intratumoral de novo steroidogenesis during progression of castration-resistant prostate cancer. Cancer Res. 2008; 68: 6407-15. doi: 10.1158/0008-5472.CAN-07-5997.
37. Persson B, Kallberg Y, Bray JE, Bruford E, Dellaporta SL, Favia AD, Duarte RG, Jornvall H, Kavanagh KL, Kedishvili N, Kisiela M, Maser E, Mindnich R, et al. The SDR (short-chain dehydrogenase/reductase and related enzymes) nomenclature initiative. Chem Biol Interact. 2009; 178: 94-8. doi: 10.1016/j.cbi.2008.10.040.
38. Ishizaki F, Nishiyama T, Kawasaki T, Miyashiro Y, Hara N, Takizawa I, Naito M, Takahashi K. Androgen deprivation promotes intratumoral synthesis of dihydrotestosterone from androgen metabolites in prostate cancer. Sci Rep. 2013; 3: 1528. doi: 10.1038/srep01528.
39. Zhang A, Zhang J, Plymate S, Mostaghel EA. Classical and Non-Classical Roles for Pre-Receptor Control of DHT Metabolism in Prostate Cancer Progression. Horm Cancer. 2016; 7: 104-13. doi: 10.1007/s12672-016-0250-9.
40. Klein KA, Reiter RE, Redula J, Moradi H, Zhu XL, Brothman AR, Lamb DJ, Marcelli M, Belldegrun A, Witte ON, Sawyers CL. Progression of metastatic human prostate cancer to androgen independence in immunodeficient SCID mice. Nat Med. 1997; 3: 402-8.
41. Horoszewicz JS, Leong SS, Kawinski E, Karr JP, Rosenthal H, Chu TM, Mirand EA, Murphy GP. LNCaP model of human prostatic carcinoma. Cancer Res. 1983; 43: 1809-18.
42. Thalmann GN, Anezinis PE, Chang SM, Zhau HE, Kim EE, Hopwood VL, Pathak S, von Eschenbach AC, Chung LW. Androgen-independent cancer progression and bone metastasis in the LNCaP model of human prostate cancer. Cancer Res. 1994; 54: 2577-81.
43. Wu HC, Hsieh JT, Gleave ME, Brown NM, Pathak S, Chung LW. Derivation of androgen-independent human LNCaP prostatic cancer cell sublines: role of bone stromal cells. Int J Cancer. 1994; 57: 406-12.
44. Gregory CW, Johnson RT, Jr., Mohler JL, French FS, Wilson EM. Androgen receptor stabilization in recurrent prostate cancer is associated with hypersensitivity to low androgen. Cancer Res. 2001; 61: 2892-8.
45. Mickey DD, Stone KR, Wunderli H, Mickey GH, Paulson DF. Characterization of a human prostate adenocarcinoma cell line (DU 145) as a monolayer culture and as a solid tumor in athymic mice. Prog Clin Biol Res. 1980; 37: 67-84.
46. Wainstein MA, He F, Robinson D, Kung HJ, Schwartz S, Giaconia JM, Edgehouse NL, Pretlow TP, Bodner DR, Kursh ED, Resnick MI, Seftel A, Pretlow TG. CWR22: androgen-

dependent xenograft model derived from a primary human prostatic carcinoma. Cancer Res. 1994; 54: 6049-52.
47. Nagabhushan M, Miller CM, Pretlow TP, Giaconia JM, Edgehouse NL, Schwartz S, Kung HJ, de Vere White RW, Gumerlock PH, Resnick MI, Amini SB, Pretlow TG. CWR22: the first human prostate cancer xenograft with strongly androgen-dependent and relapsed strains both in vivo and in soft agar. Cancer Res. 1996; 56: 3042-6.
48. Papadopoulos JS, Agarwala R. COBALT: constraint-based alignment tool for multiple protein sequences. Bioinformatics. 2007; 23: 1073-9. doi: 10.1093/bioinformatics/btm076.
49. Wilton J, Titus M, Efstathiou E, Fetterly G, Mohler J. Androgenic biomarker profiling in human matrices and cell culture samples using high throughput, electrospray tandem mass spectrometry. Prostate. 2014; 74: 722-31.
50. Gregory CW, Hamil KG, Kim D, Hall SH, Pretlow TG, Mohler JL, French FS. Androgen receptor expression in androgen-independent prostate cancer is associated with increased expression of androgen-regulated genes. Cancer Res. 1998; 58: 5718-24.
51. Kim D, Gregory CW, Smith GJ, Mohler JL. Immunohistochemical quantitation of androgen receptor expression using color video image analysis. Cytometry. 1999; 35: 2-10.
52. Kim D, Gregory CW, French FS, Smith GJ, Mohler JL. Androgen receptor expression and cellular proliferation during transition from androgen-dependent to recurrent growth after castration in the CWR22 prostate cancer xenograft. Am J Pathol. 2002; 160: 219-26. doi: 10.1016/S0002-9440(10)64365-9.

Figure Legends

Figure 1: HSD17B6, RDH16, DHRS9 and RDH5 expression in AS-BP, AS-CaP and CRPC

Androgen metabolism pathways for DHT synthesis (A). Diagram of 3α-oxidoreductase activity (B). COBALT 3α-oxidoreductase protein sequence alignment with the catalytic site highlighted (green box) (C). IHC of four endogenous 3α-oxidoreductases in AS-BP, AS-CaP and CRPC (D). Positive and negative control images were shown in Supplemental Fig. S1. Scores showed that HSD17B6 and RDH16 were expressed at higher levels in CRPC than ASBP or AS-CaP tissue (E). Data were presented as the mean +/- SEM. Protein expression was modeled as a function of tissue type (AS-BP, AS-CaP or CRCP), compartment (cytosol or nuclear), their interaction, and a random rater effect using a linear mixed model (LMM). Mean expression was compared among tissue types and between compartments using Tukey-Kramer adjusted tests about the least square means. *P*-values were listed in Supplemental Table S4.

Figure 2: 3α-oxidoreductases were expressed in CaP cell lines and xenografts

qRT-PCR results were shown for 3α-oxidoreductase (A), SRD5A (B), and AR (C) mRNA levels for CaP cell lines and CWR22 and rCWR22 xenografts. Data were presented as mean +/-

SEM. Gene expression was modeled as a function of cell line and a random replicate effect using a LMM. Mean expression was compared among cell lines using Tukey-Kramer adjusted tests about the least square means.

Figure 3: DHT levels increased when RDH16 was expressed in LAPC-4 cells

Androgen levels were measured using LC-MS/MS from media and cell pellets of LAPC-4 cells transfected with empty plasmid or expression plasmids encoded with HSD17B6, RDH16, DHRS9 or RDH5. Media and cell pellet androgen levels were combined. Cells were treated for 12 h in SFM alone (A) or SFM with 20 nM DIOL (B) or 1 nM T (C) or 20 nM AND (D). Western blot analysis using DDK antibody was used to confirm enzyme expression (E). Data were presented as mean +/- SEM. Androgen levels were modeled as a function of treatment (SFM, DIOL, T or AND), enzyme (HSD17B6, RDH16, DHRS9 or RDH5), and their interaction using a general linear model (GLM). Mean androgen levels were compared among DIOL, T or AND treated LAPC-4 cells against SFM treated LAPC-4 cells for each analyte. Comparisons were made among LAPC-4 cells that expressed each 3α-oxidoreductase and LAPC-4 cells with empty plasmid for each treatment using Dunnett adjusted post-hoc tests. *P*-values were reported in Supplemental Table S6. * $p < 0.05$

Figure 4: Mutation of conserved residues impaired 3α-oxidoreductase activity

CV-1 cells were analyzed for 3α-oxidoreductase gene expression (A). 5α-dione levels were measured in CV-1 cells that transiently expressed wild-type HSD17B6, RDH16, DHRS9 or RDH5 wild-type 3α-oxidoreductases catalytic site deletion mutant (Δcat) or double mutant (Y→F,K→R) (B). Transient 3α-oxidoreductase expression was confirmed using western blotting with DDK antibody (C). Data were presented as the mean +/- SEM. Mean media androgen levels were compared between AND or SFM treated CV-1 cells using one-sided Tukey-Kramer adjusted Welch-Satterthwaite T-tests; corresponding *P*-values were listed in Supplemental Table S6. Media androgen levels of AND treated CV-1 cells were modeled as a function of enzyme (HSD17B6, RDH16, DHRS9 or RDH5, or empty plasmid), plasmid type (wild-type,

Y→F,K→R or ∆cat 3α-oxidoreductases) and their interaction using a GLM. Mean levels were compared among plasmid types for each 3α-oxidoreductase, and among 3a-oxidoreductases and the empty plasmid for each plasmid type using Tukey-Kramer adjusted post-hoc tests. *P*-values were reported in Supplemental Table S8. * $p < 0.05$

Figure 5: 3α-oxidoreductases were expressed in AS-BP and AS-CaP tissues from research subjects treated with finasteride

HSD17B6, RDH16 and RDH5 (A) were detected using IHC in androgen stimulated-benign prostate (AS-BP) and CaP (AS-CaP) tissues. Visual scoring showed 3α-oxidoreductase expression levels did not change with or without finasteride treatment (B). Data were presented as mean +/- SEM. Protein expression levels were modeled as a function of treatment (finasteride and no finasteride), tissue type (AS-BP or AS-CaP), their interaction, and a random subject effect using a LMM. Mean levels were compared between treatments within each tissue type, and between tissue types for each treatment using Tukey-Kramer adjusted tests about the least-square means. *P*-values were reported in Supplemental Table S9.

Figure 6: The combination of dutasteride and 3α-oxidoreductase mutants decreased DHT levels greater than dutasteride alone

The effect of dutasteride on DHT levels was determined in LAPC-4 cells that transiently overexpressed wild-type, ∆cat or Y→F,K→R enzymes (A). DHT levels were measured in VCaP, C4-2 and CWR-R1 cells transfected with empty plasmid or over-expressing plasmids of wild-type RDH16 or RDH16 Y176F,K180R (B-D). Western blot analysis using DDK antibody confirmed transiently expressed enzymes in LAPC-4, VCaP, C4-2 and CWR-R1 (E-H). Data were presented as mean +/- SEM. DHT was modeled as a function of treatment (dutasteride or SFM), enzyme (HSD17B6, RDH16, DHRS9 or RDH5) or empty plasmid, and plasmid type (wild-type, ∆cat or Y→F,K→R) using a GLM. Mean DHT levels were compared between dutasteride and SFM treated LAPC-4 cells using one-sided Tukey-Kramer adjusted tests about the least-square means. Mean levels were compared among LAPC-4 cells that expressed HSD17B6,

RDH16, DHRS9 or RDH5, or empty plasmid, for each 3α-oxidoreductase-treatment combination using Tukey-Kramer adjusted tests about the least square means. *P*-values were reported in Supplemental Table S10. * $p < 0.05$

Fig. 1

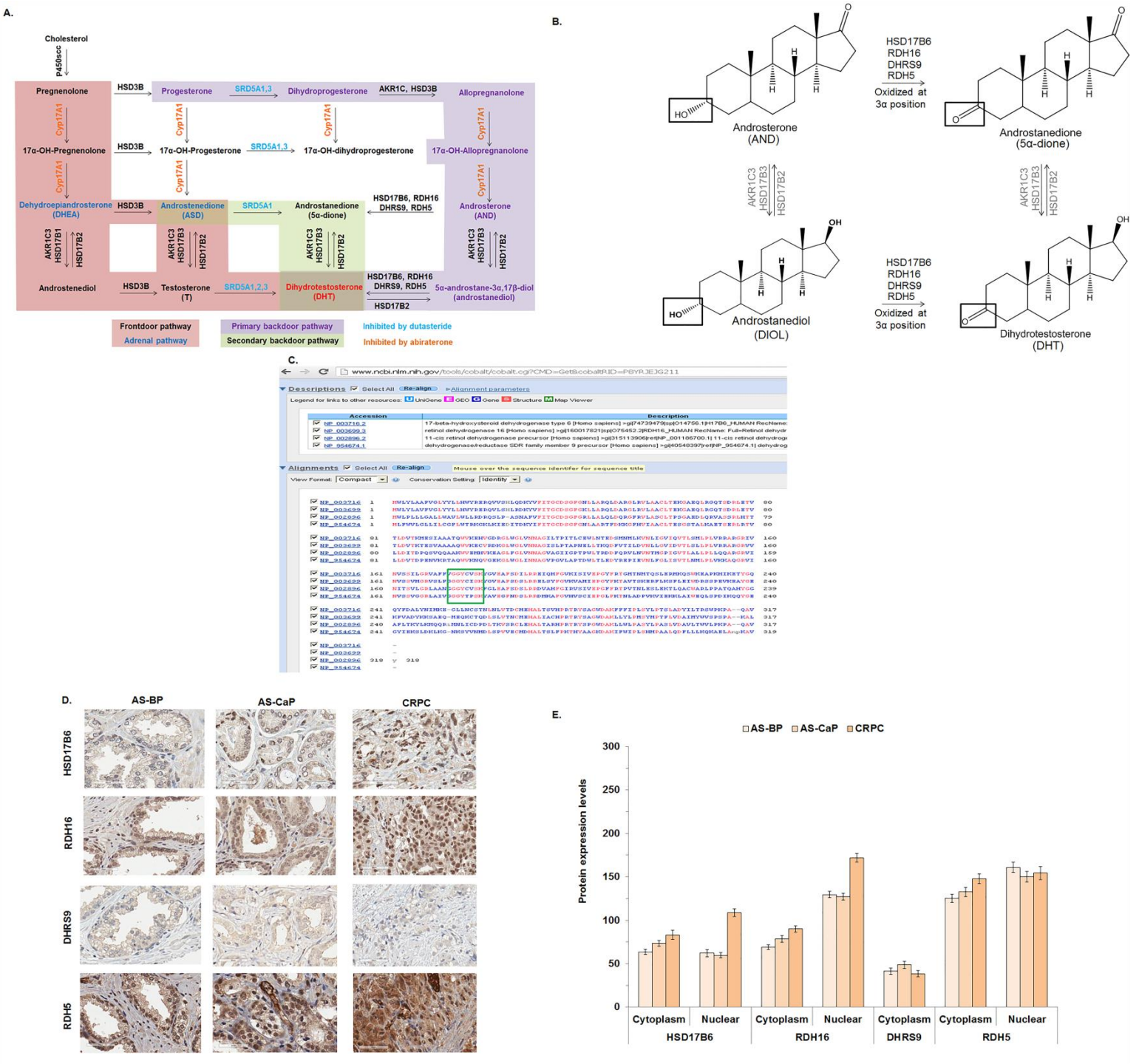
A.
Cholesterol
P450scc
Pregnenolone
HSD3B
Progesterone
SRD5A1,3
Dihydroprogesterone
AKR1C, HSD3B
Allopregnanolone
Cyp17A1
17α-OH-Pregnenolone
17α-OH-Progesterone
17α-OH-dihydroprogesterone
17α-OH-Allopregnanolone
Dehydroepiandrosterone (DHEA)
Androstenedione (ASD)
SRD5A1
Androstanedione (5α-dione)
HSD17B6, RDH16 DHRS9, RDH5
Androsterone (AND)
AKR1C3 HSD17B3 HSD17B2
AKR1B1 HSD17B2
Androstenediol
Testosterone (T)
SRD5A1,2,3
Dihydrotestosterone (DHT)
5α-androstane-3α,17β-diol (androstanediol)
Frontdoor pathway
Adrenal pathway
Primary backdoor pathway
Secondary backdoor pathway
Inhibited by dutasteride
Inhibited by abiraterone
B.
Androsterone (AND)
HSD17B6 RDH16 DHRS9 RDH5
Oxidized at 3α position
Androstanedione (5α-dione)
Androstanediol (DIOL)
Dihydrotestosterone (DHT)
C.
www.ncbi.nlm.nih.gov/tools/cobalt/cobalt.cgi?CMD=Get&cobaltR.ID=PBYRJEJG211
Descriptions
Alignments
Accession
Description
NP_003716.2
NP_003699.3
NP_002896.2
NP_954674.1
D.
AS-BP
AS-CaP
CRPC
HSD17B6
RDH16
DHRS9
RDH5
E.
AS-BP
AS-CaP
CRPC
Protein expression levels
300
250
200
150
100
50
0
Cytoplasm
Nuclear
HSD17B6
RDH16
DHRS9
RDH5

Fig. 2

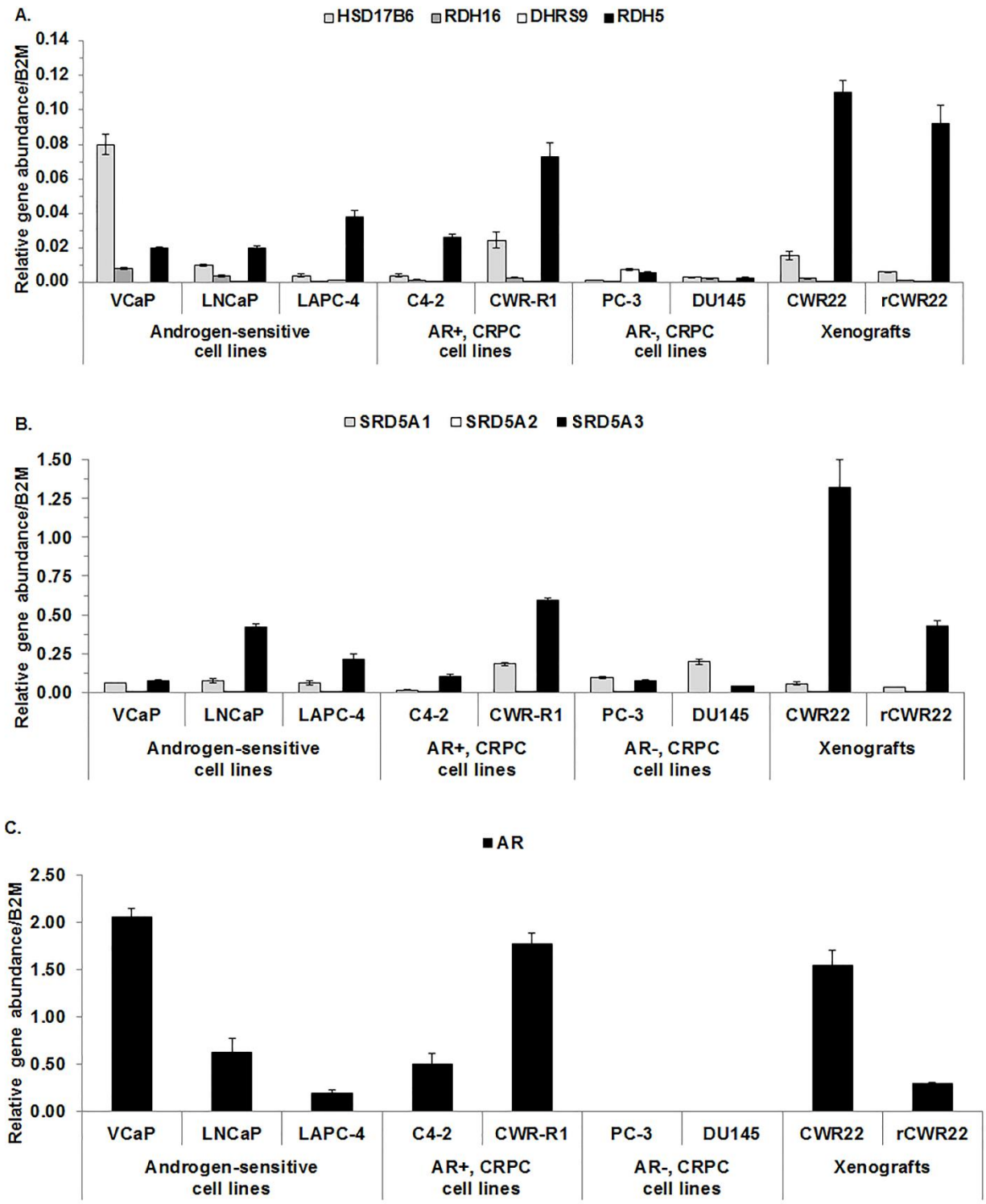
A.
HSD17B6
RDH16
DHRS9
RDH5
Relative gene abundance/B2M
0.14
0.12
0.10
0.08
0.06
0.04
0.02
0.00
VCaP
LNCaP
LAPC-4
C4-2
CWR-R1
PC-3
DU145
CWR22
rCWR22
Androgen-sensitive cell lines
AR+, CRPC cell lines
AR-, CRPC cell lines
Xenografts
B.
SRD5A1
SRD5A2
SRD5A3
Relative gene abundance/B2M
1.50
1.25
1.00
0.75
0.50
0.25
0.00
VCaP
LNCaP
LAPC-4
C4-2
CWR-R1
PC-3
DU145
CWR22
rCWR22
Androgen-sensitive cell lines
AR+, CRPC cell lines
AR-, CRPC cell lines
Xenografts
C.
AR
Relative gene abundance/B2M
2.50
2.00
1.50
1.00
0.50
0.00
VCaP
LNCaP
LAPC-4
C4-2
CWR-R1
PC-3
DU145
CWR22
rCWR22
Androgen-sensitive cell lines
AR+, CRPC cell lines
AR-, CRPC cell lines
Xenografts

Fig. 3

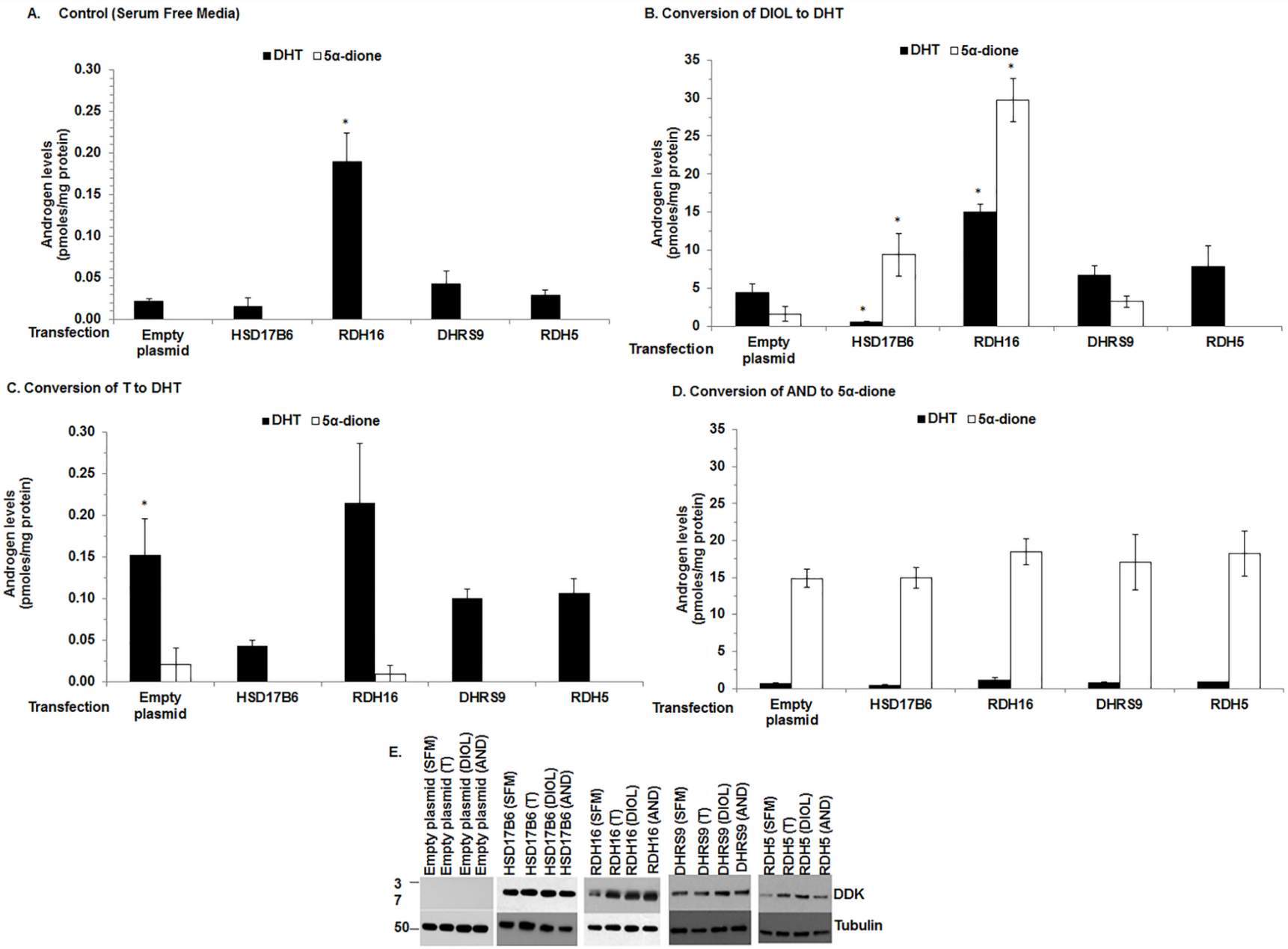
A. Control (Serum Free Media)
DHT
5α-dione
Androgen levels (pmoles/mg protein)
0.30
0.25
0.20
0.15
0.10
0.05
0.00
Transfection
Empty plasmid
HSD17B6
RDH16
DHRS9
RDH5
B. Conversion of DIOL to DHT
DHT
5α-dione
Androgen levels (pmoles/mg protein)
35
30
25
20
15
10
5
0
Transfection
Empty plasmid
HSD17B6
RDH16
DHRS9
RDH5
C. Conversion of T to DHT
DHT
5α-dione
Androgen levels (pmoles/mg protein)
0.30
0.25
0.20
0.15
0.10
0.05
0.00
Transfection
Empty plasmid
HSD17B6
RDH16
DHRS9
RDH5
D. Conversion of AND to 5α-dione
DHT
5α-dione
Androgen levels (pmoles/mg protein)
35
30
25
20
15
10
5
0
Transfection
Empty plasmid
HSD17B6
RDH16
DHRS9
RDH5
E.
Empty plasmid (SFM)
Empty plasmid (T)
Empty plasmid (DIOL)
Empty plasmid (AND)
HSD17B6 (SFM)
HSD17B6 (T)
HSD17B6 (DIOL)
HSD17B6 (AND)
RDH16 (SFM)
RDH16 (T)
RDH16 (DIOL)
RDH16 (AND)
DHRS9 (SFM)
DHRS9 (T)
DHRS9 (DIOL)
DHRS9 (AND)
RDH5 (SFM)
RDH5 (T)
RDH5 (DIOL)
RDH5 (AND)
3
7
50
DDK
Tubulin

Fig. 4

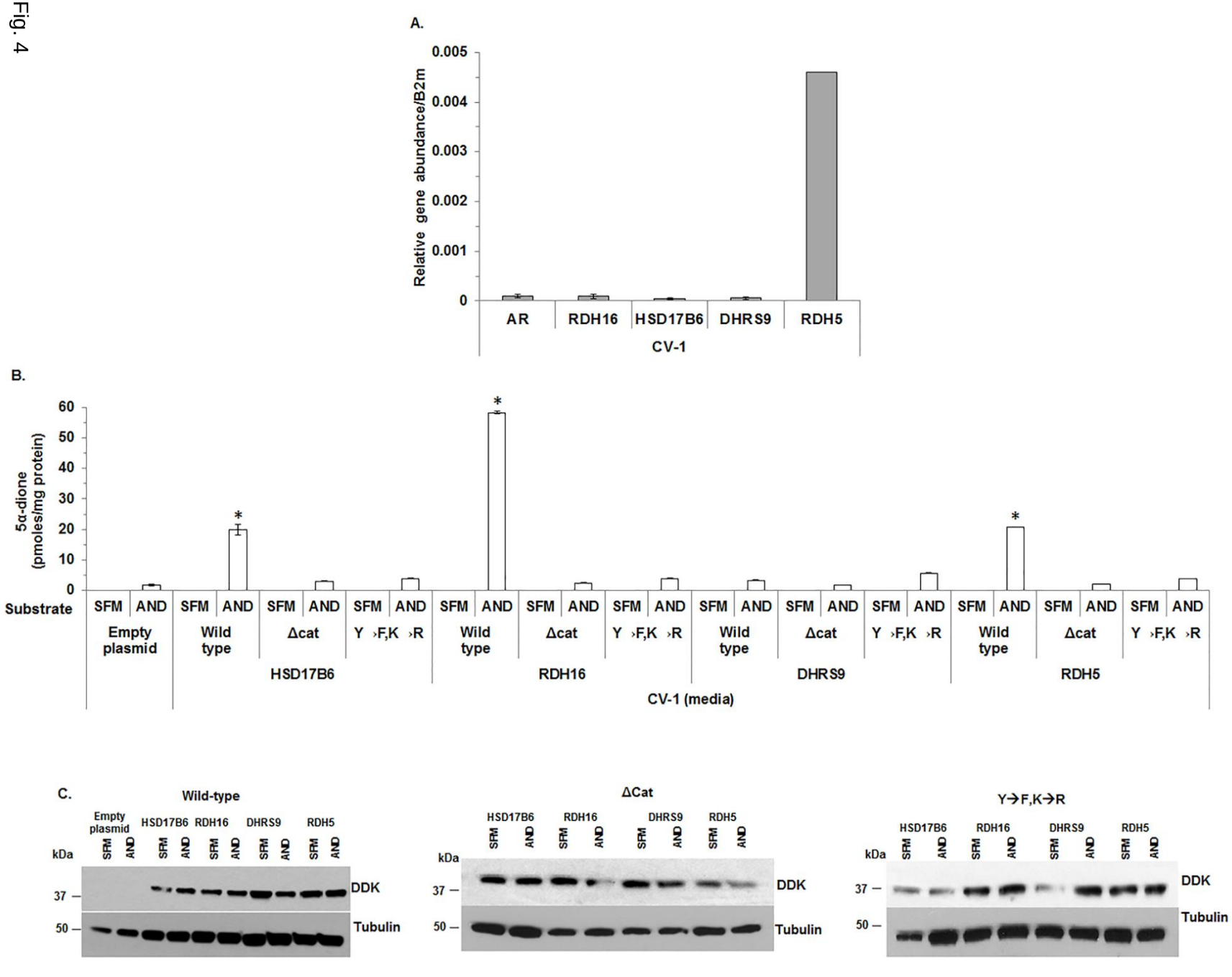
A.
Relative gene abundance/B2m
0.005
0.004
0.003
0.002
0.001
0
AR
RDH16
HSD17B6
DHRS9
RDH5
CV-1
B.
5α-dione (pmoles/mg protein)
60
50
40
30
20
10
0
Substrate
SFM
AND
Empty plasmid
Wild type
Δcat
Y →F,K →R
HSD17B6
RDH16
DHRS9
RDH5
CV-1 (media)
C.
Wild-type
ΔCat
Y→F,K→R
Empty plasmid
HSD17B6
RDH16
DHRS9
RDH5
kDa
37
50
DDK
Tubulin

Fig. 5

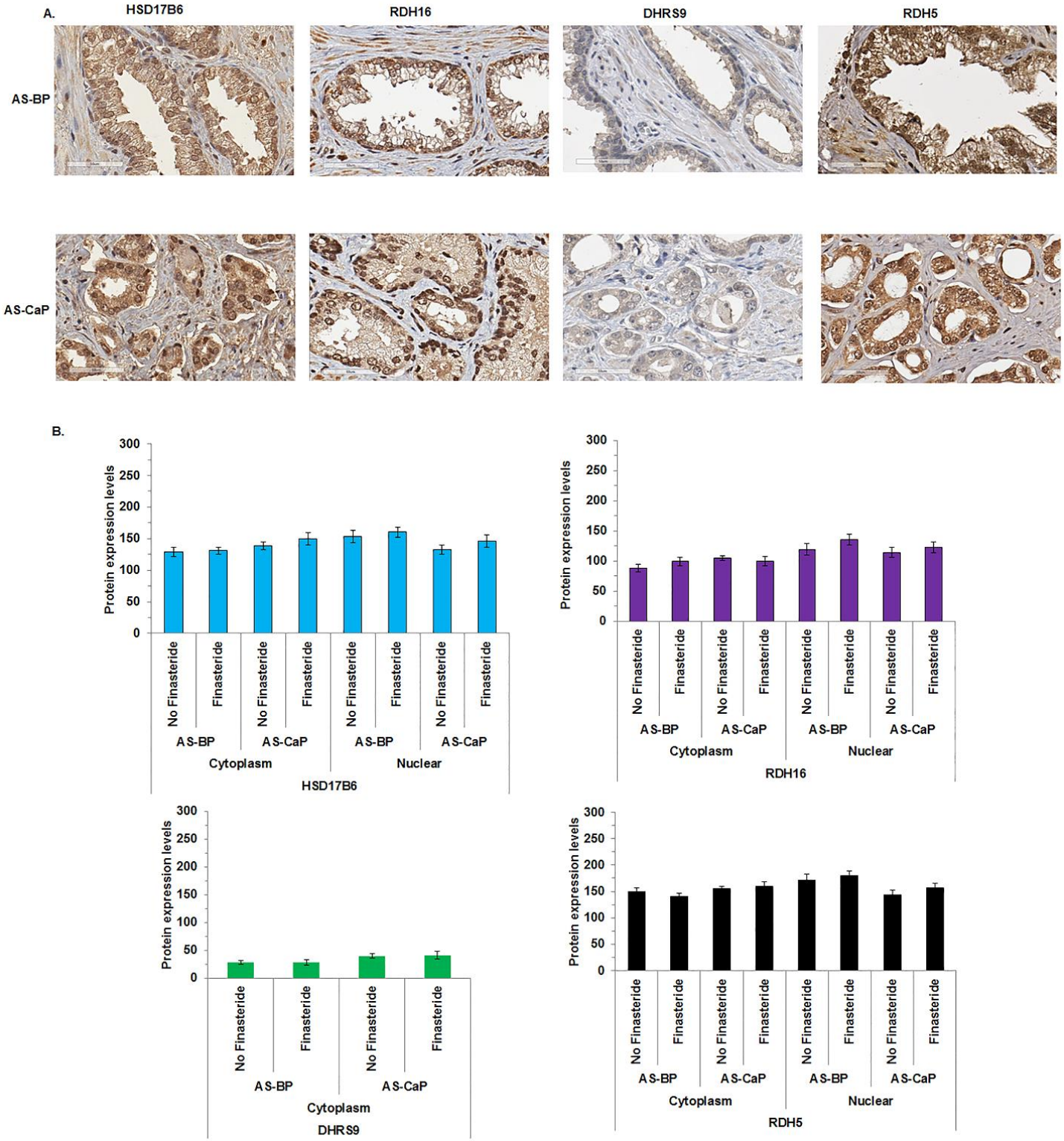
A.
HSD17B6
RDH16
DHRS9
RDH5
AS-BP
AS-CaP
B.
Protein expression levels
300
250
200
150
100
50
0
No Finasteride
Finasteride
AS-BP
AS-CaP
Cytoplasm
Nuclear
HSD17B6
RDH16
DHRS9
RDH5

Fig. 6

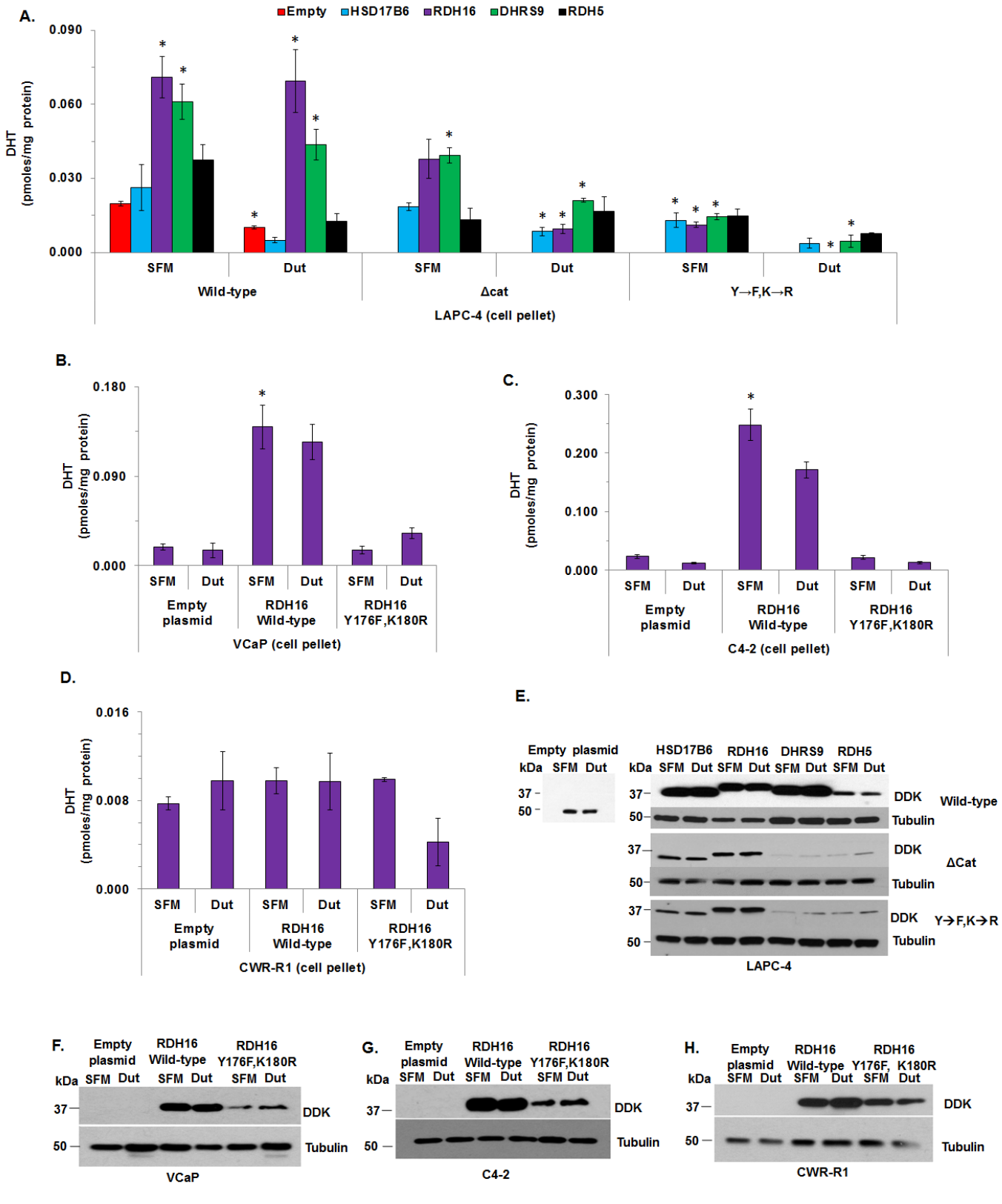
A.
Empty
HSD17B6
RDH16
DHRS9
RDH5
DHT (pmoles/mg protein)
0.090
0.060
0.030
0.000
SFM
Dut
Wild-type
Δcat
Y→F,K→R
LAPC-4 (cell pellet)
B.
0.180
0.090
0.000
Empty plasmid
RDH16 Wild-type
RDH16 Y176F,K180R
VCaP (cell pellet)
C.
0.300
0.200
0.100
0.000
C4-2 (cell pellet)
D.
0.016
0.008
0.000
CWR-R1 (cell pellet)
E.
Empty plasmid
kDa
37
50
DDK
Tubulin
Wild-type
ΔCat
Y→F,K→R
LAPC-4
F.
VCaP
G.
C4-2
H.
CWR-R1

Send Orders for Reprints to reprints@benthamscience.ae

Efficient Synthesis of Aurone Mannich Bases and Evaluation of their Antineoplastic Activity in PC-3 Prostate Cancer Cells

Antonina V. Popova,[a] Mykhaylo S. Frasinyuk,[a,b,c] Svitlana P. Bondarenko,[d] Wen Zhang,[b,e] Yanqi Xie,[b,c] Zachary M. Martin,[b,c] Xianfeng Cai,[b,e] Michael V. Fiandalo,[f] James L. Mohler,[f] Chunming Liu,[b,e] David S. Watt[b,c,e] and Vitaliy M. Sviripa[c,g,*]

[a]*Department of Chemistry of Bioactive Nitrogen Containing Heterocyclic Bases, Institute of Bioorganic and Petrochemistry, National Academy of Sciences of Ukraine, Kyiv 02094, Ukraine;* [b]*Department of Molecular and Cellular Biochemistry, College of Medicine, University of Kentucky, Lexington, KY 40536-0509, USA;* [c]*Center for Pharmaceutical Research and Innovation, College of Pharmacy, University of Kentucky, Lexington, KY 40536-0509, USA;* [d] *National University of Food Technologies, Kyiv 01601, Ukraine;* [e] *Lucille Parker Markey Cancer Center, University of Kentucky, Lexington, KY 40536-0509, USA;* [f] *Department of Urology, Elm & Carlton Streets, Roswell Park Cancer Institute, Buffalo, New York 14263, USA;* [g] *Department of Pharmaceutical Sciences, College of Pharmacy, University of Kentucky, Lexington, KY 40536-0509, USA*

Abstract: An efficient method for regioselective synthesis of C-7 Mannich bases of 6-hydroxyaurones was accomplished by the *N*,*N*-dialkylaminomethylation using aminals prepared from dimethylamine, dipropylamine, bis(2-methoxyethyl)amine, *N*-methylbutylamine, *N*-methylbenzylamine, morpholine, piperidine, and 1-methylpiperazine. Further transformation of 7-(*N*,*N*-dialkylamino)methyl group in these aurones led to formation of C-7 acetoxymethyl and methoxymethyl derivatives of 6-hydroxyaurones, some of which showed promising inhibition of PC-3 cancer cell proliferation in the high nanomolar to low micromolar range.

Keywords: 6-hydroxyaurones • Mannich base • aminomethylation • antineoplastic • PC-3 cells • prostate cancer.

1. INTRODUCTION

The 2-Benzylidenebenzofuran-3(2*H*)-ones, commonly known as aurones, represent a subclass of flavonoids with pharmacological potential [1-3]. Semisynthetic aurones display antitubercular [4], anticancer [5], antimalarial [6] activity, and aurones with tertiary amines, including Mannich bases, were reported as inhibitors of AChE [7] PIM1 [8], p38 MAP kinase [9]. Structure-activity relationships among the flavonoids, isoflavonoids, and semisynthetic aurones do not necessarily parallel one another [10] but the high CDK1/Cyclin B inhibitory activity of flavonoid Mannich bases [11, 12] prompted us to consider auronoid Mannich bases for evaluation as potential antineoplastic agents. In contrast to flavonoids and isoflavonoids, reports on the synthesis and evaluation of auronoid Mannich bases were scarce.

We ascribed part of this deficiency to poor yields encountered in the application of "classical Mannich reactions" to 6-hydroxyaurones **2a** using aqueous paraformaldehyde and secondary amines in ethanol [6].

*Address correspondence to this author at the Department of Pharmaceutical Sciences, College of Pharmacy, University of Kentucky, Lexington, KY 40536-0509, USA Tel/Fax: ++1-859-420-8879, +1-859-257-7585; E-mail: vitaliy.sviripa@uky.edu

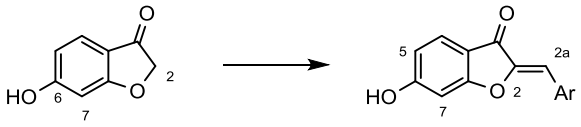

Fig. (1). 6-Hydroxybenzofuran-3-(2*H*)-ones **1** and 6-hydroxyaurones **2**.

Alternative methods for the synthesis of semisynthetic aurones introduced aminomethyl groups on alkoxy- or hydroxy-substituted benzofuran-3(2*H*)-one derivatives [8, 13] **1** prior to condensation with aryl or heteroaryl aldehydes to secure the semisynthetic aurones **2** (Ar = aryl or heteroaryl). Aminomethylation of benzofuran-3(2*H*)-one (**1a)** generally proceed in poor yields because of competitive condensation at C-2 leading to 2,2-bis-(*N*,*N*-dialkylamino)methyl 6-hydroxybenzofuran-3(2*H*)-one derivatives [14, 15]. As a consequence, we explored a procedure for the direct aminomethylation of semisynthetic 6-hydroxyaurones **2** as a means of acquiring compounds for biological evaluation.

2. MATERIALS AND METHOD

2.1 Chemical Synthesis

^{1}H and ^{13}C NMR spectra were recorded on a Varian 500 spectrometer (at 500 MHz or at 125 MHz, respectively) or

XXX-XXX/14 $58.00+.00

on a Varian 400 spectrometer (at 400 MHz or at 100 MHz, respectively) in deuteriochloroform ($CDCl_3$) or deuterated dimethylsulfoxide (DMSO-d_6). ^{13}C NMR IR spectra were recorded on a Bruker Vertex 70 FT/IR spectrometer. Melting points were determined in open capillarity tubes with a Buchi B-535 apparatus and were uncorrected. Mass spectra were obtained with an Agilent 1100 spectrometer under chemical ionization conditions.

General procedure for the synthesis of 6-hydroxyaurones 2a-2f.

To a stirred solution of 0.75 g (5 mmol) 6-hydroxybenzofuranone (**1**) in ethanol (5 mL) and DMF (5 mL) was added aldehyde (5 mmol) and 1.15 mL of 50% KOH. The mixture was stirred at room temperature for 4-6 h. The reaction mixture was poured into 30 mL of hot water with vigorous stirring and neutralized with conc. HCl at pH of 1-2. The precipitate was filtered, washed with water, dried and recrystallized from DMF-MeOH.

(2*Z*)-2-Benzylidene-6-hydroxy-1-benzofuran-3(2*H*)-one (2a). Yellow solid (87% yield); mp: 259-260^{o}C; IR (KBr): ν_{max} 3072, 2960, 1674, 1644, 1580, 1455, 1376, 1285, 1109, 770 cm^{-1}; ^1H NMR (400 MHz, DMSO-d_6): δ 6.72 (1H, dd, ^3J = 8.4 Hz, ^4J = 1.7 Hz, H-5), 6.78 (1H, s, H-2a), 6.80 (1H, d, ^4J=1.7 Hz, H-7), 7.38 –7.53 (3H, m, H-3′, 4′, 5′), 7.63 (1H, d, ^3J = 8.4 Hz, H-4), 7.94 (2H, d, ^3J = 8.5 Hz, H-2′, 6′), 11.30 ppm (1H, br. s, OH-6); ^{13}C NMR (100 MHz, DMSO-d_6): δ 98.71, 110.41, 112.79, 113.18, 126.08, 129.04, 129.72, 131.12, 132.14, 147.45, 166.70, 168.05, 181.55 ppm; MS (CI): *m/z* 238.9 (MH$^+$, 100). Anal. calcd for $C_{15}H_{10}O_3$: C, 75.62; H, 4.23. Found: C, 75.41; H, 4.05.

(2*Z*)-6-Hydroxy-2-(4-methoxybenzylidene)-1-benzofuran-3(2*H*)-one (2b). Yellow solid (85% yield); mp: 268 - 270^{o}C; IR (KBr): ν_{max} 3081, 2899, 2598, 1675, 1566, 1455, 1285, 1256, 1108 cm^{-1}; ^1H NMR (400 MHz, DMSO-d_6): δ 3.81 (3H, s, OMe-4′), 6.71 (1H, dd, ^3J = 8.5 Hz, ^4J = 2.0 Hz, H-5), 6.77 – 6.81 (2H, m, H-2a, H-7), 7.05 (2H, d, ^3J = 8.4 Hz, H-3′, 5′), 7.61 (1H, d, ^3J = 8.5 Hz, H-4), 7.91 (2H, d, ^3J = 8.4 Hz, H-2′, 6′), 11.17 ppm (1H, s, OH-6); ^{13}C NMR (100 MHz, DMSO-d_6): δ 55.28, 98.46, 110.62, 112.81, 112.96, 114.48, 124.50, 125.65, 132.82, 146.05, 160.30, 166.11, 167.47, 181.08 ppm; MS (CI): *m/z* 269.1 (MH$^+$, 100). Anal. calcd for $C_{16}H_{12}O_4$: C, 71.64; H, 4.51. Found: C, 71.45; H 4.38.

(2*Z*)-2-(3,4-Dimethoxybenzylidene)-6-hydroxy-1-benzofuran-3(2*H*)-one (2c). Yellow solid (87% yield); mp: 224 - 226^{o}C; IR (KBr): ν_{max} 3122, 1679, 1582, 1509, 1259, 1235, 1125, 1092, 1015 cm^{-1}; ^1H NMR (400 MHz, DMSO-d_6): δ 3.82, 3.83 (each 3H, 2s, OMe-3′,4′), 6.68 (1H, dd, ^3J = 8.5 Hz, ^4J = 1.8 Hz, H-5), 6.73 (1H, s, H-2a), 6.75 (1H, d, ^4J = 1.8 Hz, H-7), 7.07 (1H, d,^3J = 8.5 Hz, H-5′), 7.54-7.60 ppm (3H, m, H-4, 2′, 6′); ^{13}C NMR (100 MHz, DMSO-d_6): δ 55.50, 55.55, 98.56, 111.07, 111.86, 112.83, 112.96, 114.13, 124.65, 124.98, 125.66, 146.11, 148.61, 150.25, 166.11, 167.45, 181.06 ppm; MS (CI): *m/z* 299.1 (MH$^+$, 100). Anal. calcd for $C_{17}H_{14}O_5$: C, 68.45; H, 4.73. Found: C, 68.31; H 4.51.

(2*Z*)-2-(1,3-Benzodioxol-5-ylmethylene)-6-hydroxy-1-benzofuran-3(2*H*)-one (2d). Yellow solid (91% yield); mp: 321 - 323^{o}C (decomp); IR (KBr): ν_{max} 3057, 2890, 1668, 1616, 1542, 1446, 1405, 1329, 1253, 1102, 1034 cm^{-1}; ^1H NMR (400 MHz, DMSO-d_6): δ 6.11 (2H, s, OCH_2O), 6.71 (1H, dd, ^3J = 8.5 Hz, ^4J = 1.8 Hz, H-5), 6.74 (1H, s, H-2a), 6.81 (1H, d, ^4J = 1.8 Hz, H-7), 7.04 (1H, d, ^3J = 8.1 Hz, H-7′), 7.47 (1H, dd, ^3J = 8.1 Hz, ^4J = 1.7 Hz, H-6′), 7.55 (1H, d, ^4J = 1.7 Hz, H-4′), 7.60 ppm (1H, d, ^3J = 8.5 Hz, H-4); ^{13}C NMR (100 MHz, DMSO-d_6): δ 98.58, 101.59, 108.80, 109.95, 110.64, 112.78, 112.93, 125.66, 126.12, 126.79, 146.15, 147.70, 148.50, 166.35, 167.52, 181.04 ppm; MS (CI): *m/z* 283.3 (MH$^+$, 100). Anal. calcd for $C_{16}H_{10}O_5$: C, 68.09; H, 3.57. Found: C, 67.95; H, 3.68.

(2*Z*)-6-Hydroxy-2-(3,4,5-trimethoxybenzylidene)-1-benzofuran-3(2*H*)-one (2e). Yellow solid (81% yield); mp: 254 - 256^{o}C; IR (KBr): ν_{max} 3271, 1678, 1637, 1582, 1454, 1315, 1242, 1129, 1108, 998 cm^{-1}; ^1H NMR (400 MHz, DMSO-d_6): δ 3.72 (3H, s, OMe-4′), 3.85 (6H, s, OMe-3′, 5′), 6.72 (1H, dd, ^3J = 8.4 Hz, ^2J = 2.0 Hz, H-5), 6.75 (1H, s, H-2a), 6.82 (1H, d, ^4J = 2.0 Hz, H-7), 7.30 (2H, s, H-2′, 6′), 7.61 (1H, d, ^3J = 8.4 Hz, H-4), 11.19 ppm (1H, br. s, OH-6); ^{13}C NMR (100 MHz, DMSO-d_6): δ 55.94, 60.12, 98.68, 108.73, 110.73, 112.74, 112.92, 125.73, 127.38, 139.03, 146.68, 152.83, 166.28, 167.61, 181.13 ppm; MS (CI): *m/z* 329.1 (MH$^+$, 100). Anal. calcd for $C_{18}H_{16}O_6$: C, 65.85; H, 4.91. Found: C, 65.62; H; 5.04.

(2*Z*)-6-Hydroxy-2-(2,3,4-trimethoxybenzylidene)-1-benzofuran-3(2*H*)-one (2f). Yellow solid (78% yield); mp: 249 - 251^{o}C; IR (KBr): ν_{max} 3169, 2941, 1680, 1582, 1492, 1266, 1136, 1103, 1090, 976 cm^{-1}; ^1H NMR (400 MHz, DMSO-d_6): δ 3.78, 3.87, 3.88 (each 3H, s, OMe-2′, 3′, 4′), 6.71 (1H, dd, ^3J = 8.3 Hz, ^4J = 1.9 Hz, H-5), 6.77 (1H, d, ^4J = 1.9 Hz, H-7), 6.90 (1H, s, H-2a), 6.98 (1H, d, ^3J = 8.9 Hz, H-5′), 7.61 (1H, d, ^3J = 8.3 Hz, H-4), 7.93 (1H, d, ^3J = 8.9 Hz, H-6′), 11.15 ppm (1H, br. s, OH-6); ^{13}C NMR (100 MHz, DMSO-d_6): δ 55.96, 60.42, 61.61, 98.50, 104.01, 108.45, 112.86, 112.92, 118.25, 125.73, 126.25, 141.55, 146.79, 152.80, 154.95, 166.19, 167.48, 181.09 ppm; MS (CI): *m/z* 329.1 (MH$^+$, 100). Anal. calcd for $C_{18}H_{16}O_6$: C, 65.85; H, 4.91. Found: C, 65.98; H, 5.12.

General procedure for the synthesis of Mannich bases 3–11.

To a suspension of 2 mmol of **2a-f** in 10 mL of isopropyl alcohol or 1,4-dioxane (in case of compound **1d**) was added 2.2 mmol of aminal, and the mixture was refluxed for 4-6 h. The mixture was diluted with 10 mL hexane and cooled. The residue was filtered and recrystallized from isopropanol-hexane mixture.

(2*Z*)-2-Benzylidene-7-[(dimethylamino)methyl]-6-hydroxy-1-benzofuran-3(2*H*)-one (3a). Yellow solid (77% yield); mp: 248 - 250^{o}C; IR (KBr): ν_{max} 3051, 2394, 1682, 1598, 1507, 1444, 1333, 1272, 1123, 1049 cm^{-1}; ^1H NMR (500 MHz, $CDCl_3$): δ 2.51 (6H, s, NMe_2), 3.99 (2H, s, CH_2-7), 6.67 (1H, d, ^3J = 8.4 Hz, H-5), 6.78 (1H, s, H-2a), 7.36 – 7.49 (3H, m, H-3′, 4′, 5′), 7.61 (1H, d, ^3J = 8.4 Hz, H-4), 7.82 (2H, d, ^3J = 8.8 Hz, H-2′, 6′), 10.69 ppm (1H, br. s, OH-7); ^{13}C NMR (125 MHz, $CDCl_3$): δ 44.55, 54.64, 104.19, 111.37, 113.16, 113.84, 125.53, 129.00, 129.55, 131.21, 132.72, 148.08, 165.86, 168.12, 182.78 ppm; MS (CI): *m/z* 296.2 (MH$^+$, 100). Anal. calcd for $C_{18}H_{17}NO_3$: C, 73.20; H, 5.80; N, 4.74. Found: C, 73.04; H, 5.54; N, 4.61.

(2*Z*)-7-[(Dimethylamino)methyl]-6-hydroxy-2-(4-methoxybenzylidene)-1-benzofuran-3(2*H*)-one (3b). Yellow solid (83% yield); mp: 171-173^{o}C; IR (KBr): ν_{max} 2960, 2836, 1692, 1600, 1509, 1252, 1126, 1036, 821 cm^{-1};

^{1}H NMR (400 MHz, $CDCl_3$): δ 2.49 (6H, s, NMe_2), 3.85 (3H, s, OMe-4′), 3.96 (2H, s, CH_2-7), 6.64 (1H, d, ^3J = 8.5 Hz, H-5), 6.74 (1H, s, H-2a), 6.97 (2H, d, ^3J = 8.9 Hz, H-3′, 5′), 7.58 (1H, d, ^3J = 8.5 Hz, H-4), 7.77 (2H, d, ^3J = 8.9 Hz, H-2′, 6′), 7.95 ppm (1H, br. s, OH-6); ^{13}C NMR (100 MHz, $CDCl_3$): δ 44.55, 54.72, 55.46, 104.21, 111.68, 113.43, 113.62, 114.56, 125.27, 125.35, 133.00, 146.97, 160.76, 165.48, 167.74, 182.73 ppm; MS (CI): *m/z* 326.2 (MH^+, 100). Anal. calcd for $C_{19}H_{19}NO_4$: C, 70.14; H, 5.89; N, 4.30. Found: C, 69.90; H, 5.62; N, 4.55.

(2*Z*)-2-(3,4-Dimethoxybenzylidene)-7-[(dimethylamino)methyl]-6-hydroxy-1-benzofuran-3(2*H*)-one (3c). Yellow solid (78% yield); mp: 91 - 93°C; IR (KBr): ν_{max} 3451, 3387, 2834, 1672, 1588, 1514, 1455, 1336, 1266, 1122 cm^{-1}; ^{1}H NMR (400 MHz, $CDCl_3$): δ 2.45 (6H, s, NMe_2), 3.91 (2H, s, CH_2-7), 3.95, 3.98 (each 3H, 2s, OMe-3′,4′), 6.65 (1H, d, ^3J = 8.3 Hz, H-5), 6.77 (1H, s, H-2a), 6.96 (1H, d,^3J = 8.4 Hz, H-5′), 7.42 (1H, dd, ^3J = 8.3 Hz, ^4J = 1.9 Hz, H-6′), 7.50 (1H, d, ^4J = 1.9 Hz, H-2′), 7.61 ppm (1H, d, ^3J = 8.4 Hz, H-4); ^{13}C NMR (125 MHz, $CDCl_3$): δ 44.74, 54.78, 55.85, 56.08, 104.22, 111.40, 111.95, 113.54, 113.63, 125.39, 125.43, 125.63, 147.10, 149.04, 150.54, 165.39, 167.46, 182.63 ppm; MS (CI): *m/z* 356.2 (MH^+, 100). Anal. calcd for $C_{20}H_{21}NO_5$: C, 67.59; H, 5.96; N, 3.94. Found: C, 67.83; H, 6.17; N, 4.07.

(2*Z*)-2-(1,3-Benzodioxol-5-ylmethylene)-7-[(dimethylamino)methyl]-6-hydroxy-1-benzofuran-3(2*H*)-one (3d). Yellow solid (84% yield); mp: 158 - 160°C; IR (KBr): ν_{max} 2963, 2899, 1689, 1601, 1444, 1331, 1242, 1038 cm^{-1}; ^{1}H NMR (400 MHz, $CDCl_3$): δ 2.47 (6H, s, NMe_2), 3.94 (2H, s, CH_2-7), 6.05 (2H, s, OCH_2O), 6.64 (1H, d, ^3J = 8.5 Hz, H-5), 6.72 (1H, s, H-2a), 6.89 (1H, d, ^3J = 8.1 Hz, H-7′), 7.24 – 7.27 (1H, m, H-6′), 7.47 (1H, d, ^4J = 1.6 Hz, H-4′), 7.60 ppm (1H, d, ^3J = 8.4 Hz, H-4); ^{13}C NMR (125 MHz, $CDCl_3$): δ 44.62, 54.98, 101.61, 104.50, 108.91, 110.31, 111.61, 113.37, 113.68, 125.17, 126.96, 127.12, 147.02, 148.20, 148.91, 165.37, 167.82, 182.64 ppm; MS (CI): *m/z* 340.0 (MH^+, 100). Anal. calcd for $C_{19}H_{17}NO_5$: C, 67.25; H, 5.05; N, 4.13. Found: C, 66.98; H, 5.31; N, 4.42.

(2*Z*)-7-[(Dimethylamino)methyl]-6-hydroxy-2-(3,4,5-trimethoxybenzylidene)-1-benzofuran-3(2*H*)-one (3e). Yellow solid (76% yield); mp: 191 - 193°C; IR (KBr): ν_{max} 3433, 2955, 1670, 1614, 1510, 1450, 1344, 1273, 1130, 1051 cm^{-1}; ^{1}H NMR (400 MHz, $CDCl_3$): δ 2.43 (6H, s, NMe_2), 3.88 (2H, s, CH_2-7), 3.92 (3H, s, OMe-4′), 3.95 (6H, s, OMe-3′, 5′), 6.66 (1H, d, ^3J = 8.5 Hz, H-5), 6.73 (1H, s, H-2a), 7.14 (2H, s, H-2′, 6′), 7.62 ppm (1H, d, ^3J = 8.5 Hz, H-4); ^{13}C NMR (100 MHz, DMSO-d_6): δ 43.62, 52.26, 55.82, 60.14, 103.65, 108.15, 108.89, 109.11, 115.07, 124.78, 127.90, 138.43, 147.63, 152.80, 166.27, 171.55, 179.71 ppm; MS (CI): *m/z* 386.2 (MH^+, 100). Anal. calcd for $C_{21}H_{23}NO_6$: C, 65.44; H, 6.02; N, 3.63. Found: C, 65.21; H, 6.15; N, 3.49.

(2*Z*)-7-[(Dimethylamino)methyl]-6-hydroxy-2-(2,3,4-trimethoxybenzylidene)-1-benzofuran-3(2*H*)-one (3f). Yellow solid (87% yield); mp: 152-154°C; IR (KBr): ν_{max} 2940, 1678, 1599, 1496, 1453, 1278, 1122, 1090 cm^{-1}; ^{1}H NMR (400 MHz, $CDCl_3$): δ 2.47 (6H, s, NMe_2), 3.90, 3.95, 3.97 (each 3H, 3s, OMe-2′, 3′, 4′), 3.93 (2H, s, CH_2-7), 6.65 (1H, d, ^3J = 8.4 Hz, H-5), 6.84 (1H, d, ^3J = 8.9 Hz, H-5′), 7.21 (1H, s, H-2a), 7.62 (1H, d, ^3J = 8.5 Hz, H-4), 7.94 (1H, d, ^3J = 8.9 Hz, H-6′), 8.24 ppm (1H, br. s, OH-7); ^{13}C NMR (100 MHz, $CDCl_3$): δ 44.37, 54.32, 56.07, 60.90, 61.84, 103.80, 105.74, 107.73, 113.47, 119.63, 125.36, 126.53, 142.21, 147.57, 153.86, 155.13, 165.38, 167.43, 182.51 ppm; MS (CI): *m/z* 386.2 (MH^+, 100). Anal. calcd for $C_{21}H_{23}NO_6$: C, 65.44; H, 6.02; N, 3.63. Found: C, 65.17; H, 5.83; N, 3.90.

(2*Z*)-7-{[Butyl(methyl)amino]methyl}-6-hydroxy-2-(4-methoxybenzylidene)-1-benzofuran-3(2*H*)-one (4b). Yellow solid (76% yield); mp: 112 - 114°C; IR (KBr): ν_{max} 3421, 2958, 1664, 1606, 1510, 1460, 1257, 1130 cm^{-1}; ^{1}H NMR (400 MHz, DMSO-d_6): δ 0.88 (3H, t, ^3J = 7.3 Hz, $CH_2CH_2CH_2C\underline{H}_3$), 1.24– 1.38 (2H, m, $CH_2CH_2C\underline{H}_2CH_3$), 1.52 – 1.69 (2H, m, $CH_2C\underline{H}_2CH_2CH_3$), 2.43 (3H, s, NMe), 2.63– 2.78 (2H, m, $C\underline{H}_2CH_2CH_2CH_3$), 3.82 (3H, s, OMe-4′), 4.04 (2H, s, CH_2-7), 6.48 (1H, d, ^3J = 8.6 Hz, H-5), 6.68 (1H, s, H-2a), 7.05 (2H, d, ^3J = 8.8 Hz, H-3′, 5′), 7.45 (1H, d, ^3J = 8.6 Hz, H-4), 7.90 ppm (2H, d, ^3J = 8.8 Hz, H-2′, 6′); ^{13}C NMR (100 MHz, DMSO-d_6): δ 13.71, 19.75, 27.87, 40.68, 51.17, 55.24, 55.73, 104.07, 109.03, 109.52, 114.41, 114.67, 124.33, 124.93, 132.53, 146.83, 159.91, 165.85, 171.15, 179.93 ppm; MS (CI): *m/z* 368.1 (MH^+, 100). Anal. calcd for $C_{22}H_{25}NO_4$: C, 71.91; H, 6.86; N, 3.81. Found: C, 72.09; H, 6.63; N, 3.65.

(2*Z*)-7-{[Butyl(methyl)amino]methyl}-2-(3,4-dimethoxybenzylidene)-6-hydroxy-1-benzofuran-3(2*H*)-one (4c). Yellow solid (73% yield); mp: 101 - 102°C; IR (KBr): ν_{max} 2959, 1676, 1605, 1512, 1458, 1260, 1118 cm^{-1}; ^{1}H NMR (400 MHz, $CDCl_3$): δ 0.92 (3H, t, ^3J = 7.4 Hz, $CH_2CH_2CH_2C\underline{H}_3$), 1.27– 1.46 (2H, m, $CH_2CH_2C\underline{H}_2CH_3$), 1.48 – 1.70 (2H, m, $CH_2C\underline{H}_2CH_2CH_3$), 2.41 (3H, s, NMe), 2.53– 2.65 (2H, m, $C\underline{H}_2CH_2CH_2CH_3$), 3.92, 3.95 (each 3H, 2s, OMe-3′,4′), 3.98 (2H, s, CH_2-7), 6.65 (1H, d, ^3J = 8.5 Hz, H-5), 6.73 (1H, s, H-2a), 6.93 (1H, d,^3J = 8.5 Hz, H-5′), 7.38 (1H, dd, ^3J = 8.5 Hz, ^4J = 2.0 Hz, H-6′), 7.45 (1H, d, ^4J = 2.0 Hz, H-2′), 7.58 ppm (1H, d, ^3J = 8.5 Hz, H-4); ^{13}C NMR (100 MHz, $CDCl_3$): δ 13.95, 20.41, 28.72, 41.37, 53.31, 55.83, 56.07, 57.09, 104.08, 111.39, 111.86, 113.47, 113.61, 113.67, 125.35, 125.40, 125.64, 147.12, 149.05, 150.52, 165.50, 167.62, 182.56 ppm; MS (CI): *m/z* 398.2 (MH^+, 100). Anal. calcd for $C_{23}H_{27}NO_5$: C, 69.50; H, 6.85; N, 3.52. Found: C, 69.77; H, 7.03; N, 3.64.

(2*Z*)-7-{[Butyl(methyl)amino]methyl}-6-hydroxy-2-(3,4,5-trimethoxybenzylidene)-1-benzofuran-3(2*H*)-one (4e). Yellow solid (82% yield); mp: 147 - 149°C; IR (KBr): ν_{max} 2959, 1677, 1603, 1511, 1459, 1334, 1274, 1117 cm^{-1}; ^{1}H NMR (400 MHz, $CDCl_3$): δ 0.93 (3H, t, ^3J = 7.4 Hz, $CH_2CH_2CH_2C\underline{H}_3$), 1.31– 1.43 (2H, m, $CH_2CH_2C\underline{H}_2CH_3$), 1.56 – 1.68 (2H, m, $CH_2C\underline{H}_2CH_2CH_3$), 2.43 (3H, s, NMe), 2.55– 2.77 (2H, m, $C\underline{H}_2CH_2CH_2CH_3$), 3.91 (3H, s, OMe-4′), 3.93 (6H, s, OMe-3′, 5′), 3.99 (2H, s, CH_2-7), 6.58 – 6.78 (2H, m, H-2a, 5), 7.12 (2H, s, H-2′, 6′), 7.60 (1H, d, ^3J = 8.5 Hz, H-4), 10.29 ppm (1H, br. s, OH-6); ^{13}C NMR (100 MHz, $CDCl_3$): δ 13.95, 20.40, 28.50, 41.34, 53.12, 56.18, 57.10, 61.13, 103.95, 108.64, 111.67, 113.34, 113.84, 125.61, 128.08, 139.75, 147.67, 153.37, 165.69, 167.71, 182.50 ppm; MS (CI): *m/z* 428.2 (MH^+, 100). Anal. calcd for $C_{24}H_{29}NO_6$: C, 67.43; H, 6.84; N, 3.28. Found: C, 67.18; H, 7.07; N, 3.08.

(2*Z*)-7-{[Benzyl(methyl)amino]methyl}-2-(3,4-dimethoxybenzylidene)-6-hydroxy-1-benzofuran-3(2*H*)-one (5c). Yellow solid (71% yield); mp: 141 - 143°C; IR (KBr): ν_{max} 2946, 2835, 1698, 1601, 1515, 1420, 1261, 1142,

1117, 1024 cm^{-1}; ^1H NMR (400 MHz, $CDCl_3$): δ 2.38 (3H, s, NMe), 3.73 (2H, s, NCH_2Ph), 3.92, 3.96 (each 3H, 2s, OMe-3′, 4′), 3.98 (2H, s, CH_2-7), 6.68 (1H, d, ^3J = 8.5 Hz, H-5), 6.77 (1H, s, H-2a), 6.95 (1H, d,^3J = 8.4 Hz, H-5′), 7.28 – 7.43 (6H, m, H-6′, NCH_2Ph), 7.49 (1H, d, ^4J = 1.9 Hz, H-2′), 7.62 ppm (1H, d, ^3J = 8.4 Hz, H-4); ^{13}C NMR (100 MHz, DMSO-d_6): δ 40.87, 50.48, 55.30, 55.54, 60.46, 106.10, 110.50, 111.60, 111.78, 113.41, 124.32, 124.88, 125.13, 127.29, 128.23, 129.06, 137.02, 146.41, 148.56, 150.07, 165.58, 167.56, 180.79 ppm; MS (CI): *m/z* 432.2 (MH^+, 100). Anal. calcd for $C_{26}H_{25}NO_5$: C, 72.37; H, 5.84; N, 3.25. Found: C, 72.16; H, 5.95; N, 3.42.

(2*Z*)-2-(1,3-Benzodioxol-5-ylmethylene)-7-{[benzyl(methyl)amino]methyl}-6-hydroxy-1-benzofuran-3(2*H*)-one (5d). Yellow solid (69% yield; mp: 159 - 161°C; IR (KBr): ν_{max} 2851, 1697, 1602, 1499, 1243, 1188, 1035 cm^{-1}; ^1H NMR (400 MHz, $CDCl_3$): δ 2.40 (3H, s, NMe), 3.77 (2H, s, NCH_2Ph), 4.03 (2H, s, CH_2-7), 6.07 (2H, s, OCH_2O), 6.68 (1H, d, ^3J = 8.4 Hz, H-5), 6.74 (1H, s, H-2a), 6.90 (1H, d, ^3J = 8.1 Hz, H-7′), 7.22 – 7.43 (6H, m, H-6′, NCH_2Ph), 7.48 (1H, d, ^4J = 1.7 Hz, H-4′), 7.62 ppm (1H, d, ^3J = 8.4 Hz, H-4); ^{13}C NMR (100 MHz, $CDCl_3$): δ 41.38, 52.52, 61.31, 100.09, 101.64, 104.46, 108.94, 110.34, 111.76, 113.66, 125.35, 126.90, 127.16, 128.31, 128.93, 129.67, 135.39, 146.95, 148.23, 148.97, 165.49, 167.31, 182.62 ppm; MS (CI): *m/z* 416.2 (MH^+, 100). Anal. calcd for $C_{25}H_{21}NO_5$: C, 72.28; H, 5.10; N, 3.37. Found: C, 72.43; H, 5.36; N, 3.09.

(2*Z*)-7-{[Benzyl(methyl)amino]methyl}-6-hydroxy-2-(3,4,5-trimethoxybenzylidene)-1-benzofuran-3(2*H*)-one (5e). Yellow solid (68% yield); mp: 144 - 146°C; IR (KBr): ν_{max} 2938, 2837, 1685, 1599, 1452, 1262, 1132 cm^{-1}; ^1H NMR (400 MHz, $CDCl_3$): δ 2.39 (3H, s, NMe), 3.73 (2H, s, NCH_2Ph), 3.91 (6H, s, OMe-3′, 5′), 3.94 (3H, s, OMe-4′), 3.97 (2H, s, CH_2-7), 6.70 (1H, d, ^3J = 8.4 Hz, H-5), 6.74 (1H, s, H-2a), 7.14 (2H, s, H-2′, 6′), 7.29 – 7.41 (5H, m, NCH_2Ph), 7.64 ppm (1H, d, ^3J = 8.4 Hz, H-4); ^{13}C NMR (100 MHz, $CDCl_3$): 41.63, 52.22, 56.12, 61.13, 61.36, 104.45, 108.60, 111.75, 113.61, 113.70, 125.52, 128.06, 128.41, 128.95, 129.76, 134.88, 139.71, 147.62, 153.34, 165.50, 167.24, 182.59 ppm; MS (CI): *m/z* 462.0 (MH^+, 100). Anal. calcd for $C_{27}H_{27}NO_6$: C, 70.27; H, 5.90; N, 3.03. Found: C, 70.50; H, 6.18; N, 3.31.

(2*Z*)-7-{[Benzyl(methyl)amino]methyl}-6-hydroxy-2-(2,3,4-trimethoxybenzylidene)-1-benzofuran-3(2*H*)-one (5f). Yellow solid (76% yield); mp: 139 - 141°C; IR (KBr): ν_{max} 2940, 1692, 1601, 1460, 1256, 1133, 1091 cm^{-1}; ^1H NMR (400 MHz, $CDCl_3$): δ 2.40 (3H, s, NMe), 3.78 (2H, s, NCH_2Ph), 3.89, 3.95, 3.96 (each 3H, 3s, OMe-2′, 3′, 4′), 4.04 (2H, s, CH_2-7), 6.71 (1H, d, ^3J = 8.5 Hz, H-5), 6.82 (1H, d, ^3J = 8.9 Hz, H-5′), 7.21 (1H, s, H-2a), 7.29 – 7.44 (5H, m, NCH_2Ph), 7.63 (1H, d, ^3J = 8.5 Hz, H-4), 7.92 ppm (1H, d, ^3J = 8.9 Hz, H-6′); ^{13}C NMR (100 MHz, $CDCl_3$): δ 41.40, 52.43, 56.23, 61.04, 61.30, 61.98, 104.34, 105.93, 107.87, 113.51, 113.97, 119.82, 125.46, 126.71, 128.33, 128.95, 129.72, 135.33, 142.40, 147.70, 154.05, 155.29, 165.47, 167.01, 182.69 ppm; MS (CI): *m/z* 462.0 (MH^+, 100). Anal. calcd for $C_{27}H_{27}NO_6$: C, 70.27; H, 5.90; N, 3.03. Found: C, 70.02; H, 5.65; N, 2.84.

(2*Z*)-2-(3,4-Dimethoxybenzylidene)-7-[(dipropylamino)methyl]-6-hydroxy-1-benzofuran-3(2*H*)-one (6c). Yellow solid (73% yield); mp: 135 - 137°C; IR (KBr): ν_{max} 2966, 1666, 1597, 1514, 1458, 1263, 1114, 1019 cm^{-1}; ^1H NMR (400 MHz, $CDCl_3$): δ 0.91 (6H, t, ^3J = 7.4 Hz, $N(CH_2CH_2CH_3)_2$), 1.53 –1.72 (4H, m, $N(CH_2CH_2CH_3)_2$), 2.50 – 2.67 (4H, m, $N(CH_2CH_2CH_3)_2$), 3.91, 3.94 (each 3H, 2s, OMe-3′,4′), 4.01 (2H, s, CH_2-7), 6.61 (1H, d, ^3J = 8.5 Hz, H-5), 6.71 (1H, s, H-2a), 6.91 (1H, d,^3J = 8.2 Hz, H-5′), 7.36 (1H, dd, ^3J = 8.2 Hz, ^4J = 2.0 Hz, H-6′), 7.45 (1H, d, ^4J = 2.0 Hz, H-2′), 7.56 (1H, d, ^3J = 8.5 Hz, H-4), 8.30 ppm (1H, br. s, OH-6); ^{13}C NMR (100 MHz, $CDCl_3$): δ 11.77, 19.27, 50.41, 55.71, 55.73, 56.02, 104.33, 111.32, 111.70, 113.26, 113.49, 113.71, 125.12, 125.37, 125.65, 147.14, 148.98, 150.44, 165.45, 167.94, 182.51 ppm; MS (CI): *m/z* 412.2 (MH^+, 100). Anal. calcd for $C_{24}H_{29}NO_5$: C, 70.05; H, 7.10; N, 3.40. Found: C, 69.86; H, 7.35; N, 3.12.

(2*Z*)-2-(1,3-Benzodioxol-5-ylmethylene)-7-[(dipropylamino)methyl]-6-hydroxy-1-benzofuran-3(2*H*)-one (6d). Yellow solid (72% yield); mp: 117 - 119°C; IR (KBr): ν_{max} 2963, 2875, 1690, 1596, 1486, 1442, 1254, 1188, 1110, 1040 cm^{-1}; ^1H NMR (400 MHz, $CDCl_3$): δ 0.94 (6H, t, ^3J = 7.4 Hz, $N(CH_2CH_2CH_3)_2$), 1.59 –1.76 (4H, m, $N(CH_2CH_2CH_3)_2$), 2.59 – 2.70 (4H, m, $N(CH_2CH_2CH_3)_2$), 4.05 (2H, s, CH_2-7), 6.04 (2H, s, OCH_2O), 6.64 (1H, d, ^3J = 8.5 Hz, H-5), 6.71 (1H, s, H-2a), 6.88 (1H, d, ^3J = 8.1 Hz, H-7′), 7.21 – 7.27 (1H, m, H-6′), 7.45 (1H, d, ^4J = 1.7 Hz, H-4′), 7.59 ppm (1H, d, ^3J = 8.4 Hz, H-4); ^{13}C NMR (125 MHz, $CDCl_3$): δ 11.86, 19.67, 50.76, 56.01, 101.63, 104.66, 108.97, 110.35, 111.47, 113.21, 113.90, 125.09, 127.11, 127.12, 147.18, 148.24, 148.89, 165.56, 168.34, 182.67 ppm; MS (CI): *m/z* 396.0 (MH^+, 100). Anal. calcd for $C_{23}H_{25}NO_5$: C, 69.86; H, 6.37; N, 3.54. Found: C, 69.60; H, 6.20; N, 3.48.

(2*Z*)-7-[(Dipropylamino)methyl]-6-hydroxy-2-(3,4,5-trimethoxybenzylidene)-1-benzofuran-3(2*H*)-one (6e). Yellow solid (65% yield); mp: 172 - 174°C; IR (KBr): ν_{max} 3472, 2962, 1686, 1603, 1460, 1269, 1134, 1009 cm^{-1}; ^1H NMR (400 MHz, $CDCl_3$): δ 0.94 (6H, t, ^3J = 7.4 Hz, $N(CH_2CH_2CH_3)_2$), 1.57 –1.65 (4H, m, $N(CH_2CH_2CH_3)_2$), 2.57– 2.60 (4H, m, $N(CH_2CH_2CH_3)_2$), 3.91 (3H, s, OMe-4′), 3.94 (6H, s, OMe-3′, 5′), 4.00 (2H, s, CH_2-7), 6.63 (1H, d, ^3J = 8.5 Hz, H-5), 6.72 (1H, s, H-2a), 7.14 (2H, s, H-2′,6′), 7.61 ppm (1H, d, ^3J = 8.5 Hz, H-4); ^{13}C NMR (100 MHz, DMSO-d_6): δ 11.41, 18.21, 49.35, 54.41, 55.72, 60.11, 103.92, 108.31, 109.78, 110.21, 114.28, 124.45, 127.67, 138.61, 147.28, 152.76, 165.26, 170.30, 180.21 ppm; MS (CI): *m/z* 442.3 (MH^+, 100). Anal. calcd for $C_{25}H_{31}NO_6$: C, 68.01; H, 7.08; N, 3.17. Found: C, 68.15; H, 6.79; N, 2.99.

(2*Z*)-2-Benzylidene-7-{[bis(2-methoxyethyl)amino]methyl}-6-hydroxy-1-benzofuran-3(2*H*)-one (7a). Yellow solid (69% yield); mp: 81 - 82°C; IR (KBr): ν_{max} 2879, 1697, 1604, 128, 1187, 1128, 1105, 1039 cm^{-1}; ^1H NMR (400 MHz, $CDCl_3$): δ 2.96 (4H, t, ^3J = 5.3 Hz, $N(CH_2CH_2OMe)_2$), 3.35 (6H, s, CH_2OCH_3), 3.59 (4H, t, ^3J = 5.3 Hz, $N(CH_2CH_2OMe)_2$), 4.19 (2H, s, CH_2-7), 6.68 (1H, d, ^3J = 8.4 Hz, H-5), 6.79 (1H, s, H-2a), 7.33 – 7.51 (3H, m, H-3′, 4′, 5′), 7.61 (1H, d, ^3J = 8.4 Hz, H-4), 7.85 ppm (2H, d, ^3J = 8.8 Hz, H-2′, 6′); ^{13}C NMR (125 MHz, $CDCl_3$): δ 50.15, 53.62, 58.93, 69.87, 105.39, 111.28, 113.35, 113.92, 125.25, 128.95, 129.51, 131.22, 132.76, 148.12, 165.94, 167.58, 182.94 ppm; MS (CI): *m/z* 384.0 (MH^+, 100). Anal. calcd for $C_{22}H_{25}NO_5$: C, 68.91; H, 6.57; N, 3.65. Found: C, 69.15; H, 6.39; N, 3.71.

(2*Z*)-7-{[Bis(2-methoxyethyl)amino]methyl}-6-hydroxy-2-(4-methoxybenzylidene)-1-benzofuran-3(2*H*)-

one (7b). Yellow solid (83% yield); mp: 109 - 111°C; IR (KBr): ν_{max} 3421, 2935, 1687, 1601, 1512, 1400, 1255, 1132, 1038 cm^{-1}; ^1H NMR (400 MHz, DMSO-d_6): δ 2.84 (4H, t, ^3J = 5.3 Hz, N($C\underline{H}_2CH_2OMe)_2$), 3.22 (6H, s, $CH_2OC\underline{H}_3$), 3.51 (4H, t, ^3J = 5.5 Hz, N($CH_2C\underline{H}_2OMe)_2$), 3.82 (3H, s, OMe-4′), 4.10 (2H, s, CH_2-7), 6.63 (1H, d, ^3J = 8.4 Hz, H-5), 6.76 (1H, s, H-2a), 7.05 (2H, d, ^3J = 8.8 Hz, H-3′, 5′), 7.52 (1H, d, ^3J = 8.4 Hz, H-4), 7.91 ppm (2H, d, ^3J = 8.8 Hz, H-2′, 6′); ^{13}C NMR (100 MHz, DMSO-d_6): δ 48.68, 52.56, 55.30, 57.99, 69.13, 106.22, 110.44, 112.22, 113.18, 114.49, 124.14, 124.62, 132.83, 146.19, 160.26, 165.12, 166.96, 181.10 ppm; MS (CI): *m/z* 414.0 (MH^+, 100). Anal. calcd for $C_{23}H_{27}NO_6$: C, 66.81; H, 6.58; N, 3.39. Found: C, 66.93; H, 6.73; N, 3.53.

(2*Z*)-7-{[Bis(2-methoxyethyl)amino]methyl}-2-(3,4-dimethoxybenzylidene)-6-hydroxy-1-benzofuran-3(2*H*)-one (7c). Yellow solid (83% yield); mp: 80 - 82°C; IR (KBr): ν_{max} 2835, 1687, 1593, 1519, 1322, 1261, 1123, 1021 cm^{-1}; ^1H NMR (400 MHz, $CDCl_3$): δ 2.95 (4H, t, ^3J = 5.2 Hz, N($C\underline{H}_2CH_2OMe)_2$), 3.32 (6H, s, $CH_2OC\underline{H}_3$), 3.59 (4H, t, ^3J = 5.2 Hz, N($CH_2C\underline{H}_2OMe)_2$), 3.93, 3.96 (each 3H, 2s, OMe-3′,4′), 4.18 (2H, s, CH_2-7), 6.69 (1H, d, ^3J = 8.4 Hz, H-5), 6.74 (1H, s, H-2a), 6.93 (1H, d,^3J = 8.4 Hz, H-5′), 7.40 (1H, dd, ^3J = 8.4 Hz, ^4J = 2.0 Hz, H-6′), 7.49 (1H, d, ^4J = 2.0 Hz, H-2′), 7.59 ppm (1H, d, ^3J = 8.4 Hz, H-4); ^{13}C NMR (125 MHz, $CDCl_3$): δ 50.23, 53.67, 55.88, 56.07, 58.96, 69.80, 105.09, 111.35, 111.86, 113.60, 113.67, 113.81, 125.24, 125.47, 125.69, 147.12, 149.06, 150.53, 165.56, 167.08, 182.69 ppm; MS (CI): *m/z* 444.2 (MH^+, 100). Anal. calcd for $C_{24}H_{29}NO_7$: C, 65.00; H, 6.59; N, 3.16. Found: C, 64.81; H, 6.82; N, 3.00.

(2*Z*)-2-(1,3-Benzodioxol-5-ylmethylene)-7-{[bis(2-methoxyethyl)amino]methyl}-6-hydroxy-1-benzofuran-3(2*H*)-one (7d). Yellow solid (77% yield); mp: 114 - 116°C; IR (KBr): ν_{max} 3421. 1645, 1614, 1564, 1450, 1402, 1257, 1107, 1036 cm^{-1}; ^1H NMR (400 MHz, $CDCl_3$): δ 2.97 (4H, t, ^3J = 5.3 Hz, N($C\underline{H}_2CH_2OMe)_2$), 3.35 (6H, s, $CH_2OC\underline{H}_3$), 3.60 (4H, t, ^3J = 5.3 Hz, N($CH_2C\underline{H}_2OMe)_2$), 4.19 (2H, s, CH_2-7), 6.03 (2H, s, OCH_2O), 6.68 (1H, d, ^3J = 8.5 Hz, H-5), 6.71 (1H, s, H-2a), 6.87 (1H, d, ^3J = 8.0 Hz, H-7′), 7.25 (1H, dd, ^3J = 8.0 Hz, ^4J = 1.8 Hz, H-6′), 7.48 (1H, d, ^4J = 1.8 Hz, H-4′), 7.59 ppm (1H, d, ^3J = 8.5 Hz, H-4); ^{13}C NMR (125 MHz, $CDCl_3$): δ 50.32, 53.61, 58.97, 70.03, 101.63, 105.54, 108.93, 110.36, 111.58, 113.56, 113.83, 125.07, 127.08, 127.15, 147.12, 148.26, 148.93, 165.60, 167.42, 182.81 ppm; MS (CI): *m/z* 428.1 (MH^+, 100). Anal. calcd for $C_{23}H_{25}NO_7$: C, 64.63; H, 5.90; N, 3.28. Found: C, 64.78; H, 5.67; N, 3.52.

(2*Z*)-7-{[Bis(2-methoxyethyl)amino]methyl}-6-hydroxy-2-(3,4,5-trimethoxybenzylidene)-1-benzofuran-3(2*H*)-one (7e). Yellow solid (88% yield); mp: 119 - 120°C; IR (KBr): ν_{max} 2878, 1692, 1602, 1502, 1344, 1185, 1117 cm^{-1}; ^1H NMR (400 MHz, $CDCl_3$): δ 2.91 (4H, t, ^3J = 5.2 Hz, N($C\underline{H}_2CH_2OMe)_2$), 3.33 (6H, s, $CH_2OC\underline{H}_3$), 3.58 (4H, t, ^3J = 5.2 Hz, N($CH_2C\underline{H}_2OMe)_2$), 3.92 (3H, s, OMe-4′), 3.95 (6H, s, OMe-3′, 5′), 4.14 (2H, s, CH_2-7), 6.67 (1H, d, ^3J = 8.5 Hz, H-5), 6.72 (1H, s, H-2a), 7.15 (2H, s, H-2′, 6′), 7.61 ppm (1H, d, ^3J = 8.5 Hz, H-4); ^{13}C NMR (125 MHz, $CDCl_3$): δ 50.26, 53.64, 56.17, 58.95, 61.11, 69.69, 105.08, 108.61, 111.60, 113.46, 113.94, 125.37, 128.11, 139.68, 147.67, 153.34, 165.67, 167.25, 182.63 ppm; MS (CI): *m/z* 474.2 (MH^+, 100). Anal. calcd for $C_{25}H_{31}NO_8$: C, 63.41; H, 6.60; N, 2.96. Found: C, 63.30; H, 6.86; N, 3.11.

(2*Z*)-7-{[Bis(2-methoxyethyl)amino]methyl}-6-hydroxy-2-(2,3,4-trimethoxybenzylidene)-1-benzofuran-3(2*H*)-one (7f). Yellow solid (79% yield); mp: 105 - 107°C; IR (KBr): ν_{max} 2943, 1691, 1605, 1594, 1303, 1130, 1091, 1041 cm^{-1}; ^1H NMR (400 MHz, $CDCl_3$): δ 2.93 (4H, t, ^3J = 5.2 Hz, N($C\underline{H}_2CH_2OMe)_2$), 3.35 (6H, s, $CH_2OC\underline{H}_3$), 3.59 (4H, t, ^3J = 5.2 Hz, N($CH_2C\underline{H}_2OMe)_2$), 3.90, 3.94, 3.97 (each 3H, 3s, OMe-2′, 3′, 4′), 4.15 (2H, s, CH_2-7), 6.66 (1H, d, ^3J = 8.4 Hz, H-5), 6.82 (1H, d, ^3J = 8.9 Hz, H-5′), 7.20 (1H, s, H-2a), 7.61 (1H, d, ^3J = 8.4 Hz, H-4), 7.96 ppm (1H, d, ^3J = 8.9 Hz, H-6′); ^{13}C NMR (125 MHz, $CDCl_3$): δ 50.24, 53.71, 56.15, 58.90, 60.97, 61.92, 70.01, 105.35, 105.58, 107.80, 113.59, 113.71, 119.84, 125.00, 126.67, 142.30, 147.74, 153.93, 155.15, 165.46, 167.08, 182.74 ppm; MS (CI): *m/z* 474.2 (MH^+, 100). Anal. calcd for $C_{25}H_{31}NO_8$: C, 63.41; H, 6.60; N, 2.96. Found: C, 63.70; H, 6.36; N, 2.75.

(2*Z*)-2-Benzylidene-6-hydroxy-7-(piperidin-1-ylmethyl)-1-benzofuran-3(2*H*)-one (8a). Yellow solid (85% yield); mp: 187 - 189°C; IR (KBr): ν_{max} 2950, 1678, 1608, 1502, 1451, 1371, 1279, 1179, 1117, 1066 cm^{-1}; ^1H NMR (400 MHz, $CDCl_3$): δ 1.36 – 3.46 (10H, m, piperidine moiety), 4.06 (2H, s, CH_2-7), 6.73 (1H, d, ^3J = 8.5 Hz, H-5), 6.79 (1H, s, H-2a), 7.35 – 7.50 (3H, m, H-3′, 4′, 5′), 7.62 (1H, d, ^3J = 8.5, H-4), 7.82 (2H, d, ^3J = 8.5 Hz, H-2′, 6′), 10.08 ppm (1H, br. s, OH-6); ^{13}C NMR (100 MHz, $CDCl_3$): δ 23.40, 25.35, 53.43, 53.87, 103.34, 111.49, 113.26, 113.97, 125.74, 129.05, 129.63, 131.21, 132.69, 148.05, 166.21, 168.01, 182.76 ppm; MS (CI): *m/z* 336.1 (MH^+, 100). Anal. calcd for $C_{21}H_{21}NO_3$: C, 75.20; H, 6.31; N, 4.18. Found: C, 75.03; H, 6.09; N, 4.34.

(2*Z*)-6-Hydroxy-2-(4-methoxybenzylidene)-7-(piperidin-1-ylmethyl)-1-benzofuran-3(2*H*)-one (8b). Yellow solid (91% yield); mp: 125 - 126°C; IR (KBr): ν_{max} 2935, 1692, 1598, 1509, 14477, 1256, 1187, 1124, 1035 cm^{-1}; ^1H NMR (400 MHz, $CDCl_3$): δ 1.24 – 1.95, 2.21 – 3.37 (6H, 4H, 2m, piperidine moiety), 3.80 (3H, s, OMe-4′), 3.92 (2H, s, CH_2-7), 6.57 (1H, d, ^3J = 8.5 Hz, H-5), 6.69 (1H, s, H-2a), 6.92 (2H, d, ^3J = 8.5 Hz, H-3′, 5′), 7.52 (1H, d, ^3J = 8.5 Hz, H-4), 7.72 (2H, d, ^3J = 8.8 Hz, H-2′, 6′), 11.51 ppm (1H, br. s, OH-6); ^{13}C NMR (100 MHz, $CDCl_3$): δ 23.64, 25.66, 53.97, 54.16, 55.38, 103.94, 111.41, 113.27, 113.57, 114.48, 124.89, 125.32, 132.89, 146.95, 160.65, 165.52, 167.83, 182.60 ppm; MS (CI): *m/z* 366.0 (MH^+, 100). Anal. calcd for $C_{22}H_{23}NO_4$: C, 72.31; H, 6.34; N, 3.83. Found: C, 72.39; H, 6.62; N, 3.59.

(2*Z*)-2-(3,4-Dimethoxybenzylidene)-6-hydroxy-7-(piperidin-1-ylmethyl)-1-benzofuran-3(2*H*)-one (8c). Yellow solid (82% yield); mp: 180 - 182°C; IR (KBr): ν_{max} 3446, 2937, 2677, 1676, 1616, 1512, 1458, 1269, 1144, 1022 cm^{-1}; ^1H NMR (400 MHz, $CDCl_3$): δ 1.33– 3.46 (10H, m, piperidine moiety), 3.92 (2H, s, CH_2-7), 3.95, 3.98 (each 3H, 2s, OMe-3′,4′), 6.63 (1H, d, ^3J = 8.4 Hz, H-5), 6.76 (1H, s, H-2a), 6.95 (1H, d, ^3J = 8.4 Hz, H-5′), 7.40 (1H, dd, ^3J = 8.4 Hz, ^4J = 2.0 Hz, H-6′), 7.51 (1H, d, ^4J = 2.0 Hz, H-2′), 7.59 ppm (1H, d, ^3J = 8.4 Hz, H-4); ^{13}C NMR (100 MHz, DMSO-d_6): δ 23.05, 24.85, 52.06, 53.05, 55.29, 55.54, 104.08, 110.17, 110.65, 111.80, 113.39, 114.05, 124.34, 124.92, 125.02, 146.54, 148.55, 149.99, 165.53, 169.26, 180.35 ppm; MS (CI): *m/z* 396.2 (MH^+, 100). Anal. calcd for $C_{23}H_{25}NO_5$:

C, 69.86; H, 6.37; N, 3.54. Found: C, 69.97; H, 6.51; N, 3.36.

(2*Z*)-2-(1,3-Benzodioxol-5-ylmethylene)-6-hydroxy-7-(piperidin-1-ylmethyl)-1-benzofuran-3(2*H*)-one (8d). Yellow solid (74% yield); mp: 163 - 165°C; IR (KBr): ν_{max} 3406, 2949, 1678, 1595, 1448, 1331, 1250, 1132, 1038 cm^{-1}; ^1H NMR (400 MHz, $CDCl_3$): δ 1.32– 3.56 (10H, m, piperidine moiety), 3.95 (2H, s, CH_2-7), 6.05 (2H, s, OCH_2O), 6.62 (1H, d, ^3J = 8.4 Hz, H-5), 6.72 (1H, s, H-2a), 6.88 (1H, d, ^3J = 8.1 Hz, H-7′), 7.14 – 7.33 (1H, m, H-6′), 7.46 (1H, d, ^4J = 1.7 Hz, H-4′) 7.59 (1H, d, ^3J = 8.4 Hz, H-4), 10.08 ppm (1H, br. s, OH-6); ^{13}C NMR (100 MHz, DMSO-d_6): δ 23.15, 25.00, 51.88, 53.08, 101.49, 104.46, 108.75, 109.21, 109.68, 109.74, 114.57, 124.19, 126.43, 126.57, 146.87, 147.69, 148.15, 165.91, 170.67, 180.02 ppm; MS (CI): *m/z* 380.0 (MH^+, 100). Anal. calcd for $C_{22}H_{21}NO_5$: C, 69.65; H, 5.58; N, 3.69. Found: C, 69.74; H, 5.47; N, 3.88.

(2*Z*)-2-(3,4-Dimethoxybenzylidene)-6-hydroxy-7-(morpholin-4-ylmethyl)-1-benzofuran-3(2*H*)-one (9c). Yellow solid (67% yield); mp: 179 - 181°C; IR (KBr): ν_{max} 2928, 2836, 1671, 1601,1435, 1264, 1133 cm^{-1}; ^1H NMR (500 MHz, $CDCl_3$): δ 2.55 – 2.88 (4H, m, N($C\underline{H}_2CH_2$)O), 3.74 – 3.86 (4H, m, N($CH_2C\underline{H}_2$)O), 3.93, 3.96 (each 3H, 2s, OMe-3′,4′), 3.97 (2H, s, CH_2-7), 6.66 (1H, d, ^3J = 8.4 Hz, H-5), 6.75 (1H, s, H-2a), 6.94 (1H, d,^3J = 8.4 Hz, H-5′), 7.39 (1H, dd, ^3J = 8.3 Hz, ^4J = 1.9 Hz, H-6′), 7.45 (1H, d, ^4J = 1.9 Hz, H-2′), 7.60 ppm (1H, d, ^3J = 8.4 Hz, H-4); ^{13}C NMR (125 MHz, $CDCl_3$): δ 53.22, 53.76, 55.84, 56.07, 66.55, 103.40, 103.47, 111.41, 112.28, 113.52, 113.60, 114.02, 125.48, 125.52, 146.92, 149.06, 150.65, 165.58, 166.34, 182.56 ppm; MS (CI): *m/z* 398.0 (MH^+, 100). Anal. calcd for $C_{22}H_{23}NO_6$: C, 66.49; H, 5.83; N, 3.52. Found: C, 66.21; H, 6.08; N, 3.30.

(2*Z*)-2-(1,3-Benzodioxol-5-ylmethylene)-6-hydroxy-7-(morpholin-4-ylmethyl)-1-benzofuran-3(2*H*)-one (9d). Yellow solid (59% yield); mp: 189 - 191°C; IR (KBr): ν_{max} 3419, 1668, 1599, 1502, 1442, 1254, 1119, 1038 cm^{-1}; ^1H NMR (400 MHz, DMSO-d_6): δ 2.52 – 2.61 (4H, m, N($C\underline{H}_2CH_2$)O), 3.57 – 3.65 (4H, m, N($CH_2C\underline{H}_2$)O), 3.78 (2H, s, CH_2-7), 6.10 (2H, s, OCH_2O), 6.65 – 6.77 (2H, m, H-2a, 5), 7.03 (1H, d, ^3J = 8.1 Hz, H-7′), 7.45 (1H, dd, ^3J = 8.1 Hz, ^4J = 1.7 Hz, H-6′), 7.52 (1H, d, ^3J = 8.3 Hz, H-4), 7.58 ppm (1H, d, ^4J = 1.6 Hz, H-4′); ^{13}C NMR (100 MHz, DMSO-d_6): δ 50.80, 52.93, 66.04, 101.60, 106.36, 108.79, 109.79, 110.64, 112.44, 112.74, 124.31, 126.25, 126.95, 146.18, 147.75, 148.51, 165.49, 165.86, 181.24 ppm; MS (CI): *m/z* 382.3 (MH^+, 100). Anal. calcd for $C_{21}H_{19}NO_6$: C, 66.14; H, 5.02; N, 3.67. Found: C, 65.96; H, 5.21; N, 3.90.

(2*Z*)-6-Hydroxy-7-(morpholin-4-ylmethyl)-2-(3,4,5-trimethoxybenzylidene)-1-benzofuran-3(2*H*)-one (9e). Yellow solid (74% yield); mp: 197 - 199°C; IR (KBr): ν_{max} 2956, 2835, 1691, 1603, 1504, 1448, 1120 cm^{-1}; ^1H NMR (400 MHz, $CDCl_3$): δ 2.48 – 2.93 (4H, m, N($C\underline{H}_2CH_2$)O), 3.78 – 3.87 (4H, m, N($CH_2C\underline{H}_2$)O), 3.91 (3H, s, OMe-4′), 3.94 (6H, s, OMe-3′, 5′), 3.99 (2H, s, CH_2-7),6.63 – 6.78 (2H, m, H-2a, 5), 7.11 (2H, s, H-2′, 6′), 7.62 ppm (1H, d, ^3J = 8.4 Hz, H-4); ^{13}C NMR (100 MHz, $CDCl_3$): δ 53.23, 53.53, 56.20, 61.15, 66.38, 103.26, 108.68, 112.14, 113.76, 113.91, 125.85, 127.90, 139.90, 147.46, 153.39, 165.81, 166.43, 182.53 ppm; MS (CI): *m/z* 428.2 (MH^+, 100). Anal. calcd for $C_{23}H_{25}NO_7$: C, 64.63; H, 5.90; N, 3.28. Found: C, 64.37; H, 6.18; N, 3.50.

(2*Z*)-6-Hydroxy-2-(4-methoxybenzylidene)-7-[(4-methylpiperazin-1-yl)methyl]-1-benzofuran-3(2*H*)-one (10b). Yellow solid (80% yield); mp: 156 - 158°C; IR (KBr): ν_{max} 2801, 1692, 1601, 1509, 1257, 1183, 1129, 1032, 813 cm^{-1}; ^1H NMR (400 MHz, $CDCl_3$): δ 2.36 (3H, s, N′-CH_3), 2.39 – 3.15 (8H, m, piperazine moiety), 3.85 (3H, s, OMe-4′), 3.98 (2H, s, CH_2-7), 6.62 (1H, d, ^3J = 8.5 Hz, H-5), 6.75 (1H, s, H-2a), 6.97 (2H, d, ^3J = 8.9 Hz, H-3′, 5′), 7.58 (1H, d, ^3J = 8.5 Hz, H-4), 7.77 (2H, d, ^3J = 8.8 Hz, H-2′, 6′), 10.25 ppm (1H, br. s, OH-6); ^{13}C NMR (100 MHz, $CDCl_3$): δ 45.64, 52.40, 53.39, 54.64, 55.37, 103.93, 111.74, 113.33, 113.75, 114.49, 125.03, 125.18, 132.94, 146.77, 160.72, 165.40, 166.68, 182.62 ppm; MS (CI): *m/z* 381.2 (MH^+, 100). Anal. calcd for $C_{22}H_{24}N_2O_4$: C, 69.46; H, 6.36; N, 7.36. Found: C, 69.73; H, 6.55; N, 7.49.

(2*Z*)-2-(3,4-Dimethoxybenzylidene)-6-hydroxy-7-[(4-methylpiperazin-1-yl)methyl]-1-benzofuran-3(2*H*)-one (10c). Yellow solid (86% yield); mp: 173 - 175°C; IR (KBr): ν_{max} 3423, 2941, 2692, 1662, 1595, 1514, 1452, 1334, 1263, 1128 cm^{-1}; ^1H NMR (400 MHz, $CDCl_3$): δ 2.09 – 3.47 (11H, m, piperazine moiety), 3.95 (3H, s) and 3.97 (5H, m, CH_2-7, OMe-3′,4′,), 6.65 (1H, d, ^3J = 8.4 Hz, H-5), 6.78 (1H, s, H-2a), 6.95 (1H, d, ^3J = 8.5 Hz, H-5′), 7.38 (1H, dd, ^3J = 8.5 Hz, ^4J = 1,7 Hz, H-6′), 7.55 (1H, d, ^4J = 1.7 Hz, H-2′), 7.62 ppm (1H, d, ^3J = 8.4 Hz, H-4); ^{13}C NMR (100 MHz, DMSO-d_6): δ 45.53, 50.86, 52.23, 54.35, 55.34, 55.58, 105.74, 110.79, 111.83, 111.92, 113.24, 113.37, 124.35, 124.81, 125.32, 146.26, 148.58, 150.16, 165.57, 166.78, 180.95 ppm; MS (CI): *m/z* 411.1 (MH^+, 100). Anal. calcd for $C_{23}H_{26}N_2O_5$: C, 67.30; H, 6.38; N, 6.82. Found: C, 67.53; H, 6.54; N, 6.65.

(2*Z*)-2-(1,3-Benzodioxol-5-ylmethylene)-6-hydroxy-7-[(4-methylpiperazin-1-yl)methyl]-1-benzofuran-3(2*H*)-one (10d). Yellow solid (69% yield); mp: 190 - 912°C; IR (KBr): ν_{max} 3410, 2937, 1689, 1603, 1500, 1446, 1342, 1257, 1188, 1036 cm^{-1}; ^1H NMR (400 MHz, DMSO-d_6): δ 2.17 (3H, s, N′-CH_3), 2.25 – 2.48 (4H, m) and 2.52 – 2.78 (4 H, m, piperazine ring), 3.84 (2H, s, CH_2-7), 6.11 (2H, s, OCH_2O), 6.65 (1H, d, ^3J = 8.5 Hz, H-5), 6.72 (1H, s, H-2a), 7.03 (1H, d, ^3J = 8.1 Hz, H-7′), 7.38 – 7.61 ppm (3H, m, H-4, 4′ 6′); ^{13}C NMR (100 MHz, DMSO-d_6): δ 45.49, 50.77, 52.16, 54.36, 101.58, 105.96, 108.83, 109.81, 110.27, 111.67, 113.34, 124.25, 126.33, 126.84, 146.37, 147.74, 148.43, 165.75, 167.10, 180.90 ppm; MS (CI): *m/z* 395.1 (MH^+, 100). Anal. calcd for $C_{22}H_{22}N_2O_5$: C, 66.99; H, 5.62; N, 7.10. Found: C, 66.84; H, 5.83; N, 6.92.

(2*Z*)-6-Hydroxy-7-[(4-methylpiperazin-1-yl)methyl]-2-(3,4,5-trimethoxybenzylidene)-1-benzofuran-3(2*H*)-one (10e). Yellow solid (82% yield); mp: 201-203°C; IR (KBr): ν_{max} 2936, 2810, 1692, 1603, 1422, 1262, 1124, 1048 cm^{-1}; ^1H NMR (400 MHz, $CDCl_3$): δ 2.02 – 3.31 (11H, m, piperazine moiety), 3.91 (3H, s, OMe-4′), 3.93 (6H, s, OMe-3′, 5′), 3.94 (2H, s, CH_2-7), 6.66 (1H, d, ^3J = 8.5 Hz, H-5), 6.73 (1H, s, H-2a), 7.14 (2H, s, H-2′, 6′), 7.62 ppm (1H, d, ^3J = 8.5 Hz, H-4); ^{13}C NMR (125 MHz, $CDCl_3$): δ 45.80, 52.95, 53.54, 54.67, 56.06, 61.10, 103.98, 108.54, 111.80, 113.59, 113.61, 125.33, 127.98, 139.69, 147.54, 153.30, 165.49, 166.87, 182.56 ppm; MS (CI): *m/z* 441.0 (MH^+, 100). Anal. calcd for $C_{24}H_{28}N_2O_6$: C, 65.44; H, 6.41; N, 6.36. Found: C, 65.15; H, 6.30; N, 6.15.

(2*Z*)-6-Hydroxy-7-[(4-methylpiperazin-1-yl)methyl]-2-(2,3,4-trimethoxybenzylidene)-1-benzofuran-3(2*H*)-one (10f). Yellow solid (81% yield); mp: 188 - 190°C; IR (KBr): ν_{max} 3425, 1635, 1608, 1556, 1456, 1402, 1279, 1093 cm^{-1}; ^1H NMR (400 MHz, DMSO-d_6): δ 2.17 (3H, s, N′-CH_3), 2.27 – 2.44 (4H, m) and 2.55 – 2.72 (4H, m, piperazine moiety), 3.78 (3H, s) and 3.88 (8H, s, OMe-2′, 3′, 4′, CH_2-7), 6.65 (1H, d, ^3J = 8.6 Hz, H-5), 6.88 (1H, s, H-2a), 7.01 (1H, d, ^3J = 8.9 Hz, H-5′), 7.52 (1H, d, ^3J = 8.6 Hz, H-4), 7.97 ppm (1H, d, ^3J = 8.9 Hz, H-6′); ^{13}C NMR (100 MHz, DMSO-d_6): δ 45.43, 50.87, 51.99, 54.34, 56.01, 60.42, 61.62, 103.62, 105.67, 108.62, 111.90, 113.19, 118.36, 124.31, 126.16, 141.57, 146.90, 152.80, 154.88, 165.53, 166.80, 180.97 ppm; MS (CI): *m/z* 441.2 (MH^+, 100). Anal. calcd for $C_{24}H_{28}N_2O_6$: C, 65.44; H, 6.41; N, 6.36. Found: C, 65.21; H, 6.67; N, 6.48.

(2*Z*)-6-Hydroxy-7-{[4-(2-hydroxyethyl)piperazin-1-yl]methyl}-2-(4-methoxybenzylidene)-1-benzofuran-3(2*H*)-one (11b). Yellow solid (58% yield); mp: 179 - 181°C; IR (KBr): ν_{max} 3410, 2958, 1668, 1605, 1510, 1443, 1254, 1132, 1028 cm^{-1}; ^1H NMR (400 MHz, DMSO-d_6): δ 2.40 (2H, t, ^3J = 6.1 Hz, N′C$\underline{H}_2$$CH_2$OH), 2.52 – 2.69 (8H, m, CH_2-2″,3″, 5″,6″), 3.49 (2H, t, ^3J = 6.1 Hz, N′CH_2C$\underline{H}_2$OH), 3.83 (3H, s, OMe-4′), 3.91 (2H, s, CH_2-7), 6.65 (1H, d, ^3J = 8.4 Hz, H-5), 6.75 (1H, s, H-2a), 7.07 (2H, d, ^3J = 8.7 Hz, H-3′, 5′), 7.51 (1H, d, ^3J = 8.4 Hz, H-4), 7.92 ppm (2H, d, ^3J = 8.7 Hz, H-2′, 6′); ^{13}C NMR (100 MHz, DMSO-d_6): δ 50.97, 52.14, 52.84, 55.33, 58.44, 59.96, 105.57, 110.26, 111.82, 113.27, 114.55, 124.25, 124.70, 132.83, 146.27, 160.22, 165.59, 167.09, 180.96 ppm; MS (CI): *m/z* 411.0 (MH^+, 100). Anal. calcd for $C_{23}H_{26}N_2O_5$: C, 67.30; H, 6.38; N, 6.82. Found: C, 67.51; H, 6.24; N, 6.66.

(2*Z*)-2-(3,4-Dimethoxybenzylidene)-6-hydroxy-7-{[4-(2-hydroxyethyl)piperazin-1-yl]methyl}-1-benzofuran-3(2*H*)-one (11c). Yellow solid (63% yield); mp: 180 - 182°C; IR (KBr): ν_{max} 2947, 1682, 1600, 1513, 1298, 1270, 1139, 1123, 1039 cm^{-1}; ^1H NMR (400 MHz, $CDCl_3$): δ 2.08 – 3.36 (10H, m, N′C$\underline{H}_2$$CH_2$OH and piperazine ring), 3.65 (2H, t, ^3J = 5.4 Hz, N′CH_2C$\underline{H}_2$OH), 3.95, 3.98 (each 3H, 2s, OMe-3′,4′), 3.97 (2H, s, CH_2-7), 6.65 (1H, d, ^3J = 8.4 Hz, H-5), 6.78 (1H, s, H-2a), 6.95 (1H, d,^3J = 8.4 Hz, H-5′), 7.41 (1H, dd, ^3J = 8.4 Hz, ^4J = 2.0 Hz, H-6′), 7.50 (1H, d, ^4J = 2.0 Hz, H-2′), 7.62 ppm (1H, d, ^3J = 8.4 Hz, H-4); ^{13}C NMR (125 MHz, $CDCl_3$): δ 52.68, 52.87, 53.56, 55.88, 56.10, 57.93, 59.33, 103.93, 111.43, 112.19, 113.52, 113.63, 113.92, 125.31, 125.54, 125.56, 147.02, 149.08, 150.64, 165.45, 166.66, 182.66 ppm; MS (CI): *m/z* 441.1 (MH^+, 100). Anal. calcd for $C_{24}H_{28}N_2O_6$: C, 65.44; H, 6.41; N, 6.36. Found: C, 65.72; H, 6.70; N, 6.09.

(2*Z*)-2-(1,3-Benzodioxol-5-ylmethylene)-6-hydroxy-7-{[4-(2-hydroxyethyl)piperazin-1-yl]methyl}-1-benzofuran-3(2*H*)-one (11d). Yellow solid (55% yield); mp: 162 - 164°C; IR (KBr): ν_{max} 2944, 1690, 1608, 1499, 1451, 1291, 1262, 1115, 1042 cm^{-1}; ^1H NMR (400 MHz, $CDCl_3$): δ 2.47 – 2.91 (10H, m, N′C$\underline{H}_2$$CH_2$OH and piperazine ring), 3.64 (2H, t, ^3J = 5.3 Hz, N′CH_2C$\underline{H}_2$OH), 3.96 (2H, s, CH_2-7), 6.01 (2H, s, OCH_2O), 6.60 (1H, d, ^3J = 8.3 Hz, H-5), 6.68 (1H, s, H-2a), 6.84 (1H, d, ^3J = 8.0 Hz, H-7′), 7.19 – 7.27 (1H, m, H-6′), 7.40 (1H, d, ^4J = 1.6 Hz, H-4′), 7.56 ppm (1H, d, ^3J = 8.3 Hz, H-4); ^{13}C NMR (100 MHz, $CDCl_3$): δ 52.65, 52.69, 53.51, 57.90, 59.28, 101.64, 104.04, 108.93, 110.32, 111.93, 113.55, 113.75, 125.21, 126.83, 127.20, 146.88, 148.23, 149.02, 165.48, 166.87, 182.66 ppm; MS (CI): *m/z* 425.2 (MH^+, 100). Anal. calcd for $C_{23}H_{24}N_2O_6$: C, 65.08; H, 5.70; N, 6.60. Found: C, 65.29; H, 5.93; N, 6.88.

(2*Z*)-6-Hydroxy-7-{[4-(2-hydroxyethyl)piperazin-1-yl]methyl}-2-(3,4,5-trimethoxybenzylidene)-1-benzofuran-3(2*H*)-one (101e). Yellow solid (68% yield); mp: 187 - 189°C; IR (KBr): ν_{max} 2939, 2820, 1688, 1602, 1451, 1309, 1262, 1133, 1120 cm^{-1}; ^1H NMR (400 MHz, $CDCl_3$): δ 2.39 – 3.08 (10H, m, N′C$\underline{H}_2$$CH_2$OH and piperazine ring), 3.66 (2H, t, ^3J = 5.4 Hz, N′CH_2C$\underline{H}_2$OH), 3.93 (3H, s, OMe-4′), 3.95 (8H, s, CH_2-7, OMe-3′, 5′), 6.67 (1H, d, ^3J = 8.5 Hz, H-5), 6.74 (1H, s, H-2a), 7.15 (2H, s, H-2′, 6′), 7.63 ppm (1H, d, ^3J = 8.5 Hz, H-4); ^{13}C NMR (100 MHz, $CDCl_3$): δ 52.59, 53.06, 53.50, 56.12, 58.03, 59.29, 61.10, 103.93, 108.59, 108.67, 111.85, 113.62, 125.35, 127.97, 139.72, 147.53, 153.31, 165.50, 166.85, 182.57 ppm; MS (CI): *m/z* 471.2 (MH^+, 100). Anal. calcd for $C_{25}H_{30}N_2O_7$: C, 63.82; H, 6.43; N, 5.95. Found: C, 64.10; H, 6.71; N, 6.13.

General procedure for the synthesis of diacetates 12.

A mixture of a Mannich base **3a-3d** (2 mmol) and 200 mg (2 mmol) of potassium acetate in 5 mL of acetic anhydride was refluxed for 5 min and cooled to room temperature. The mixture was diluted with water to afford a precipitate of **11a-11d**, that was recrystallized from acetonitrile-water.

[(2*Z*)-6-(Acetyloxy)-2-benzylidene-3-oxo-2,3-dihydro-1-benzofuran-7-yl]methyl acetate (12a). Yellow solid (93% yield); mp: 145-147°C; IR (KBr): ν_{max} 1770, 1738, 1706, 1605, 1434, 1255, 1188, 1129 cm^{-1}; ; ^1H NMR (500 MHz, $CDCl_3$): δ 2.09 (3H, s, CH_3COO-6), 2.39 (3H, s, C$\underline{H}_3$$COCH_2$-7), 5.36 (2H, s, CH_2-7), 6.93 (1H, s, H-2a), 7.00 (1H, d, ^3J = 8.3 Hz, H-5), 7.39 – 7.51 (3H, m, H-3′, 4′, 5′), 7.82 (1H, d, ^3J = 8.4 Hz, H-4), 7.91 ppm (2H, d, ^3J = 8.3 Hz, H-2′, 6′); ^{13}C NMR (125 MHz, $CDCl_3$): δ 20.81, 20.94, 54.73, 114.02, 114.44, 118.87, 119.77, 125.70, 129.16, 130.34, 131.80, 132.15, 147.22, 156.25, 165.79, 168.60, 170.63, 183.39 ppm; MS (CI): *m/z* 353.0 (MH^+, 100). Anal. calcd for $C_{20}H_{16}O_6$: C, 68.18; H, 4.58. Found: C, 68.33; H, 4.45.

[(2*Z*)-6-(Acetyloxy)-2-(4-methoxybenzylidene)-3-oxo-2,3-dihydro-1-benzofuran-7-yl]methyl acetate (12b). Yellow solid (81% yield); mp: 135-137°C; IR (KBr): ν_{max} 2936, 2840, 1771, 1735, 1650, 1601, 1512, 1431, 1256, 1195, 1134 cm^{-1}; ^1H NMR (400 MHz, $CDCl_3$) δ 2.09 (3H, s, CH_3COO-6), 2.39 (3H, s, C$\underline{H}_3$$COCH_2$-7), 3.88 (3H, s, OMe-4′), 5.36 (2H, s, CH_2-7), 6.92 (1H, s, H-2a), 6.96 – 7.03 (3H, m, H-5, 3′, 5′), 7.82 (1H, d, ^3J = 8.3 Hz, H-4), 7.88 ppm (2H, d, ^3J = 8.8 Hz, H-2′, 6′); ^{13}C NMR (100 MHz, $CDCl_3$): δ 20.77, 20.87, 54.61, 55.45, 114.10, 114.27, 114.67, 118.51, 119.97, 124.71, 125.49, 133.63, 146.07, 155.81, 161.35, 165.26, 168.60, 170.58, 183.02 ppm; MS (CI): *m/z* 383.2 (MH^+, 100). Anal. calcd for $C_{21}H_{18}O_7$: C, 65.97; H, 4.75. Found: C, 66.11; H, 5.03.

[(2*Z*)-6-(Acetyloxy)-2-(3,4-dimethoxybenzylidene)-3-oxo-2,3-dihydro-1-benzofuran-7-yl]methyl acetate (12c). Yellow solid (91% yield); mp: 190-192°C; IR (KBr): ν_{max} 2963, 2845, 1772, 1736, 1647, 1595, 1514, 1259, 1184, 1127, 1065, 1021 cm^{-1}; ^1H NMR (400 MHz, $CDCl_3$): δ 2.06 (3H, s, CH_3COO-6), 2.38 (3H, s, C$\underline{H}_3$$COCH_2$-7), 3.94,

3.96 (each 3H, 2s, OMe-3′, 4′), 5.32 (2H, s, CH_2-7), 6.89 (1H, s, H-2a), 6.94 (1H, d, ^3J = 8.3 Hz, H-5), 6.98 (1H, d,^3J = 8.4 Hz, H-5′), 7.35 – 7.47 (1H, m, H-6′), 7.62 (1H, d, ^4J = 2.0 Hz, H-2′), 7.81 ppm (1H, d, ^3J = 8.3 Hz, H-4); ^{13}C NMR (125 MHz, $CDCl_3$): δ 20.81, 20.97, 54.68, 55.92, 56.10, 111.32, 113.56, 114.06, 114.68, 118.74, 120.00, 125.08, 125.70, 126.52, 146.22, 149.29, 151.26, 156.07, 165.25, 168.72, 170.59, 183.00 ppm; MS (CI): *m/z* 413.2 (MH^+, 100). Anal. calcd for $C_{22}H_{20}O_8$: C, 64.08; H, 4.89. Found: C, 63.92; H, 4.60.

[(2*Z*)-6-(Acetyloxy)-2-(1,3-benzodioxol-5-ylmethylene)-3-oxo-2,3-dihydro-1-benzofuran-7-yl]methyl acetate (12d). Yellow solid (88% yield); mp: 170-172°C; IR (KBr): ν_{max} 1765, 1737, 1704, 1649, 1611, 1257, 1200, 1031 cm^{-1}; ^{1}H NMR (400 MHz, $CDCl_3$): δ 2.09 (3H, s, CH_3COO-6), 2.39 (3H, s, C<u>H</u>$_3$COOCH_2-7), 5.35 (2H, s, CH_2-7), 6.05 (2H, s, OCH_2O), 6.86 (1H, s, H-2a), 6.89 (1H, d, ^3J = 8.3 Hz, H-5), 6.99 (1H, d, ^3J = 8.3 Hz, H-7′), 7.29 – 7.35 (1H, m, H-6′), 7.58 (1H, d, ^4J = 1.6 Hz, H-4′), 7.81 ppm (1H, d, ^3J = 8.3 Hz, H-4); ^{13}C NMR (125 MHz, $CDCl_3$): δ 20.87, 20.99, 54.71, 101.85, 109.03, 110.75, 114.34, 114.46, 118.74, 119.98, 125.61, 126.42, 128.12, 146.20, 148.51, 149.74, 155.95, 165.36, 168.74, 183.12 ppm; MS (CI): *m/z* 397.0 (MH^+, 100). Anal. calcd for $C_{21}H_{16}O_8$: C, 63.64; H, 4.07. Found: C, 63.87; H, 4.22.

General procedure for the synthesis of 7-methoxymethyl-6-hydroxyaurones 13a-13d.

A mixture of diacetate **12a-12d** (2 mmol) and 0.1 mL of concentrated hydrochloric acid in 10 mL of methanol was refluxed for 16-24 h. The mixture was cooled and diluted with water, and the resulting precipitate was collected by filtration. The products were purified by chromatography using 1:20 methanol-dichloromethane.

(2*Z*)-2-Benzylidene-6-hydroxy-7-(methoxymethyl)-1-benzofuran-3(2*H*)-one (13a). Yellow solid (43% yield); mp: 332-333°C; IR (KBr): ν_{max} 2893, 1677, 1583, 1442, 1305, 1284, 1135, 1061 cm^{-1}; ^{1}H NMR (400 MHz, DMSO-d_6): δ 3.34 (3H, s, C<u>H</u>$_3$OCH_2-7), 4.59 (2H, s, CH_2-7), 6.76 – 6.86 (2H, m, H-2a, 5), 7.41 – 7.55 (3H, m, H-3′, 4′, 5′), 7.61 (1H, d, ^3J = 8.5 Hz, H-4), 7.95 – 8.01 (2H, d, ^3J = 8.8 Hz, H-2′, 6′), 11.34 ppm (1H, br. s, OH-6); ^{13}C NMR (100 MHz, DMSO-d_6): δ 57.63, 61.60, 108.36, 110.43, 112.47, 112.61, 125.49, 129.02, 129.68, 131.08, 132.17, 147.37, 164.88, 166.86, 181.70 ppm; MS (CI): *m/z* 251.0 (MH^+-32, 100). Anal. calcd for $C_{17}H_{14}O_4$: C, 72.33; H, 5.00. Found: C, 72.46; H, 5.19.

(2*Z*)-6-Hydroxy-2-(4-methoxybenzylidene)-7-(methoxymethyl)-1-benzofuran-3(2*H*)-one (13). Yellow solid (53% yield); mp: 185-187cels ; IR (KBr): ν_{max} 3097, 2926, 1674, 1600, 1446, 1287, 1263, 1137, 1064 cm^{-1}; ^{1}H NMR (400 MHz, DMSO-d_6): δ 3.33 (3H, s, C<u>H</u>$_3$OCH_2-7), 3.83 (3H, s, OMe-4′), 4.59 (2H, s, CH_2-7), 6.76 – 6.84 (2H, m, H-2a, 5), 7.09 (2H, d, ^3J = 8.5 Hz, H-3′, 5′), 7.59 (1H, d, ^3J = 8.4 Hz, H-4), 7.94 (2H, d, ^3J = 8.5 Hz, H-2′, 6′), 11.25 ppm (1H, br. s, OH-6); ^{13}C NMR (100 MHz, DMSO-d_6): δ 55.37, 57.62, 61.62, 108.27, 110.86, 112.44, 112.78, 114.67, 124.66, 125.28, 132.99, 146.16, 160.49, 164.54, 166.50, 181.49 ppm; MS (CI): *m/z* 313.2 (MH^+, 100). Anal. calcd for C18H16O5: C, 69.22; H, 5.16. Found: C, C, 69.48; H, 5.41.

(2*Z*)-2-(3,4-Dimethoxybenzylidene)-6-hydroxy-7-(methoxymethyl)-1-benzofuran-3(2*H*)-one (13c). Yellow solid (69% yield); mp: 225 - 227°C; IR (KBr): ν_{max} 2917, 1664, 1605, 1581, 1515, 1303, 1303, 1274, 1136 cm^{-1}; ^{1}H NMR (500 MHz, DMSO-d_6): δ 3.30 (3H, s, C<u>H</u>$_3$OCH_2-7), 3.82, 3.86 (each 3H, 2s, OMe-3′,4′), 4.57 (2H, s, CH_2-7), 6.77 (1H, s, H-2a), 6.80 (1H, d, ^3J = 8.4 Hz, H-5), 7.07 (1H, d,^3J = 8.4 Hz, H-5′), 7.48 (1H, dd, ^3J = 8.3 Hz, ^4J = 1.9 Hz, H-6′), 7.58 (1H, d, ^3J = 8.4 Hz, H-4), 7.69 (1H, d, ^4J = 1.9 Hz, H-2′), 11.24 ppm (1H, br. s, OH-6); ^{13}C NMR (125 MHz, DMSO-d_6): δ 55.21, 55.56, 57.54, 61.72, 108.20, 111.28, 111.84, 112.42, 112.80, 113.32, 124.80, 125.25, 125.57, 146.15, 148.70, 150.37, 164.52, 166.42, 181.40 ppm; MS (CI): *m/z* 343.2 (MH^+, 100). Anal. calcd for $C_{19}H_{18}O_6$: C, 66.66; H, 5.30. Found: C, 66.90; H, 5.48.

(2*Z*)-2-(1,3-Benzodioxol-5-ylmethylene)-6-hydroxy-7-(methoxymethyl)-1-benzofuran-3(2*H*)-one (13d). Yellow solid (54% yield); mp: 310-311°C; IR (KBr): ν_{max} 2900, 1671, 1603, 1442, 1295, 1258, 1147, 1033 cm^{-1}; ^{1}H NMR (400 MHz, DMSO-d_6): δ 3.32 (3H, s, C<u>H</u>$_3$OCH_2-7), 4.56 (2H, s, CH_2-7), 6.11 (2H, s, OCH_2O), 6.76 (1H, s, H-2a), 6.79 (1H, d, ^3J = 8.5 Hz, H-5), 7.04 (1H, d, ^3J = 8.1 Hz, H-7′), 7.43 – 7.50 (1H, m, H-6′), 7.53 – 7.61 (2H, m, H-4, 4′), 11.26 ppm (1H, br. s, OH-6); ^{13}C NMR (100 MHz, DMSO-d_6): δ 57.66, 61.77, 101.68, 108.28, 108.93, 109.87, 110.92, 112.48, 112.71, 125.27, 126.29, 127.10, 146.22, 147.87, 148.69, 164.50, 166.49, 181.43 ppm; MS (CI): *m/z* 327.0 (MH^+, 100). Anal. calcd for $C_{18}H_{14}O_6$: C, 66.26; H, 4.32. Found: C, 66.03; H, 4.58.

2.2 **Cell Proliferation Assay**

Prostate cancer PC-3 cells were cultured in DMEM/F-12 HAM Mixture (Sigma D8437) containing 10% Fetal Bovine Serum (Atlanta Biological S11150). Cells ($3.5x10^4$ cells per well) were split into 12-well plates. After 24 h, 10mM of each compound were added to each well. DMSO was used as a control. Each experiment was done in triplicate. Cell viability and number were analyzed using the Vi-Cell XR Cell Viability Analyzer (Beckman Coulter).

3. RESULTS AND DISCUSSIONS

The important criteria to consider in developing of a synthesis of *N,N*-dialkylaminomethyl derivatives of 6-hydroxyaurones included efficiency, simplicity and regioselectivity. 6-Hydroxy-2-benzylidenbenzofuran-3(2*H*)-one **2** (Ar = C_6H_5) possessed two nucleophilic centers at C-5 and C-7, excluding possible centers in the benzylidene ring, for Mannich reactions. The efficient and selective aminomethylation of unsymmetrical phenols depended on the structure of the substrate, the dialkylamine, solvent, the catalyst, the pH, and in particular, the aminomethylating agent. These agents include iminium salts or hemiaminals [16,17], imines [18-20], and aminals [21, 22] that effect the aminomethylation of a wide range of phenolic substrates.

For these reasons, we investigated the aminomethylation of 6-hydroxyaurones using various reagents and conditions including [1] 40% aqueous formaldehyde and a secondary amine in refluxing ethanol; [2] 40% aqueous formaldehyde and a secondary amine hydrochloride in refluxing ethanol; and [3] 40% aqueous formaldehyde and a secondary amine under basic catalysis by 4-dimethylaminopyridine (DMAP), 1,8-diazabicyclo[5.4.0]undec-7-ene (DBU) or Et_3N in refluxing ethanol. The best yield was observed using DMAP

as a catalyst and using paraformaldehyde in place of aqueous formaldehyde. For example, aminomethylation of aurone **2a** with 1-methylpiperazine gave 21% yield of the compound **10b** using aqueous formaldehyde without base, 32% yield using aqueous formaldehyde with DMAP, and 46% yield using paraformaldehyde with DMAP. The formation of 5,7-bisaminomethyl derivatives was observed in all cases under these reaction conditions. Carrying out the aminomethylation using *N*-hydroxymethylamines and *N*,*N*-bisaminomethanes (aminals) provided the most promising pathway for the synthesis of aurone Mannich bases. For example, aminomethylation of aurone **2a** using 4,4'-methylenebis(1-methylpiperazine) increased the yield of **10b** to 80% of target product and simplified the purification of target compound by minimizing the amount of the 5,7-bisaminomethyl derivatives.

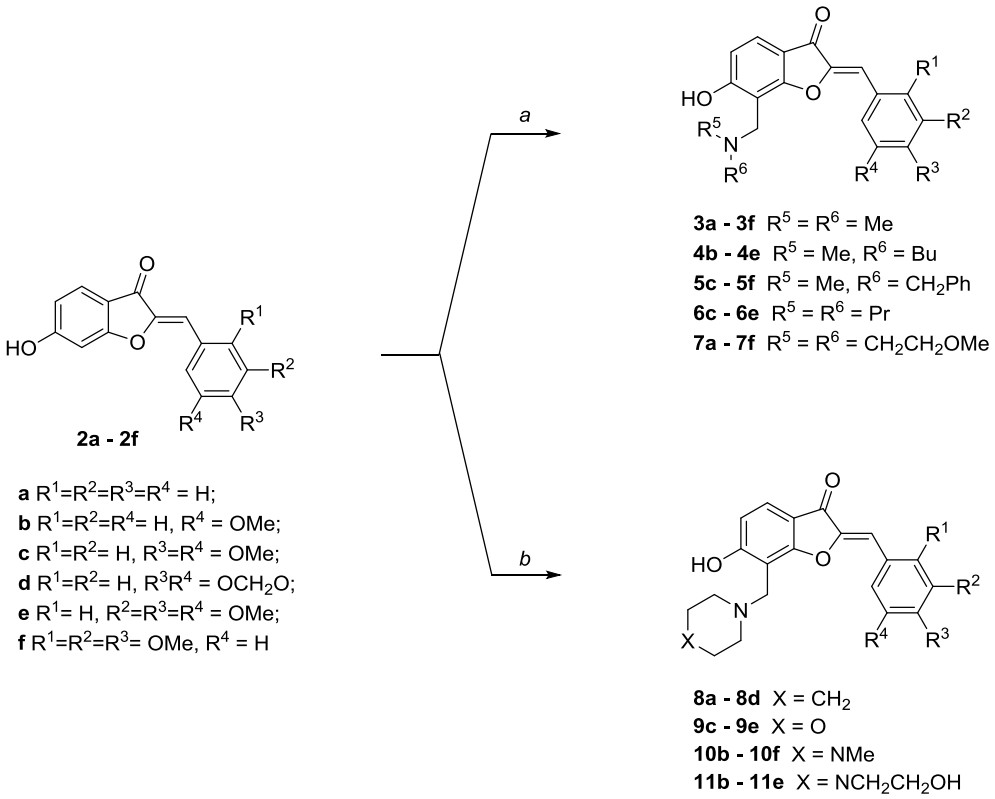

a $R^1=R^2=R^3=R^4$ = H;
b $R^1=R^2=R^4$= H, R^4 = OMe;
c $R^1=R^2$= H, $R^3=R^4$ = OMe;
d $R^1=R^2$= H, R^3R^4 = OCH_2O;
e R^1= H, $R^2=R^3=R^4$ = OMe;
f $R^1=R^2=R^3$= OMe, R^4 = H

Scheme 1. Synthesis of Mannich bases of 6-hydroxyaurones **3-11**. Reagents and conditions: *a*) $CH_2(NR^5R^6)_2$, *i*-PrOH, 80°C, 4-8 h; *b*) $CH_2(NC_4H_8X)_2$, *i*-PrOH, 80°C, 4-6 h

Further studies revealed that the aminomethylation of most 6-hydroxyaurones with aminals in isopropanol or, as in case of aurone **2d,** in 1,4-dioxane gave the best yields. In these cases, we observed the regiospecific formation of 7-*N*,*N*-dialkylaminomethyl aurone derivatives. When using aminals prepared from dimethylamine, dipropylamine, bis(2-methoxyethyl)amine, *N*-methylbutylamine, *N*-methylbenzylamine, morpholine, piperidine, and 1-methylpiperazine, we did not observe formation of any 5,7-bisaminomethyl derivatives. The desired 7-(N,N-dialkylamino)methyl-6-hydroxyaurones were isolated in 51-86% yield (Scheme 1). Formation of 7-(*N*,*N*-dialkylamino)methyl derivatives was confirmed by ^{1}H NMR in which the coupling constant (J = 8.4-8.5 Hz) between H-4 and H-5 excluded the regioisomeric 5-(*N*,*N*-dialkylamino)methyl-6-hydroxyaurones.

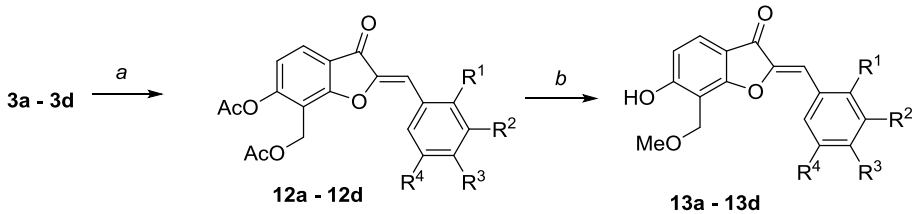

Scheme 2. Conversion of *N*,*N*-dimethylaminomethyl derivatives **3a-d** to acetoxymethyl- and methoxymethyl derivatives. Legend: *a*, Ac_2O, KOAc*; b*, HCl, MeOH.

Table 1. Percent inhibition of prostate cancer PC-3 cell proliferation by select aurones

Aurone	R^1	R^2	R^3	R^4	C-7	Inhibition at 10 μM (%)
2a	H	H	H	H	H	7.1±22.6
2e	H	OMe	OMe	OMe	H	52.9±31.7
3a	H	H	H	H	CH_2NMe_2	9.3±6.5
3e	H	OMe	OMe	OMe	CH_2NMe_2	22.4±8.3
5c	H	OMe	OMe	H	$CH_2N(Me)CH_2Ph$	25.9±12.9
5d	H	OCH_2O		H	$CH_2N(Me)CH_2Ph$	8.8±13.8
5e	H	OMe	OMe	OMe	$CH_2N(Me)CH_2Ph$	63.0±4.8
6d	H	OCH_2O		H	CH_2NPr_2-*i*	84.51±0
8a	H	H	H	H	1-piperidinylmethyl	6.5±19.5
8d	H	OCH_2O		H	1-piperidinylmethyl	11.7±4.8
9e	H	OMe	OMe	OMe	4-morpholinomethyl	31.4±2.5
10b	H	H	OMe	H	4-(1-methylpiperazinyl)methyl	40.6±5.6
10c	H	OMe	OMe	H	4-(1-methylpiperazinyl)methyl	45.8±10.0
10c	H	OMe	OMe	H	4-(1-(2hudroxyethyl) piperazinyl)-methyl	47.9±19.8
12c	H	OMe	OMe	H	acetoxymethyl	99.5±0.1
12d	H	OCH_2O		H	acetoxymethyl	87.9±2.3

Heating 7-*N*,*N*-dialkylaminomethyl-8-hydroxymethylaurones **3a-3d** with acetic anhydride in presence of potassium acetate afforded the corresponding diacetates **12a-12d** in excellent yield (Scheme 2). Hydrolysis of **12** in methanol using hydrochloric acid led directly to formation of 7-methoxymethyl derivatives **13a-13d**.

A screening program using inhibition of the proliferation of PC-3 prostate cancer cells revealed that several 6-hydroxyaurones **2-13** with C-7 *N*,*N*-dialkylaminomethyl, acetoxymethyl or methoxymethyl substituents exhibited antineoplastic activity in the low micromolar range (Table 1). In general, 7-(*N*,*N*-dialkylamino)methyl-6-hydroxyaurones possessed weak activity at these concentration but provided access to 7-acetoxymethylaurones that were the most potent. Thus, compounds **12c** and **12d** inhibited the growth of PC-3 cells at 1 μM concentration to the extent of 86.0±2.2% and 87.1±4.0, respectively. Additional testing of **12c** at a concentration of 300 nM showed good retention of this inhibition of cell proliferation (75.4±15.6%).

CONCLUSION

Various aminals (*i.e.*, bis(*N*,*N*-dialkylamino)methanes) derived from aliphatic and alicyclic amines afforded the regiospecific aminomethylation of 6-hydroxyaurones. The resulting products in turn provided ready access to aurones bearing acetoxy or methoxy groups with the capacity to inhibit prostate cancer PC-3 cell proliferation. Additional studies of these agents will be reported in due course.

LIST OF ABBREVIATIONS

If abbreviations are used in the text either they should be defined in the text where first used, or a list of abbreviations can be provided.

CONFLICT OF INTEREST

CL and DSW have partial ownership of a new-start company, Epionc, Inc., that seeks to develop these compounds as commercial agents. CL and DSW disclosed this information and complied with requirements to mitigate any potential conflicts of interest in accord with University of Kentucky policy.

ACKNOWLEDGEMENTS

CL and DSW were supported by CA172379 from the NIH. DSW was also supported by the Office of the Dean of the College of Medicine, by the Center for Pharmaceutical Research and Innovation in the College of Pharmacy, and by NIH Grant Number P30 GM110787 from the National Institute of General Medical Sciences to L. Hersh, PI. Its contents are solely the responsibility of the authors and do not necessarily represent the official views of the NIH or the NIGMS. DSW was also supported by the Office of the Assistant Secretary of Defense for Health Affairs, through the Prostate Cancer Research Program under Award No. W81XWH-16-1-0635. Opinions, interpretations, conclusions and recommendations are those of the author and are not necessarily endorsed by the Department of Defense.

Guest or honorary authorship based solely on position (e.g. research supervisor, departmental head) is discouraged.

SUPPLEMENTARY MATERIAL

Supplementary material is available on the publisher's web site along with the published article.

REFERENCES

[1] Haudecoeur, R.; Boumendjel, A. Recent Advances in the Medicinal Chemistry of Aurones. *Curr. Med. Chem.*, **2012**, *19*(18), 2861-2875.

[2] Boumendjel, A. Aurones: A Subclass of Flavones with Promising Biological Potential. *Curr. Med. Chem.*, **2003**, *10*(23), 2621-2630.

[3] Sim, H. M.; Loh, K. Y.; Yeo, W. K.; Lee, C. Y.; Go, M. L.; Yeo, W. K. Aurones as Modulators of ABCG2 and ABCB1: Synthesis and Structure-Activity Relationships. *ChemMedChem*, **2011**, *6*(4), 713 - 724.

[4] Horváti, K.; Bacsa, B.; Szabó, N.; Dávid, S.; Mező, G.; Grolmusz, V.; Vértessy, B.; Hudecz, F.; Bősze, S. Enhanced Cellular Uptake of a New, *in Silico* Identified Antitubercular Candidate by Peptide Conjugation. *Bioconjugate Chem.*, **2012**, *23*(5), 900-907.

[5] Schoepfer, J.; Fretz, H.; Chaudhuri, B.; Muller, L.; Seeber, E.; Meijer, L.; Lozach, O.; Vangrevelinghe, E.; Furet, P. Structure-Based Design and Synthesis of 2-Benzylidene-benzofuran-3-ones as Flavopiridol Mimics. *J. Med. Chem.*, **2002**, *45*(9), 1741-1747.

[6] Carrasco, M. P.; Newton, A. S.; Gonçalves, L.; Góis, A.; Machado, M.; Gut, J.; Nogueira, F.; Hänscheid, T.; Guedes, R. C.; dos Santos, D. J. V. A.; Rosenthal, P. J.; Moreira, R. Probing the aurone scaffold against *Plasmodium falciparum*: Design, synthesis and antimalarial activity. *Eur. J. Med. Chem.*, **2014**, *80*(0), 523-534.

[7] Sheng, R.; Xu, Y.; Hu, C.; Zhang, J.; Lin, X.; Li, J.; Yang, B.; He, Q.; Hu, Y. Design, synthesis and AChE inhibitory activity of indanone and aurone derivatives. *Eur. J. Med. Chem.*, **2009**, *44*(1), 7-17.

[8] Nakano, H.; Saito, N.; Parker, L.; Tada, Y.; Abe, M.; Tsuganezawa, K.; Yokoyama, S.; Tanaka, A.; Kojima, H.; Okabe, T.; Nagano, T. Rational Evolution of a Novel Type of Potent and Selective Proviral Integration Site in Moloney Murine Leukemia Virus Kinase 1 (PIM1) Inhibitor from a Screening-Hit Compound. *J. Med. Chem.*, **2012**, *55*(11), 5151-5164.

[9] Choi, H.; Park, H. J.; Shin, J. C.; Ko, H. S.; Lee, J. K.; Lee, S.; Park, H.; Hong, S. Structure-based virtual screening approach to the discovery of p38 MAP kinase inhibitors. *Bioorg. Med. Chem. Lett.*, **2012**, *22*(6), 2195-2199.

[10] Lewin, G.; Aubert, G.; Thoret, S.; Dubois, J.; Cresteil, T. Influence of the skeleton on the cytotoxicity of flavonoids. *Bioorg. Med. Chem.*, **2012**, *20*(3), 1231-1239.

[11] Liu, T.; Xu, Z.; He, Q.; Chen, Y.; Yang, B.; Hu, Y. Nitrogen-containing flavonoids as CDK1/Cyclin B inhibitors: design, synthesis, and biological evaluation. *Bioorg. Med. Chem. Lett.*, **2007**, *17*(1), 278 - 281.

[12] Zhang, S.; Ma, J.; Bao, Y.; Yang, P.; Zou, L.; Li, K.; Sun, X. Nitrogen-containing flavonoid analogues as CDK1/cyclin B inhibitors: synthesis, SAR analysis, and biological activity. *Bioorg. Med. Chem.*, **2008**, *16*(15), 7128-7133.

[13] Gao, M.; Wang, M.; Miller, K. D.; Zheng, Q.-H. Synthesis of (*Z*)-2-((1*H*-indazol-3-yl)methylene)-6-[^{11}C]methoxy-7-(piperazin-1-ylmethyl)benzofuran-3(2H)-one as a new potential PET probe for imaging of the enzyme PIM1. *Bioorg. Med. Chem. Lett.*, **2013**, *23*(15), 4342-4346.

[14] Bandgar, B. P.; Patil, S. A.; Korbad, B. L.; Biradar, S. C.; Nile, S. N.; Khobragade, C. N. Synthesis and biological evaluation of a novel series of 2,2-bisaminomethylated aurone analogues as anti-inflammatory and antimicrobial agents. *Eur. J. Med. Chem.*, **2010**, *45*(7), 3223-3227.

[15] Lipeeva, A. V.; Shul'ts, E. E.; Shakirov, M. M.; Bagryanskaya, I. Y.; Tolstikov, G. A. Plant coumarins: XIII. Synthesis of 2,3,9-trisubstituted furocoumarins. *Russ. J. Org. Chem.*, **2013**, *49*(3), 403-411.

[16] Nguyen, T. B.; Wang, Q.; Guéritte, F. An Efficient One-Step Synthesis of Piperidin-2-yl and Pyrrolidin-2-yl Flavonoid Alkaloids through Phenolic Mannich Reactions. *Eur. J. Org. Chem.*, **2011**, *2011*(35), 7076-7079.

[17] Frasinyuk, M. S.; Bondarenko, S. P.; Khilya, V. P.; Liu, C.; Watt, D. S.; Sviripa, V. M. Synthesis and tautomerization of hydroxylated isoflavones bearing heterocyclic hemi-aminals. *Org. Biomol. Chem.*, **2015**, *13*(4), 1053-1067.

[18] MacLeod, P. D.; Li, Z.; Li, C.-J. Self-catalytic, solvent-free or in/on water protocol: aza-Friedel–Crafts reactions between 3,4-dihydroisoquinoline and 1- or 2-naphthols. *Tetrahedron*, **2010**, *66*(5), 1045-1050.

[19] Cimarelli, C.; Fratoni, D.; Mazzanti, A.; Palmieri, G. Betti Reaction of Cyclic Imines with Naphthols and Phenols - Preparation of New Derivatives of Betti's Bases. *Eur. J. Org. Chem.*, **2011**, *2011*(11), 2094-2100.

[20] Nguyen, T. B.; Lozach, O.; Surpateanu, G.; Wang, Q.; Retailleau, P.; Iorga, B. I.; Meijer, L.; Guéritte, F. Synthesis, Biological Evaluation, and Molecular Modeling of Natural and Unnatural Flavonoidal Alkaloids, Inhibitors of Kinases. *J. Med. Chem.*, **2012**, *55*(6), 2811-2819.

[21] Mrug, G. P.; Bondarenko, S. P.; Khilya, V. P.; Frasinyuk, M. S. Synthesis and aminomethylation of 7-hydroxy-5-methoxyisoflavones. *Chem. Nat. Compd.*, **2013**, *49*(2), 235-241.

[22] Bondarenko, S. P.; Levenets, A. V.; Frasinyuk, M. S.; Khilya, V. P. Synthesis of Analogs of Natural Isoflavonoids Containing Phloroglucinol. *Chem. Nat. Compd.*, **2003**, *39*(3), 271-275.

Received: March 20, 2014 Revised: April 16, 2014 Accepted: April 20, 2014